






Universitat Autònoma de Barcelona

ADVERTIMENT. L'accés als continguts d'aquesta tesi queda condicionat a l'acceptació de les condicions d'ús establertes per la següent llicència Creative Commons:  http://cat.creativecommons.org/?page_id=184

ADVERTENCIA. El acceso a los contenidos de esta tesis queda condicionado a la aceptación de las condiciones de uso establecidas por la siguiente licencia Creative Commons:  <http://es.creativecommons.org/blog/licencias/>

WARNING. The access to the contents of this doctoral thesis it is limited to the acceptance of the use conditions set by the following Creative Commons license:  <https://creativecommons.org/licenses/?lang=en>



UAB

**Universitat Autònoma
de Barcelona**

PhD Thesis

***Neuropathological and molecular alterations in a novel
neuromelanin-producing transgenic mouse model:
relevance to Parkinson's disease and brain aging***

Núria Peñuelas Peñarroya

Directors: Dr. Miquel Vila Bover i Dr. Ariadna Laguna Tuset

Tutor: Dr. Joan Xavier Comella Carnicé

PhD in Neurosciences

Institut de Neurociències

Universitat Autònoma de Barcelona

Barcelona, 2022

TABLE OF CONTENTS

LIST OF FIGURES	¡Error! Marcador no definido.
LIST OF TABLES	viii
LIST OF ABBREVIATIONS	ix
ABSTRACT	2
INTRODUCTION	4
1. Parkinson’s disease	4
1.1 Brief history.....	4
1.1.1 Early clinical descriptions	4
1.1.2 Early neuropathological descriptions	4
1.1.3 Early treatments	4
1.2 Epidemiology.....	5
1.3 Neuropathological hallmarks.....	6
1.3.1 Selective neurodegeneration	6
1.3.2 Lewy pathology.....	7
1.3.3 Neuroinflammation	10
1.4 Determinants of neuronal vulnerability	11
1.4.1 Neuronal pigmentation	12
1.4.2 DA toxicity	12
1.4.3 Iron load	12
1.4.4 Axonal arborization size and activity	13
1.4.5 Bioenergetic failure.....	13
1.5 Symptomatology	14
1.6 Disease staging and therapeutic window	15
1.7 Treatment	17
1.8 Etiology	18
1.8.1 Genetics.....	18
1.8.2 Non-genetic factors.....	20
1.9 PD experimental models	20
1.9.1 Toxic animal models	21
1.9.2 Genetic animal models.....	23
2. Neuromelanin	25
2.1 Brief history.....	25
2.2 Species distribution	25
2.3 Synthesis of melanin and neuromelanin	25

2.4	Structure	29
2.5	Function	29
2.6	Brain-wide topographical distribution	30
3.	NM relation to PD pathogenesis.....	32
3.1	NM distribution and levels in relation to PD cell death	32
3.1.1	NM distribution	32
3.1.2	NM levels.....	35
3.2	NM in relation to PD hallmarks.....	35
3.2.1	Aging	35
3.2.2	Lewy pathology.....	37
3.2.3	Neuroinflammation	38
3.2.4	Generation of the first <i>in vivo</i> NM-producing rodent model	39
4.	Genome-wide transcriptomic analysis in PD.....	41
	HYPOTHESIS AND OBJECTIVES	44
	MATERIALS AND METHODS	47
1.	Human tissue	47
2.	Animals.....	47
3.	Histological analysis	49
4.	Real-Time quantitative PCR (qPCR)	53
5.	Western blot (WB)	56
6.	In vivo microdialysis.....	56
7.	Chromatographic determination of metabolites by UPLC-MS/MS.	57
8.	Behavioral analysis	60
9.	Assessment of peripheral functions	62
10.	Laser capture microdissection	62
11.	Transcriptomic microarrays and data analysis	64
12.	Lysosomal enzymatic activity	68
13.	ELISA.....	70
14.	Statistical analysis.....	71
	RESULTS – CHAPTER 1. Generation and characterization of a new brain-wide NM accumulating rodent model	73
1.	Endogenous expression of melanogenic enzymes in the rodent and human brain.....	73
2.	Generation of tyrosinase transgenic mouse lines	76
2.1	Initial characterization of distinct tyrosinase transgenic lines	76
2.2	TgNM basic colony characterization	78
2.3	Brain TYR expression and NM accumulation in tgNM	79
2.4	Consequences of NM accumulation in dopaminergic SN and VTA nuclei.....	84
2.4.1	Behavioral alterations related to dopaminergic dysfunction	84

2.4.2	Dopaminergic dysfunction and early neurodegenerative changes in SN-VTA from tgNM mice.....	85
2.4.3	PD-like neuropathological alterations in SN-VTA from tgNM mice.....	89
2.5	Consequences of NM accumulation in noradrenergic LC nucleus	90
2.5.1	Behavioral alterations related to noradrenergic dysfunction.....	90
2.5.2	Neurodegeneration and PD-like neuropathology in LC from tgNM mice.....	91
2.6	Consequences of NM accumulation in cholinergic and serotonergic nuclei	93
2.7	Consequences of NM accumulation in medullary nuclei	95
2.7.1	PD-like neuropathology in DVC from tgNM mice.....	95
2.7.2	Peripheral alterations associated to medullary brainstem nuclei dysfunction	97
RESULTS - CHAPTER 2. TgNM transcriptomic characterization and identification of potential therapeutic targets		
1.	Transcriptional profiling of anatomically-defined pigmented areas in tgNM mice	101
1.1	Sample collection and transcriptomic microarrays.....	101
1.2	Differential expression analysis	103
1.2.1	Common DEGs between all pigmented regions	105
1.2.2	Two-region overlapping DEGs	106
1.2.3	Region-specific DEGs.....	107
1.2.4	Non-coding microRNA.....	108
1.3	Gene set enrichment analysis.....	108
2.	Transcriptional profiling of pigmented neurons in tgNM mice	110
2.1	Sample collection and microarrays	111
2.2	Differential Expression Analysis.....	111
2.2.1	Common DEGs between SN and VTA neurons	114
2.2.2	Subtype-specific DEGs.....	114
2.3	Gene set enrichment analysis.....	116
3.	Differences in the splicing events	118
4.	Evidence of the translational value of tgNM mice as a model of human-like NM accumulation	120
5.	Validation of potential NM-related pathways and targets.....	124
6.	Pan-regional neuroinflammatory NM-related genes	128
7.	GPNMB as a possible NM-linked therapeutic target	131
8.	GPNMB interplay with NM.....	135
DISCUSSION		
1.	Generation of a new TYR-expressing NM-accumulating model of PD	139
1.1	TYR overexpression in mice	139
1.2	Modelling brain pigmentation distribution and accumulation	140
1.3	Dopaminergic dysfunction.....	140

1.4	Noradrenergic neurodegeneration	142
1.5	Medullary nuclei alterations.....	142
1.6	Cholinergic and serotonergic alterations.....	144
1.7	PD-like neuropathological hallmarks	145
1.8	Relevance of tgNM as a new PD model.....	147
2.	Transcriptomic characterization of the effects of progressive NM accumulation in neurons	150
2.1	Characterization of progressively pigmented distinct regions	150
2.2	TOP individual DEGs	150
2.3	NM-related biological pathways.....	154
2.4	Translational value of the NM-induced transcriptomic profile identified in tgNM mice	155
2.5	Splicing events.....	155
2.6	Validation of the main NM-related candidates and biological pathways.....	156
2.7	DAM profile.....	157
2.8	Neuroinflammatory cytokines	160
2.9	GPNMB as a new NM-related biomarker or therapeutic target.....	161
2.10	Relevance of the transcriptomic characterization in tgNM animals.....	163
	CONCLUSIONS	166
	REFERENCES	168
	ANNEX	195

LIST OF FIGURES

Figure 1. Cellular vulnerability in PD	7
Figure 2. Staging of Lewy pathology in clinical PD	9
Figure 3. Summary of the converging hypotheses that may explain the origins of the selective vulnerability of neurons in PD	14
Figure 4. Clinical symptoms associated with PD progression	17
Figure 5. Molecular mechanisms involved in PD	24
Figure 6. Peripheral melanin synthesis pathway and proposed mechanism for NM organelles formation	27
Figure 7. NM distribution in human brain catecholaminergic groups	30
Figure 8. Distribution of pigmentation in the human brain	33
Figure 9. Age-dependent PD incidence and NM accumulation	37
Figure 10. NM in relation to PD neuropathological hallmarks	38
Figure 11. Age-dependent human-like NM production in rat SNpc triggers PD pathology	40
Figure 12. Transcriptomic microarray quality control analysis: Normalization, batch/sex effect correction, and outlier removal	66
Figure 13. Endogenous expression of melanogenic enzymes in the rodent and human brain	74
Figure 14. Characterization of the different transgenic mouse lines generated	78
Figure 15. TgNM colony characterization	79
Figure 16. TYR expression within catecholaminergic areas in TgNM	80
Figure 17. Accumulation of human-like NM in different brain catecholaminergic nuclei	81
Figure 18. Brain-wide NM distribution in catecholaminergic nuclei	82
Figure 19. NM accumulation in the main catecholaminergic nuclei in tgNM mice	83
Figure 20. Dopaminergic-related behavioral analysis in tgNM mice	85
Figure 21. Dopaminergic dysfunction in tgNM mice	87
Figure 22. Neuropathological alterations in SN-VTA from tgNM mice	89
Figure 23. Noradrenergic-related behavior analysis in tgNM mice	91
Figure 24. LC neurodegeneration and PD-like neuropathology in tgNM mice	92
Figure 25. Cholinergic and serotonergic alterations in tgNM mice	94
Figure 26. Medullary catecholaminergic nuclei alterations in tgNM mice	96
Figure 27. Peripheral alterations in tgNM mice	98

Figure 28. Isolation of histologically-defined PD-vulnerable regions in mice.....	102
Figure 29. Quality control of collection method and microarray experimental design	103
Figure 30. Differential expression analysis (DEA) between pigmented and non-pigmented catecholaminergic nuclei.....	104
Figure 31. Differentially-expressed genes and NM accumulation	104
Figure 32. Pan-regional NM-linked transcriptional changes.....	106
Figure 33. Gene set enrichment analysis with GO database in tgNM compared to wt SN-VTA-LC	109
Figure 34. Gene set enrichment analysis with Reactome database in tgNM compared to wt SN-VTA-LC	110
Figure 35. Experimental design and quality control of neuronal-enriched samples.....	111
Figure 36. Comparison of DEGs identified in pigmented areas using two distinct LCM collection methods (region vs neurons)	112
Figure 37. Differential expression analysis between tgNM and wt SNpc and VTA neurons	113
Figure 38. Comparison between SN and VTA neurons specific DEGs.....	115
Figure 39. Gene set enrichment analysis with GO database in tgNM compared to wt SN-VTA neurons.....	116
Figure 40. Gene set enrichment analysis with Reactome database in tgNM compared to wt SN-VTA neurons	117
Figure 41. Alternative Splicing events in tgNM pigmented areas.....	119
Figure 42. TgNM profiles in relation to single-cell postmortem SN dataset.....	123
Figure 43. Biological pathway validation at the RNA level.....	125
Figure 44. Biological pathway validation at the protein level	126
Figure 45. Lysosomal activity in tgNM mice	127
Figure 46. DAM-associated genes increased in all NM-accumulating areas in tgNM.....	129
Figure 47. Cytokine profile in pigmented areas of tgNM mice	130
Figure 48. Peripheral neuroinflammatory markers in tgNM mice	131
Figure 49. GPNMB expression in tgNM mice	133
Figure 50. GPNMB expression in PD postmortem SN	134
Figure 51. GPNMB overexpression attenuates NM-linked deficits.....	136
Figure 52. Schematic evolution of the prodromal phase modelled by tgNM mice.....	149
Figure 53. The intron-exon architecture of GPNMB in relation to protein domains	156
Figure 54. Proposed shared mechanism between microglial activation in tgNM mice with other neurodegenerative diseases	159

LIST OF TABLES

Table 1. PARK loci and identified genes that segregate with familial forms of PD	19
Table 2. Genes associated with single nucleotide polymorphisms that modulate PD risk. 19	
Table 3. Degree of PD cell loss in specific medullary nuclei.	34
Table 4. Primary antibodies used in immunohistochemistry (IHC), immunofluorescence (IF) and western blot (WB)	51
Table 5. Primers designed using Primer-BLAST for mouse and human transcripts.	56
Table 6. MRM acquisition settings^a	60
Table 7. Expression of melanogenic enzymes in human brain datasets from PD and control samples	75
Table 8. Nomenclature of pigmented catecholaminergic cell groups in tgNM and their qualitatively assessed cytoplasmic NM levels.	82
Table 9. DEGs in pigmented (tgNM) compared to non-pigmented (wt) SN-VTA-LC regions.	105
Table 10. Top DEGs in pigmented (tgNM) compared to non-pigmented (wt) SN-VTA neurons.	114
Table 11. PD postmortem datasets correlation with tgNM SN at different ages.	121
Table 12. PD postmortem datasets correlation with tgNM LC at different ages	121
Table 13. Gene-lists linked to PD genetically and experimentally	122
Table 14. Gene-lists linked to PD genetically and experimentally	122

LIST OF ABBREVIATIONS

μ l	Microliter
μ M	Micromolar
3MT	3-methoxytyramine
5HIAA	5-hydroxyindole-3-acetic acid
5HT	Serotonin
5HT-d4	Serotonin-d4 Hydrochloride
5SCD	5-S-cysteinyl-dopa
5SCDA	5-S-cysteinyl-dopamine
6-OHDA	6-hydroxydopamine
AAV	adeno-associated viral vector
ABC	avidin-biotin-peroxidase complex
AC	aminochrome
Ach	acetylcholine
ALP	autophagy-lysosomal pathways
BBB	Blood-brain barrier
BIOBANC-MUR	Biobanco en Red de la Región de Murcia
BSA	Biological Significance Analysis
BTX-A	Botulinum toxin A
BTX-B	Botulinum toxin B
Ca ²⁺	Calcium
CD4	Cluster of differentiation 4
CD68	Cluster of Differentiation 68
CD8	Cluster of differentiation 8
cDNA	Complementary DNA
ChAT	Choline acetyltransferase
CIBER-BBN	Centro de Investigación Biomédica en Red—Bioingeniería, Biomateriales y Nanomedicina
COMT	Catechol-O-methyltransferase
CT	Threshold cycle
Ctrl	Control
DA	Dopamine or dopaminergic
DA-d4	Dopamine-d4 hydrochloride

DAM	Disease-associated-microglia
DAT	Dopamine transporter
DCT	Dopachrome tautomerase
DEA	Differential expression analysis
DEGs	Differentially expressed genes
DHI	5,6-dihydroxyindole
DHICA	5,6-dihydroxyindole-2-carboxylic acid
DMNV	Dorsal motor nucleus of the vagus nerve
DNA	Deoxyribonucleic acid
DOMA	3,4-dihydroxymandelic acid
DOPAC	3,4-Dihydroxyphenylacetic acid
DRN	Dorsal Raphe
DVC	Dorsal vagal complex
e.g.	<i>exempli gratia</i> (example given)
eNM	Extraneuronal NM
EtOH	Ethanol
FA	Formic acid
FC	Frontal cortex
FDR	False Discovery Rate
GBA	β -glucocerebrosidase
GFAP	Glial fibrillary acidic protein
GO	Gene-Ontology
GSEA	Gene set enrichment analysis
GWAS	Genome-wide association studies
h	hours
H&E	Hematoxylin and eosin
H ₂ O	Water
HCl	Hydrochloric acid
HIP	Hippocampus
Hyp	Hypothalamus
i.e.	<i>id est</i> (that is)
Iba1	Ionized calcium binding adaptor molecule 1
ICAM1	Intercellular Adhesion Molecule 1
IF	Immunofluorescence

IHC	Immunohistochemistry
ILBD	Incidental Lewy Body disease
IS	Internal standard
LB	Lewy bodies
LC	Locus Coeruleus
LCM	Laser capture microdissection
L-DOPA	Levodopa
LFA-1	Lymphocyte function-associated antigen 1
LOD	Limit of detection
LOQ	Limit of quantitation
LRRK2	Leucine-rich repeat kinase 2
M	Molar
m	Months
MAOB	Monoamine oxidase type B
MB	Marinesco bodies
MDS	Movement Disorders Society
MHC	Major histocompatibility complex
mM	Millimolar
MPP+	1-methyl-4-phenylpyridinium
MPTP	1-methyl-4-phenyl-1,2,3,6-tetrahydropyridine
NA	Noradrenergic or noradrenaline
NAT	Noradrenaline transporter
NBM	Nucleus basalis of Meynert
NDS	Normal donkey Serum
Ng	Nanograms
NGS	Normal Goat Serum
NM	Neuromelanin
NM-MRI	NM-sensitive Magnetic Resonance Imaging
NTS	Nucleus of the solitary tract
OB	Olfactory Bulb
°C	Degree Celsius
OD	Optical densitometry
Paraquat	(N,N'-dimethyl-4-4'-bypiridinium)
PB	Pale body

ProtB	Protein-bound
PBS	Phosphate buffered saline
PCA	Principal Component Analysis
PD	Parkinson's disease
PET	Positron emission tomography
PFC	Prefrontal cortex
pg	Picograms
PINK1	PTEN induced kinase 1
PNMT	Phenylethanolamine N-Methyltransferase
PPN	Pedunculopontine nucleus
qPCR	Real-Time quantitative PCR
RBD	REM sleep behavior disorders
REM	Rapid eye movement
RIN	RNA integrity number
RN	Raphe nuclei
RNA	Ribonucleic acid
RNAseq	RNA sequencing
ROS	Reactive oxygen species
RRF	Retrorubral field
RT	Room temperature
s	Seconds
SD	Standard deviation
SNpc	Substantia Nigra pars compacta
snRNAseq	Single-nuclei RNAseq
Str	Striatum
TBS	Tris buffered saline
TFEB	Transcription factor EB
Tg	Transgenic
TH	Tyrosine hydroxylase
Thal	Thalamus
Thy-1	Thymocyte differentiation antigen 1
TPH	Tryptophan hydroxylase
Trp	Tryptophan
TYR	Tyrosinase

Tyrp1	Tyrosinase-related protein 1
TYRP2	Tyrosinase-related protein-2
UAB	Universitat Autònoma de Barcelona
Ub	Ubiquitin
US-FDA	United States Food and Drug Administration
VHIR	Vall d'Hebron Research Institute
VMA	Vanillylmandelic acid
VMAT2	Vesicular monoamine transporter 2
VTA	Ventral tegmental area
λ	Wavelength
λ_{em}	Emission wavelength
λ_{ex}	Excitation wavelength

ABSTRACT

ABSTRACT

Parkinson's disease is characterized by a preferential degeneration of neuromelanin-containing neurons, especially neurons from substantia nigra and locus coeruleus. Here, we generated a new neuromelanin-producing rodent model based on the tissue-specific constitutive expression of the human tyrosinase under the tyrosine hydroxylase promoter (tgNM). TgNM mouse model mimics the progressive accumulation and cerebral distribution of neuromelanin within the aging human brain (i.e. catecholaminergic groups A1-A14). In parallel to neuromelanin intracellular buildup, tgNM mice exhibited major Parkinson's disease features, including multisystem neurochemical deficits, motor and non-motor behavioral alterations, cytoplasmic inclusions, and degeneration of specific catecholaminergic neuronal groups. Transcriptomic analysis of neuromelanin-laden neurons revealed alterations in Parkinson's disease-related biological pathways that correlate with human Parkinson's disease postmortem studies. Our results show that modelling human neuromelanin accumulation in mice leads to age-dependent catecholaminergic dysfunction and molecular alterations resulting in motor and non-motor deficits relevant to Parkinson's disease and brain aging. Additionally, the transcriptomic profiles identified here may point to new neuromelanin-induced potential therapeutic targets for the treatment of Parkinson's disease and, in a broader sense, brain aging.

INTRODUCTION

INTRODUCTION

1. Parkinson's disease

1.1 Brief history

1.1.1 Early clinical descriptions

Parkinson's disease was first described more than two centuries ago, in 1817, by the British physician James Parkinson in his *Essay on the Shaking Palsy*, where he described the main motor symptoms and their progressive nature (Parkinson, 1817). Fifty years later, in 1872, Charcot thoroughly described the wide spectrum of clinical signs, remarking bradykinesia (slowness of movement) and rigidity as key features of the disease. He decided to use for the first time the eponym Parkinson's disease (PD) to identify the disease refusing the term "paralysis agitans" or "shaking palsy" because he recognized that PD patients were not markedly weak and did not necessarily show tremor (Charcot, 1872; Goetz, 2011; Obeso et al., 2017).

1.1.2 Early neuropathological descriptions

In 1890s, Blocq, Marinesco, and Brissaud first suggested *Substantia Nigra* pars compacta (SNpc) as the main area affected in PD when they noticed restring tremor in a patient with a tuberculoma contralateral to the side of the body affected by PD (Fénelon & Walusinski, 2021). Two decades later, during the 1920s, Trétiakoff first described neuropathological alterations in the SNpc of PD patients. He reported the loss of neuromelanin (NM) containing neurons together with the presence of cytoplasmic inclusions termed Lewy bodies (LB). From that moment onward, these two neuropathological observations were established as neuropathological hallmarks and neuropathological diagnostic criteria of PD (Del Rey et al., 2018).

1.1.3 Early treatments

Shortly after the discovery of decreased dopamine (DA) levels in the striatum of PD patients by Ehringer and Hornykiewicz in 1960 (Ehringer & Hornykiewicz, 1960), levodopa (L-DOPA) was injected intravenously for the first time to PD patients showing antiakinetic effects (Birkmayer & Hornykiewicz, 1962; Goetz, 2011). Then, Cotzias and colleagues reported first large scale trials assessing oral-preparations of L-DOPA, confirming the beneficial effects and demonstrating long-term benefits (Cotzias, Papavasiliou, & Gellene, 1969).

1.2 Epidemiology

In 1855, forty years after James Parkinson first described the condition, approximately 22 people of the 15 million population in England were reported to die of the condition. Currently, PD is the most common neurodegenerative movement disorder and the second most common neurodegenerative disease after Alzheimer's disease, affecting 2–3% of the population ≥ 65 years of age (Poewe et al., 2017). Aging is the main risk factor for developing PD since it is rare before 50 years of age but its incidence increases sharply from the sixth to the ninth decade of life (Poewe et al., 2017).

According to the global burden of neurological disorders study, PD prevalence and disability is increasing faster than for any other neurological disease, surpassing that of Alzheimer's disease (Feigin et al., 2019). In 2019, the global prevalence of PD reached 8,5 million individuals, increasing 155.50% from 1990 to 2019. Prevalence of PD was higher among men and was clearly associated with age, showing the highest prevalence number in individuals aged over 65 years (Ou et al., 2021).

Not only the prevalence, which might be associated with increasing survival of PD individuals, but also the incidence is increasing. Globally, the incident number of PD was 1.08 million people in 2019, which increased 159.73% since 1990, increasing an average of 0.61% from 1990 to 2019. Incidence showed higher increase rates in men and in the age-group of over 80 years (Ou et al., 2021). It is unclear if these differences in the incidence rate might be confounded by possible changes in diagnostic patterns. A study correcting for these differences showed no incidence rate changes in the UK from 2006-2016 (Okunoye, Marston, Walters, & Schrag, 2022).

Considering that prevalence and incidence are highly associated with increasing age and world's population is aging, it is estimated that by 2040, the number of people with PD will exceed 12 million (Dorsey & Bloem, 2018). Several studies are now identifying this rapid increase in PD as a pandemic-like episode that should be addressed accordingly (i.e. prevention of risks, expert health care, research funding, access to therapies) (Barker, 2020; Dorsey & Bloem, 2018; Dorsey, Sherer, Okun, & Bloem, 2018).

1.3 Neuropathological hallmarks

Current major neuropathological hallmarks of PD are neuronal loss of pigmented neurons in the SNpc with the consequent depletion of DA in the striatum, together with widespread intracellular α -synuclein accumulation in the form of LB, as noted by Trétiakoff in 1920s. When these two features are presented together, they are pathognomonic for a definitive postmortem diagnosis of idiopathic PD (Poewe et al., 2017). Besides SNpc neuronal death, other neuronal groups are reported to be affected in PD (Giguère, Nanni, & Trudeau, 2018). Additionally, neuroinflammatory reaction concomitant with cell death has been consistently reported in PD postmortem brains (Grottemeyer, McFleder, Wu, Wischhusen, & Ip, 2022). All these neuropathological hallmarks will be further discussed in the next sections.

1.3.1 Selective neurodegeneration

Studies evaluating cell death in PD postmortem brains have elucidated that cell death in PD is not restricted to SNpc nor to dopaminergic (DA) neurons but is much more extended than classically thought. A recent comprehensive review of all the studies analyzing cell death throughout the brain in PD postmortem cases highlighted the importance of cell death in other brain areas (Fig. 1). Many studies analyzing PD postmortem brains have identified neurodegeneration in the locus coeruleus (LC), the dorsal vagal complex (DVC), the nucleus basalis of Meynert (NBM), the pedunculopontine nucleus (PPN), the ventral tegmental area (VTA), the raphe nuclei (RN), the thalamus (Thal) and hypothalamus (Hyp) (Giguère et al., 2018). The percentages of cell death found by manual, computer-assisted and stereological counting in these areas were in decreasing order as follows (mean % cell loss \pm SD): SN 69 \pm 9.3, LC:67 \pm 10, DVC:60 \pm 19, NBM:56 \pm 17, PPN:50 \pm 10, VTA:49 \pm 15, RN: 49 \pm 31, Thal:27 \pm 31, Hyp:19 \pm 21 (Fig. 1). Interestingly, there are studies that report increased DA cells in the olfactory bulb (OB) (mean % cell loss \pm SD): OB:164 \pm 72.

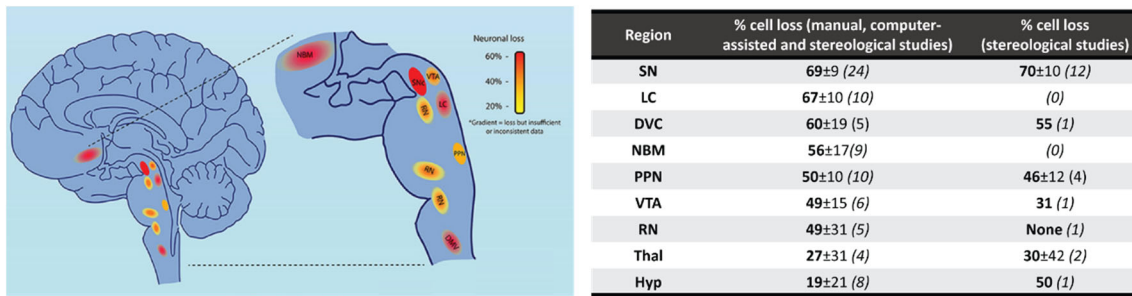


Figure 1. Cellular vulnerability in PD. Left, Schematic representation of brain regions demonstrating cell loss in Parkinson's disease. Color represents evidence of cell loss. Red = 60%, orange = 40%, and yellow = 20%. Color gradients indicate uncertainty in the extent of this cell loss. Right, Percentage of cell loss reported in manual, computer-assisted and stereological studies assessing neurodegeneration in PD postmortem brains. The number of studies considered is stated in parentheses. Adapted from (Giguère et al., 2018).

Neurodegeneration in these multiple areas leads to the consequent perturbation of multiple neurotransmitter systems in PD brains. Neurodegeneration of DA-producing neurons in SNpc and associated DA denervation of the striatum not only leads to the classical motor symptoms of PD but it is also associated to non-motor symptoms (e.g. anxiety, depression, sensory perception) (Schapira, Chaudhuri, & Jenner, 2017). Additionally, cell loss in other cell types may contribute to the spectrum of non-motor symptoms of the disease: cell loss of noradrenergic (NA) LC and the consequent depletion of NA innervation in targeted projections has been linked to alterations in attention, mood, sleep, and memory (Delaville, de Deurwaerdère, & Benazzouz, 2011; Espay, Lewitt, & Kaufmann, 2014); cell loss in cholinergic cells of the NBM has been linked to cognitive impairments independent of nigrostriatal terminal losses (Bohnen et al., 2022); structural changes in the medulla oblongata of PD patients have been linked to autonomic alterations, in particular cardiovascular and respiratory (Pyatigorskaya et al., 2016). Overall, the detection of neurodegeneration in different anatomical structures involving various neurotransmitter systems defines PD as a multisystem disorder (Klingelhofer & Reichmann, 2017).

1.3.2 Lewy pathology

Besides neuronal loss, the other characteristic hallmark of the disease, is the widespread presence of cytoplasmic inclusions, named LBs. Classical brainstem LBs are spherical cytoplasmic neuronal inclusions with a hyaline eosinophilic core and a peripheral halo typically identified by immunoreactivity for α -synuclein and p62 in the halo and ubiquitin

(Ub) in the core. Recent studies indicated the additional presence of Parkin, components of the Ub-proteasome system, molecular chaperones, crowded organelles and lipid membranes in LBs (Choong & Mochizuki, 2022). Another type of inclusion, considered precursors of LBs, are Pale bodies (PB). These are characterized by rounded granular, pale-staining eosinophilic material displacing NM in brainstem neurons (Choong & Mochizuki, 2022). Kuusisto, et al. performed a careful examination of the different steps in LB formation using postmortem SN tissue of PD cases and suggested that LBs first appear as α -synuclein-positive punctate structures in perikaryal areas of sparse NM that after incorporation of p62 and Ub yield PB structures. PBs gradually displace NM adopting different irregular morphologies before their final compactation into the classical LBs (Kuusisto, Parkkinen, & Alafuzoff, 2003b).

In 1997, the identification of the genetic link of α -synuclein with PD and the identification of α -synuclein as one of the principal components of LBs (Polymeropoulos et al., 1997; Spillantini et al., 1997) meant a far-reaching revolution for PD research. In 2003, Braak and colleagues analyzed alpha-synuclein staining in a large number of autopsy PD cases confirming LB pathology in many brain areas and suggested that their topographical location was indicative of an ascending caudo-rostral course of LB pathology (H. Braak et al., 2003). In the proposed scheme, LB pathology started in the OB and DVC (Stage 1), followed by LC (Stage 2) and SNpc (Stage 3) affection and finally reaching cortical areas (Stage 4-6) (Fig. 2). Later studies reported some degree of Braak stereotypic staging applicability in the majority of PD cases but not all (~7% of cases with typical clinical features of PD showed no DVC pathology) (K. A. Jellinger, 2003b; Kalaitzakis, Graeber, Gentleman, & Pearce, 2008) and less applicability in other synucleopathies (67% for incidental LBs; 86% for progressive supranuclear palsy with LBs; 86% for pure LB disease; and 84% for LB disease with Alzheimer's; and only 6% for Alzheimer's disease with amygdala predominant LBs) (Dickson, Uchikado, Fujishiro, & Tsuboi, 2010; K. A. Jellinger, 2003b).

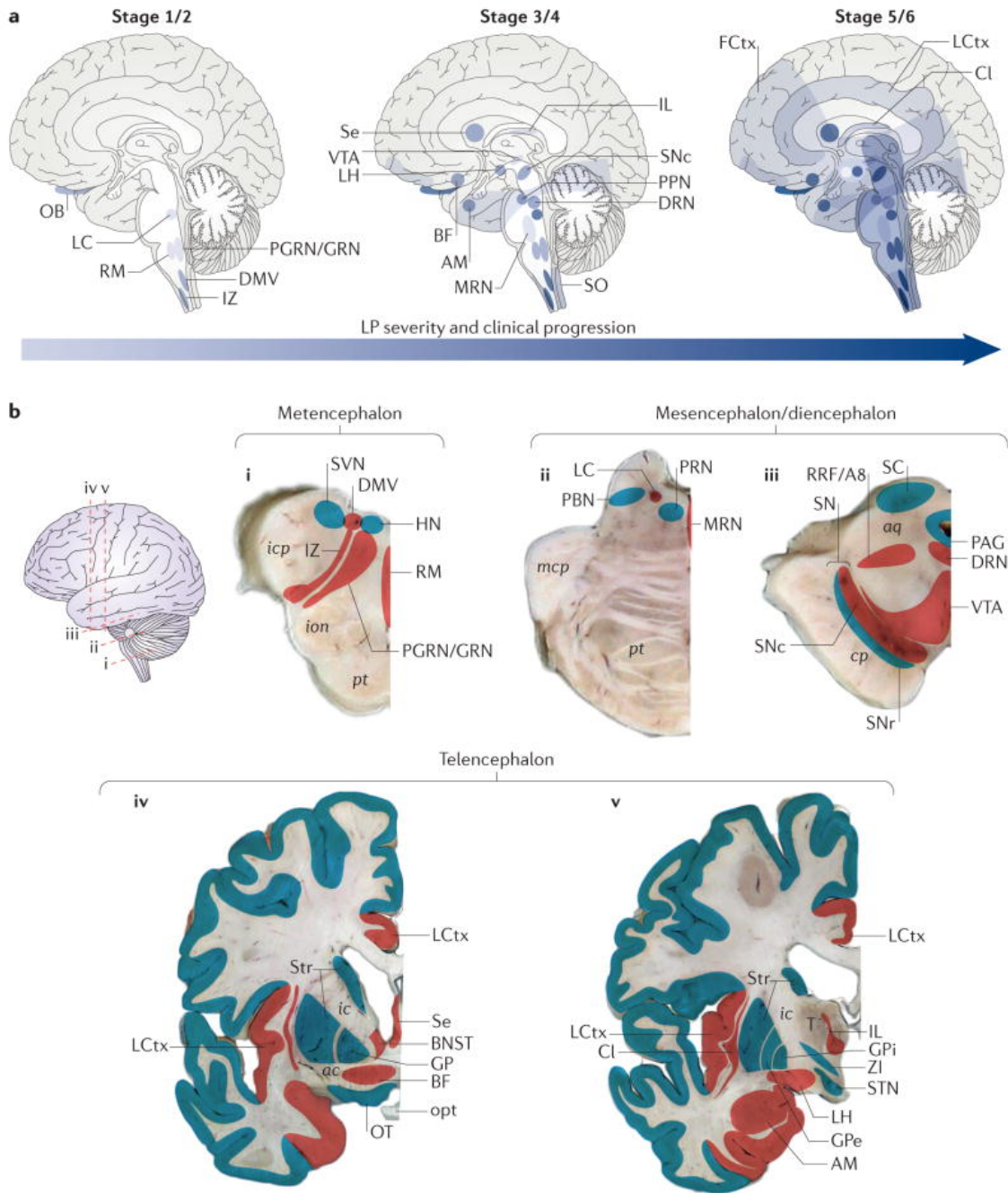


Figure 2. Staging of Lewy pathology in clinical PD. **a)** Schematic representation of the spread of Lewy pathology (LP) within different brain structures, based on the stages proposed by Braak (H. Braak et al., 2003). The anatomical progression of disease through the brain increases over time (from left to right), and the darker the color the more LP is present in each region at a given stage. **b)** A lateral external surface of a representative brain identifies the levels of each cross-sectional brain slice (in the figure, i–v). Regions (which are not to scale) that contain LP at any stage are represented in red, whereas those that only rarely show LP, or that only show mild LP, are indicated in blue. ac, anterior commissure; aq, aqueduct; AM, amygdala; BF, magnocellular nuclei of the basal forebrain; BNST, bed nucleus of the stria terminalis; Cl, claustrum; cp, cerebral peduncle; DMV, dorsal motor nucleus of the vagus; DRN, dorsal raphe nucleus; FCtx, frontal cortex; GP, globus pallidus; GPe, GP externa; GPi, GP interna; HN, hypoglossal nucleus; ic,

internal capsule; icp, inferior cerebellar peduncle; IL, intralaminar nuclei of the thalamus; ion, inferior olivary nucleus; IZ, intermediate reticular zone; LC, locus coeruleus and subcoeruleus; LCtx, limbic cortex; LH, lateral hypothalamus; mcp, middle cerebellar peduncle; MRN, median raphe nucleus; OB, olfactory bulb; opt, optic tract; OT, olfactory tubercle; PAG, periaqueductal grey; PBN, parabrachial nucleus; PGRN/GRN, paragigantocellular and gigantocellular reticular nucleus; PPN, pedunculopontine nucleus; PRN, pontine reticular nucleus; pt, pyramidal tract; RM, raphe magnus; RRF/A8, retrorubral fields/A8 dopaminergic cell group; SC, superior colliculus; Se, septum; SNc, substantia nigra pars compacta; SNr, substantia nigra pars reticulata; SO, solitary tract nuclei; STN, subthalamic nucleus; Str, striatum; SVN, spinal vestibular nucleus; T, thalamus; VTA, ventral tegmental area; ZI, zona incerta. From (D. James Surmeier, Obeso, & Halliday, 2017).

The pathophysiological significance of LBs remains uncertain. LB pathology does not correlate with PD clinical severity, being present in clinically healthy subjects (incidental LB disease) (up to Braak stages 4-6) (Burke, Dauer, & Vonsattel, 2008; K. A. Jellinger, 2003b; Parkkinen, Kauppinen, Pirttilä, Autere, & Alafuzoff, 2005) and does not strictly correlate with cell loss patterns (Parkkinen et al., 2011; D. James Surmeier et al., 2017). Also, some genetic forms of PD cases (LRRK2-PD or Parkin-PD) do not show consistent LB pathology (Schneider & Alcalay, 2017). So, although clearly related to PD pathology, the relationship between abnormal α -synuclein deposition and PD etiopathology remains to be clarified.

Another common type of inclusion found in PD pigmented neurons from SNpc and LC are marinesco bodies (MB), which unlike LBs, are localized inside the cellular nucleus. Their frequency increases with age and is high in Alzheimer's disease, dementia with LBs, and other neurodegenerative disorders (Beach et al., 2004; Yuen & Baxter, 1963). In the elderly brain, MB frequency inversely correlates with striatal concentrations of the DA neuron markers [DA transporter (DAT) and DA synthesizing enzyme tyrosine hydroxylase (TH)] (Beach et al., 2004). A recent study analyzing 131 autopsied cases revealed that MB were less common in PD brains than in controls, and that MB frequency in PD correlated with disease duration and SNpc cell death (Abbott et al., 2017). However, no clear pathological association has ever been established.

1.3.3 Neuroinflammation

A broad spectrum of neurodegenerative diseases are associated with chronic inflammation, including PD. A large body of evidence supports increases in immune cell markers in PD postmortem brains, including: (i) increases in microglia, either as major

histocompatibility complex (MHC)II-positive cells (Croisier, Moran, Dexter, Pearce, & Graeber, 2005; P. L. McGeer, Itagaki, Boyes, & McGeer, 1988; Orr, Rowe, Mizuno, Mori, & Halliday, 2005), as Cd68-positive cells (Croisier et al., 2005) or as CR3/43-positive cells (Banati, Daniel, & Blunt, 1998; Mirza, Hadberg, Thomsen, & Moos, 1999); (ii) inconsistent increases in astrocytes, either as GFAP-positive cells (Banati et al., 1998; Damier, Hirsch, Zhang, Agid, & Javoy-Agid, 1993; Mirza et al., 1999) or as ICAM-1-positive cells (Miklossy et al., 2006); (iii) increases in peripheral monocytes/macrophages as CD163-positive cells (Pey, Pearce, Kalaitzakis, Griffin, & Gentleman, 2014); (iv) increases in leukocytes as LFA-1-positive cells (Miklossy et al., 2006), and (v) increases in T CD8 and CD4 lymphocytes (Brochard et al., 2009; Galiano-Landeira, Torra, Vila, & Bové, 2020).

Classically, neuroinflammation was viewed as a mere consequence of neuronal cell death. Nowadays, the exact role of neuroinflammation in the etiology of PD is still a matter of debate. Some studies performing positron emission tomography with a radiotracer specific for activated microglia report an early microglial activation in midbrain of early-stage drug-naïve PD patients and patients with idiopathic rapid eye movement (REM) sleep behavior disorder (RBD, considered a prodromal form of PD) (Ouchi et al., 2005; Stokholm et al., 2017). Additionally, this microglial activation showed a positive correlation with disease severity and an inverse correlation with levels of the DAT ligand (i.e. a marker of DA terminals) in the striatum (Ouchi et al., 2005). Also, CD8-positive T lymphocyte infiltration in SNpc has been reported in early stages of synucleinopathy before the onset of neuronal death, correlating with cell death in later synucleinopathy stages (Galiano-Landeira et al., 2020). Also, supporting a direct involvement of neuroinflammation in the pathological process, serum levels of immune markers, genetic alterations in immune regulators and use of immune-modifying drugs, modify the risk for developing PD (E. C. Hirsch & Hunot, 2009). These findings suggest that the neuroinflammatory reaction might be participating in the onset of neurodegeneration, leading to a vicious cycle of neuronal death causing chronification of neuroinflammation in later stages.

1.4 Determinants of neuronal vulnerability

Identifying determinants of selective vulnerability to cell death in PD represents an opportunity to understand the etiology of its pathogenesis, and has therefore been

extensively studied. There are some important characteristics shared by neuronal populations that are at risk in PD.

1.4.1 Neuronal pigmentation

Since the early description of NM-containing neurons being lost in the SNpc of PD patients in 1919, NM has long been suspected to play a role in PD selective vulnerability. The presence of NM as a basic characteristic of this group of vulnerable cells, the loss of which leads to the typical motor symptoms and represents the cardinal pathologic diagnostic criteria, suggests that NM may be acting as a vulnerability factor for these cells (Fedorow et al., 2005). The numerous evidences that point to a role of this pigment in PD cell specific vulnerability will be addressed further in this introduction (Section 3. NM relation to PD pathogenesis).

1.4.2 DA toxicity

DA toxicity has been suggested to act as a vulnerability factor for SNpc cells. The neurotransmitter DA is highly reactive and gets easily oxidized in the cytoplasm when not encapsulated in synaptic vesicles, generating toxic quinones. These quinones increase oxidative stress and have been shown to react with numerous proteins (e.g. mitochondrial protein complexes, TH, DAT, α -synuclein) (Giguère et al., 2018). However, this hypothesis is challenged by the fact that DA cell loss is not aggravated by increases in DA levels with L-DOPA treatment and that it does not explain non-DA cell neurodegeneration. So even if DA toxicity might participate in pathogenesis, it is certainly not the sole factor driving neuronal death in PD.

1.4.3 Iron load

Iron is the most abundant transition metal in the brain, participating in numerous essential cellular processes, such as neurotransmitter synthesis, myelination of neurons, and mitochondrial function (Hare, Ayton, Bush, & Lei, 2013). When not bound to ferritin, free iron may undergo redox reactions by Fenton Reaction resulting in cytotoxic damage of proteins, DNA or lipids (Götz, Double, Gerlach, Youdim, & Riederer, 2006). Iron has been shown to accumulate in NM granules in SNpc and LC neurons of the aging brain (L. Zecca et al., 1996, 2004) and also in PD postmortem brains (K. Jellinger et al., 1992), exclusively localized in intraneuronal NM granules, while absent in non-melanized SNpc cells. However the relation between iron and cell damage in PD is not clear since iron

increases in PD are only seen in late stages (Sian-Hülsmann, Mandel, Youdim, & Riederer, 2011).

1.4.4 Axonal arborization size and activity

The shape and electrical activity of neurons might also render them especially vulnerable. All the areas reporting consistent cell loss in PD represent the main sites of neurotransmitter synthesis of the different mammalian neuromodulatory systems (i.e. SN and VTA for DA, LC for NA, DVC for NA and adrenergic, NBM and PPN for cholinergic and RN for serotonergic (5HT) system). They represent small pools of neurons located in the brainstem and basal forebrain areas showing widespread ascending projections to broad areas of the brain and/or descending projections to peripheral organs (Avery & Krichmar, 2017). Additionally, it is known that SNpc, LC, RN, PPN, DVC and NBM all have unusually long and highly branched axons that are unmyelinated or thinly myelinated (D. J. Surmeier & Sulzer, 2013), implicating high oxidative stress levels and a high dependency on energy, protein delivery and proteasomal systems (Y. C. Wong et al., 2019). Areas like the SN, VTA, LC, DVC and PPN also share an autonomous pace-maker activity, showing a slow and rhythmic spiking without any excitatory input. This tonic activity implies constant intracellular oscillation in calcium (Ca²⁺) levels which in turn induces mitochondrial oxidative stress (D. James Surmeier et al., 2017). However, these vulnerability factors cannot be modified because all cognitive functions depend on these neuromodulatory systems. Instead, specific molecular factors needed for these vulnerable characteristics, including proper mitochondrial function, antioxidant capacity and proteostasis are being investigated for potential new therapeutic targets.

1.4.5 Bioenergetic failure

All the above-mentioned characteristics impose high levels of oxidative stress (quinone production, free iron, unmyelinated axons) and high demand of energy and substrate production (neurotransmitter release, pace-maker activity) (Fig. 3). These particularities require neurons to have good antioxidant capacity, maintain mitochondrial homeostasis and ensure proper protein quality control. At the same time, these requirements may be easily disturbed by PD known triggerings, like toxic insults or genetic defects. Indeed, several familial PD linked genes participate in mitophagy and mitochondrial antigen presentation pathways (PARK2-Parkin and PARK6- PTEN induced kinase 1, PINK1), oxidative stress response (PARK7-DJ1), or vesicular trafficking (PARK8- Leucine-rich repeat kinase 2, LRRK2) (Giguère et al., 2018). Also, PD-causing toxins (i.e., MPTP,

rotenone, paraquat) are clearly associated with increased oxidative stress and inhibition of mitochondrial complexes (Blesa, Phani, Jackson-Lewis, & Przedborski, 2012). Overall, the general hypothesis of PD-associated vulnerability is associated with the combination of all the aforementioned characteristics.

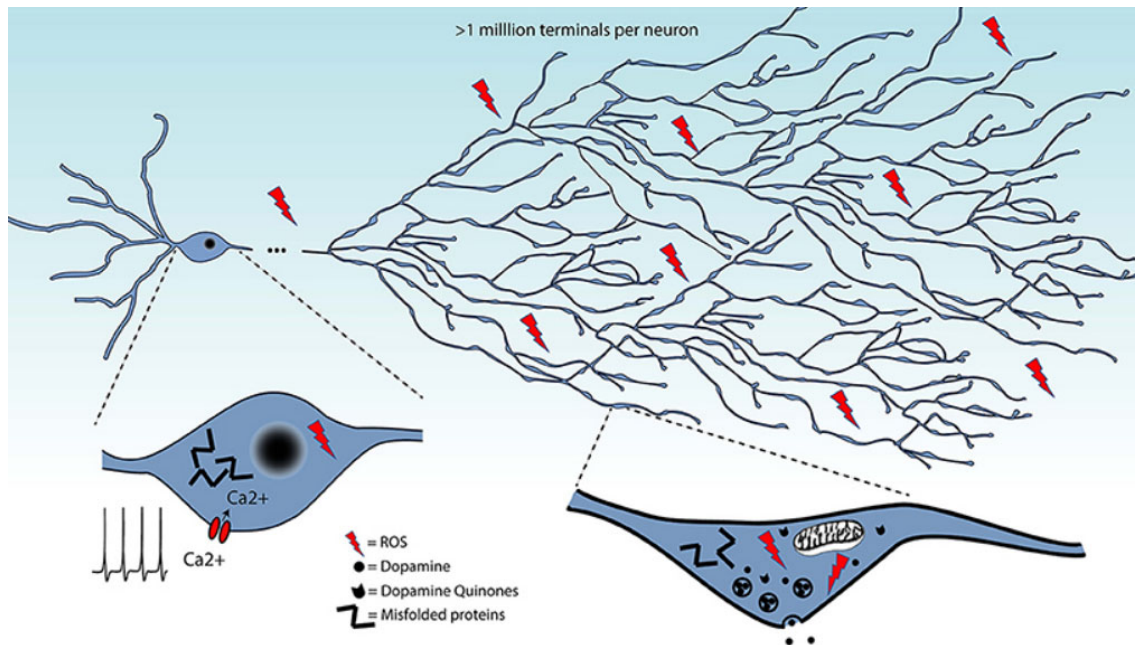


Figure 3. Summary of the converging hypotheses that may explain the origins of the selective vulnerability of neurons in PD. This includes the exceptionally large axonal arbor of PD-affected neurons, their electrophysiological properties including calcium-dependent pacemaking, high levels of oxidant stress, pathological protein aggregation and reactive dopamine quinones. ROS, reactive oxygen species; Ca²⁺, Calcium. From (Giguère et al., 2018)

1.5 Symptomatology

Loss of DA neurons in the SNpc leading to striatal dopamine depletion is the core mechanism underlying the cardinal motor features of PD. The cardinal motor signs that determine a clinical diagnosis of idiopathic PD are resting tremor, bradykinesia, rigidity and loss of postural reflexes. Non-motor symptoms are also present in virtually all PD patients and usually have a greater impact in patients's quality-of-life measures (Chaudhuri, Healy, & Schapira, 2006). Non-motor symptoms might appear before disease diagnosis (e.g. constipation, olfactory deficit, RBD and depression) and continue with advancing age and disease severity (e.g. neuropsychiatric symptoms, sleep disorders, autonomic and gastrointestinal symptoms and sensory alterations) (Chaudhuri et al., 2006). In 2015, the Movement Disorders Society (MDS) re-defined the diagnostic criteria for PD, incorporating some of the non-motor symptoms. Following their guidelines, a PD

diagnosis is determined when parkinsonism is observed (bradykinesia together with tremor and/or rigidity) with additional supportive criteria including the presence of either olfactory loss or cardiac sympathetic denervation (Daniela Berg et al., 2015).

1.6 Disease staging and therapeutic window

PD, as with all neurodegenerative diseases, shows an indefinite start. The slow appearance of symptomatology was already noted by James Parkinson “... *so slight and nearly imperceptible are the first inroads of this malady, and so extremely slow is its progress, that it rarely happens, that the patient can form any recollection of the precise period of its commencement.*”(Gálvez-Jiménez, 2007; Parkinson, 1817). The unclear start of the disease implies early stages during which the disease has started but not progressed to the classically known PD motor symptoms. Indeed, it is estimated that when a clinical PD diagnosis is determined, at least 30% of the pigmented SNpc cells are lost (Burke & O’Malley, 2013). Kordower and colleagues, performed an evaluation of the melanized DA SNpc cells in 28 PD postmortem brains ranging from 1 to 27 years post-diagnosis. This study revealed only a 10% cell death in the one case evaluated 1 year post-diagnosis, and a variable (30-80%) loss during the first years (3-7years) of the disease (Kordower et al., 2013). They also assessed the number of TH-positive neurons and found that at all stages of the disease, loss of melanized neurons was less than the loss of TH-positive neurons. Indeed, pigmented catecholaminergic neurons reduce their capacity to synthesize catecholamines before cell death. This phenomenon is known as TH-downregulation or TH-phenotypic loss and has been consistently reported in the SNpc of PD postmortem brains (Huynh, Fu, Kirik, Shine, & Halliday, 2021). This downregulation of TH expression suggests a state in which cells have lost the DA phenotype but are still potentially capable of being restored by neuroprotective/restorative therapies. In line with this, TH downregulation (NM-positive cells without TH immunoreactivity) can also be observed in the aged brain (in SNpc and LC) (Chu & Kordower, 2007; Manaye, McIntire, Mann, & German, 1995) and in early Braak stages (stages 1 and 2, incidental Lewy body disease, ILBD) (Milber et al., 2012).

Markers that identify subjects at early stages of disease are needed to determine the etiopathogenic mechanisms driving the triggering of the disease to further design disease-modifying therapeutic strategies. Also, it is important to better identify patients at risk to

develop PD for their inclusion in novel neuroprotective trials testing new potential disease-modifying agents. In recent years, there has been increasing efforts to identify risk factors and biomarkers that are associated with a later diagnosis of PD in epidemiological studies. Diagnosis of PD occurs with the onset of motor symptoms (early-stage PD) but is usually preceded by a prodromal phase characterized mainly by non-motor symptoms (prodromal PD) (Fig. 4) (Poewe et al., 2017). Markers of the prodromal phase include sleep alterations, hyposmia, autonomic dysfunction, depression and anxiety, mild motor signs, and altered imaging markers of the DA system and the cardiac sympathetic system (Daniela Berg et al., 2021). RBD is the prodromal symptom with the highest risk of phenoconversion to PD (Bloem, Okun, & Klein, 2021). Multicenter studies have shown that >80% of patients with RBD will develop a synucleinopathy, including PD, DLB or Multiple system atrophy (Daniela Berg et al., 2021).

Recently, the MDS has published an update in the research criteria for prodromal PD, including, in order of likelihood ratios; polysomnography -proven RBD, DA positron emission tomography (PET) clearly abnormal, subthreshold parkinsonism, orthostatic hypotension, olfactory loss, among others (Heinzel et al., 2019). These criteria have to be constantly updated and further validated to understand their specific predictive validity and usefulness in selecting populations for the study of early-PD mechanisms and for their inclusion in disease-prevention trials.

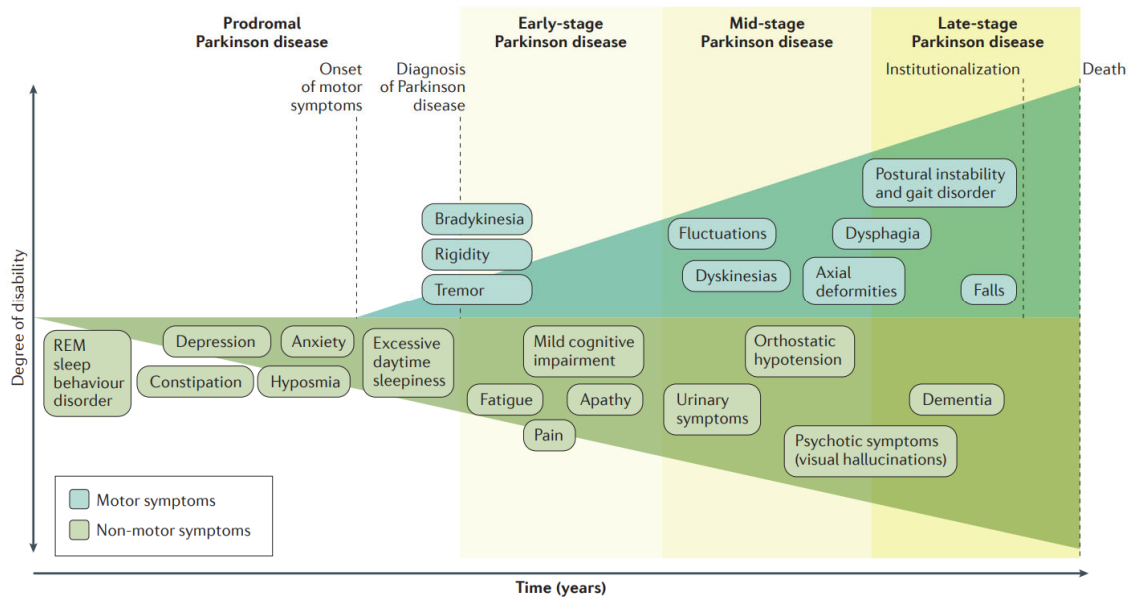


Figure 4. Clinical symptoms associated with PD progression. Schematic representation of the different clinical stages of PD. REM, rapid eye movement. From (Poewe et al., 2017).

1.7 Treatment

Restoring striatal DA levels via systemic administration of the DA precursor L-DOPA has remained the gold standard treatment for PD since its discovery during the 1960s (Poewe et al., 2017). However, this therapy is only capable to transiently restore motor deficits since after 2-5 years of treatment it might induce motor response oscillations and drug-induced dyskinesia in patients (Poewe et al., 2017).

Advances in the understanding of the nigrostriatal pathway have led to the development of new drugs directed to counteract DA depletion, including DA agonists and inhibitors of DA degradation enzymes that enhance the bioavailability of DA. DA agonists are in some cases recommended as monotherapy in *de novo* PD patients to avoid L-DOPA-related motor complications, although they have secondary effects such as compulsive behaviors (Grall-Bronnec et al., 2018). Because of the longer half-life of DA agonists, sometimes these are used in combination with L-DOPA to avoid motor fluctuations (Connolly & Lang, 2014). Motor fluctuations induced by L-DOPA can also be ameliorated by increasing the bioavailability of L-DOPA using degradation enzyme inhibitors like Catechol-O-methyltransferase (COMT) and Monoamine oxidase type B (MAOB) inhibitors (Poewe et al., 2017).

L-DOPA treatment is able to reverse only some non-motor symptoms (Chaudhuri & Schapira, 2009; Del Rey et al., 2018) while the majority persist and even arise as a

consequence of increasing DA transmission (e.g. impulse control disorders) (Del Rey et al., 2018). The persisting non-motor symptoms have to be treated with supplemental drugs. An MDS revision of the studies evaluating clinical efficiency of current drugs in the treatment of non-motor symptoms identified efficacy of: pramipexole (DA agonist) and tricyclic antidepressants (modulating 5HT and NA) for the treatment of depressive symptoms; clozapine (modulating DA and 5HT) for the treatment of psychosis; rivastigmine (cholinesterase inhibitor) for the treatment of dementia; botulinum toxin A and B (BTX-A and BTX-B) (blocking acetylcholine transmission in nerves) for the treatment of sialorrhea; and macrogol (osmotically acting laxative) for the treatment of constipation (Seppi et al., 2011). The efficacy of the different neurotransmitter-targeting drugs strengthen the involvement of multiple neurotransmitter systems in PD.

Finally, and most relevant, L-DOPA is an exclusively symptomatic treatment and does not halt disease progression as it does not stop neuronal loss, subsequently turning PD into a chronic incurable neurodegenerative disease. Bearing in mind all the limitations of the current therapeutic options for PD, it appears necessary to better understand the mechanisms that are driving neurodegeneration in selective neuronal populations to develop new disease-modifying or even restorative treatments.

1.8 Etiology

1.8.1 Genetics

Advances in genetic research methods have provided major insights into genetic contributions to the development of PD. The discovery of a mutation in the α -synuclein gene in families with PD was the first causative PD gene identified (Polymeropoulos et al., 1997). Since then, mutations in 24 more genes have been linked to familial forms of PD (Funayama, Nishioka, Li, & Hattori, 2022) (Table 1). Despite only representing 5-10% of all PD cases, heritable forms of PD provide essential information about pathological mechanisms underlying PD pathology (Poewe et al., 2017). Additionally, genetic contributors to idiopathic PD, accounting for the rest of PD cases, have also been studied with large genome-wide association studies (GWAS). More than 90 single-nucleotide polymorphisms (SNP) that confer increased risk for developing PD have been identified so far (Vázquez-Vélez, Zoghbi, & Duncan, 2021) (Table 2).

PARK loci	Gene	Function
PARK1/4	SNCA	Protein aggregation/prion-like-transmission/synaptic function
PARK2	PARKIN	Mitochondrial maintenance/mitophagy/ubiquitin-proteasome
PARK3	Unknown	Unknown
PARK5	UCH-L1	Ubiquitin hydrolase
PARK6	PINK1	Mitochondrial function/mitophagy
PARK7	DJ-1	Mitochondrial function/cell stress response
PARK8	LRRK2	Protein and membrane trafficking/neurite structure/lysosomal autophagy/synaptic function
PARK9	ATP13A2	Lysosomal autophagy/mitochondrial function
PARK10	Unknown	Unknown
PARK11	GIGYF2	Tyrosine kinase receptor signaling/insulin like growth factor pathway
PARK12	Unknown	Unknown
PARK13	HTRA2	Mitochondrial function
PARK14	PLA2G6	Mitochondrial function
PARK15	FBX07	Mitochondrial maintenance/mitophagy/ubiquitin-proteasome
PARK16	RAB7L1	Protein and membrane trafficking/lysosomal autophagy
PARK17	VPS35	Lysosomal autophagy/endocytosis
PARK18	EIF4G1	Protein translation
PARK19	DNAJC6	Synaptic function/endocytosis
PARK20	SYNJ1	Synaptic function/endocytosis
PARK21	DNAJC13	Membrane trafficking/endocytosis
PARK22	CHCHD2	Mitochondria-mediated apoptosis
PARK23	VPS13C	Mitochondrial maintenance/mitophagy/lipid transport
PARK24	PSAP	Lysosomal autophagy

Table 1. PARK loci and identified genes that segregate with familial forms of PD. Adapted from (Kumaran & Cookson, 2015).

Category	Candidate genes
Cytoskeleton	CAB39L, TUBG2, MAPT, DNAH17, ANK2, PDLIM2, SORBS3
Endosomal and vesicular trafficking	VAMP4, SIPA1L2, SNCA, CHMP2B, LRRK2, BIN3, RIMS1, DDRGK1, SYT4, ATP6V0A1, GBF1, ARHGAP27, SH3GL2
Immune system	FCGR2A, IL1R2, HLA-DRB6, HLA-DQA1, FYN, CD19, CD38, NOD2, TRIM40, FAM49B, ITIH3, ITIH4, TLR9, STAB1
Ion channels, transporters, and neurotransmitter signaling	KCNS3, KCNIP3, TMEM163, SCN3A, CHRN1, CLCN3, GCH1, NCKIPSD, CAMK2D
Lipid metabolism and signaling	SPTSSB, ELOVL7, DGKQ
Lysosome and autophagosome	GBA, CTSB, GALC, KAT8, TMEM175
Mitochondria	SLC41A1, COQ7, VPS13C, BAG3, MCCC1, CRLS1, MICU3
Nucleus and gene regulation	NUCKS1, CCNT2, SATB1, KPNA1, MED12L, LCORL, MBNL2, MEX3C, MIR4697, TOX3, UBTF, LSM7, BRIP1, ASXL3, RP S6KL1, PSMC3IP, SREBF1, RAI1, KANSL1, RNF141, RPS12, CDC71, PHF7, NUPL2, ZNF184
Ubiquitin pathway	UBAP2, BAP1, KLHL7
Miscellaneous	ITPKB, LINC00693, DYRK1A, OGFOD2, FAM171A2, ZNF646, FAM47E, FBRSL1, MIPOL1, SCAF11, PAM, TMEM229B, CR HR1, STH, SPPL2C, DLG2, C5orf24, C8orf58, GS1-124K5-11, ALAS1, NISCH, GPNMB, FAM200B, STK39

Table 2. Genes associated with single nucleotide polymorphisms that modulate PD risk. From (Vázquez-Vélez et al., 2021).

Genetic contribution to familial forms of PD are mainly linked to mitochondrial and autophagy-lysosomal pathways (ALP), highlighting the importance of these processes in PD pathology (Table 1) (Kumaran & Cookson, 2015). Moreover, genetic risk factors associated to the disease have confirmed such pathways might play a role also in idiopathic PD. Indeed, genetic mutations in the lysosomal hydrolase β -glucocerebrosidase (GBA), which is essential for correct lysosomal function, have been

identified as the most common genetic risk factor for PD (Y. C. Wong et al., 2019) and decreased GBA activity has been shown also in idiopathic PD (Gegg et al., 2012). Additionally, genetic PD risk factors associated to the disease have identified other pathways that might be linked to idiopathic PD, including cytoskeleton organization, vesicular trafficking, neurotransmission, lipid metabolism, nucleus and gene regulation, ubiquitin-proteasome system, immune system and others (Table 2) (Vázquez-Vélez et al., 2021).

1.8.2 Non-genetic factors

There are numerous well established non-genetic factors that contribute to an increased risk for developing PD. Aging is the main risk factor since its incidence increases sharply with age (Poewe et al., 2017). PD risk factors include also male sex and geographic location. A meta-analysis evaluating forty-seven epidemiological studies of PD found increased prevalence of PD in men compared to women, but only for individuals aged 50-59 years; and also a decreased prevalence of PD in Asia compared to Europe, North America and Australia in individuals from 70 to 79 years (Pringsheim, Jette, Frolkis, & Steeves, 2014). Specific lifestyles and health-related factors have also been shown to influence PD risk. Smoking, coffee drinking and alcohol consumption have been linked with decreased PD risk (Periñán et al., 2022; Yuan, Tian, Liu, & Zhang, 2022). On the other hand, pesticide exposure (agricultural occupation and well-water drinking), metal exposure, viral infections, gut alterations (e.g. inflammatory bowel disease), dietary product consumption, air pollution and higher education have been linked with higher PD risk (Periñán et al., 2022; Yuan et al., 2022).

1.9 PD experimental models

Animal models of human diseases are crucial to understand the etiopathogenic mechanisms and evolution/stages of diseases. The knowledge gained from modelling diseases in animals remains a fundamental core in today's biomedical research including therapeutic target identification and evaluation of novel therapeutic agents' toxicity/safety, pharmacokinetics, pharmacodynamics and efficacy. Indeed, preclinical drug research in animal models currently remains a mandatory asset for regulatory approval for human studies in United States Food and Drug Administration (US-FDA) guidelines (Singh & Seed, 2021).

Evidences from genetic contributors to familial forms of PD and epidemiological studies linking specific PD risk factors have enabled the generation of numerous PD animal models that have been extensively studied. Additionally, a plethora of human cellular models have also been designed over the last decades. These models are useful for certain applications and patient-specific studies (e.g. patient derived induced pluripotent stem cells). However, they are limited in terms of maturation and complexity, lack of neuronal circuits and absence of vascular and immunologic components (Dawson, Golde, & Lagier-Tourenne, 2018). Considering the scope of this thesis, only animal rodent models of PD will be presented.

Animal rodent models in PD can be categorized in two main groups: neurotoxic and genetic. Neurotoxic models are based on the acute neurodegeneration of the nigrostriatal system concurring with SNpc neuronal death. On the other hand, genetic models show a wide variability of phenotypes, with some failing to reproduce SNpc neurodegeneration but still providing crucial clues in the molecular understanding of PD pathophysiology.

1.9.1 Toxic animal models

MPTP

The neurotoxicity of 1-methyl-4-phenyl-1,2,3,6-tetrahydropyridine (MPTP) was discovered when in early 1980s, several drug users were diagnosed with Parkinsonism after having used the opioid 1-methyl-4-phenyl-4-propionoxypiperidine (MPPP) contaminated with MPTP. MPTP was then used to model PD in animals. Since MPTP is highly lipophilic and easily crosses the blood brain barrier (BBB) is usually administrated systemically. After reaching the brain, MPTP is metabolized by astrocytic MAO-B to MPP⁺, its active metabolite, which can enter neurons via DAT. Once inside neurons, MPP⁺ inhibits the complex I of the mitochondrial electron transport chain consequently increasing reactive oxygen species (ROS) and decreasing energy production. The major advantage of MPTP is its reproducible and PD-like neurotoxic pattern on the nigrostriatal system (i.e. greater loss of DA neurons in SNpc than in VTA or retrorubral field (RRF) and greater degeneration of DA nerve terminals in the putamen than in the caudate nucleus) (Blesa & Przedborski, 2014). One major disadvantage of this model is the rare detection of LB-like inclusions, despite increases of α -synuclein expression levels have been reported in MPTP-treated mice (Vila et al., 2000). Intraneuronal inclusions are only found in MPTP-treated non-human primates (Forno, Langston, DeLanney, Irwin, & Ricaurte, 1986; Kowall et al., 2000).

6-OHDA

The 6-hydroxydopamine (6-OHDA) model was the first model ever used for PD research 50 years ago (Ungerstedt, 1968). Injection of 6-OHDA has to be performed intracerebrally as it does not cross the BBB when injected systemically. Traditionally, 6-OHDA is injected unilaterally so that neurodegeneration is inflicted into one sole hemisphere and motor impairments can be detected by drug-induced rotation tests (Blesa & Przedborski, 2014). As a NA analog, 6-OHDA shows high affinity for DAT and noradrenaline transporter (NAT) enabling entrance inside the cell (Bové, Prou, Perier, & Przedborski, 2005). Once inside neurons, 6-OHDA is highly oxidative and produces its toxic effect by a combination of ROS and quinone production (Bové et al., 2005). Like MPTP, 6-OHDA fails to reproduce LB-like pathology.

Paraquat and rotenone

Paraquat (N,N'-dimethyl-4,4'-bipyridinium) is a widely used herbicide in agriculture that was identified as neurotoxic because of its structural similarity to MPP⁺. When injected systemically, paraquat is able to cross the BBB and is transported into DA neurons via DAT. Once inside neurons, paraquat exerts its toxic effects through mechanisms of oxidative stress (Bastías-Candia, Zolezzi, & Inestrosa, 2019). Rotenone is both an herbicide and an insecticide. It is highly lipophilic and when injected systemically can easily cross the BBB and cellular membranes. In mitochondria, rotenone impairs oxidative phosphorylation by inhibiting complex I (Bové et al., 2005). The characteristic feature of rotenone and paraquat induced models of PD is that, contrarily to 6-OHDA and MPTP models, they succeed in reproducing formation of LB-like structures in DA SNpc neurons (Bové et al., 2005).

The main drawback of toxic models for studying PD etiopathogenic mechanisms is the acute nature of the toxic insult compared to the progressive neurodegenerative nature of the disease. While in toxic models the neurodegeneration is established within days or weeks (when chronic administration is performed), the PD-linked neurodegeneration process in humans spans decades. Although they have been extremely valuable to understand specific SNpc cell death mechanisms and to assay symptomatic therapies for PD motor symptoms, they fail to reproduce the multisystemic nature and more progressive cascade of events happening in PD.

1.9.2 Genetic animal models

Genetic models have been developed with the idea to investigate etiopathogenic mechanisms in familial forms of PD, which might also shed some light on the etiopathogenic mechanisms of idiopathic PD. After the discovery of the distinct PD causative genes, numerous animal models replicating these same genetic alterations have been developed and extensively characterized over the last two decades.

These models show a wide range of cellular and molecular alterations in DA SNpc cells that have contributed to the identification of PD-linked pathological pathways (e.g. α -synuclein proteostasis, mitochondrial function, oxidative stress, calcium homeostasis, axonal transport and neuroinflammation) (Fig. 5) (Poewe et al., 2017). However, most of them fail to reproduce the neurodegeneration of the nigrostriatal system, including (i) transgenic mice modelling point mutations (PARK1/ α -synuclein [A53T, A30P, E46K]) and overexpression of α -synuclein (PARK4/ α -synuclein duplication/triplication), except when using neuronal specific promoters like thymocyte differentiation antigen 1 (Thy-1); (ii) knockout mice modelling loss-of-function mutation in PARK2/Parkin, PARK6/PINK, PARK7/DJ; and (iii) transgenic mice modelling LRRK2 mutations (PARK8/LRRK [G2019S, R1441C/G]) (Blesa & Przedborski, 2014; Konnova & Swanberg, 2018).

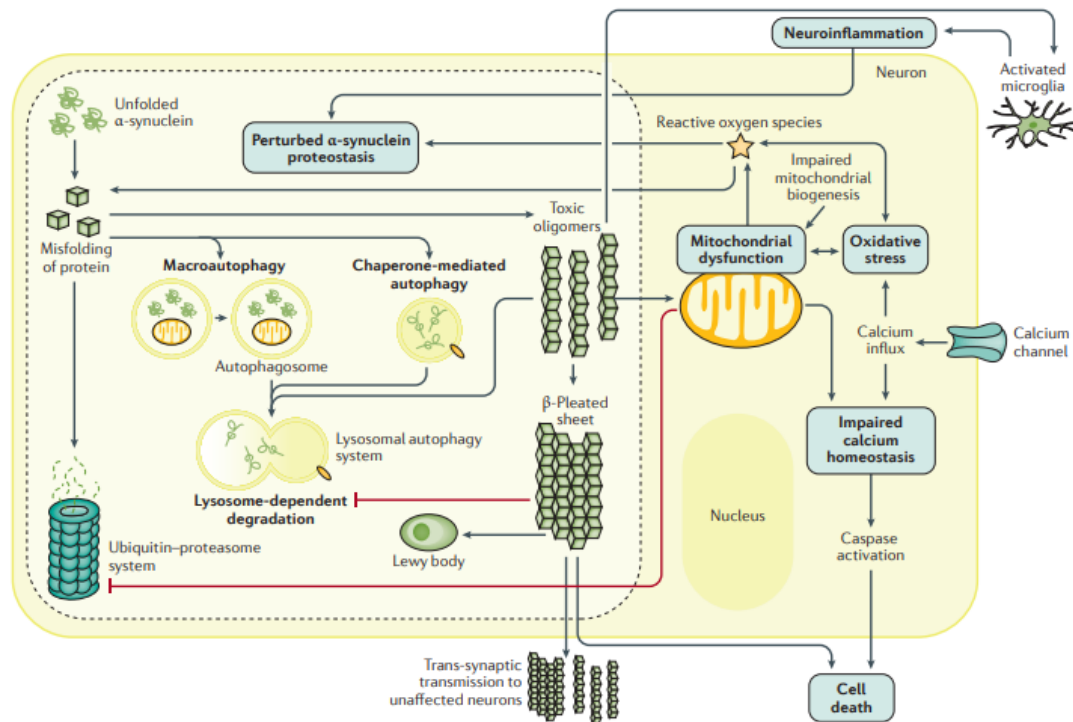


Figure 5. Molecular mechanisms involved in PD. Schematic diagram depicting interactions between major molecular pathways that are implicated in the pathogenesis of Parkinson's disease (Poewe et al., 2017).

Some more aggressive strategies like viral vector overexpression of α -synuclein by stereotaxic injection directly into the SNpc (Decressac, Mattsson, Lundblad, Weikop, & Björklund, 2012; Oliveras-Salva et al., 2013) and the injection of already aggregated forms of α -synuclein (preformed fibrils) (Luk et al., 2012; Paumier et al., 2015), or the combination of both (Thakur et al., 2017), enhance the pathological insult resulting in DA neurodegeneration.

The ultimate goal of an animal model of a disease is to identify, develop and test new therapeutic agents for human diseases. Promising new agents tested in PD toxic or genetic models have failed to demonstrate any efficacy as disease modifying therapies in clinical trials (Dawson et al., 2018; C. W. Olanow, Kiebertz, & Katz, 2017). This failure to translate the findings from preclinical models to humans is in part due to the lack of PD animal models that precisely reflect the multifactorial etiology and the multisystem pathophysiology of the disease and its chronic and progressive nature (C. Warren Olanow, Kiebertz, & Schapira, 2008).

2. Neuromelanin

2.1 Brief history

The SN was first described by Félix Vicq d'Azyr, with remarkable illustrations in 1786. Vicq d'Azyr noted the dark pigmented nature of this structure that he aptly called *tache noirâtre* or *locus niger crurum cerebri*. This was one century before Blocq and Marinesco alluded to a possible link between this structure and PD (Parent & Parent, 2010). In 1939, Adler, first reported pigmentation in the brain of other animals and in humans, being “*sharply localized in three centers, the substantia nigra, locus coeruleus, and the dorsal vagus nucleus*”. During the beginning of the 1960s, the pigment was named NM because its resemblance to peripheral melanins (Fedorow et al., 2005; Lillie, 1957). Then, an extensive study published in 1968 by Fenichel and Bazelon analyzing 44 brains from the 34th gestational week to 16 years of age, reported an age-dependent increase in the NM content in SN, LC and DVC (Fenichel & Bazelon, 1968). Pigmentation was later described to be present in other parts of the human brain in detailed atlases that proposed a correspondence between catecholaminergic cell groups and pigmentation (Bogerts, 1981; C. Saper & Petit, 1982).

2.2 Species distribution

NM pigment has been found not only in the human brain but also, at moderate levels, in non-human primates and other animals like dolphins, whales, horses, sheep, dogs, cats, giraffes and even frogs (Itzev, Ovtscharoff, Marani, & Usunoff, 2002; Sacchini et al., 2018, 2022; Sukhorukova, Alekseeva, & Korzhevsky, 2014). However, the great abundance of NM in the brainstem is unique to humans, as macroscopic dark pigmentation of main pigmented areas is not observed in other animal species (Marsden, 1961; Scherer, 1939). On the contrary, the absence of NM accumulation has been consistently reported in rodents (Itzev et al., 2002). This is highly relevant for the study of NM since the most commonly used animal models in experimental research lack this pigment. For these reasons, its implications in health and disease conditions have not been properly studied in *in vivo* models yet.

2.3 Synthesis of melanin and neuromelanin

Currently, the mechanism leading to NM synthesis in the brain is still a matter of debate. However, synthesis of peripheral melanins is well-established and can thus shed light to potential NM synthesis pathways. In the skin, two distinct types of melanins are produced

and both types of pigment derive from the common precursor dopaquinone which is formed *via* the oxidation of tyrosine by the melanogenic enzyme tyrosinase (TYR) (Ito & Wakamatsu, 2008) (Fig. 6a). Dopaquinone is highly reactive and in the absence of sulfur groups (cysteine) undergoes autooxidation to dopachrome. Dopachrome then gradually and spontaneously rearranges to form 5,6-dihydroxyindole (DHI) and to a lesser extent 5,6-dihydroxyindole-2-carboxylic acid (DHICA), the ratio of which is determined by dopachrome tautomerase (Dct), also known as tyrosinase-related protein-2 (TYRP2) (Ito & Wakamatsu, 2008). In mice, another tyrosinase-related protein (tyrosinase-related protein-1, Tyrp1) can oxidize DHICA, although in humans TYR participates in this step (Ito & Wakamatsu, 2008). Oxidation and subsequent polymerization of these dihydroxyindoles leads to the production of eumelanin. Alternatively, when cysteine is present, dopaquinone reacts with cysteine or cysteinyl groups and forms cysteinylquinones which eventually lead to the production of pheomelanin. Thus, TYR enzyme represents the rate-limiting enzyme for both types of melanins since it participates in the generation of the common precursor dopaquinone, while the other melanogenic enzymes (Tyrp1 and TYRP2) only participate in the formation of eumelanin.

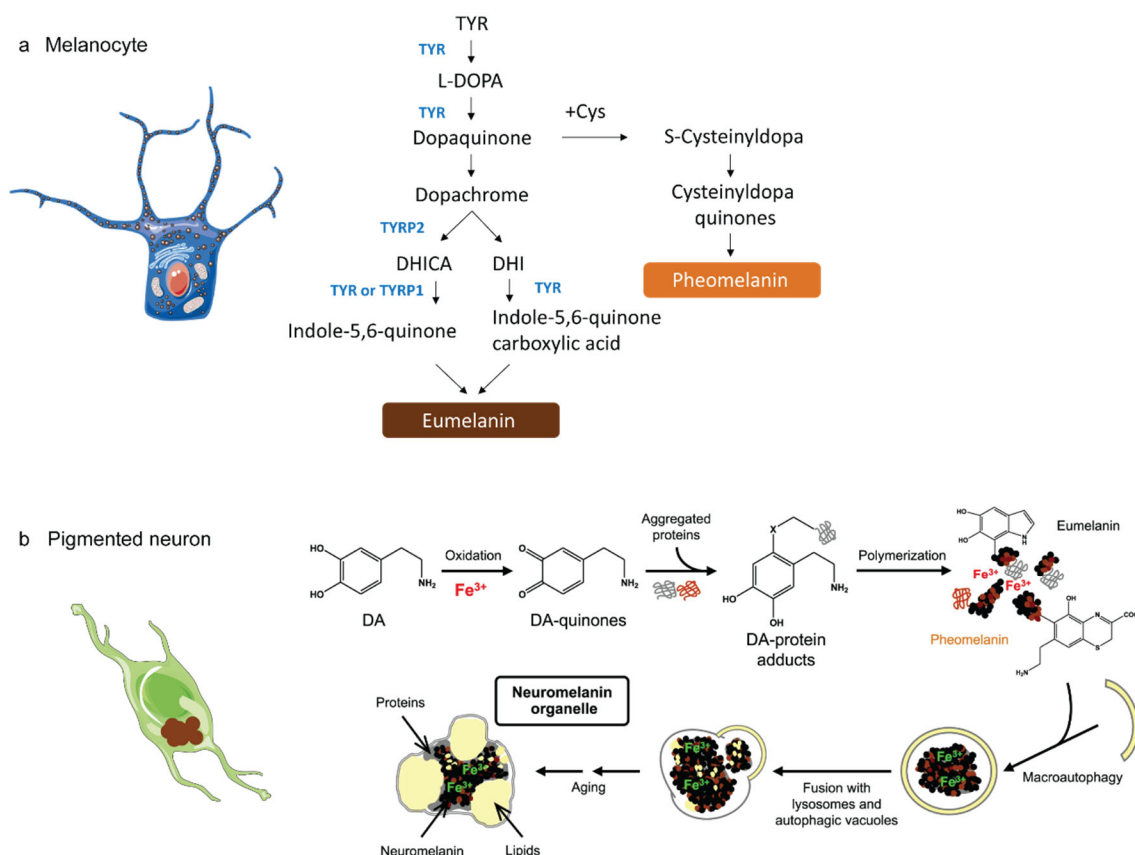


Figure 6. Peripheral melanin synthesis pathway and proposed mechanism for NM organelles formation. a) Peripheral melanin synthesis biochemical pathway: tyrosinase (TYR) is the rate-limiting enzyme catalyzing three different reactions along the pathway. Modified from (Ito & Wakamatsu, 2008; X. T. Zhang et al., 2018). b) Proposed mechanisms for biosynthesis of NM pigment and for the formation of NM-containing organelles in human SN. Excess dopamine in the cytosol of SN neurons can be oxidized to quinones by ferric iron. These highly reactive compounds can bind to aggregated and β -structured proteins that accumulate in the cytosol. An oxidative polymerization initiates formation of the melanin-protein component with eumelanin and pheomelanin moieties. Via macroautophagy, the resulting undegradable material is taken into autophagic vacuoles that fuse with lysosomes and other autophagic vacuoles containing lipid and protein components, thus forming the final NM-containing organelles. Based on (David Sulzer et al., 2018).

It has long been debated whether NM synthesis is enzymatically controlled as peripheral melanin synthesis or whether it arises as a simple autooxidation byproduct of catecholamine metabolism. Sulzer and colleagues (D. Sulzer et al., 2000) tried to address this issue and reported that NM formation *in vitro* was driven by excess cytosolic catecholamines not accumulated by synaptic vesicles. They showed that L-DOPA addition into cultures was able to induce formation and accumulation of NM granules which were reduced by the overexpression of vesicular monoamine transporter 2

(VMAT2) (increasing DA uptake by synaptic vesicles) and by an iron chelator. Thus, both levels of free cytosolic DA and iron stimulate NM formation. Also, albino individuals (which in some cases, but not all (Fernández et al., 2021), is associated with a loss of TYR activity) show the presence of NM in SNpc (Foley & Banter, 1958). Thus, the possibility of inducing NM by increasing cytosolic DA, together with the lack of strong evidences for an enzymatic activity linked to NM production in the brain have led to the widely accepted hypothesis of DA autoxidation as the NM synthesis mechanism (Fig. 6b).

On the contrary, the restriction of NM production to most but not all catecholaminergic neurons in the human brain and the lack of this pigment in most animal species, despite the presence of DA in these animals, suggest that the formation of NM is unlikely to result simply as a consequence of DA autoxidation. In addition, PD patients treated with large quantities of L-DOPA do not exhibit increased NM levels within their surviving SN neurons, as it might be expected if NM represents a mere process of autoxidized DA (David M.A. Mann & Yates, 1983; David Sulzer & Surmeier, 2013). Similarly, rats chronically treated with L-DOPA do not produce NM despite exhibiting increased intracellular levels of DA (Murer et al., 1998). Also, the specific pattern of age-dependent NM accumulation in humans is suggestive of an enzymatic synthesis of this pigment (Fedorow et al., 2006). Finally, synthetic NM formed via DA autoxidation alone differs from the complex ultrastructure of NM granules naturally present in the human brain (Double et al., 2000). In this line, one possible candidate enzyme for NM synthesis is TYR, the rate-limiting enzyme in peripheral melanogenesis. Indeed, TYR-like activity and expression (mRNA levels and promoter activity) have been reported in the human and mouse brain, including the SNpc (Greggio et al., 2005; Miranda, Botti, Bonfigli, Ventura, & Arcadi, 1984; Tief, Schmidt, & Beermann, 1998; Xu et al., 1997). However, TYR protein levels in the human brain have only been described in one study by immunoprecipitation with TYR antibodies (Greggio et al., 2005), while most studies using immunohistochemistry, western blot or mass spectrometry show no evidence of TYR protein in the human brain (Ikemoto et al., 1998; Plum et al., 2016; Tribl, Arzberger, Riederer, & Gerlach, 2007). Another piece of evidence pointing to Tyr activity in the brain of *in vivo* models comes from studies showing that Tyr possesses catecholamine-synthesizing activity in the absence of TH (Rios et al., 1999) and that Tyr null mice show aggravated methamphetamine-induced DA neurotoxicity (Miyazaki et al., 2006).

Importantly, a genetic association between rare variants of TYR and PD has been reported (Lubbe et al., 2016), suggesting at least some role of TYR in PD pathophysiology. Other enzymes than TYR might also be involved in NM synthesis, but so far, a neuron-specific enzymatic pathway has not been unequivocally demonstrated (Zucca et al., 2014).

2.4 Structure

Similar to peripheral melanin, NM has also been described to contain both eumelanin and pheomelanin (Odh et al., 1994), specifically NM granules have been proposed to be organized as a dense pheomelanin core surrounded by eumelanin (Bush et al., 2006). Indeed NM and peripheral melanins share some important general histochemical and spectroscopic properties (e.g. electron paramagnetic resonance spectra, ultraviolet spectra, reduction of silver salts, basophilia) while differing in some specific properties (e.g. reacting to specific stains) (Usunoff, Itzev, Ovtscharoff, & Marani, 2002). In addition to the melanic pigment, NM granules are heterogeneous organelles that contain other cellular components like different lipids (18 %) and peptides (12–15 %) (Zucca et al., 2014). Electron microscopy studies analyzing NM granules in the human brain have consistently reported the presence of lipid droplets intermingled with the NM pigment and that these heterogeneous organelles are entrapped within single- or double-membranes (D. Sulzer et al., 2000, 2008; Zucca et al., 2018). During autophagy, structures targeted for degradation are sequestered into large double-membrane vesicles called autophagosomes that are later fused with lysosomes for content degradation (Mari, Tooze, & Reggiori, 2011). So the observation of double-membrane limited NM organelles together with the identification of many lysosomal proteins within these organelles suggests that NM might represent pigmented autophagic vacuoles (Zucca et al., 2018). These observations suggest a possible scenario in which NM granules together with other aggregated or misfolded proteins are engulfed by the phagophore resulting in autolysosomes containing undegradable material (Zucca et al., 2018) (Fig. 6b).

2.5 Function

The functional significance of NM remains speculative. Until recently, NM was considered merely as a waste product of cellular metabolism that was devoid of any physiological function. More recently, it has been speculated that NM may possess a dual role; protective and/or toxic depending mostly on the cellular context (Zucca et al., 2014). It has been proposed that the NM synthesis *per se* prevents the accumulation of toxic catechol derivatives by their incorporation into the polymer (L. Zecca, Zucca, Wilms, &

Sulzer, 2003). Under normal physiological conditions NM might serve as an antioxidant since it is able to bind ions such as metals (e.g. iron, zinc, copper) and toxic compounds (e.g. MPTP, paraquat). On the other hand, NM could also have a direct pro-oxidant effect when intracellular iron levels exceed the NM-binding capacity, leading to the release of redox active iron (Zucca et al., 2014). Additionally, although the formation of autophagic vacuoles trapping NM via macroautophagy could be initially protecting the neuron from cellular stress, the continuous accumulation of pigmented autophagic vacuoles may eventually interfere with normal degradative pathways and endocytic/secretory tasks, such as appropriate response to growth factors (D. Sulzer et al., 2000, 2008), and result in detrimental effects in neuron survival. Finally, when released in the extracellular space, NM triggers microglia activation and could become an agent of chronic inflammation slowly releasing metals and toxic compounds trapped in its structure (Zucca et al., 2014). After all, one hypothesis could be that the age-dependent accumulation of intracellular NM, until occupying most of the neuronal cytoplasm, could lead to cellular dysfunction followed by cell death and subsequent release of NM in the extracellular space, resulting in a self-perpetuating cycle of neuroinflammation and neurodegeneration.

2.6 Brain-wide topographical distribution

NM distribution in the human brain follows a similar pattern as the catecholaminergic neuronal groups A1-A14 defined in the brains of other animal species (Björklund & Dunnett, 2007; Matsushita et al., 2002; C. Saper & Petit, 1982) (Fig. 7). Catecholaminergic neurons of the OB and the retina correspond to groups A16 and A17, respectively (Sukhorukova et al., 2014) and to date have not been reported to contain any pigmentation in the human brain.

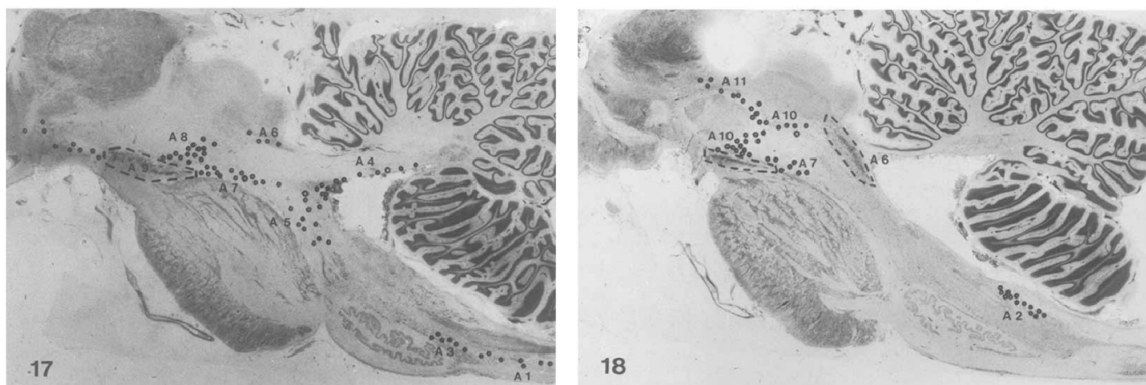


Figure 7. NM distribution in human brain catecholaminergic groups. Sagittal sections at a magnification of three, showing the distribution of melanin schematically. From (Bogerts, 1981).

Medulla. In the medulla, pigmented cells can be divided into two groups, situated in the dorsal (A2) and the ventral medulla (A1). A1 group is found primarily along the dorsal aspect of the lateral reticular nucleus and the nucleus ambiguus complex. A2 group is found in the DVC, intermingled with neurons from dorsal motor nucleus of the vagus nerve (DMNV) and nucleus of the solitary tract (NTS) reaching into the area postrema (Bogerts, 1981; Halliday et al., 1988; C. Saper & Petito, 1982).

Pons. The most densely packed accumulation at the pontine level is located within the LC (A6). A7 represents a separate compact group of pigmented neurons situated ventrally to A6. Other groups in the pons include A4, situated in the roof of the fourth ventricle, along the middle cerebellar peduncle and A5, scattered cells localized along the ventrolateral reticular formation from the medulla up into the pons being more concentrated at the level of superior olivary nucleus (Bogerts, 1981; C. Saper & Petito, 1982).

Midbrain. The main accumulation of melanized cells is found in the SNpc (A9). The second one corresponds to VTA (A10) and the third one corresponds to RRF (A8) (Bogerts, 1981; C. Saper & Petito, 1982).

Diencephalon. Melanin pigment in the diencephalon of the human brain is controversial. Catecholaminergic groups consist in a group of cells lining the wall of the third ventricle in the hypothalamus, posterior hypothalamus (A11), dorsal to arcuate nucleus (A12-A13) and medial to periventricular nucleus of the hypothalamus (A14). Some studies identify pigmented cells in these groups (Sanghera, Zamora, & German, 1995; Usunoff et al., 2002), while others report that NM in these cell groups is not visible in unstained sections (Bogerts, 1981) but otherwise detectable with NM-specific stains like Fontana-Masson or the Schmorl method (C. Saper & Petito, 1982; Spencer et al., 1985).

3. NM relation to PD pathogenesis

3.1 NM distribution and levels in relation to PD cell death

3.1.1 NM distribution

The most pigmented catecholaminergic areas in the human brain are the two most vulnerable brain areas in PD (Zucca et al., 2014): DA neurons in SNpc/A9 and VTA/A10 (*black substance*) and NA neurons in LC/A6 (*blue spot*) (Mai & Paxinos, 2012; Poe et al., 2020) (Sukhorukova et al., 2014; David Sulzer & Surmeier, 2013; Zucca et al., 2014) (Fig. 8a-b). Studies analyzing cell death in the SNpc of PD brains are numerous and show consistent neurodegeneration (Giguère et al., 2018) (Fig. 1). Although not evaluated by stereological methods, PD postmortem studies analyzing cell death in LC also show consistent neurodegeneration ranging from “some” to 94% (Giguère et al., 2018) (Fig. 1). As expected by the great loss of pigmented cells, the macroscopic pigmentation of these areas in PD patients is greatly reduced (Sasaki et al., 2006) (Fig. 8b). Compared with other catecholamine cell groups, neurons in the human SNpc and LC consistently contain considerable amounts of NM (SNpc: 84%, LC: 83% pigmented neurons from the total population) (Usunoff et al., 2002) (Fig. 8c). Studies analyzing the VTA, the DA region adjacent to SNpc, report that this area contains less pigmented cells than SNpc (VTA:51%) as well as less degree and consistency of neurodegeneration in PD postmortem studies, although less studies have evaluated cell death in this area (Giguère et al., 2018) (Fig.1).

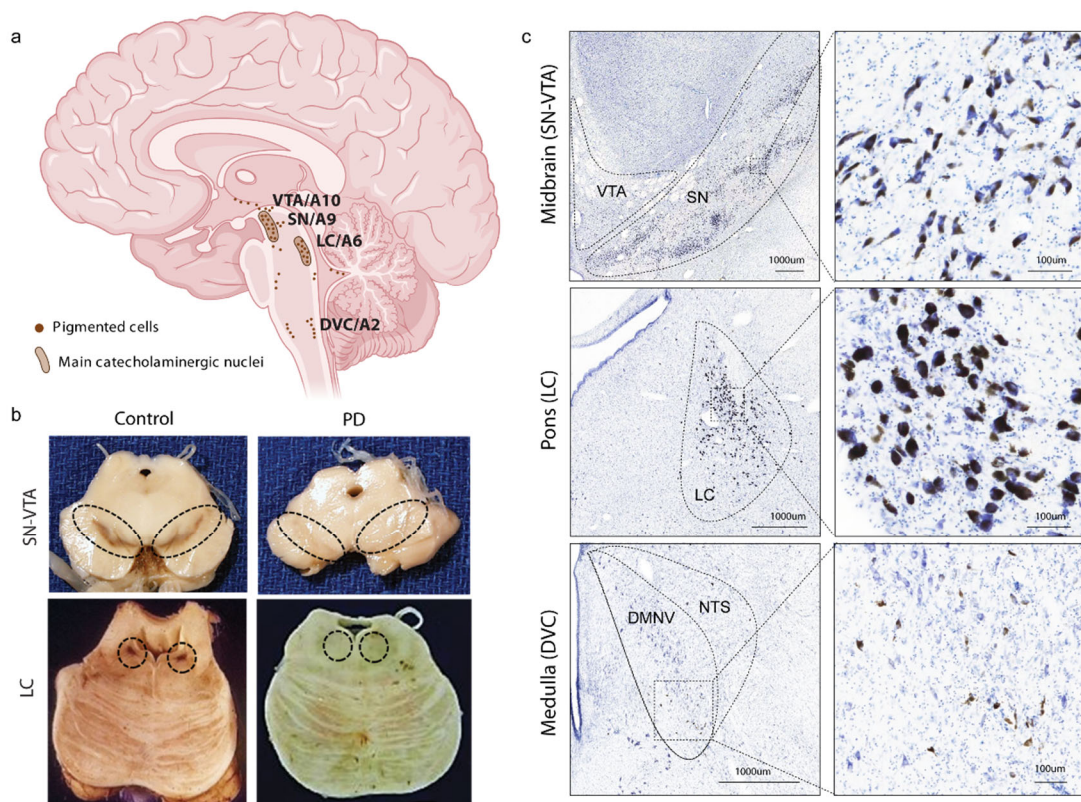


Figure 8. Distribution of pigmentation in the human brain. a) Distribution of NM-containing cells in the human brain based on (Bogerts, 1981). **b)** Macroscopic loss of pigmented areas in PD compared to control postmortem brains. **c)** Microscopic pigmentation in control brains in SN and VTA (midbrain), LC (pons) and DVC (medulla oblongata). Melanin is visualized as a brown-black pigment in Nissl stained sections. From Nissl Human atlas presented in (Ding et al., 2016) http://www.brainspan.org/ish/experiment/dual_view?id=100149965&imageId=102339919&imageType=nissl&initImage=nissl&z=2

The third area affected in PD in terms of consistency and degree of cell loss (~60%) is the DVC (Giguère et al., 2018). This area encompasses different nuclei: (i) the NTS, a viscerosensory nucleus integrating information from the gut, heart and lungs, (ii) the DMNV, containing cholinergic visceral motor neurons, and (iii) the area postrema, a circumventricular organ in the fourth ventricle (Binder, Hirokawa, & Windhorst, 2008). The pigmented A2 catecholaminergic neuronal group intermingles with the NTS and the DMNV cholinergic cells (Fig. 7c), being some of them double immunopositive for TH and choline acetyltransferase (ChAT). Altogether, the DVC represents the major integrative center for the autonomic nervous system. In the A2 group, unlike midbrain and pontine areas, only 15-65% from all catecholaminergic cells are pigmented (Halliday et al., 1988). Usually the cell loss reported in this area is interpreted as a loss of cholinergic cells in the DMNV (Giguère et al., 2018), yet a lot of studies evaluating cell loss in

medullary nuclei use catecholaminergic specific markers, such as TH, the adrenergic synthesizing enzyme Phenylethanolamine N-Methyltransferase (PNMT) and/or pigmentation (Table 3). Some of them show evidence of pigmented cell loss in both the dorsal and the ventral medulla and others show loss of Nissl-stained motoneurons in the DMNV (Benarroch, Schmeichel, Sandroni, Low, & Parisi, 2006; Eadie, 1963; Gai, Blumbergs, Geffen, & Blessing, 1992; Gai, Geffen, Denoroy, & Blessing, 1993; Halliday et al., 1990; Rajput & Rozdilsky, 1976; C. B. Saper, Sorrentino, German, & Lacalle, 1991). Thus, the exact population at risk in medullary nuclei is still not well characterized and more studies are needed to clarify the specific PD-vulnerable cell type in this area.

Study	Disease	% cell loss (marker used)
Eadie, et al. 1963	Typical paralysis agitans	Dorsal: 30%(Nissl), no change (Pigment)
Rajput, et al. 1976	iPD	Dorsal: Some (Pigment)
Halliday, et al. 1990	iPD	Medulla: 41% (PNMT), no change (TH), 70% (NPY) Dorsal: 70% (SP) Ventral: 85% (SP)
Saper, et al. 1991	PD, MSA, Postencephalitic parkinsonism	Dorsal: 19% (TH), 19% (Pigment)
Gai, et al. 1992	iPD	Dorsal: 45% (Nissl)
Gai, et al. 1993	iPD	Dorsal: 21% (Pigment), no change (PNMT) Ventral: 50% (Pigment), 53% (PNMT)
Benarroch, et al. 2006	MSA, LBD	Dorsal: MSA 60% (ChAT), LBD 51% (ChAT)

Table 3. Degree of PD cell loss in specific medullary nuclei. The percentage of cell loss compared to controls is shown. Cell loss is reported in dorsomedial (Dorsal) and ventrolateral (Ventral) medulla in human PD or related disorders. iPD, idiopathic PD; MSA, Multiple system atrophy; LBD, Lewy body disease; PNMT, Phenylethanolamine N-Methyltransferase; ChAT, Choline acetyltransferase; SP, substance P; NPY, Neuropeptide Y.

Finally, there are numerous non-catecholaminergic, non-pigmented regions that show degeneration in PD postmortem studies. However, their cell loss is not as consistent as the most pigmented areas (some studies reporting no cell death) (i.e. Hypothalamus, RN, Thalamus, Cortex) (Giguère et al., 2018) and sometimes considered to be a consequence of cell death in pigmented areas, like the case of cholinergic neurons from PPN (Bensaid, Michel, Clark, Hirsch, & François, 2016) and NBM (Szego et al., 2011), in which *in vivo* experimental studies showed loss of neurons resulting from a previously induced SNpc lesion.

3.1.2 NM levels

Several findings in relation to the amount of NM in midbrain DA cells support the role of pigmentation in PD cellular differential vulnerability. First, in 1983, Mann and Yates reported a 15% decrease in the NM content of surviving pigmented cells of the SNpc in PD patients, suggesting a preferential loss of neurons that contain the greatest amount of melanin pigment (Mann and Yates, 1983). Second, in 1988, Hirsch and colleagues reported a positive correlation between the percentage of NM-pigmented neurons normally present in the main catecholaminergic nuclei in the midbrain in healthy controls (52% in A8, 51% in A10 and 84% in A9) and the cell loss found in the same nuclei in PD cases (43% in A8, 48% in A10 and 77% in A9) (E. Hirsch, Graybiel, & Agid, 1988). Additionally, they noted that within these groups there is a greater relative sparing of non-pigmented neurons than of pigmented neurons. Third, in 1992, Kastner and colleagues, showed an inverse correlation between intracellular NM levels and the percentage of surviving neurons in PD cases compared to controls, suggesting that the vulnerability of the DA neurons is related to their NM content (Kastner et al., 1992). Finally, in 2005, Halliday reported a decrease in the levels of NM per cell in DA neurons from SNpc, but only in late stages of degeneration (with a concurrent presence of LB pathology), while adjacent vulnerable (but yet morphologically intact) DA neurons exhibited significantly increased NM levels (Halliday et al., 2005). In line with this, our group has recently reported increased levels of intracellular NM in PD and ILBD patients (Carballo-Carbajal et al., 2019). These observations indicate that increased intracellular levels of NM may precede neuronal loss, and thus could predispose these neurons to degeneration in PD. Overall, the number of pigmented cells and the intracellular NM amounts in PD-vulnerable neurons correlates with neuronal dysfunction and/or neurodegeneration in PD cases, suggesting a role of this vulnerability factor in the pathophysiology of the disease.

3.2 NM in relation to PD hallmarks

3.2.1 Aging

Considering that aging is the main risk factor for PD, another evidence that suggests a potential role of NM in PD pathogenesis is the age-dependent and progressive accumulation of this pigment in PD-vulnerable neuronal populations.

Macroscopic pigmentation detected by NM-sensitive Magnetic Resonance Imaging (NM-MRI) increases gradually with age in SN (Xing, Sapuan, Dineen, & Auer, 2018)

and LC (Shibata et al., 2006) of control healthy human brains, reaching a plateau phase at middle age (40 to 59 years for the LC, 45 and 53 years for the SN) after which it starts decreasing gradually. Intracellular NM content in SNpc becomes evident at approximately 3 years of age and accumulates progressively with age until occupying most of the neuronal cytoplasm in aged individuals (Fedorow et al., 2006; D.M.A. Mann & Yates, 1974; Luigi Zecca et al., 2002) (Fig. 9a). This is explained by the apparent inability of neurons to degrade or eliminate this insoluble pigment, either by the resistance of the pigments to lysosomal degradation and/or by inadequate fusion of the NM-containing vacuoles with lysosomes (D. Sulzer et al., 2008). Studies evaluating NM content in other catecholaminergic pigmented areas like LC and DVC show that pigmentation can consistently be detected at 3 years of age in the LC and at 6 years of age in the DVC and that they increase gradually with age (Fenichel & Bazelon, 1968; Manaye et al., 1995). Interestingly, LC intracellular NM content is higher than that of SNpc in the first decades of life, while after middle life SNpc NM levels exceed those in the LC (D. M.A. Mann & Yates, 1979; D.M.A. Mann & Yates, 1974; L. Zecca et al., 2004) (Fig.9b).

The hypothesis that progressive accumulation of NM is a vulnerability factor increasing with age and predisposing to the manifestation of PD is consistent with the fact that neuronal loss in most pigmented areas, like SNpc and LC, can be observed as well in elder individuals without PD (about 10% per decade) (Cabello, Thune, Pakkenberg, & Pakkenberg, 2002; German et al., 1988; Ma, Røyttä, Collan, & Rinne, 1999; Manaye et al., 1995; Patrick L. McGeer, McGeer, & Suzuki, 1977; Rudow et al., 2008; S.Y. Ma et al., 1999; Vijayashankar & Brody, 1979) (Fig. 9c). This cell death seems specific to these neuronal groups since cellular counts of non-pigmented brain regions from elder subjects do not show the consistency seen in pigmented ones (no loss or incomplete) (e.g. superior temporal sulcus, hippocampus) (Gómez-Isla et al., 1997; Morrison & Hof, 1997; West, Coleman, Flood, & Troncoso, 1994). Additionally, extracellular NM, indicative of its release from dying neurons, is commonly seen in the aged compared with the young adult brain, in association with sustained microglial activation (Beach et al., 2007; Korzhhevskii et al., 2021). These evidences point to a possible impact of NM accumulation also in normal brain aging, thus reinforcing the idea that NM accumulation could be acting as a vulnerability factor, establishing a certain threshold of accumulation above which PD would develop (Fig. 9d).

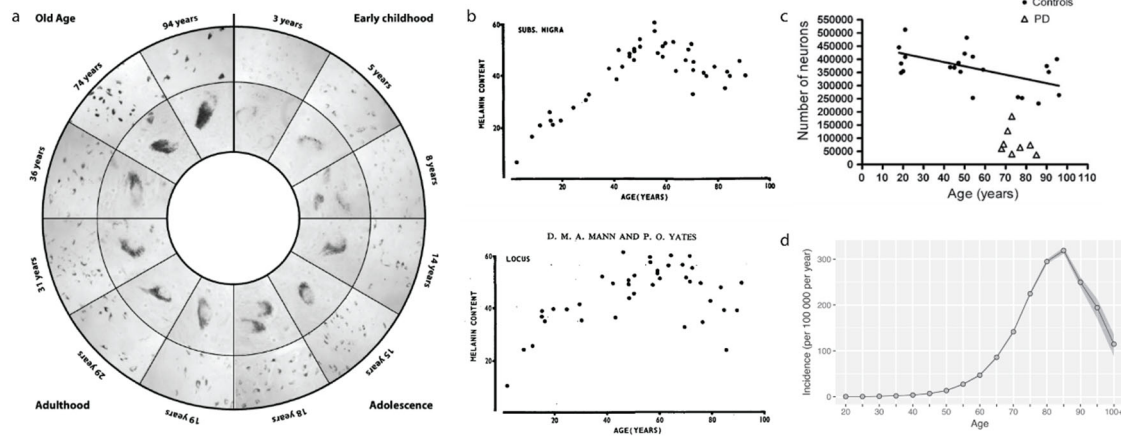


Figure 9. Age-dependent PD incidence and NM accumulation. a) Intermediate and high magnification photomicrographs of representative unstained NM-pigmented neurons from the ventral region of the human SN at various ages (Halliday et al., 2006). **b)** NM content (absorption of the Prussian blue-melanin complex of the Schmorl reaction) in SN (upper panel) and LC (lower panel) in healthy subjects at different ages (D.M.A. Mann & Yates, 1974). **c)** Decrease in the number of SN pigmented neurons throughout life in healthy controls (black circles) and PD cases (white triangles) (Rudow et al., 2008). **d)** Age-dependent increase in PD incidence (Myall et al., 2017).

3.2.2 Lewy pathology

Further indicating a link between NM and PD pathology, LB formation seems to be clearly related to pigmentation. Classical brainstem LBs (i.e., eosinophilic cytoplasmic inclusions with a dense core surrounded by a pale halo of radiating fibrils in hematoxylin and eosin (H&E) staining) are present in pigmented neurons and confined to the inside portion of the pigment accumulation (E. Braak et al., 2001; K. A. Jellinger, 2003a; Kuusisto et al., 2003b) (Fig. 10). On the other hand, cortical LBs appear in irregular shapes (i.e., rounded, angular, or reniform structures) without an obvious halo, and cannot be easily distinguished by classical H&E staining (E. J. Chung et al., 2022; McKeith et al., 2005). Also, α -synuclein is a major protein component of NM granules extracted from PD patients' brains but not control brains (Fasano, Giraudo, Cocha, Bergamasco, & Lopiano, 2003).

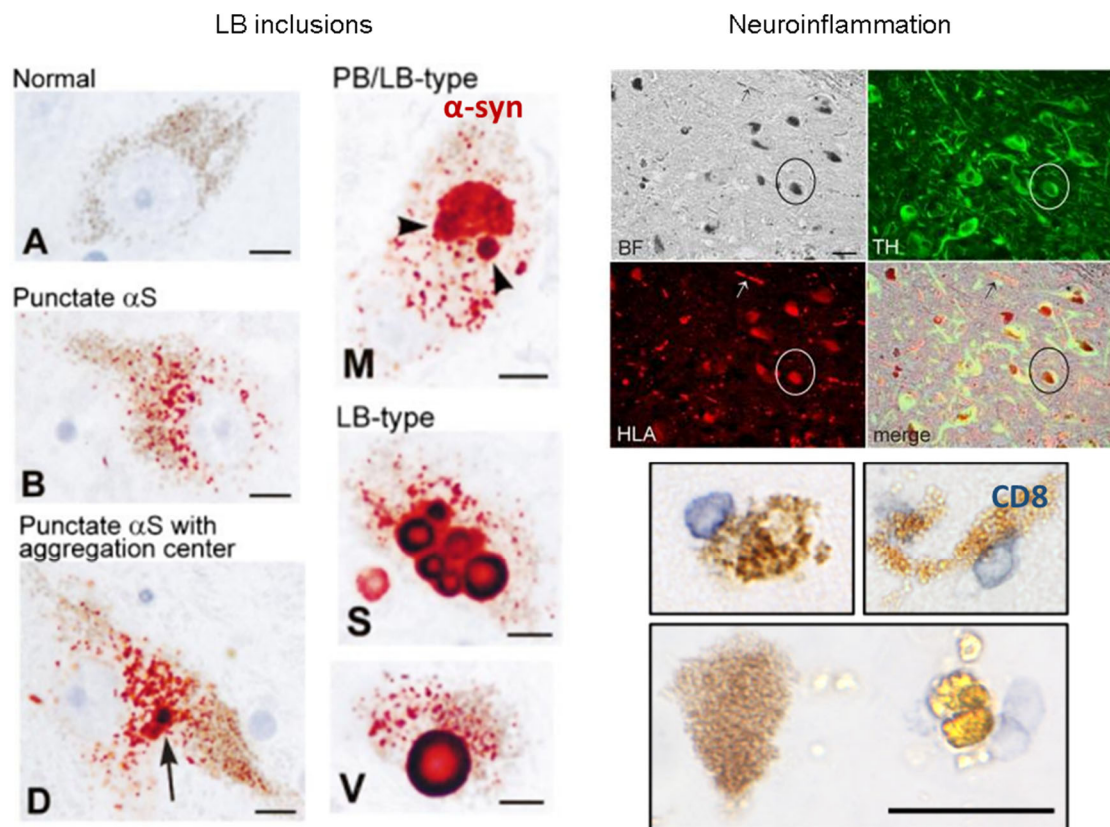


Figure 10. NM in relation to PD neuropathological hallmarks. *LB inclusions.* Morphological spectrum of nigral α -synuclein accumulations in NM-accumulating neurons in cases with abundant PBs and LBs, as visualized by immunodetection using α -synuclein antibody (orange-red to black). The sections were counterstained with hematoxylin to reveal nuclei (light blue). Abbreviations: α S, α -synuclein; LB, Lewy body; PB, pale body; Ub, ubiquitin. From (Kuusisto, Parkkinen, & Alafuzoff, 2003a). *Neuroinflammation.* *Upper panel,* Brightfield and immunofluorescence images of human postmortem SN stained for HLA A, B, and C (red) and TH (green). NM was identified under brightfield illumination. Encircled neurons demonstrate that TH⁺ neurons display HLA immunolabel, overlapping in particular with NM. *Lower panel,* Photomicrographs showing CD8 T cells in close contact with DA neurons. Neurons in contact with one to three T cells are shown (Galiano-Landeira et al., 2020).

3.2.3 Neuroinflammation

There are numerous evidences as well of a NM role in PD-linked neuroinflammation processes. First, microgliosis, astrogliosis and lymphocyte infiltration in PD postmortem brains are highly localized within NM-containing regions (SNpc, LC and some in DVC) and particularly concentrated in areas with high NM-containing cells and extraneuronal NM (eNM) (E. C. Hirsch & Hunot, 2009; Miklossy et al., 2006; Pey et al., 2014). Second, expression of MHC I, needed for antigen presentation, has been reported only in pigmented neurons and colocalizing with NM granules from SN and LC, while absent in other regions (hippocampus with adjacent entorhinal cortex). These findings suggest that

NM could be acting as a possible antigen and that pigmented neurons might thus be more vulnerable to a potential T-cell mediated cytotoxic attack (Cebrián et al., 2014) (Fig. 10). Indeed, close physical contacts of CD8-positive T cells with NM-containing neurons and eNM have been reported (Galiano-Landeira et al., 2020) (Fig. 10). Third, eNM released from dying neurons is surrounded by or contained within microglial cells in aged controls and PD cases (Beach et al., 2007; Langston et al., 1999; P. L. McGeer et al., 1988), correlates with microglial cells in aged human SN (Beach et al., 2007), and it has been described to induce a pro-inflammatory microglial phenotype in *in vitro* and *in vivo* studies (Wilms et al., 2003; L. Zecca et al., 2008; W. Zhang et al., 2011). Finally, anti-NM antibodies were found increased in a study with PD patients' sera (Double et al., 2009).

3.2.4 Generation of the first *in vivo* NM-producing rodent model

Considering all the data reported, there seems to be a link, whether as a vulnerability factor or as a triggering event, between NM and PD pathophysiology. However, NM has long been omitted in PD animal research because species commonly used in experimental laboratory studies, like mice and rats, lack this pigment (Bnirrr & Rullrrin, 1983; Sukhorukova et al., 2014). Thus, in order to be able to assess a potential involvement of NM in PD pathogenesis, an adequate experimental *in vivo* model that recapitulates the progressive age-dependent NM production and accumulation seen in humans should be used in experimental research.

In a previous study from our group, we tested the hypothesis that NM could be synthesized enzymatically by the rate-limiting melanogenic enzyme TYR in the SNpc of rats, which normally do not accumulate NM (Carballo-Carbajal et al., 2019). An adeno-associated viral vector (AAV)-driven overexpression of human TYR was achieved by unilateral stereotaxic injection into the rat SNpc (Fig. 11a). This experiment showed that overexpression of TYR in SNpc DA neurons is sufficient to produce macroscopically visible NM (Fig. 11b) with authentic human-like properties based on evidences from magnetic resonance, electron microscopy and histological studies (Fig. 11c). Moreover, quantifications of intracellular NM levels showed an age-dependent accumulation up to levels reached in elderly humans (Fig. 11d). In this rat model, progressive intracellular NM accumulation ultimately compromised neuronal function and triggered age-dependent pathological PD features, including impaired DA release, nigrostriatal neurodegeneration, motor alterations and intracellular inclusion body formation (Fig.

11e-g). Interestingly, the formation of cytoplasmic inclusions was also detected in the absence of α -synuclein (i.e. α -synuclein knockout mice), suggesting that this process was independent of α -synuclein and occurred as a consequence of NM accumulation. Further proving a link between NM accumulation and cell dysfunction/neurodegeneration, reducing levels of intracellular NM by overexpression of the master autophagy regulator transcription factor EB (TFEB) attenuated inclusion formation, prevented nigrostriatal neurodegeneration and reversed motor deficits in these animals (Carballo-Carbajal et al., 2019).

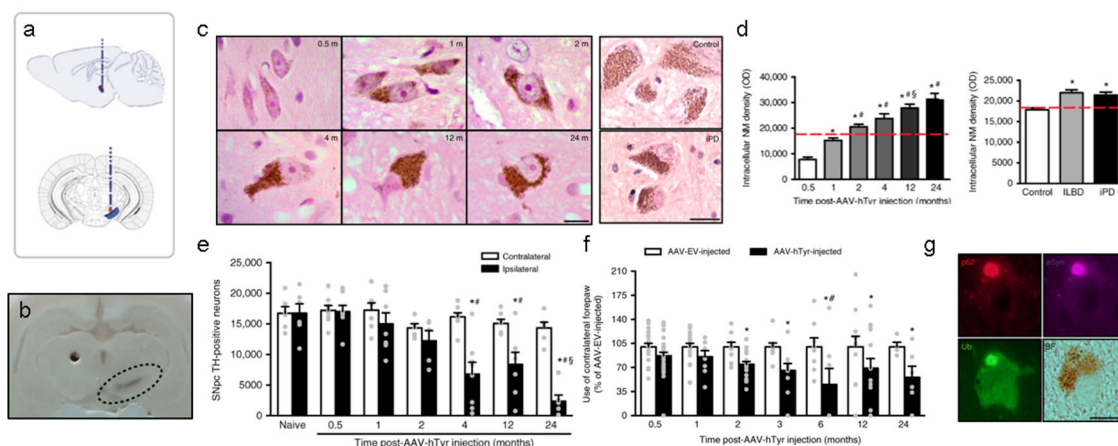


Figure 11. Age-dependent human-like NM production in rat SNpc triggers PD pathology. **a)** Schematic representation of stereotaxic injection. **b)** Representative unstained AAV-TYR injected rat brain (2 months post-injection) in which ipsilateral SNpc can be detected macroscopically as a brown darkened area. **c)** Representative photomicrographs of H&E-stained brain sections showing progressive intracellular NM accumulation (brown) within ipsilateral SNpc DA neurons from AAV-TYR-injected rats (*left*) and humans (*right* panel). **d)** Quantification of intracellular NM levels by optical densitometry in AAV-TYR-injected rats and human controls, ILBD and idiopathic PD cases. **e)** Use of contralateral forepaw in AAV-TYR compared to Empty Vector (EV)-injected rats. **f)** Progressive loss of DA SNpc neurons in AAV-TYR injected rats. **g)** LB-like inclusion formation, immunopositive for p62, ubiquitin (Ub) and α -synuclein (aSyn), in NM-containing SNpc neurons from AAV-TYR injected rats (2 months post-injection). ILBD, Incidental Lewy Body disease. iPD, idiopathic Parkinson’s Disease. From (Carballo-Carbajal et al., 2019).

This study lead to a novel pathogenic scenario in which the continuous, age-dependent buildup of NM within autophagic compartments obstructs the ALP and alters endocytic/secretory tasks, creating a cellular traffic jam eventually leading to LB pathology and PD-linked neuronal dysfunction/degeneration (Vila, Laguna, & Carballo-Carbajal, 2019).

4. Genome-wide transcriptomic analysis in PD

The genomic era has enabled a wide range of technologies for measuring high-throughput genomic expression in biological samples. Contrarily to the assessment of individual gene expression, high throughput whole-genome platforms enable data-driven discoveries without a prior etiological hypothesis. Since 2000s, genome-wide approaches have been extensively applied to the analysis of gene expression in PD to identify pathways and genes involved in PD-specific neurodegeneration. Over the last two decades, RNA microarrays-based analysis, in particular, were the most frequently used technique (Mariani et al., 2016). Since the beginning of 2000s, numerous gene expression studies showed differential expression profiles in the bulk SN of post-mortem brain tissues of PD patients compared to controls using microarray techniques (Bossers et al., 2009; Dijkstra et al., 2015; Duke et al., 2006; Durrenberger et al., 2012; Grünblatt et al., 2004; Hauser et al., 2005; Moran et al., 2006; Y. Zhang, James, Middleton, & Davis, 2005). One important consideration about these array studies is that most use homogenized tissue of a specific brain area and thus reflect the gene expression profiles of the heterogeneous neuronal and glial populations that exist in the region being analyzed. Overcoming the obstacle of tissue complexity, the technique of laser capture microdissection (LCM), which combined with the use of immunohistochemical stains allows the isolation of specific cell populations, has been applied in some studies to specifically isolate DA neurons from the SNpc of control and PD subjects followed by transcriptomic microarray analysis (Cantuti-Castelvetri et al., 2007; Elstner et al., 2011; Simunovic et al., 2009) and microRNA-based microarrays (Briggs et al., 2015; Kim et al., 2014). These studies enabled the detection of DA neuron-specific differential expression profiles in PD versus control SNpc. During the last decade, RNA sequencing (RNAseq) emerged as a new tool to investigate genome-wide changes and has also been applied in studies with PD brain tissue (Dumitriu et al., 2016; Henderson-Smith et al., 2016; Riley et al., 2014). Still, until 2018, oligonucleotide microarrays had been the most widely-used platform for the transcriptomic characterization of PD brain, particularly the Affymetrix Gene Array family of microarrays (14 studies using microarrays out of 33) (Borragero, Haylett, Seedat, Kuivaniemi, & Bardien, 2017), while studies using RNAseq had been much less used (3 studies using RNA-seq out of 33, 2 of which characterized cortex or striatum (Dumitriu et al., 2016; Henderson-Smith et al., 2016) and only one study used SN tissue (Riley et al., 2014)). Recently, the new methodology of single-cell RNAseq allows

transcription profiling at the single cell level, overcoming the heterogeneity of the tissue and enabling a deeper understanding of gene expression regulation and dynamics (Borrageiro et al., 2017). Still, this approach is technically compelling since it requires freshly dissected tissue in order to avoid membrane disruption during cryopreservation. For this reason, single-nuclei RNAseq (snRNAseq), which enables analysis from cryopreserved biospecimens, has been used instead to characterize the more readily available frozen human specimens. The application of snRNAseq in human control SN tissue has identified different cell clusters within human control SN (Agarwal et al., 2020; Welch et al., 2019), which together with the data from PD-associated risk loci from GWAS studies gives us a cell-specific context of the molecular pathways involved in PD etiology (Agarwal et al., 2020). Very recently, studies performing snRNAseq on SN tissue from PD postmortem subjects have identified cell-specific gene expression changes and defined especially vulnerable neuronal subtypes in PD (Adams, Kyung Song, Tanaka, & Kim, 2022; Kamath et al., 2022; Smajić, et al., 2022; Q. Wang et al., 2022).

Independently of the approach used, the characterization of SN from PD postmortem tissue have consistently identified PD-related molecular pathways associated to neuroinflammation, ubiquitin-proteasome system, mitochondrial function, iron and oxidative stress responses, protein folding, cell-adhesion pathways, vesicle-mediated transport and translation (Duke et al., 2006; Dumitriu et al., 2016; Durrenberger et al., 2012; Grünblatt et al., 2004). However, most of the postmortem PD tissue used in these studies represents a final end-point of the disease and consequently altered molecular pathways might have little or nothing to do with the etiopathogenic factor that triggered the disease in the first stages. For this reason, other studies guided to identify etiopathogenic factors attempt to characterize (i) molecular determinants of regional PD-vulnerability (Aguila et al., 2021; Keo et al., 2020), (ii) molecular determinants of the aging process and its relation to PD (Adams et al., 2022; Glaab & Schneider, 2015), (iii) early/prodromal stages of the disease (e.g. initial Braak stages) (Dijkstra et al., 2015; Keo et al., 2020). Under these scenarios, the key etiopathogenic triggering factors might be detected and used as potential targets to develop a therapeutic intervention to halt or reverse disease progression.

HYPOTHESIS AND OBJECTIVES

HYPOTHESIS AND OBJECTIVES

The main aim of this PhD thesis is to generate a new NM-based model that accumulates NM in all PD-vulnerable catecholaminergic groups and to characterize the consequences of NM accumulation in these groups through a multidisciplinary approach involving behavioral, neurochemical, histological and transcriptomic techniques.

Aim 1

Previously, our group has generated the first *in vivo* rodent model of NM accumulation. This model, based on the AAV-mediated overexpression of TYR (AAV-TYR), induces pigmentation unilaterally and exclusively in the SNpc of rodents. Here we want to generate the first *in vivo* model of NM accumulation that reproduces the brain-wide bilateral distribution and age-dependent accumulation of NM pigment that occurs in the human brain (i.e. all catecholaminergic groups). By fulfilling this goal, we will be able to characterize the consequences of pigment accumulation in all PD-vulnerable neuronal groups. The major assets of this characterization will consist on the assessment of: (i) neuronal viability, (ii) presence of PD neuropathological hallmarks, and (iii) behavioral consequences. The results from these outcomes will confront or validate the hypothesis that NM accumulation interferes with normal functioning of distinct neuronal cell types, becoming an essential triggering factor for PD vulnerability in specific neuronal groups.

This first global aim can be subdivided into the following specific objectives:

- 1- To generate a transgenic mouse line with overexpression of TYR specifically in catecholaminergic neuronal groups.
- 2- To assess TYR expression and NM accumulation in different brain nuclei at different ages.
- 3- To perform behavioral assessment of NM-accumulating mice at different ages.
- 4- To perform stereological cell counts in the main PD-vulnerable cell groups in NM-accumulating mice at different ages.
- 5- To characterize neurotransmission in the main PD-vulnerable cell groups in NM-accumulating mice at different ages.
- 6- To determine the presence of LB pathology in the main PD-vulnerable neuronal groups in NM-accumulating mice at different ages.

- 7- To characterize the neuroinflammatory response in the main PD vulnerable neuronal groups in NM-accumulating mice at different ages.

Aim 2

Moreover, since we hypothesize that NM accumulation in different catecholaminergic groups disrupts cellular homeostasis leading to PD-like pathology (Aim1), as seen in our previously generated NM-accumulating model (AAV-TYR), our second aim is to characterize the molecular events that might be driving this disturbance. By fulfilling this goal we will be able to characterize the molecular consequences of NM accumulation. The major assets of this characterization will consist in the assessment of: (i) NM-induced altered gene expression profiles in different pigmented brain nuclei, (ii) similarity between NM-induced transcriptomic alterations in our model with reported PD postmortem transcriptomic profiles, and (iii) new potential NM-induced therapeutic targets for PD.

This second global aim can be subdivided into the following specific objectives:

- 1- To specifically collect pigmented areas from NM-accumulating mice by LCM for its transcriptomic characterization at different ages.
- 2- To perform transcriptomic microarrays and differential expression analysis in the pigmented areas compared to non-pigmented areas at different ages.
- 3- To compare the transcriptomic profile identified in NM-mice pigmented areas to the human PD postmortem transcriptomic profile from published studies.
- 4- To validate the identified pathways involved in NM-induced pathology.
- 5- To identify new potential NM-related systemic biomarkers and NM-related therapeutic targets and validate them in NM-accumulating mice.

MATERIALS AND METHODS

MATERIALS AND METHODS

1. Human tissue

Human post-mortem brain tissue. Paraffin-embedded midbrain sections (5 μm) from healthy control subject *BK1749* (female, 70 years old) for H&E staining and BCM-65 (male, 81 years old) for Masson-Fontana staining were provided by the *Neurological Tissue BioBank at IDIBAPS-Hospital Clinic (Barcelona)* and *Biobanco en Red de la Región de Murcia (BIOBANC-MUR) (Murcia)*, respectively. All procedures were conducted in accordance with guidelines established by the BPC (CPMP/ICH/135/95) and the Spanish regulation (223/2004) and approved by the Vall d'Hebron Research Institute (VHIR) Ethical Clinical Investigation Committee (PR(AG)370/2014). Standard H&E and Masson-Fontana stainings were performed on 5 μm -thick paraffin-embedded SNpc and LC sections. Identification of DA neurons was ascertained by the visualization of unstained NM pigment. Magnetic resonance images from human SN-VTA and LC were kindly provided by Alex Rovira, Director of the Magnetic Resonance Unit and of the Section of Neuroradiology at University Hospital Vall d'Hebron, Barcelona (Spain).

2. Animals

TgNM mouse colony. Transgenic (tg) mice were obtained by pronuclear microinjection (classical transgenesis) of the full-length human TYR complementary DNA (cDNA) fused to the rat tyrosine hydroxylase (Th) promoter (tg-Th-TYR) into C57Bl6-SJL mouse zygotes [Centre for Animal Biotechnology and gene Therapy (CBATEG)]. Mice were backcrossed for 8-10 generations using C57BL/6J mice (Charles River) and maintained in heterozygosis. Animals were housed two to five per cage with *ad libitum* access to food and water during a 12 hours (h) light/dark cycle. All the experimental and surgical procedures were conducted in strict accordance with the European (Directive 2010/63/UE) and Spanish laws and regulations (Real Decreto 53/2013; Generalitat de Catalunya Decret 214/97) on the protection of animals used for experimental and other scientific purposes and approved by the Vall d'Hebron Research Institute (VHIR) Ethical Experimentation Committee. Male and female wt and tgNM mice were randomly distributed into the different experimental groups and wt and tgNM animals were processed at once to minimize bias.

Genotyping. DNA was routinely extracted from mice ear punches with the kit AccuStart™ II Mouse Genotyping Kit (QuantaBio, #95135) and a PCR was performed mixing 1ul of DNA with the primers TYR-Forward (TTCAGACCCAGACTCTTTTCAA), TYR-Reverse (GCTGCTTTCTCTTGTGACGA) at a concentration of 500nM using a 9800 Fast Thermal Cycler (Applied Biosystems). Amplification product was loaded into 1.8% agarose gel and visualized using a GelDoc XR (BioRad).

Survival analysis and reproduction. All animals were followed throughout their lifespan and a survival analysis (log-rank test and Gehan-Breslow-Wilcoxon test) was performed considering all natural deaths as positive events and all animals used for experimental purposes as censored data. Animals used for experimental purposes were chosen randomly and for reasons unrelated to their health status, thus avoiding a potential bias due to censoring (Ranganathan & Pramesh, 2012). For reproduction analysis all heterozygous matings were registered and the mean number of pups was assessed.

Magnetic resonance Imaging. Proton nuclear magnetic resonance imaging (¹H-MRI) studies were performed at the joint nuclear magnetic resonance facility of the *Universitat Autònoma de Barcelona* and *Centro de Investigación Biomédica en Red—Bioingeniería, Biomateriales y Nanomedicina* (CIBER-BBN) (Cerdanyola del Vallès, Spain), Unit 25 of NANBIOSIS. Experiments were conducted on a 7T Bruker BioSpec 70/30USR scanner (Bruker BioSpin GmbH, Ettlingen, Germany) equipped with a mini-imaging gradient set (400mT/m) and using a 72-mm inner diameter linear volume coil as a transmitter and a dedicated mouse brain surface coil as a receiver. All MRI data were acquired and processed on a Linux computer using Paravision 5.1 software (Bruker BioSpin GmbH, Karlsruhe, Germany). Mice were anesthetized (1.5-2% isoflurane in 1 L/min oxygen for maintenance) and placed into an animal bed with bite-bar and ear-bars for optimal head immobilization. An animal monitoring and control system (SA Instruments, Stony Brook, NT) was used to control the respiration rate (50-100 bpm) and core body temperature ($37 \pm 1^\circ\text{C}$) was maintained via integrated water hoses in animal's bed during the whole session. High resolution T1-weighted spin-echo images were acquired afterwards in the axial plane with and without fat saturation pulses. Two slice packages of 7 contiguous slices each were acquired containing the SNpc and LC regions and using the following parameter: TE=7 ms; TR= 500 ms; NA=56; FOV=1.92×1.92

cm²; MTX=128×128; ST= 0.25 mm; thus, resulting in a spatial resolution of 150×150×250 μm³; Acqt= 1h per image.

3. Histological analysis

Brain processing. Animals were deeply anesthetized with sodium pentobarbital intraperitoneally and then perfused through the left ventricle with saline [0.9% (wt/vol)] at room temperature (RT), followed by ice-cold formaldehyde solution 4% phosphate buffered for histology (Panreac). Brains were removed and post-fixed for 24 h in the same fixative and subsequently processed for paraffin embedding following standard procedures or cryoprotected for 24-48 h in 30% sucrose at 4°C and frozen. Sectioning was performed with a sliding microtome (Leica, Germany) at 5 μm-thickness for paraffin samples or in a cryostat at 30 μm-thickness for frozen samples (Leica, Germany).

Immunohistochemistry. Deparaffinized sections or cryosections were quenched for 10 min in 3% H₂O₂-10% (vol/vol) methanol. Antigen retrieval in paraffin sections was performed with a 10 mM citric acid solution at pH 6.0 at 95°C for 20 min. Sections were rinsed 3 times in 0.1 M Tris buffered saline (TBS) between each incubation period. Blocking for 1 h with 5-10% (vol/vol) normal goat or rabbit serum (NGS or NRS) (Vector Laboratories, #S-1000 and #S-5000) was followed by incubation with the primary antibody at 4°C for 24 or 48h in 2% (vol/vol) serum and with the corresponding biotinylated antibody (Vector Laboratories) or alkaline-phosphatase antibody (Abcam #ab6722) for 1h at room temperature. Sections were visualized by incubation with avidin-biotin-peroxidase complex (Thermo Fisher Scientific, ABC Peroxidase Standard Staining Kit #32020 or Ultra-Sensitive ABC Peroxidase Standard Staining Kit #32050), VectorSG Peroxidase Substrate Kit (Vector Laboratories, #SK-4700) or ImmPACT Vector Red Substrate (Vector, #SK-5105) and then mounted and coverslipped with DPX mounting medium (Sigma-Aldrich 06522). Bright-field section images were examined with Zeiss Imager.D1 microscope coupled to an AxioCam MRc camera and with Pannoramic 250 Flash III (3D Histech), and processed with ZEN 2011 software (Zeiss, Germany) and Caseviewer 3D HISTECH Ltd, respectively.

Immunofluorescence. Blocking was performed with 5-10% (vol/vol) normal goat (Vector Laboratories, #S-1000) or donkey serum (Abcam, #ab7475) and 0.1% (vol/vol) Triton X-100 (Sigma-Aldrich) in phosphate buffered saline (PBS) solution.

Corresponding primary antibodies described in Table 4 were incubated together overnight at 4°C in 2-10% (vol/vol) NGS or NDS and adequate Alexa 488, 594, and 647-conjugated secondary antibodies (1:1000 Thermo Fisher Scientific, 1:400 Anti-Goat (Donkey)-594 Gibco, #A11058) were incubated simultaneously for 1h at RT in 2-10% (vol/vol) serum. Nuclei were stained with Hoechst 33342 (1:2000, Thermo Fisher Scientific) in 1x PBS for 10 min. Sections were coverslipped using the DakoCytomation Fluorescent Mounting Medium (Dako, #S302380-2). Immunofluorescence section images were examined using ZEISS LSM 980 with Airyscan 2 and processed with ZEN 2011 software (Zeiss, Germany).

Masson-Fontana. To stain NM granules, the Masson-Fontana Staining Kit (DiaPath) was performed on 5 µm-thick paraffin-embedded human and mouse representative sections of SN-VTA and LC regions. This procedure is based on the ability of NM to chelate metals by reducing silver nitrate to a visible metallic state. Briefly, paraffin tissue sections were dewaxed and rehydrated by heating at 60°C for 10 min, followed by xylene (5 min, 3 times) and ethanol serial washes (100-95-70% and H₂O, 5 min each). Staining was performed by incubating the sections with ammoniac solution for 40 min at 56°C, followed by sodium thiosulphate for 2 min and a final counterstain with Kernechtrot for 7 min. Between each step, samples were rinsed in distilled water.

Nissl and Hematoxylin-Eosin (H&E) stainings. To perform the NM brain map, standard Nissl staining was performed for each animal in serial 30 µm-thick cryosections spanning the whole brain from the olfactory bulb to the beginning of the spinal cord. Areas from A16 to A12 were imaged with Zeiss Imager.D1 microscope coupled to an AxioCam MRc camera. Standard H&E staining was performed in 5 µm-thick paraffin-embedded representative sections of SN-VTA and LC regions for each animal. In these sections, catecholaminergic neurons were identified by the visualization of unstained NM pigment.

Primary Antibody	Manufacturer	Dilution
Anti-TH	Calbiochem (657012)	1:1000 (WB)
		1:40000 (IHC for SN-VTA and
		1:5000 (IHC for Str)
		1:3000-1:20000 (IHC)
Anti-DAT	Chemicon #MAB369	1:1000 (IF)
		1:500 (WB)
		1:500 (IHC)

Anti-VMAT2	Courtesy of G.Miller, Emory University	1:20000 (IHC)
Anti-ChAT	Millipore #AB144P	1:500 (IHC for PPN/NBM) 1:100- 1:2500 (IHC for DVC)
Anti-TPH	Chemicon #AB1541	1:500 (IHC)
Anti-GFAP	Sigma-Aldrich #G3893	1:1000 (IHC) 1:1000 (WB)
Anti-Iba-1	Wako #019-19741(IHC) Wako #016-20001(WB)	1:1000 (IHC) 1:500 (IF) 1:1000 (WB)
Anti-p62	Progen #GP62-C	1:500 (IF) 1:1000 (WB)
Anti-α-synuclein	BD Biosciences #610786	1:500 (IF)
Anti-β-actin	Sigma Aldrich #A5441	1:10000 (WB)
Anti- Ubiquitin	Sigma-Aldrich #U 5379	1:1000 (WB)
Anti-VDAC1/ Porin	Abcam #ab15895	1:1000 (WB)
Anti-LC3	Novus #NB100-2220	1:1000 (WB)
Anti-Lamp1	Abcam #ab24170	1:1000 (WB)
Anti-Cathepsin D	Sigma-Aldrich #C0715	1:1000 (WB)
Anti-Parkin	Abcam #ab77924	1:2000 (WB)
Anti-GPNMB (mo)	R&D Systems-Biogen #AF2330	1:1000 (IHC and WB)
Anti-GPNMB (hu)	R&D Systems- Biogen #AF2550	1:200 (IHC and IF)
Anti-Drp1	BD #611738	1:1000 (WB)
Anti-OPA1	BD #612606	1:1000 (WB)

Table 4. Primary antibodies used in immunohistochemistry (IHC), immunofluorescence (IF) and western blot (WB). IF was performed on paraffin sections for LB characterization (p62, α -synuclein, and TH) and on free-floating cryosections for GPNMB co-localization (GPNMB, Iba1 and TH). IHC was performed on free-floating cryosections, except for TPH staining that was performed on paraffin sections.

Intracellular NM quantification. 5 μ m-thick paraffin-embedded H&E-stained sections and Nissl or unstained 30 μ m-thick cryopreserved sections representative of the different regions of interest (SN, VTA, LC, DVC) at different ages were selected and all neurons per section were analyzed. Catecholaminergic neurons were identified by the visualization of unstained NM brown pigment. H&E sections were scanned using the Panoramic Midi II FL, HQ SCIENTIFIC 60x and section images were acquired with CaseViewer software at an objective magnification of 63x. Alternatively, Nissl or bright-field pictures from unstained sections were taken with the Zeiss Imager.D1 microscope coupled to an AxioCam MRC camera. All NM-positive neurons from each brain nuclei were analyzed by means of optical densitometry using ImageJ software (NIH, USA) to quantify the percentage (%) of cytosolic area occupied by NM pigment in H&E and the intracellular optical density (OD) of NM in Nissl or unstained sections as previously

reported (Carballo-Carbajal et al., 2019). For NM pigment OD measurements the pixel brightness values for all individual NM-positive cells (excluding the nucleus) in all acquired images were measured and corrected for non-specific background staining by subtracting values obtained from the neuropil in the same images. All quantifications were performed by an investigator blinded to the experimental groups.

Stereological Cell Counting. Assessment of (i) the total number of SNpc, VTA, LC and DVC TH-positive neurons, (ii) the number of NM-laden neurons, (iii) the total number of DA/NA neurons in the different regions of interest, (iv) the total number of ChAT-positive neurons in DVC, PPN and NBM, and (v) the total number of TPH-positive neurons in the DR, was performed according to the fractionator principle, using the MBF Bioscience StereoInvestigator 11 (64 bits) Software (Micro Brightfield). Serial 30 μm -thick cryosections (every fourth section for SNpc, VTA, LC; every sixth section for PPN, NBM and DVC), or 5 μm -thick paraffin sections for the DR (every tenth section), covering the entire nuclei were included in the counting procedure. For SNpc, VTA, LC, PPN and NBM a 25% of the area was analyzed with the following sampling parameters: (i) a fixed counting frame with a width and length of 50 μm ; (ii) a sampling grid size of 125 x 100 μm . The counting frames were placed randomly by the software at the intersections of the grid within the outlined structure of interest. For DR and DVC, 100% of the area was analyzed. Cells in both brain hemispheres were counted following the unbiased sampling rule using a 100x lens and included in the measurement when they came into focus within the dissector. A coefficient of error of <0.10 was accepted. Data for the total numbers of TH-positive neurons, TPH-positive and ChAT-positive neurons are expressed as absolute numbers. The total number of catecholaminergic SNpc, VTA, LC and DVC neurons was calculated by considering all TH⁺NM⁺, TH⁻NM⁺ and TH⁺NM⁻ neurons. The percentage (%) of TH down-regulation was calculated by considering the total number of TH⁻NM⁺ with respect to the total number of neurons containing NM in the different experimental groups. All quantifications were performed by an investigator blinded to the experimental groups.

Quantification of neuropathological parameters. The absolute number of extracellular NM (eNM) aggregates was estimated using the stereological parameters used for the stereological cell counting and in the same sections where the neurodegeneration was assessed (SNpc, VTA, LC and DVC). The number of p62-immunopositive MB and LB-like inclusions were counted from SNpc, VTA, LC and DVC sections fluorescently

immunostained with guinea pig anti-p62 (1:500, Progen #GP62-C), mouse anti- α -synuclein (1:500, BD Biosciences #610786) and TH (1:1000, Calbiochem #657012). The total number of p62-positive inclusions falling into each category was counted from one representative coronal section of the SNpc, VTA, LC and DVC nuclei in each animal. All quantifications were performed by an investigator blinded to the experimental groups.

Optical densitometry analyses. The density of TH/DAT/VMAT2-positive fibers in the striatum was measured by densitometry in serial coronal sections covering the whole region (4 sections/animal). TH-immunostained 30 μ m-thick cryosections were scanned with an Epson Perfection v750 Pro scanner and the resulting images were quantified using ImageJ. Striatal densitometry values were corrected for non-specific background staining by subtracting densitometric values obtained from the cortex. Data are expressed as optical density or absorbance defined by the logarithmic intensity of the light transmitted through the material using the formula: $-\log_{10}(\text{Striatum Intensity}/\text{Cortex Intensity})$.

Quantification of neuroinflammation parameters. Quantification of Iba-1, CD68 and GFAP-positive cells was performed in one SNpc, VTA, LC, DVC representative section. Sections were scanned using the Panoramic 250 Flash III (3D Histech) scanner and images were acquired with CaseViewer software (3D Histech, Hungary). For quantification of Iba-1, CD68 and GFAP-positive cells, specific artificial intelligence (AI)-based algorithms were used as previously described (Gonzalez-Sepulveda et al., 2022) using the Aiforia platform (Aiforia Technologies, Finland). Iba-1-positive cells were counted separately in two different groups according to their activation state: non-reactive (branched) and reactive (amoeboid). CD68- and GFAP-positive cells were counted individually. All quantifications were performed by an investigator blinded to the experimental groups.

4. Real-Time quantitative PCR (qPCR)

Genomic TYR detection. Genomic DNA was extracted using Speedtools Tissue DNA Extraction kit (BioTools #21.137) from tgNM ear punches collected throughout the course of the experiments (2015 to 2019). qPCR was performed with 10 ng of genomic DNA per well in technical triplicates using TaqMan Genotyping Master Mix (Applied Biosystems #4371355) and a customized pre-designed Copy Number Variant sensitive assay for TYR cDNA [TYR3_CYU62U6, localized within exon 2, Custom Plus

(chr11:89191160-89191460GRCh38)]. TYR CTs were normalized to the recommended Copy Number Reference Assay Tfrs reference gene (Tfrs, mouse, Taqman Copy Number Reference Assay, ThermoFisher # 4458366). Water was included in the reaction as a non-template (negative) control. The relative expression was calculated with the Δ Ct-method.

Dopaminergic markers and melanogenic enzymes cDNA gene expression. Total RNA was extracted from dissected brain regions (vMB or SN-VTA, LC, OB, DVC, PFC, HIP) and peripheral tissues (eye, retina, skin, adrenal gland, white blood cells and duodenum). mirVana PARIS RNA and Native Protein Purification Kit (Thermo Fisher Scientific # AM1556) was used for total RNA extraction and RNA concentration was determined using a NanoDrop ND-1000 Spectrophotometer. 0.5 μ g of total RNA were retrotranscribed using High-Capacity cDNA Reverse Transcription Kit (Thermo Fisher Scientific # 4368814). qPCR was performed with 10 ng (or 45ng when specified in the figure legend) of cDNA per well in technical triplicates mixed with Taqman Gene Expression Master Mix (Applied Biosystems, # 4369016) and Taqman gene expression assays [human TYR Hs00165976_m1; mouse TH Mm00447557_m1; Slc6A3 (Dat) Mm00438388_m1; Slc18a2 (Vmat2) Mm00553058_m1, Applied Biosystems] using standard procedures in a 7900HT Fast Real Time Instrument (Applied Biosystems). The arithmetic mean of triplicate thresholds cycles (CT) for each target gene were normalized to the geometric mean of one, two or three endogenous reference genes (Gapdh Mm99999915_g1, Rpl19 Mm02601633_g1 and Ppia Mm02342430_g1) as specified in the figure legend. Water was included in the reaction as a non-template (negative) control. The relative expression was calculated using the comparative method (Δ Ct-method). Relative quantities (RQ, $2^{-\Delta$ Ct) are calculated normalizing CT to endogenous controls and fold changes (FC, $2^{-\Delta\Delta$ Ct) are calculated normalizing CT to endogenous controls and to experimental control expression (i.e. wt animals).

Microarray validation and GPNMB expression. RNA extracted from microdissected tissue (mouse and human) (Methods Section 10, Laser capture microdissection) and RNA from bulk postmortem human tissues extruded using RNeasy Micro (#74004, Qiagen), was amplified with Ovation® Pico WTA System V2 (Tecan) into cDNA. This kit amplifies cDNA from total RNA (500pg-50ng of total RNA). Amplification is initiated at the 3' end as well as randomly throughout the RNA transcripts, enabling the amplification of degraded RNA. Specific primers for each validated transcript were designed using Primer-BLAST (Ye et al., 2012), a tool for designing

specific primers from the National Center for Biotechnology Information (NCBI). Primers sequences are specified in Table 5. Primers were diluted in water and stored at -20°C at a stock concentration of 100µM. For gene expression analysis, only cDNA samples amplified from good quality RNA were used (RIN>5 or RIN>4 for human microdissected DA neurons). For qPCR, 10ng of cDNA from each sample in technical triplicates were mixed with the 2X PowerUp™ SYBR™ Green Master Mix (#A25776, Applied Biosystem-ThermoFisher) and the specific primers at a working concentration of 500nM. qPCR was performed using the recommended cycling condition in a LightCycler® 480 System (Roche). Quantification analysis using Fit Points Method was performed with LightCycler Software and threshold cycles (CT) signals from each sample were obtained. Fold changes for each transcript and sample were calculated normalizing the arithmetic mean of technical replicates CTs to the geometric mean of three endogeneous control genes (Ndn, Rtn1, Ppia for mouse; FOXO1, UGGT1, GOLGA3 and HPRT1 for human bulk expression and HPRT1 and UGGT1 for human DA neurons expression) and then normalized to experimental control expression (wt for mice, Ctrl for human) using the comparative method ($\Delta\Delta$ CT method).

Assay	Type	Forward primer	Reverse primer
Aurkaip1	T	GCGACCTGATCGGTCCTAAC	CAGCGCTCAAAGCAAACAGA
B2m	T	TCACACTGAATTCACCCCA	TCACATGTCTCGATCCCAGT
Bcl2a1a	T	ATGGAGGTTGGGAAGATGGC	GCCAAGGTTCTCTCTGGTCC
Cd68	T	GGGCTCTTGGGAACACTACAG	TATGCCCAAGCCTTTCTTCC
Cst7	T	ACCATGCATCACCAACTGGA	TCAGAGTAGCAATATAGAGTCCGC
Exosc3	T	GTTACGCCTGAATGCGGGT	TGCGAGTCCACCCAGTAAAC
Extl3	T	TTGTGGGAAGCGGACTTTCA	GCTTGTTCTCCTGATCGGCT
FOXO1	R	AGGGTTAGTGAGCAGGTTACAC	TGCTGCCAAGTCTGACGAAA
Gfap	T	CCTCCAGATCCGAGAAACCAG	TTGTGCTCCTGCTTCGAGTC
GOLGA3	R	GGCGTTGTCACGGGTATCAT	CATCAGCAACAGCCAAGAGC
Gpnmb	T	ACTGCAGGAATGATTTGGGACT	GGAACCTGAGATGCTGGCTT
GNMB	T	GTTCTGACAGAGACCCAGC	CACCAAGAGGGAGATCACAGT
Grn	T	CCCGTTCTTAAGGGTGTGTC	TCTGCACTACAGTGGAAAGCC
Gsk3b	T	AGGAAGGAAAAGGTGATTCAAGA	TGCTGCCATCTTTATCTCTGCT
Hexb	T	GACCACAGTCCCAATTCCAC	AAAACATAGTTGTAATATCGCCGAA
HPRT1	R	TTGCTTTCCTTGGTCAGGCA	ATCCAACACTTCGTGGGGTC
Impact	T	ACTTGCACAGTCCGATGAG	TGCTTCGATTTCTCACTCCAT
Kif1a	T	AGCTAGTTGTGGGTGCATC	CATTTCCGAAGGAAACGCGG
Laptm5	T	CGTGCTCATCCTGAAGGTCTA	CCATGGCCGAATTCATGTGC
Lilrb4a	T	GCCCAAGAGAACAGCTACGA	TGGGTTCCAGAATAAGACCAAGG
Lyz2	T	TGAACGTTGTGAGTTTGCCAG	AGCTAAACACACCCAGTCGG
Mapk3	T	CACTGGCTTTCTGACGGAGT	GGATTTGGTGTAGCCCTTGA

Ms4a7	T	GTGCCTAGTGAAGCCACAGT	TCAGTGCACAGAGGGATCCAA
Ndn	R	CAAGAAAGATCCCCAGGCGT	CTGGGCAGCAAGATTAGCCT
Polr2l	T	CGAGTACACGGAGGGGGAT	AGGGGTGCATAGTTCAGCAG
Ppia	R	TCAACCCACCGTGTTCCTC	CCAGTGCTCAGAGCTCGAAA
Prkn	T	CCCGGTGACCATGATAGTGTT	TGCTGGTGTGAGAATCGACC
Pttg1	T	TCAAACCTCGGGCTGTAAGCA	CTTGGCCCCAATATCCCGAA
Rgl1	T	CTTGGACTCTTGGCAGCT	GGAGGCATTACGAATCTGCTAGT
Rtn1	R	GAGCTGGGGTAACGTCGTC	GGAACAGCTGCCATACCTGT
Serpina3n	T	CATCTCCACCGACTACAGCC	CCTTGTGGACCACCTGAGAG
Trem2	T	AGCACCTCCAGGCAGTTT	TTGATTCCTGGAAAGAGGAGGA
Tyrobp	T	CTGATTGCCCTGGCTGTGTA	TGTTGTTCCGGGTCCCTTC
UGGT1	R	CTGCCGGTGACAGGAGTTT	ATGGCTTTTGAGTCGGCCTT

Table 5. Primers designed using Primer-BLAST for mouse and human transcripts. Human transcripts are in capital letters. Target, T; Reference, R.

5. Western blot (WB)

Immunoblot. TgNM dissected vMB and Str were homogenized in RIPA buffer supplemented with protease inhibitors (Roche) and cell extracts clarified by centrifugation at 13000rpm g for 30 min at 4°C. Protein concentrations were quantified using the BCA (Pierce BCA Protein Assay Kit, Thermo Scientific #23227) method and subjected to SDS-PAGE. Proteins were resolved in 10 or 15 % polyacrylamide gels and transferred onto 0.45 µm nitrocellulose membranes (Amersham). Blocking with 5% milk powder in PBS was followed by overnight incubation at 4°C with the primary antibodies (Table 4). Incubation with the secondary antibodies goat anti-rat, donkey anti-rabbit and sheep anti-mouse (all 1:1000, from Amersham), was performed for 1h at RT. Band densitometry, normalized to β-actin expression, was measured using ImageJ image analysis software.

6. In vivo microdialysis

In vivo microdialysis. To assess local effects of nomifensine on striatal DA release in microdialysis experiments, the drug was dissolved in artificial cerebrospinal fluid (aCSF in mM: NaCl, 125; KCl, 2.5; CaCl₂, 1.26 and MgCl₂ 1.18) and administered by reverse dialysis at 10 and 50µM (uncorrected for membrane recovery). Concentrated solutions (1 mM; pH adjusted to 6.5–7 with NaHCO₃ when necessary) were stored at -80°C and working solutions were prepared daily by dilution in aCSF.

Extracellular DA concentration was measured by in vivo microdialysis as previously described (Alarcón-Arís et al., 2020, 2018). One concentric dialysis probe (Cuprophane membrane; 6000 Da molecular weight cut-off; 1.5 mm-long) was implanted in CPu (AP, 0.5; ML, -1.7; DV, -4.5 in mm) of isoflurane-anesthetized mice (wt and tgNM, n=7 mice per group) Microdialysis experiments were performed in freely-moving mice 24h after surgery. Probes were perfused with aCSF at 1.5 μ L/min. Following an initial 100-min stabilization period, 5 or 7 baseline samples were collected (20 min each) before local drug application by reverse dialysis and then successive dialysate samples were collected. The concentration of DA in dialysate samples was determined by HPLC coupled to electrochemical detection (+0.7 V, Waters 2465), with 3-fmol detection limit. The mobile phase containing 0.15 M NaH₂PO₄.H₂O, 0.9 mM PICB8, 0.5 mM EDTA (pH 2.8 adjusted with orthophosphoric acid), and 10 % methanol was pumped at 1 ml/min (Waters 515 HPLC pump). DA was separated on a 2.6 mm particle size C18 column (7.5 x 0.46 cm, Kinetex, Phenomenex) at 28°C. Microdialysis data are expressed as femtomoles per fraction (uncorrected for recovery) and are shown in figures as percentages of basal values (individual means of 5-7 pre-drug fractions).

7. Chromatographic determination of metabolites by UPLC-MS/MS.

Brain and peripheral samples collection. For UPLC-MS/MS analyses, heart, intestines, kidneys and several brain regions including: vMB, LC, Str, PFC, DR-PPN and DVC were dissected, frozen on dry ice, and stored at -80°C until analyzed by UPLC-MS/MS.

Sample preparation. UPLC-MS/MS analysis of mouse samples was performed using our previously validated method (Gonzalez-Sepulveda et al., 2020) with modifications. The day of analysis, samples were homogenized with 300 μ l of 250 mM formic acid (FA) and split in two: 1) 55 μ l for acetylcholine (Ach) determination, which were diluted 1:4 with 0.1% formic acid in acetonitrile containing 100 nM of Acetylcholine-d₄ Chloride as internal standard (IS); 2) 240 μ l for catecholaminergic and serotonergic determination to which a mixture (500 nM each) of dopamine-d₄ hydrochloride (DA-d₄) and serotonin-d₄ Hydrochloride (5HT-d₄) were added as IS. After centrifugation, supernatants were filtered using an Ostro™ protein precipitation and phospholipid removal plate (Waters, USA) prior the injection in the UPLC-MS/MS system. On the other hand, the pellet of the 240 μ l sample was further processed to determine the “protein-bound” (ProtB)

fraction of 5-*S*-cysteinyldopa (5SCD) and 5-*S*-cysteinyldopamine (5SCDA). 5SCD and 5SCDA standards were kindly donated by Professor Kazumasa Wakamatsu and Professor Shosuke Ito at the Fujita Health University, Aichi, Japan. Aminochrome standard (0.5 mM) was freshly prepared as previously described (Gonzalez-Sepulveda et al., 2020; Lemos-Amado et al., 2001).

Reductive hydrolysis and alumina extraction of catecholic compounds. Preparation of the ProtB fraction samples was performed using the reductive hydrolysis and alumina extraction method of Murakami et al. (Murakami et al., 2008) with some modifications. The pellet was washed with 1 ml of a 1:1 mixture of methanol and chloroform, vortex-mixed and centrifuged at 20.000 g for 10 min at 4°C. 300 µl of a mixture containing 6 M HCl, 5% thioglicolic acid and 1% phenol were added to the resulting pellet into a sealed-capped tube. Tubes are then purged with a stream of nitrogen and incubated for 16 h at 110 °C. After cooling, 100 µl of the hydrolysate were added to a tube containing 50 mg of acid-washed alumina prior the addition of 200 µl of 1% Na₂S₂O₅ – 1% EDTA.2Na and 500 µl 2.7 M Tris. HCl – 2% EDTA.2Na (pH 9.0). Tubes were vigorously mixed on a microtube mixer for 5 min and then centrifuged at 20.000 g for 10 min at 4°C. After removal of the supernatant, the alumina was washed with 1 ml of MilliQ water and centrifuged at 20.000 g for 10 min at 4°C three times. 5SCD and 5SCDA were finally eluted from alumina with 100 µl of 0.4 M HClO₄ by shaking for 2 min on a microtube mixer. 7 µl were injected into the UPLC-MS/MS system under MIX3 conditions.

UPLC-MS/MS analysis. The chromatographic separation of samples for ACh determination was performed on a Cortecs UPLC HILIC (1.6 µm; 2,1x75 mm) column coupled to a Cortecs UPLC HILIC VanGuard pre-column (Waters). Column temperature was set at 50 °C and samples were maintained at 6 °C in the thermostatic autosampler. The mobile phase consisted of solvent A (Acetonitrile + 0.1% FA) and solvent B (10 mM ammonium acetate in MilliQ water) at a flow of 0.5 mL/min with isocratic 70% A- 30% B conditions during 2.2 min. Samples for catecholaminergic and serotonergic determination were injected five times into the UPLC-MS/MS system to analyze different sets of compounds i.e. MIX1, MIX2, MIX3, MIX3-ProtB and MIX4. MIX1 includes dopamine (DA), norepinephrine (NE), 3-methoxytyramine (3MT), 3,4-dihydroxyphenylalanine (L-DOPA) and aminochrome (AC); MIX2 includes 3,4-Dihydroxyphenylacetic acid (DOPAC), 3,4-dihydroxymandelic acid (DOMA) and vanillylmandelic acid (VMA); MIX3 and MIX3-ProtB include 5SCD and 5SCDA and

finally MIX4 includes serotonin (5HT), tryptophan (Trp) and 5-hydroxyindole-3-acetic acid (5HIAA). An Acquity HSS T3 (1.8 μm , 2.1 mm \times 100 mm) column coupled to an Acquity HSS T3 VanGuard (100 \AA , 1.8 μm , 2.1 mm \times 5 mm) pre-column was used to detect MIX1-3 analytes while an Acquity UPLC BEH C18 (1.7 μm 2.1x100mm) column coupled to a Acquity BEH C18 1.7 μm VanGuard pre-column was used to detect MIX4. Column temperature was set at 45 °C for MIX1-3 and at 55° for MIX4. The mobile phase consisted of solvent A (methanol 100%) and solvent B (25 mM FA in MilliQ water) at a flow of 0.4 ml/min (0.5 ml/min for MIX4) with the following gradient profiles: 1) MIX1 and MIX2: 0.5 % B maintained for 0.5 min, 5 % B at 0.9 min maintained for 2.1 min, 50 % B at 2.8 min maintained for 1.2 min, 0.5 % B at 4.1 min maintained 0.2 min for equilibration; 2) MIX3 and MIX3-ProtB: 0.5 % B maintained for 0.5 min, 8 % B at 2.6 min, 50 % B at 2.9 min and maintained for 0.6 min, 0.5 % B at 3.7 min maintained 0.2 min for equilibration and 3) MIX4: 1% B maintained for 0.5 min, 25 % B at 3 min, 50 % B at 3.1 min and maintained for 0.5 min, 1 % B at 3.6 min maintained 0.4 min for equilibration. The mass spectrometer detector operated under the following parameters: source temperature 150°C, desolvation temperature 450°C, cone gas flow 50 L/hr, desolvation gas flow 1100 L/hr and collision gas flow 0.15 ml/min. Argon was used as the collision gas. The capillary voltage was set at: 0.5 kV (MIX1, MIX3 and MIX3-ProtB), 2 kV (MIX2) or 3 kV (MIX4, ACh). The electrospray ionization source was operated in both positive and negative modes, depending on the analyte. Multiple Reaction Monitoring (MRM) acquisition settings for the targeted metabolites are summarized in Table 6. Samples with a concentration between LOD and LOQ or bigger than LOQ were considered acceptable; samples with a concentration lower than LOD were considered as the LOD value. Catechol oxidation was measured using the formula AC+5SCDA+5SCDA-ProtB +5SCD+5SCD-ProtB / DA+DOPA. Data was normalized by the protein concentration determined by BCA (Pierce BCA Protein Assay Kit, Thermo Scientific #23227) and presented as the percentage of the WT concentration or ratio.

Analyte	MRM transition (m/z)	MIX	RT (min)	CV (V)	CE (eV)	CpV (kV)
ACh	145,98 > 86,80	ACh	1,5	10	15	3
ACh-d4	150 > 91	ACh	1,5	28	12	3
NE ^b	151,75 > 106,94	1	0,69	15	20	0,5
DA-d4 (IS)	157,83 > 94,8	01/03/2022	1,44	10	20	0,5

DA	153,93 > 90,57	1	1,46	10	20	0,5
L-DOPA	198,1 > 152,1	1	1,48	15	15	0,5
3MT^b	150,7 > 90,96	1	3,09	35	20	0,5
AC	149,61 > 121,91	1	3,36	25	25	0,5
DOMA^c	182,86 > 136,85	2	1,62	20	14	2
VMA^c	197 > 136,9	2	3,61	20	20	2
DOPAC^c	166,99 > 122,82	2	3,72	18	22	2
5SCDA	273,1 > 166,9	3	1,73	20	20	0,5
5SCD	317 > 154,86	3	2,01	24	30	0,5
5HT	177 > 160	4	0,97	10	5	3
5HT-d4 (IS)	181 > 164	4	0,97	10	5	3
5HIAA	192 > 146	4	1,5	25	20	3
Trp	205 > 188	4	2,1	15	10	3

Table 6. MRM acquisition settings^a RT, retention time; D, dwell time; CV, cone voltage; CE, collision energy; CpV, capillary voltage. ^bParent mass after loss of water. ^cDetected in negative mode.

8. Behavioral analysis

All behavioral analyses were performed at the same time of the day (9am-1pm).

Beam test. Mice were placed at the beginning of an elevated horizontal beam bar (40cm) to assess their fine movement and coordination skills. The time it took the mice to cross the beam was measured for a maximum of 120 seconds. When an animal felt, the maximum time of 120s was assigned. Animals that failed at doing the task (i.e not crossing or going backwards) were removed from the analysis.

Habituation and dishabituation (olfaction test). Two different cotton swabs were presented to mice (5 min each), the first one impregnated with water and the second one impregnated with lemon essence (Essenciales). The number of times the animal went towards each cotton swab and the time the animal spent sniffing it were measured. The discrimination index (DI) was calculated according to the formula: (Time exploring lemon essence – Time exploring water) / (Time exploring lemon essence + Time exploring water).

Rotarod. To assess motor learning, coordination, and endurance training, mice were evaluated on the constant, accelerated, and rocking Rotarod mode (Ugo basile®, Mouse

RotaRod NG). The apparatus consists of five 3 cm diameter cylinders, which are suitably machined to provide grip. Six 25 cm diameter dividers make for five lanes, each 5.7 cm wide, enable five mice to be assessed on the rotor simultaneously. The height to fall is 16 cm. The mice were placed on the rod with their back to the experimenter to measure motor learning, and the rod began to accelerate until it reached 10 rpm. The necessary tests were carried out so that each animal was kept at least 1 min on the rod with 1 min of rest between each learning trial. To measure the resistance of the animals, we used a protocol previously described (Brown & Wong, 2007) in which the mice are placed on the rotating rod in the opposite direction of the movement of the rod, with an acceleration of 0–48 rpm during a test of 6 min maximum. The test includes six trials (T1-T6) with a 1 min rest to start each. In all tasks, the latency (s) achieved by each animal was recorded.

Grip strength test. Mice were held by the middle/base of the tail and allowed to grasp a series of increasing weights consisting of tangled fine gauge stainless steel wire attached to steel chain (13.2, 19.7, 25.9, 32.1, 38.4, 44.6 g). Mice were then lifted carrying the corresponding weight with their forepaws. Time holding each weight (for a total of 5s each) was assessed, being 30 seconds the maximum time when succeeding in holding all weights. Grip latency (s) was calculated as a sum of the time holding the increasing weights.

Step down test. One of the most widespread ways to assess cognitive functions related to short-term learning and memory is fear conditioning. The passive avoidance or step down test used here (Passive Avoidance - Step Down for Mice (vibrating platform), #40570, Ugo Basile) consists of a platform located in a controllable electrified net. During training, mice were placed in the platform and received an electric shock of 0.3 mA when stepping down the platform. After 24 hours, mice were placed again in the same platform and the latency of stepping down was measured, though this second time the net was not electrified. The time on the platform was calculated by subtracting the latency time from the first day to that of the second day to normalize for the inter-individual variability in curiosity/activity of each mouse.

Open field. This protocol is used to evaluate the general locomotor activity of mouse models and allows to rule out possible motor impairments or emotional traits like anxiety. It consists of a square open field arena of 80 x 80 cm of white methacrylate, brightly lit (300 lux), where the center and the periphery can be distinguished using a tracking software (SMART 3.0 Panlab-Harvard Apparatus). Recorded data was analysed by the

Applied Research in Laboratory Animals Platform staff at Parc Científic de Barcelona (Spain).

All tests were performed by an investigator blinded to the experimental groups.

9. Assessment of peripheral functions

Heart Rate. The PhysioSuite apparatus (Kent Scientific) was used to measure the heart rate under mild anesthesia. The Isoflurane rate used was 1.5% and 1l/min O₂. The clip sensor was located in the right hind paw for 30 seconds before starting the recording and the first 10 recordings were taken and represented as average beats/minute.

Blood Pressure. Blood pressure was measured in a non-invasive way using the tail-cuff method (LE-5002 Non-Invasive Blood Pressure Meter, Panlab). The systolic and diastolic blood pressure (in mmHg) were assessed in two independent sessions for each mouse and the results were calculated as the mean from the valid values of 10 measurements in each session.

Respiratory rate. Respiration frequency was determined using microCT measurements acquired with Quantum FX imaging system (Perkin Elmer, 940 Winter St. Waltham, Massachusetts, EEUU), specifically designed for small lab animals. For the scanning procedure, animals were anesthetized with isoflurane (5% induction phase and 1% for maintenance). The air flow was set to 0.8L/minute. Defined parameters for image acquisitions were: field of view 73 mm, acquisition time 2 minutes, current voltage 70 mV and amperage 200 μ A. Image reconstruction was based on Feldkamp's method. Imaging data was analysed by the Preclinical Imaging Platform staff at Vall d'Hebron Research Institute (Spain).

All tests were performed by an investigator blinded to the experimental groups.

10. Laser capture microdissection

Brain collection. Mice aged 3, 12 and 20 months (m) (n=6 animals per genotype and age) either tgNM mice, representing different levels of NM accumulation, or wt littermates, with no-pigmentation, were sacrificed by cervical dislocation. Brains were removed, snap-frozen for 20 seconds in dry-iced cooled 2-methylbutane (isopentane) and stored at -80 °C until further processing.

Brain sectioning. Before sectioning, brain samples were tempered from -80°C to -20°C for 1h and then sectioned at 10µm in a cryostat (Leica). Serial sections covering the whole rostro-caudal extent of the SNpc and VTA regions (12 slides with 6-7 sections/slide) were collected in special membrane coated slides for LCM (PEN-membrane 2,0um, MDG3P40W, MicroDissect GmbH), previously irradiated with UV light for 1h to reduce static electricity. Slides were kept at -20°C during sectioning and then stored at -80°C until processing.

Staining. Sections were stained following the Arcturus® HistoGene® Frozen Section Staining Kit (Thermo Fisher Scientific). Briefly, slides were transferred on dry ice from -80°C immediately to a series of slide staining jars containing RNase-free solutions. Slides were kept in ethanol (EtOH) 75% for 30s, H₂O for 30s, HistoGene® solution (100 µl) for 1min and finally dehydrated with increasing concentrations of RNase-free ethanol solutions (H₂O-15s, EtOH 75%-15s, EtOH 95%-15s, EtOH 100%-15s). In order to reuse staining jars, a rigorous cleaning procedure was performed between experiments. When reused, jars were washed twice with ethanol 100%, washed twice with distilled H₂O, kept in Molecular BioProducts RNase away surface decontaminant solution (#7000TS1, ThermoScientific) overnight, washed with autoclaved miliQ H₂O for three times and dried under a fume hood for a complete removal of remaining solutions.

Laser capture microdissection. Immediately after the staining procedure was finished, the stained slide was placed under the laser capture microdissection microscope (Leica LMD6500), previously decontaminated with Molecular BioProducts RNase away surface decontaminant (#7000TS1, ThermoScientific). Neurons/regions of interests were visualized with the Leica LMD software (Leica Laser Microdissection V6.6.2), drawn manually using a 40x/5x objective, cut with a UV-laser and collected into an autoclaved RNase/DNase Free eppendorf cap (0.65 ml Low Binding MCT, #11300 Nirco (Sorenson Biosciences) containing 30µl of QIAzol Lysis Reagent solution (from miRNeasy Micro Kit, #217084, Qiagen). Approximately 300 neurons/10 regions were collected from each region and animal. The total time of the LCM procedure never exceeded 1h per slide to avoid compromising the quality of the tissue RNA. Eppendorf tubes containing collected samples were vortexed to ensure complete lysis and immediately frozen on dry ice. Samples were stored at -80°C for posterior RNA isolation.

RNA extraction and quality control. Isolation of total RNA from the microdissected tissue and neurons was performed using the miRNeasy Micro Kit (#217084, Qiagen).

This procedure combines phenol/guanidine-based lysis of samples and silica-membrane-based purification of total RNA, including long and small RNA species. Samples kept at -80°C after the LCM procedure were quickly thawed and QIAzol Lysis Reagent was added up to a volume of 152 μ l. Samples were vortexed for further lysis of tissue and cells, left for 5min at room temperature to promote dissociation of nucleoproteins, and then, chloroform was added to samples and incubated for 2-3min at room temperature and centrifuged to allow phase separation. Next, the aqueous phase was transferred to a new tube, mixed with ethanol 100% and passed through an RNeasy MinElute spin column. The column membrane was washed twice with wash buffers provided by the kit and with ethanol 80%, and finally, RNA was eluted with RNase-free water (14 μ l) and stored at -80°C for its posterior analysis.

RNA concentration and quality were assessed by electrophoresis using an Agilent 2100 BioAnalyzer instrument (Agilent technologies) and an Agilent RNA 6000 Pico Kit (0,05-5ng/ μ l) (Agilent technologies). Only samples with an RNA integrity number (RIN)>5 (or RIN>4 when stated) in a scale from 1 (highly degraded) to 10 (highest integrity) were processed for posterior analysis.

11. Transcriptomic microarrays and data analysis

Transcriptomic microarrays. RNA samples extracted from tgNM and wt animals aged 3m, 12m and 20m that passed the RNA quality control (n=4-6 mice per genotype/region/age) were analyzed using whole transcriptome microarrays Clariom D Pico Assay, mouse (#902663 and #902664) and washing kit GenChip Hyb Wash & Stain kit (#900720) (Applied Biosystems, ThermoFischer Scientific) (n=32 [SN neurons]), n=30 [VTA neurons], n=24 [LC region], n=30 [SN region] and n=36 [VTA region]) in the High Technology Unit from Vall d'Hebron Research Institute (VHIR-UAT). Clariom D mouse microarrays assess >214,000 transcripts mapping to both coding and non-coding transcripts. RNA reverse transcription is initiated at the poly-A tail as well as throughout the entire length of the RNA molecule enabling the amplification of intact, partially degraded, and compromised RNA samples (starting from 100pg of RNA). Also, Clariom D assays localize to both introns and exons, which enables not only the identification of a mean expression value per coding or non-coding transcript, but also the identification of differential splicing events within the same transcript.

Differential expression analysis (DEA) and Biological Significance Analysis (BSA).

Each region was processed in independent microarray experiments and both genotype and age variables were distributed evenly in the different experimental bathes. All experimental groups included approximately half of the animals from each sex. Basic transcriptomic data analysis was performed by the Statistics and Bioinformatics Unit at Vall d'Hebron Research Institute (UEB-VHIR) using the statistical language "R"(R version 3.6.3 (2020-02-29), Copyright (C) 2018 The R Foundation for Statistical Computing), and the libraries developed for the microarray analysis in the Bioconductor Project (Bioconductor)(Gentleman, Carey, Huber, Irizarry, & Dudoit, 2005). First, arrays were normalized using the RMA method (Gentleman et al., 2005; Irizarry et al., 2003). The exon level values were averaged to yield one expression value per gene and control probes and genes without a valid EntrezID were filtered out.

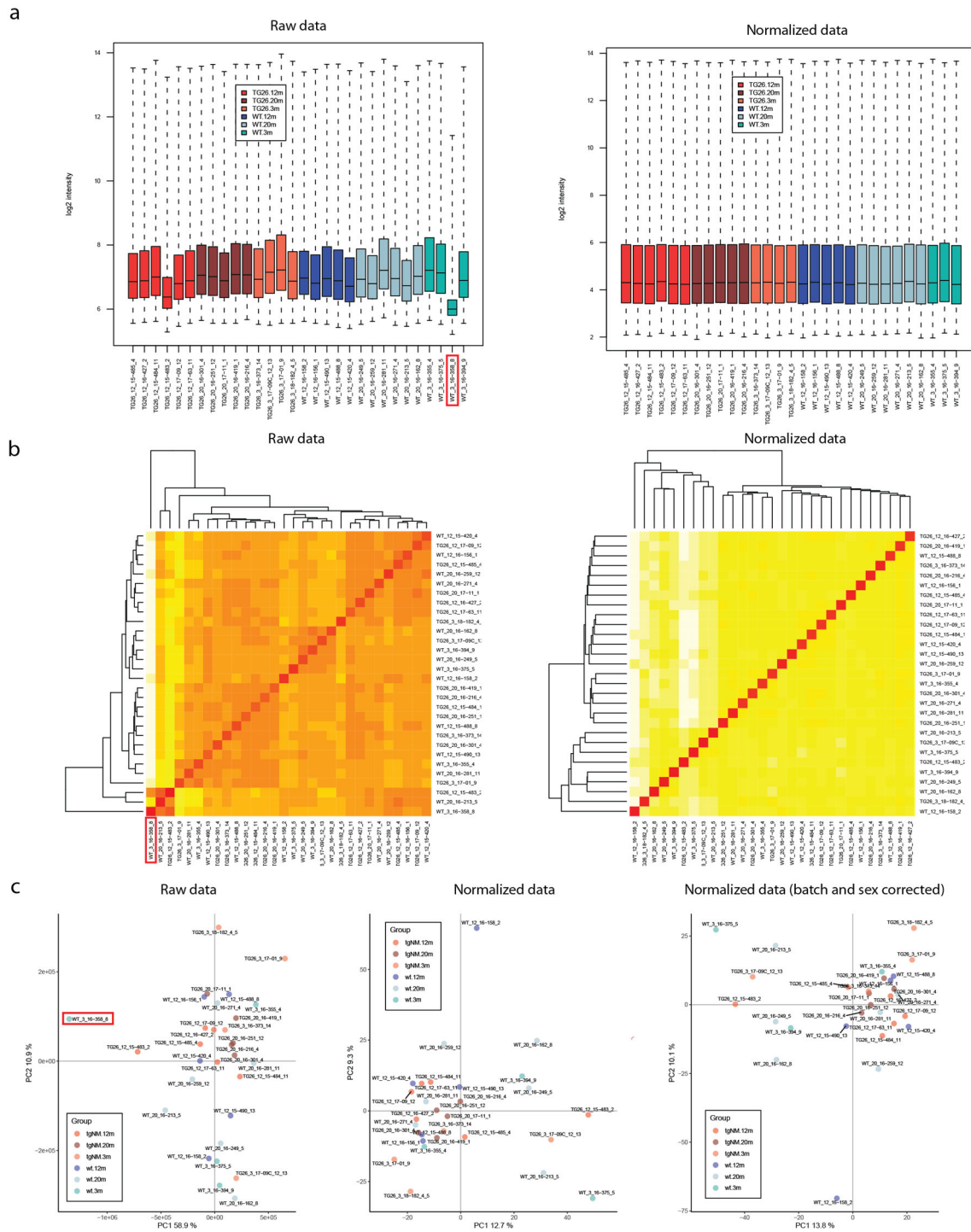


Figure 12. Transcriptomic microarray quality control analysis: Normalization, batch/sex effect correction, and outlier removal. a) Box plot representing signal intensity distributions summaries of the arrays before and after normalization. Typically, one expects the boxes to have similar positions and widths, thus the sample identified with a red rectangle was considered an outlier. **b)** Heatmap depicting distances between arrays and hierarchical clustering of samples. The color scale covers the range of distances encountered in the dataset. Patterns in this plot can indicate clustering of arrays which may be attributable either to biological, experimental or technical effects. Usually distances between arrays should be very similar, thus the sample identified with a red rectangle was considered an outlier. In hierarchical clustering

(lines grouping samples in the heatmap) distances between arrays, as a measure of similarity, are calculated to assess how the samples are grouped among them. c) PCA plots for raw data, normalized data and normalized data after correcting for batch effect and removing outliers (highlighted in red).

Four different outlier-detection approaches (Intensity plots of the raw data, Principal components Analysis (PCA), Heatmap and Hierarchical Clustering) were performed (Fig. 12). Some arrays were considered outliers by more than one criterion and thus, were consequently removed from the posterior analysis [n=3 SN neurons, n=3 VTA neurons, n=1 SN region]. During the pre-processing and normalization step, a slight batch effect was detected in all experimental groups and thus incorporated in the differential expression analysis. Sex effect was also detected in some experimental groups and thus, also incorporated in the analysis (SN, VTA, LC regions).

The analysis to select differentially expressed genes was based on adjusting a linear model with empirical Bayes moderation of the variance. This is a technique similar to ANOVA specifically developed for microarray data analysis by Gordon K Smyth (Smyth, 2004). A threshold of raw p-value <0.01 and $FC > |1.5|$ was applied to identify statistically significant differentially expressed genes (DEGs).

Biological Significance Analysis (BSA) was performed using the gene set enrichment analysis (GSEA) function and the *Gene-Ontology (GO)* and *Reactome* databases. A correction for multiple comparisons was applied for statistical significance [False Discovery Rate (FDR) threshold <0.05].

GSEA software. For the GSEA analysis comparing tgNM SN region/neurons dataset with the public dataset from Smajic, et al. 2022, we used the GSEA software (Mootha et al., 2003; Subramanian et al., 2005). We used the assay annotations file from Affymetrix (Clariom_D_Mouse.r1_MSigDB.v7.1_REMAPPED_PATCH), sample signals and phenotype labels for the SN neurons transcriptomic microarray dataset and performed GSEA (gene set-based permutations, n=1000) with the default settings. Enrichment plots were generated from GSEA software results and ggplot using R software.

Enrichment plots of specific gene sets (ShinyGO). Plots showing GO terms enriched in DEGs identified in all NM pigmented areas (pan-regional) and SN and VTA-specific DEGS were obtained using ShinyGO website (<http://bioinformatics.sdstate.edu/go/>).

Alternative Splicing Analysis. For alternative splicing analysis we used the Transcriptome Analysis Console (TAC 4.0, ThermoFisher Scientific). Microarray raw

files (CEL files) together with sample attributes for each region were uploaded. Outliers identified in the previously performed DEA were excluded from the analysis. The required library files were downloaded and installed (*MTA-1_0 version 2 Updated Transcript CSV- TaqMan Best Coverage Assay Information Added- MTA-1_0*). Batch effect was included in the analysis and comparisons for each age and region were performed. The specific parameters set for the identification of statistically significant Splicing Events were: exon FDR P-value: <0.05 ; exon splicing index: $\geq|2|$; expressed in both conditions: TRUE; exon expressed in at least one condition: TRUE.

Correlation analysis (ROAST). ROAST is a gene set test that allows for gene-wise correlation between two DEA (Wu et al., 2010). We used this test to compare DEA in the tgNM model (SN region and neurons at different ages) to published studies characterizing transcriptomic profiles in human PD postmortem samples. These studies were obtained from the public database NCBI GEO Datasets (GSE7621, GSE20164, GSE20163, GSE20292, GSE20333, GSE20141, GSE24378). The alternative hypothesis considered in this statistical test depends on whether the DEGs in the data set are expected to change in the same direction in the compared datasets or not, resulting in three different p-values representing three different alternative hypotheses tested: genes changing in the same direction in human as they do in mouse (up direction and down direction) and genes changing in mixed (up or down) directions. In our analysis, only mixed p-values are shown for simplification. Also, ROAST was used to compare the DEA performed in the tgNM model to 8 standardized PD-related gene sets from different databases, where no gene expression direction is assigned to the genes (High-priority PD genes (PUKAI), PD gene set (PUKAI), ClinVar Gene-Phenotype Associations, DISEASES Curated Gene-Disease Association Evidence Scores, DISEASES Experimental Gene-Disease Association Evidence Scores, GAD Gene-Disease Associations, GWAS Catalog SNP-Phenotype Associations, GWASdb SNP-Disease Associations).

12. Lysosomal enzymatic activity

Lysosomal enrichment. Freshly dissected samples were resuspended in sucrose 0,25M and kept at 4°C during all the procedure. Homogenization was performed gently with a douncer and the homogenate centrifuged 6800g for 5min. The supernatant was further centrifuged 17000g for 10min. The resulting pellet was washed with sucrose 0,25M and centrifuged again 17000g for 10min. The pellet was resuspended with lysis buffer (TRIS

20mM pH=7.5, EDTA 1mM, NaCl 150mM, Triton 1%) mixed with protease phosphatase inhibitors (Cell signaling #5872S) for enzymatic activities. Protein quantification was performed with BCA (Pierce BCA Protein Assay Kit, Thermo Scientific #23227).

Enzymatic activity determination. For enzymatic activities assessments, a 96-well plate was used with 5 μ g of protein per well. GBA activity was measured in technical duplicates while Beta-hexosaminidase and Alkaline phosphatase activities were measured in single assessments. Duplicate values with a CV \geq 0.05 were removed. Mean absolute absorbance from blank measurements was subtracted from samples mean absolute absorbance. Mean values of tgNM were normalized to sex-matched wt values from each experiment to avoid sex bias. Normalized values from three independent experiments were assembled together for data representation and analysis.

Glucocerebrosidase activity (GBA). Samples were resuspended in McIlvaine's buffer (0.2 M citrate/phosphate buffer pH 5.4) containing 0.25% Triton X-100, 22 mM of the activator sodium taurocholate hydrate (SIGMA, 86339), and 5 mM of the fluorescent substrate 4-Methylumbelliferyl β -d-glucopyranoside (M363; Sigma-Aldrich). A sample volume of 100 μ L per well was prepared and transferred to 96-well plates in duplicate and incubated for 5h at 37 $^{\circ}$ C. Next, a stop solution (25 μ L of 0.25 M glycine/NaOH pH 10.4) was added to terminate the reaction, and the liberated 4-methylumbelliferone was measured at λ_{ex} =365nm/ λ_{em} =450nm using an FLx800 spectrofluorimeter (BioTek, Winooski, VT, USA).

Hexosaminidase activity assay. Samples were dissolved in a reaction buffer containing 0.1 M acetate buffer pH 4.4, 1 mM of fluorescent substrate 4-methylumbelliferyl-N-acetyl-B-D-glucopyranoside (M2133; Sigma-Aldrich), and 0.125% Triton X-100 for 1h at 37 $^{\circ}$ C. Stop solution (75 μ L of 2 M glycine/Na₂CO₃) was added to terminate the reaction, and the plate was measured at λ_{ex} =360nm/ λ_{em} =450nm using an FLx800 spectrofluorimeter (BioTek, Winooski, VT, USA).

Acid phosphatase activity assay. Samples were dissolved in citrate buffer solution 0.09 M pH 4.5 and substrate 4-nitrophenyl phosphate (1 tablet/2.5 mL buffer) (N9389; Sigma-Aldrich) for 1h at 37 $^{\circ}$ C. Stop solution (200 μ L 0.5 N NaOH) was added to terminate the reaction, and the plate was measured at λ =405 nm using an ELx800 spectrophotometer (BioTek).

13. ELISA

Protein extraction from brain dissections. Protein was extracted from SN-VTA and LC bulk dissections from wt and tgNM animals using a Omni Tissue Homogenizer (TH) with ProcartaPlex Cell Lysis Buffer (#EPX-99999-000, Invitrogen-ThermoFisher) and the addition of protease/phosphatase inhibitor cocktail (Cell Signaling #5872S). After centrifugation (16.000g for 10min at 4°C), the supernatant was collected and stored at -80°C for further analysis. Protein samples were quantified using the BCA method (Pierce BCA Protein Assay Kit, Thermo Scientific #23227).

ELISA for Cytokines in brain dissections. 250µg from SN-VTA protein lysates and 150µg of LC protein lysates were analyzed using the Cytokine 10-Plex Mouse ProcartaPlex™ Panel 1B (#EPX100-26091-901, Invitrogen) (ENA-78 (CXCL5), G-CSF (CSF-3), IFN alfa, IL-1 alfa , IL-3, IL-15/IL-15R , IL-28 , IL-31 , LIF , M-CSF) and a specially designed custom 8-plex ProcartaPlex Cytokine Array (IL-17A, IFN-gamma, IL-1beta, IL-10, IL-6, MIP-1alpha, MCP-1, TNF-alpha). ELISA was read using Magpix instrument (Luminex) at the specific spectrally unique signatures from the ELISA dyed beads. Cytokine concentration was then normalized to protein loaded for each well, leading to pg cytokine/µg protein values.

Serum extraction. For serum extraction, animals were anesthetized with isoflurane 5% and placed horizontally. After opening the thoracic cavity, a direct intracardiac puncture was performed for blood collection. Approximately 500ul of blood were collected into clotting activator tubes (Micro sample tube Serum Gel, 1.1 ml, #41.1500.005, Sarstedt) and kept at room temperature for 30min. After coagulation, tubes were centrifuged at 1500g for 10 min and rapidly stored at -80°C.

ELISA for Cytokines and GPNMB in serum. For cytokine profile characterization in serum samples, serums were diluted 1:2 and then analyzed with the Cytokine 10-Plex Mouse ProcartaPlex™ Panel 1B (#EPX100-26091-901, Invitrogen) (ENA-78 (CXCL5), G-CSF (CSF-3), IFN alfa [30], IL-1 alfa , IL-3 [14], IL-15/IL-15R , IL-28 , IL-31 , LIF , M-CSF) and a specially designed custom 8-plex ProcartaPlex Cytokine Array (IL-17A, IFN-gamma, IL-1beta, IL-10, IL-6, MIP-1alpha, MCP-1, TNF-alpha). ELISA was read using Magpix instrument (Luminex) at the specific spectrally unique signatures from the ELISA dyed beads. Determination of serum GPNMB levels was performed using Mouse Osteoactivin ELISA (Bionova (RayBiotech), #ELM-Osteoactivin-1) following the

manufacturer's instructions. Serum was diluted 1:4 and read at $\lambda=450\text{nm}$ in a Varioskan LUX multimode microplate reader using the SkanIt Software 6.1.

14. Statistical analysis

Statistics. Statistical analyses were performed using GraphPad Prism software (v6, GraphPad Software Inc, USA) using the appropriate statistical tests, as indicated in each figure legend. No statistical methods were used to pre-determine sample size but our sample sizes are equivalent to those reported in previous similar publications⁸⁴. Outlier values were identified by the Grubbs' test (i.e. Extreme Studentized Deviate, ESD, method) in UPLC experiments and by ROUT test in qPCR experiments and excluded from the analyses when applicable. All data is represented as box-and-whisker plots (median, minimum, maximum and interquartile range). Non-parametric tests that do not rely on assumptions about the parameters of the underlying population distribution were performed in all comparisons, considering that the small samples sizes used in our study ($n < 30$, $n = 4-24$ mice/group) are not robust enough to reliably detect normality. Accordingly, differences among means were analyzed either by Kruskal-Wallis ANOVA on ranks, Mann-Whitney test or multiple Mann-Whitey test, as appropriate. When ANOVA showed significant differences, pairwise comparisons between means were subjected to Dunn's post-hoc testing for multiple comparisons. In all analyses, the null hypothesis was rejected at the 0.05 level. When above 0.05, the specific p-value is reported.

RESULTS - CHAPTER 1

RESULTS – CHAPTER 1. Generation and characterization of a new brain-wide NM accumulating rodent model

1. Endogenous expression of melanogenic enzymes in the rodent and human brain

As explained in the introductory section, the process of NM formation is still a matter of debate and it is not clear whether it is enzymatically-controlled, a mere product of DA autoxidation, or a combination of both. In order to elucidate the potential role of melanin-synthesizing enzymes (i.e. Tyr, Tyrp1, Dct or Tyrp2) in brain NM production, we assessed their endogenous expression in human and rodent brain samples by qPCR using Taqman probes (Thermo Fisher Scientific). We detected very low levels of melanin-synthesizing enzymes in wild-type mouse and rat midbrain dissections. Considering both rat and mouse brain samples the expression of melanogenic enzymes was 484 (Tyr), 78 (Tyrp1) and 58 (Tyrp2/Dct) times less than Th expression in the same samples (MeanCT±SD; Tyr=33.9±1.9, Tyrp1=31.3±1.4, Dct=30.9±0.2, Th=25.0±1.2) (Fig. 13a-c). Despite detection of Tyr and melanin-related enzymes expression required very high number of amplification cycles (Fig. 13d), this amplification was absent in negative controls. Confirming the suitability of our method, Tyr expression was confirmed consistently in RNA samples extracted from eyes (as expected from the pigment epithelium) and skin of mice (MeanCT±SD; Eyes Tyr=26.7±0.3, Skin Tyr=36.3±3.6) (Fig. 13e). Low amounts of Tyr expression were found in all neural tissues, while it was absent in other organs like adrenal glands, duodenum and white-blood cells (MeanCT±SD; Tyr=40±0) (Fig. 13e). Tyr cDNA expression detected here was not specifically localized in catecholaminergic regions, but ubiquitously found in all neural tissues. We also assessed TYR expression in human control SN dissections and similar to rodent brains, we detected very low levels of TYR expression in 6 out of 8 individuals tested (Fig. 13f-h, Annex Data Table 1). Considering all individuals tested, TYR expression was on average 63 times less than TH expression (MeanCT±SD:36.2±2.4). No expression was detected in the remaining 2 individuals nor in negative controls (Fig. 13f-h).

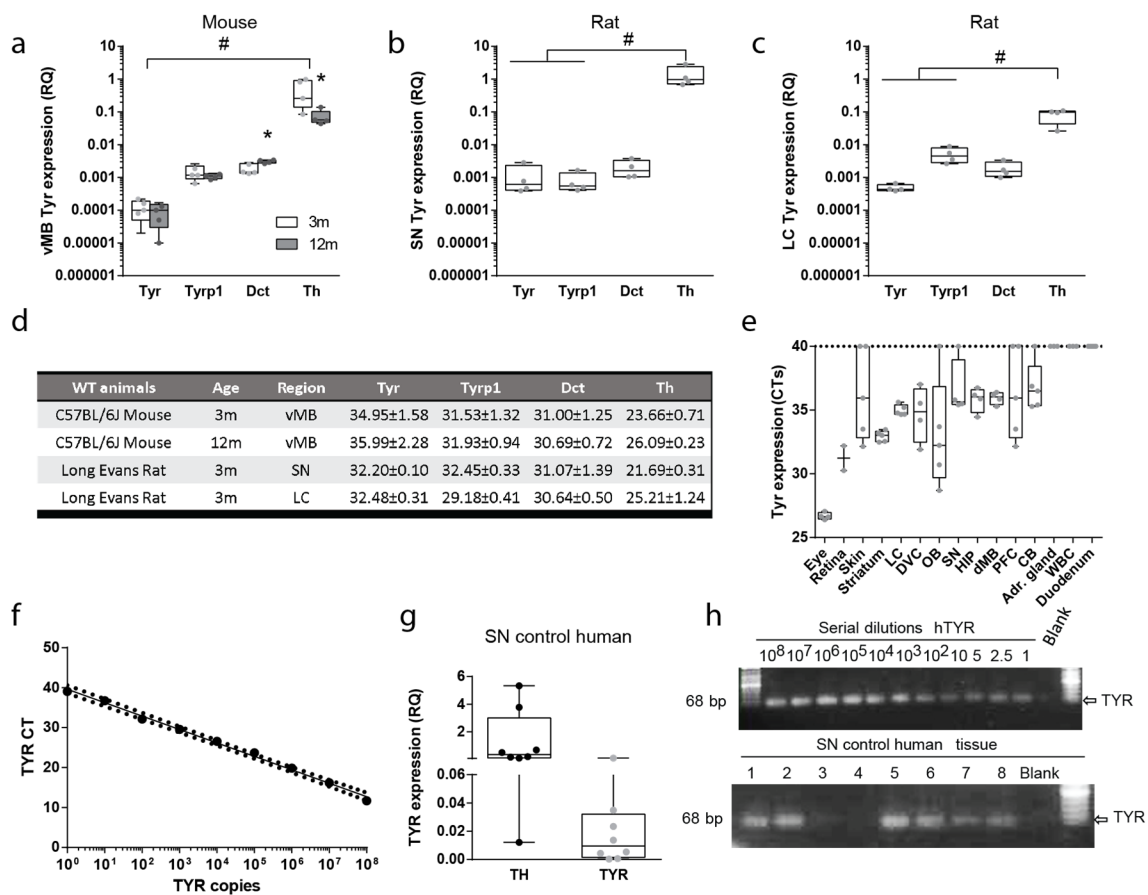


Figure 13. Endogenous expression of melanogenic enzymes in the rodent and human brain. . a-c) Tyrosinase (Tyr), Tyrosinase-related protein 1 (Tyrp1) and Dopachrome tautomerase (Dct, or Tyrp2) expression levels determined by the comparative CT method [relative quantity (RQ), $2^{-\Delta\Delta CT}$] normalized to Gapdh and Rpl19 endogenous reference genes using 45ng of cDNA in ventral midbrain dissections from C57BL/6J mice at 3m and 12m of age and in Long Evans rat SN and LC at 3m of age. * $p \leq 0.05$ compared to 3m, Mann-Whitney test; # $p \leq 0.05$ compared to Th (Kruskal Wallis, Dunn's multiple comparison test). Mice per age group [n=5(3m), n=5(12m)], rats per age group [n=4(3m), n=4(12m)]. **d)** Cycle thresholds (CT) mean values \pm standard deviation (SD) of expression values shown in (a-c). All non-template controls for the assays used were negative (CT=40). **e)** CT values of Tyr expression in neural and peripheral tissues in wild-type animals at 3m of age using 10ng of cDNA. n=2-5 per region. * $p \leq 0.05$ compared to Adr. gland, WBC and Duodenum (Kruskal-Wallis, Dunn's multiple comparison test). **f)** Serial dilutions of a DNA fragment corresponding to the full-length TYR transcript, obtained by enzymatic digestion from a pCDNA4-TYR plasmid (provided by Dr. T. Hasegawa (Department of Neurology, Tohoku University, Sendai, Japan)), were used as template for a qPCR reaction with the Taqman gene expression assay Hs00165976_m1 (Thermo Fisher Scientific) to specifically detect TYR expression. The graph represents the correlation between the number of TYR molecules and the CT values obtained. Semilog line, R square=0.9952. **g)** Measurement of TYR expression using the comparative CT method [relative quantity (RQ), $2^{-\Delta\Delta CT}$] normalized to an HPRT1 endogenous reference gene in cDNA samples from adult human postmortem SN brain tissue from control individuals (n=8) (Annex Data Table 1). **h)**

Electrophoresis gel loaded with qPCR products from (f-g). In two of the brains (#3 and #4), TYR expression was below the detection levels. No amplification products are detected in non-template controls (blank). Abbreviations: ventral midbrain, vMB; Locus coeruleus, LC; dorsal vagal complex, DVC; olfactory bulb, OB; dorsal midbrain, dMB; hippocampus, HIP; cerebellum, CB; substantia nigra, SN; adrenal gland, Adr. gland; white blood cells, WBC.

Additionally, we determined whether melanogenic-enzymes expression was detected in publically available transcriptomic microarray datasets analyzing postmortem human brain samples from PD and control subjects (Table 7). Indeed, all three enzymes were detected in 20 out of 24 datasets obtained, analyzing different regions including: frontal cortex, striatum, cerebellum, SN, LC and DMNV. In addition, some statistically significant changes in TYR (NM_000372), TYRP1 (NM_000550) and TYRP2 (NM_001922) expression were found between PD and control samples. Specifically, in the two studies analyzing microdissected DA neurons from the SNpc there was increased TYR ($p=0.06$, $p=0.08$), TYRP1 ($p=0.03$) and TYRP2 ($p=0.05$, $p=0.03$) expression in PD compared to controls. Other areas, like striatum, showed decreased expression of TYR in PD compared to controls.

GEO	Brain region(s)	TYR		TRP1		TRP2	
		logFC	p-val	logFC	p-val	logFC	p-val
GSE8397	FC	0.07	0.82	-0.08	0.60	0.17	0.10
GSE20168	FC (BA9)	0.11	0.24	-0.34	0.00	-0.10	0.20
GSE20146	Striatum (Gpi)	0.54	0.53	-0.73	0.40	-1.11	0.17
GSE23290	Striatum (Put)	-0.36	0.05	-0.44	0.01	0.28	0.07
GSE20291	Striatum (Put)	-1.22	0.04	-0.98	0.04	-1.05	0.04
GSE20314	Cerebellum	-0.31	0.32	0.47	0.53	-0.53	0.10
GSE19587	ION	0.04	0.97	0.57	0.51	1.15	0.26
GSE7621	SN	1.00	0.21	0.03	0.94	-0.52	0.27
GSE42966	SN	-0.83	0.09	-0.24	0.42	-1.11	0.11
GSE49036	SN	-0.09	0.17	-0.02	0.78	0.27	0.04
GSE20164	SN	0.24	0.51	0.86	0.02	-1.17	0.05
GSE20163	SN	0.16	0.33	0.34	0.15	0.52	0.04
GSE20292	SN	-0.82	0.17	-0.59	0.19	-0.69	0.14
GSE20333	SN	0.68	0.23	0.83	0.02	0.24	0.56
GSE24378	SN (DA neurons)	1.54	0.06	2.29	0.03	1.18	0.05
GSE20141	SN (DA neurons)	1.51	0.08	0.84	0.37	1.55	0.03
GSE8397	SN lateral	0.11	0.08	0.06	0.03	0.18	0.00
GSE8397	SN medial	0.09	0.19	-0.21	0.22	-0.15	0.14
GSE34516	LC	-0.06	0.79	-0.62	0.00	0.07	0.64
GSE19587	DMNV	0.15	0.86	0.20	0.83	2.58	0.02

Table 7. Expression of melanogenic enzymes in human brain datasets from PD and control samples. The study and the region evaluated are shown, together with the logFC and p-value associated for TYR, TRP1 and TRP2 in that specific study. Analysis was performed with GEO2R and only

microarray studies reporting TYR expression are shown (20 out of 24 GEO datasets analyzed). In four GEO datasets (analyzing Striatum, SN, LC and DMNV) TYR was not detected. Negative fold changes are represented in blue, positive fold changes are represented in light orange. Brodmann area 9, BA9; Internal globus Pallidus, Gpi; Putamen, Put; Inferior olivary nucleus, ION, Substantia Nigra, SN; Locus coeruleus, LC; Dorsal motor nucleus of the vagus nerve, DMNV.

These findings confirm other results showing very low Tyr mRNA levels in rodent and human brains (Tief et al., 1998; Xu et al., 1997). However, the relation between TYR expression and NM formation is still not clear and further experiments are needed to elucidate the potential role of melanogenic enzymes in NM formation in the brain.

2. Generation of tyrosinase transgenic mouse lines

In a recent study, our group demonstrated for the first time that overexpression of the melanin synthesizing enzyme TYR in the rodent SN leads to the formation of human-like NM. This proof-of-concept study opened a new research field addressing the consequences of NM accumulation and its potential role in PD pathophysiology. As a follow up, the group aimed at generating an *in vivo* rodent model that would not only accumulate NM in the SN but in all brain catecholaminergic nuclei in order to assess the multisystemic effect of brain pigmentation in different brain areas.

Together with the Transgenic Animal Unit of the Autonomous University of Barcelona we generated a new transgenic mouse line by classical transgenesis (T. R. Kumar, Larson, Wang, McDermott, & Bronshteyn, 2009). Specifically, pronuclear microinjection of the human TYR cDNA fused to the rat TH promoter was performed into C57Bl6-SJL mouse zygotes. This strategy allows for the constitutive expression of the TYR enzyme restricted to catecholaminergic neurons from early stages of development, since the TH promoter controls the expression of the rate-limiting enzyme for catecholamine synthesis and is first expressed at early embryonic stages (i.e. embryological day E11.5) (Matsushita et al., 2002). Twelve founder mice (Tg-Th-TYR) were obtained, 5 of which were selected by Southern Blot and expanded to generate 5 independent transgenic lines (Tg) named L11, L12, L17, L23, and L26 according to the number of the original founder.

2.1 Initial characterization of distinct tyrosinase transgenic lines

In order to identify the best transgenic line for further assessments, we considered transgene levels and NM accumulation. We measured genomic TYR levels in genomic

DNA obtained from ear punches and TYR gene expression levels in vMB homogenates at two different ages (3m and 12m of age) (Fig. 14a-d). In addition, we evaluated NM macroscopic detection in all Tg lines and quantified its levels in SNpc and LC brain sections (Fig. 14d). Within Tg lines, we obtained different amounts of genomic TYR and cDNA TYR expression levels consistent with the phenotypic display of NM accumulation. For instance, Tg L11 exhibited the lowest levels of TYR, both in genomic copies and cDNA expression, consistent with the absence of macroscopic pigmentation in the SN up to 12m of age. Also, L12 showed low amounts of genomic TYR copies and a high variability of TYR expression, correlating with the appearance of macroscopic pigmentation only at 12m of age. TYR expression variability could possibly be due to different individual characteristics affecting the transgene expression since, at this stage, the mice analyzed were still in a mixed genetic background. Also, some lines showed a trend for increased TYR expression with age, although not significant (Mann-Whitney test between 3m and 12m, not significant). The most stable lines in terms of TYR expression were L17 and L26.

Because of the very low levels of TYR and the absence of macroscopic pigmentation detected in L11 mice, we decided to exclude this line for posterior characterization. Additionally, L17 was excluded because of a sex-segregation phenomenon, possibly due to random transgene insertion into Y chromosome, which made that L17 crossings rendered only Tg males (Davis, Maillet, Miano, & Molkenin, 2012). So, we next quantified the microscopic levels of NM accumulation in the rest of transgenic lines (L12, L23, L26). We used optical densitometry of the NM pigment in Nissl-stained brain sections at three different ages (3m, 12m, 20m). L23 and L26 showed higher levels of intracellular NM accumulation than L12, especially in SNpc neurons (Fig. 14e). Overall, since L26 mice showed higher expression of TYR and higher levels of NM accumulation than L12, combined with a better reproductive performance than L23 mice, we finally selected L26 for further characterization (i.e. transgene levels, neuropathology, neurochemistry, behavior, transcriptome expression).

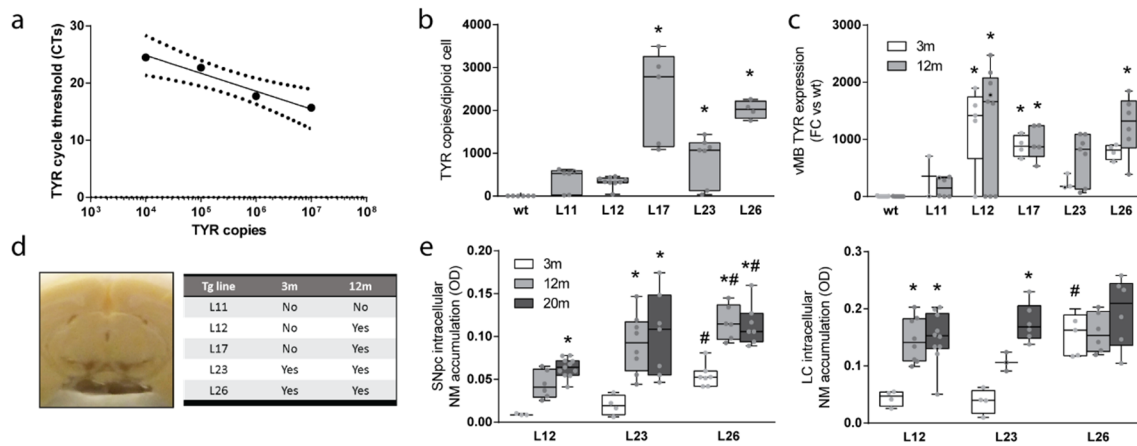


Figure 14. Characterization of the different transgenic mouse lines generated. **a)** Standard curve generated by qPCR showing the cycle threshold (CT) values obtained for TYR in serially diluted concentrations of a TYR plasmid (total number of copies per well). Semi-log line $R^2=0.9635$. **b)** TYR copy number determination (number of copies per diploid cell) in all tg lines using copy-number variant sensitive pre-designed assay [TYR3_CYU62U6, localized within exon 2, Custom Plus (chr11:89191160-89191460GRCh38)] and normalized with the recommended Copy Number Reference Assay, Tfric-VIC in singleplex. TYR CTs were obtained with 10ng of genomic DNA and a conversion factor of 5.77pg per diploid cell was applied for copy number estimation (Deng, McLaughlin, & Klinke, 2017). $*p \leq 0.05$ compared to wt (Kruskal Wallis, Dunn's multiple comparison test). **c)** TYR cDNA expression levels using Hs01099965_m1_FAM assay, calculated by the comparative method (fold change, FC) normalized to Gapdh and compared to wt in ventral midbrain (vMB) tissue homogenates from tg animals at 3m and 12m of age. $*p \leq 0.05$ compared to age-matched wt (Kruskal Wallis, Dunn's multiple comparisons test). 3m [n=11(wt), n=2(L11), n=5(L12) n=4(L17) n=3(L23), n=4(L26)] and 12m [n=7 (wt), n=6(L11), n=9(L12), n=5(L17), n=7 (L23), n=6 (L26)]. **d)** Qualitative description of midbrain macroscopic pigmentation in all tg lines. **e)** Intracellular NM accumulation quantified by optical densitometry of NM granules in SNpc and LC neurons from different transgenic lines at 3m, 12m and 20m of age. $*p \leq 0.05$ compared to same tg line at 3m (Kruskal Wallis, Dunn's multiple comparisons test), $\#p \leq 0.05$, compared to age-matched L12 (in SN, left graph) or age-matched L23 (in LC, right graph) (Kruskal Wallis, Dunn's multiple comparisons test). TgNM 3m [n=3(L12), n=4(L23), n=7(L26)], tgNM 12m [n=6(L12), n=8(L23), n=6(L26)], tgNM 20m (n=11(L12), n=7(L23), n=7(L26)).

2.2 TgNM basic colony characterization

We first confirmed that heterozygous transgenic animals from the L26 line, from now on termed tgNM mice, showed the number of pups per litter expected for their genetic background when crossed with wt animals (C57BL/6J: 5 to 11 (Finlay, Liu, Ermel, & Adamson, 2015)) (Fig. 15a). Also, the litter's genotype distribution consisted in the predicted Mendelian frequency of around 50% of transgenic animals born (Fig. 15b), consistent with a single integration site of the transgene (Davis et al., 2012).

Transgene silencing is a common phenomenon in transgenic mouse lines due to chromatin condensation and can be passed on to next generations (Davis et al., 2012). In order to detect potential transgene silencing in the tgNM mice colony, TYR expression was measured along different generations throughout the entire project. TgNM mice exhibited similar TYR expression levels from 2015 to 2019, including after rederivation of the transgenic line to a new animal facility (Fig. 15c). Although no apparent changes in transgene expression levels were detected within the years analyzed, they should be continuously monitored to prevent transgene silencing.

Another issue that must be considered in transgenic colonies is genetic drift. Some random mutations that reduce pathology burden constitute a selective advantage and might increase over generations if animals are crossed within the same colony. To prevent genetic drift, tgNM mice were back-crossed with C57BL/6J females from Jackson Laboratories on a regular basis. Most experiments shown in this thesis have been performed with mice in a F2-F5 generation and the lines are currently in an F10-F11 generation.

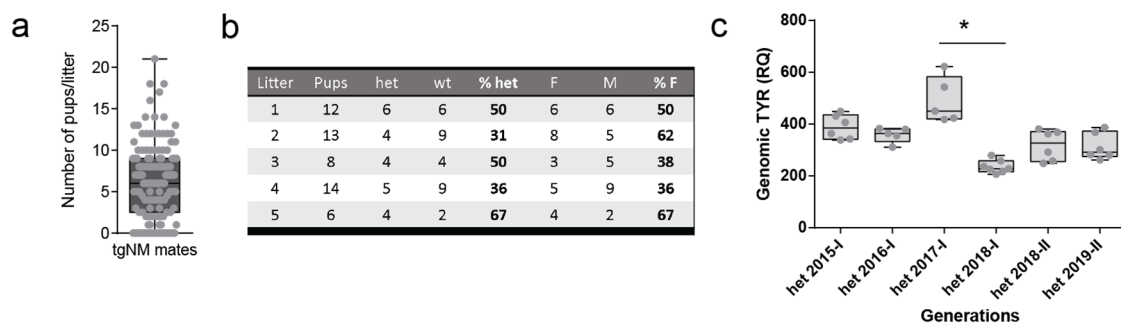


Figure 15. TgNM colony characterization. **a)** Number of pups per litter in heterozygous crossings (n=147). **b)** Representative heterozygous crossing with respective genotypes and sex percentages in the offspring. Five different litters are shown. **c)** Genomic TYR levels calculated by the comparative method normalized to Tfrc (Relative quantity, RQ) in different generations and animal facilities [Original facility (I), New facility after rederivation (II)]. *p<0.05 compared to heterozygous2017-I (Kruskal Wallis Dunn's multiple comparison test).

2.3 Brain TYR expression and NM accumulation in tgNM

To confirm the selective expression of TYR in catecholaminergic brain areas we analyzed the expression of the transgene in distinct dissected brain nuclei from tgNM mice at 12m of age (Fig. 16a). As expected, higher TYR levels were detected within catecholaminergic brain areas compared to non-catecholaminergic regions, with a positive correlation

between TYR and Th expression levels (Fig. 16b). TYR expression was also confirmed at the cellular level by *in situ* hybridization in tgNM brain tissue sections (Fig. 16c).

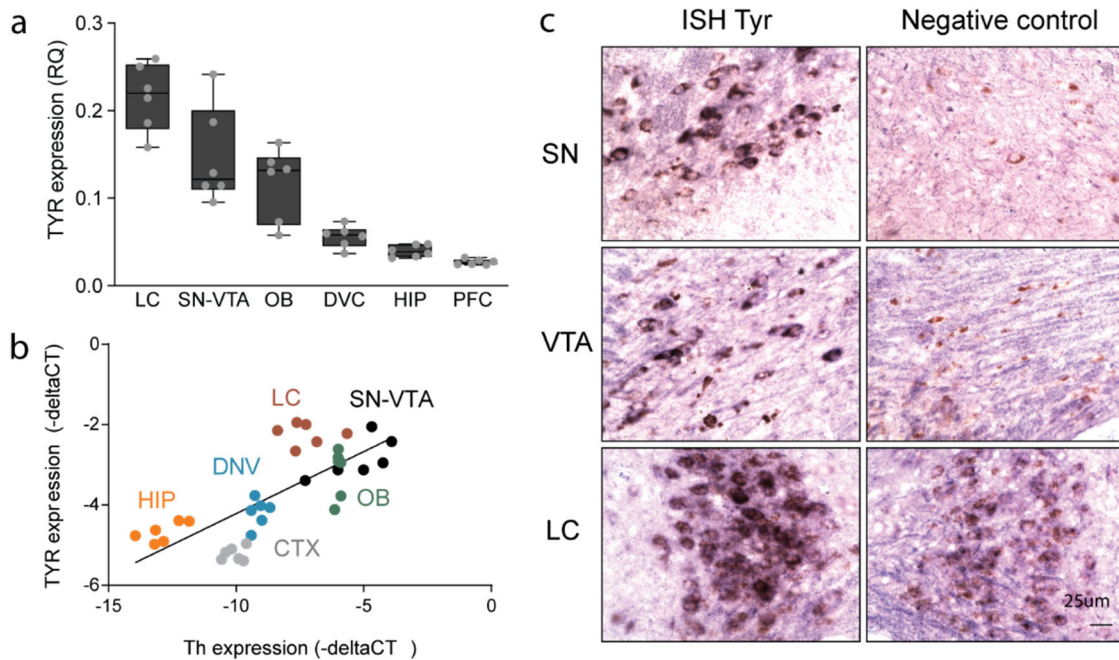


Figure 16. TYR expression within catecholaminergic areas in TgNM. **a**) TYR gene expression normalized to endogenous controls (Gapdh, Ppia, Rpl19) calculated by the comparative method (Relative Quantity, RQ) measured in samples from different catecholaminergic brain areas [Locus Coeruleus (LC), Substantia Nigra-Ventral Tegmental Area (SN-VTA), Olfactory Bulb (OB), Dorsal Vagal complex (DVC)] and non-catecholaminergic [Hippocampus (HIP) and Prefrontal Cortex (PFC)] from adult tgNM (n=6) and wt (n=6) mice. **b**) Correlation between tyrosine hydroxylase (Th) and TYR expression levels in adult tgNM (n=6). * $p \leq 0.05$, $R^2 = 0.5$ (Linear regression). Values are normalized to endogenous controls and shown in the logarithmic scale for correlation (-deltaCT). **c**) In situ hybridization using an antisense probe against TYR in adult tgNM brain sections. A TYR sense probe was used as negative control.

As expected from the previous NM-accumulating model generated (Carballo-Carbajal et al., 2019), macroscopic pigmentation was detected in the midbrain (SNpc and VTA) and in the pons (LC) of tgNM mice, appearing as macroscopically visible dark-brown colored areas in the absence of any staining, mimicking their macroscopic appearance in human specimens (Fig. 17a-c). As in humans, melanized SNpc, VTA and LC from tgNM mice could also be detected macroscopically as hyperintense areas by NM-sensitive high-resolution T1-weighted magnetic resonance imaging (NM-MRI) (Fig. 17a-c). Histologically, NM from tgNM mice appeared as a dark-brown neuronal pigment in H&E-stained sections and stained prominently with the melanin marker Masson-Fontana, similar to melanized human neurons (Fig. 17a, c). Additionally, by clarifying the brain of tgNM mice we clearly visualized the main pigmented nuclei (SNpc-VTA and LC) but

also other NM-containing brain areas like the DVC in the medulla were distinctly seen (Fig. 17c). DVC pigmentation is not easily detected macroscopically as a darkened area in a non-processed brain since the number of pigmented cells and density is much lower than those of SN-VTA and LC (Bucci et al., 2017).

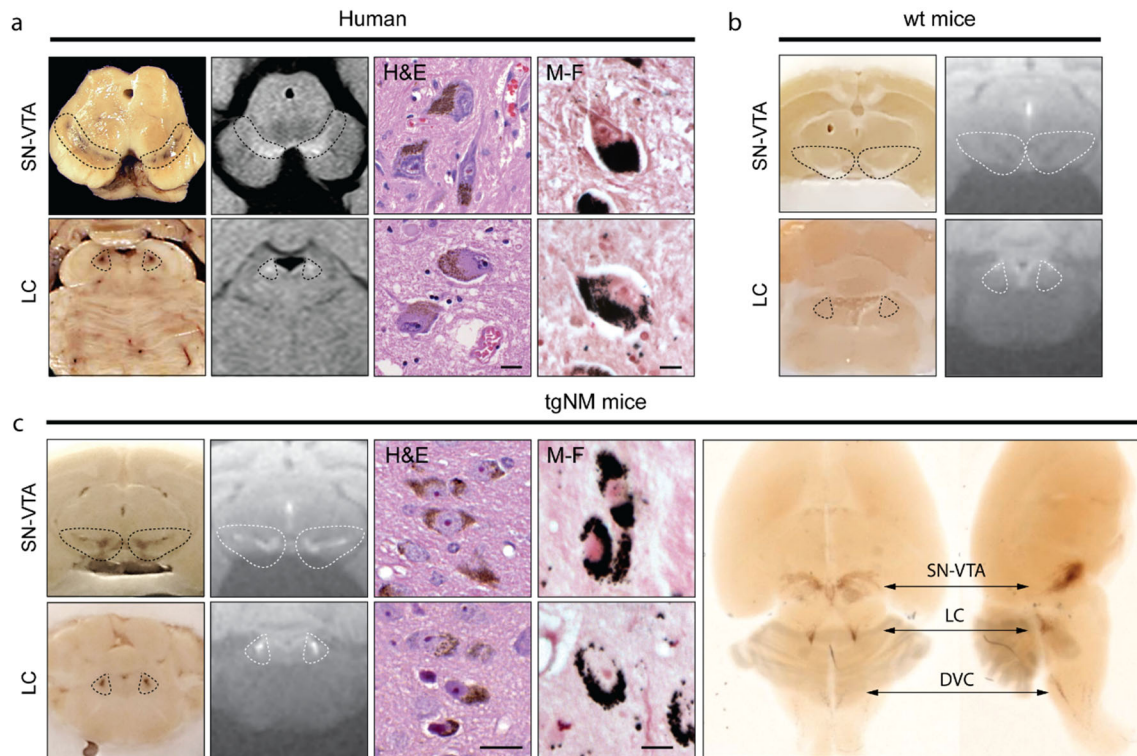


Figure 17. Accumulation of human-like NM in different brain catecholaminergic nuclei. a-c) From left to right, in a healthy human brain(a), and in wt(b) and tgNM(c) mice: unstained macroscopic view of the SN and LC region, NM-sensitive high-resolution T1-weighted magnetic resonance imaging, Hematoxylin&Eosin (H&E) and Masson-Fontana (M-F) stained neurons. In c (*right*), representative images from the macroscopic view of a clarified tgNM brain. Bars represent 20 μm (H&E) and 5 μm (M-F). Substantia nigra and Ventral tegmental area (SN-VTA), Locus coeruleus (LC), Dorsal vagal complex (DVC).

We then performed a microscopic qualitative assessment of all known catecholaminergic neuronal groups (A1-A16) in tgNM mouse brain sections. We detected different pigmented nuclei throughout the brain that showed a clear correspondence to catecholaminergic neuronal groups identified by TH-immunoreactivity in wt mice (Fig. 18 & Table 8). These results show that NM production in tgNM mice is not limited to the major catecholaminergic nuclei but is also present, at varying degrees, in all catecholaminergic cell groups (i.e. A1-A16), thereby mimicking the pattern of human NM distribution (C. Saper & Petito, 1982).

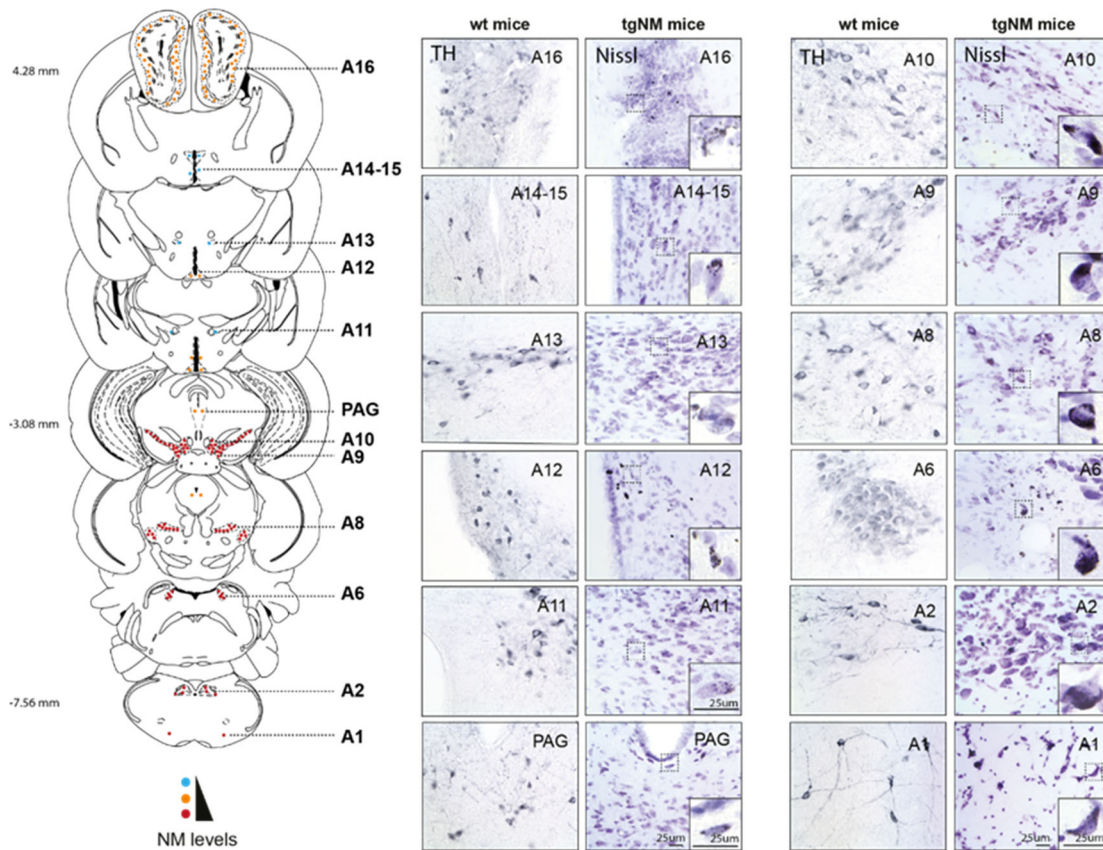


Figure 18. Brain-wide NM distribution in catecholaminergic nuclei. Qualitative brain atlas showing NM accumulation in all catecholaminergic brain groups (A1-A16) in tgNM mice. The number of dots represent the quantity of NM-accumulating cells and dot colors represent the levels of intracellular NM in each area, ranging from very low levels (yellow) to higher levels of NM accumulation (blue).

Region	Name/Location	Neuromelanin levels
A1	Medullary reticular formation	+++
A2	Dorsal Vagal Complex (DVC)	+++
A6	Locus Coeruleus (LC)	+++
A8	Retrorubral field (RRF)	+++
A9	Substantia Nigra (SN)	+++
A10	Ventral Tegmental Area (VTA)	+++
PAG	Periaqueductal gray (PAG)	++
A11	Periventricular nucleus (hypothalamus)	+
A12	Arcuate nucleus (hypothalamus)	++
A13	Zona incerta (thalamus)	+
A14-15	Preoptic periventricular nucleus	+
A16	Olfactory bulb (OB)	++

Table 8. Nomenclature of pigmented catecholaminergic cell groups in tgNM and their qualitatively assessed cytoplasmic NM levels.

To characterize the amount and accumulation rate of NM in specific cell groups with age, we quantitatively assessed the microscopic intracellular levels of NM in the main PD-vulnerable pigmented catecholaminergic cells groups (i.e. SNpc/A9, VTA/A10, LC/A6 and DVC/A2). Intracellular quantification of the optical density of NM in unstained sections of pigmented nuclei were performed in tgNM at three different ages (i.e. young [3-4m], adult [8-12m], old [18-20m]). In these animals, NM exhibits an ascending gradient of accumulation, reaching earlier higher intracellular levels in lower brainstem areas (DVC and LC) than in upper brainstem regions (SNpc and VTA) (Fig. 19a). As in humans (Fedorow et al., 2006), NM in tgNM mice is continuously produced throughout life and progressively accumulates with age until occupying a major portion of the neuronal cytoplasm (Fig. 19b).

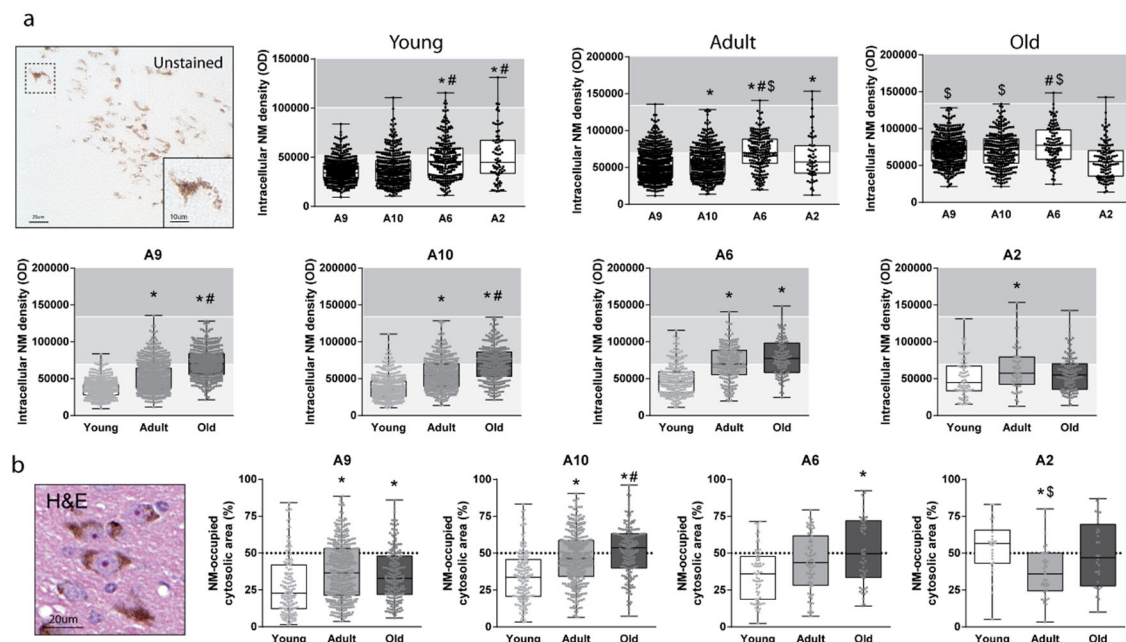


Figure 19. NM accumulation in the main catecholaminergic nuclei in tgNM mice. a) Quantification of intracellular NM optical density in unstained sections (SN/A9, VTA/A10, LC/A6, DVC/A2). Representative image of unstained SN/A9 section. Data is presented per age (upper panels) and per region (lower panels). Dots represent individual neurons. *Upper panels*, * $p \leq 0.05$ compared to A9 # $p \leq 0.05$ compared to A10, \$ $p \leq 0.05$ compared to A2 (Kruskal-Wallis test, Dunn's multiple comparison test). *Lower panels*, * $p \leq 0.05$ compared to young, # $p \leq 0.05$ compared to adult (Kruskal-Wallis test, Dunn's multiple comparison test). $n=6-14$ tgNM for each area at different ages. All neurons with a distinguished visible nucleus were measured within a representative section from each brain area (56-735 neurons for each age and area). **b)** Percentage of NM-occupied cytosolic area [(area occupied by NM/ cell cytosol area) $\times 100$] quantified in H&E stained paraffin sections. * $p \leq 0.05$ compared to young, # $p \leq 0.05$ compared to adult, \$ $p \leq 0.05$ compared to old (Kruskal-Wallis test, Dunn's multiple comparison test) $n=6$ young tgNM, $n=6-7$ adult tgNM, $n=4-5$ old tgNM.

These results indicate that TYR overexpression in tgNM mice models pigmentation in human brain, consisting in the production and accumulation of human-like NM (stained with Masson-Fontana and sensitive to NM-MRI) within all brain catecholaminergic neuronal groups (A1-A16) in an age-dependent manner.

2.4 Consequences of NM accumulation in dopaminergic SN and VTA nuclei

As explained in the introduction, SNpc and adjacent VTA constitute the main catecholaminergic nuclei in the midbrain, are the primary source of NM in the human brain and both show neurodegeneration in PD. However, while SNpc neurons degenerate extensively in PD, loss of VTA neurons is more restricted (Huynh et al., 2021; McRitchie, Cartwright, & Halliday, 1997). Using the newly-developed tgNM mice, we assessed the consequences of intracellular NM build-up in these two subtypes of midbrain DA neurons in terms of viability and function.

2.4.1 Behavioral alterations related to dopaminergic dysfunction

We characterized first the sensorimotor capacities of these animals at different ages (i.e. young [3-4m], adult [8-12m], old [18-20m]), corresponding to progressively increased levels of NM in SNpc and VTA. Adult and old tgNM mice spent more time to cross a horizontal beam (Fig. 20a) and old tgNM mice showed reduced latency to fall in a rotarod test (Fig. 20b), indicating impaired motor coordination and balance. Adult and old tgNM mice also exhibited decreased olfactory acuity to discriminate a lemon essence (Fig. 20c), indicating impaired olfaction. We also noticed a significant absence of vocalizations during the performance of the behavioral tests that was already present in young tgNM mice (Fig. 20d), a phenotype related to cranial sensorimotor deficits previously reported in α -synuclein Tg mice as an early pre-motor manifestation (Grant et al., 2014). Other behavioral tests, such as grip strength and novel object recognition, were also performed but did not reveal any differences between genotypes at any age (Fig. 20e,f).

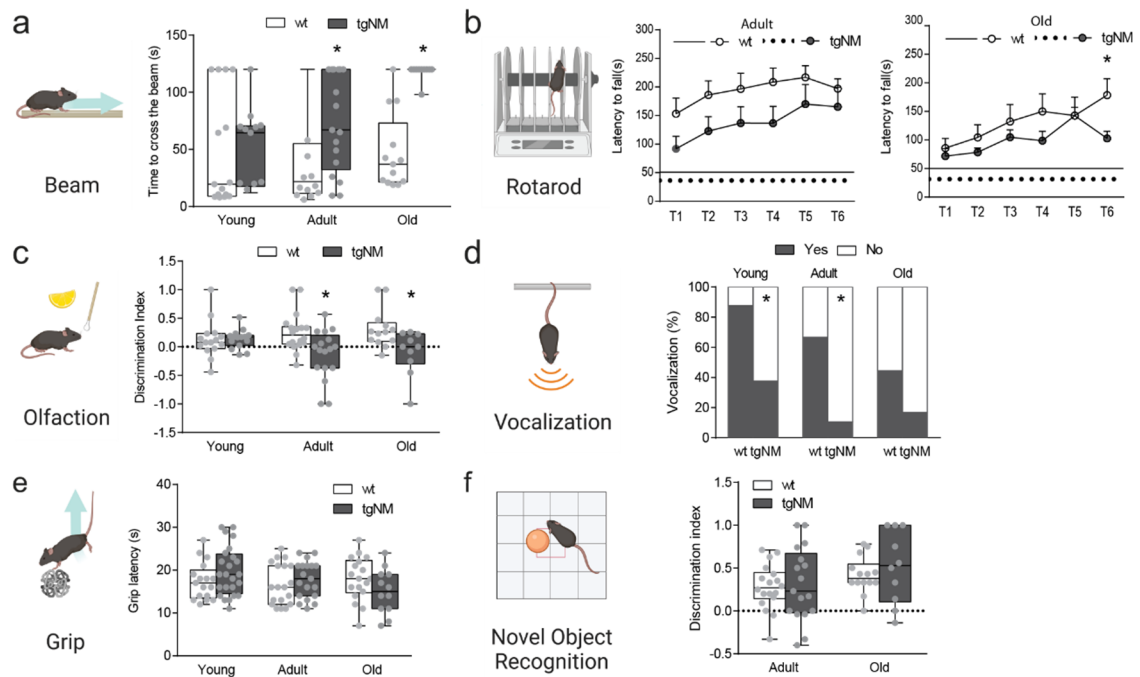


Figure 20 .Dopaminergic-related behavioral analysis in tgNM mice. a) Beam test; Quantification of the time to cross the beam on the training day compared with the time to cross the beam on the second day. * $p \leq 0.05$ compared to age-matched wt (Mann-Whitney test). Young [n=15(wt), n=13(tgNM)], Adult [n=14(wt), n=17(tgNM)], Old [n=13(wt), n=10(tgNM)]. **b)** Rotarod test; Latency to fall (s) at different acceleration rates. Mean latency to fall during the learning period is represented with a continuous line for wt and with a dashed line for tgNM. Young [n=8(wt), n=10(tgNM)], Adult [n=11(wt), n=10(tgNM)], Old [n=7(wt), n=10(tgNM)]. * $p \leq 0.05$, Multiple Mann-Whitney test. **c)** Olfaction test; Quantification of the discrimination index (time on lemon vs time on water). * $p \leq 0.05$ compared to age-matched wt (Mann-Whitney test). Young [n=15(wt), n=15(tgNM)], Adult [n=18(wt), n=17(tgNM)], Old [n=13(wt), n=10(tgNM)]. **d)** Vocalizations represented as % of vocalizing animals during a behavioral test in which animals are suspended by the tail. Young [n=16 (wt), n=16 (tgNM)], Adult [n=21 (wt) n=19(tgNM)], Old [n=18(wt), n=12 (tgNM)]. * $p \leq 0.05$ compared to wt, contingency table (Fisher's exact test). **e)** Quantification of grip latency time (s). Young [n=17(wt), n=24(tgNM)], Adult [n=19(wt), n=19(tgNM)], Old [n=18(wt), n=12(tgNM)]. Mann-Whitney tests tgNM compared to age-matched wt not significant. **f)** Quantification of the relative discrimination index in the Novel Object Recognition test. Adult [n=18(wt), n=17(tgNM)], Old [n=14(wt), n=10(tgNM)]. Mann-Whitney tests tgNM compared to age-matched wt not significant.

2.4.2 Dopaminergic dysfunction and early neurodegenerative changes in SN-VTA from tgNM mice

We then performed stereological cell counts of TH-positive neurons in tgNM mice and detected a decrease in the number of TH-immunopositive cells (TH-positive-NM-negative + TH-positive-NM-positive) at an adult and old age. However, no decrease was found when considering total DA neurons including TH-immunopositive and TH-immunonegative melanized neurons (TH-positive-NM-negative + TH-positive-NM-

positive + TH-negative-NM-positive) (Fig. 21a-b). Thus, tgNM mice showed TH phenotypic loss but no actual cell death in SN nor in VTA. TH-immunonegative pigmented neurons are also conspicuously observed in human PD and aged postmortem brains (Korzhevskii et al., 2021; Nagatsu, Nakashima, Ichinose, & Kobayashi, 2019) and represent dysfunctional neurons at early stages of degeneration (Carballo-Carbajal et al., 2019; E. Hirsch et al., 1988) (Fig. 21b). The loss of DA phenotype in SN and VTA neurons was confirmed by decreased transcript expression of DA markers in SN-VTA dissected tissue from old tgNM mice (Fig. 21c). Also, similar to humans, NM-accumulating neurons within the total population of DA neurons increased with age, being around 87% in SN and 85% in VTA in adult tgNM (Mean \pm SD; 87 \pm 6 in SN, 85.1 \pm 6 in VTA) and reaching 97% in SN (mean \pm SD; 97.1 \pm 1.3) and 93% in VTA (mean \pm SD;92.7 \pm 3.2) in old tgNM animals (Fig.21b).

The presence of eNM, which derives from dying neurons, is typically observed in PD and aged postmortem brains (Beach et al., 2007; Ishikawa, 1998; Korzhevskii et al., 2021; Langston et al., 1999). It is indicative of an active and ongoing nerve cell loss (Langston et al., 1999) and is even used as a marker of neurodegeneration in postmortem studies (Ohm et al., 2020). Thus, we next performed stereological counts of eNM granules in tgNM mice at different ages. Indeed, tgNM brain sections showed considerable amounts of eNM granules that increased with age in parallel to the phenotypic loss of Th expression (Fig. 21d). These findings further suggested an incipient neurodegenerative process ongoing in this model.

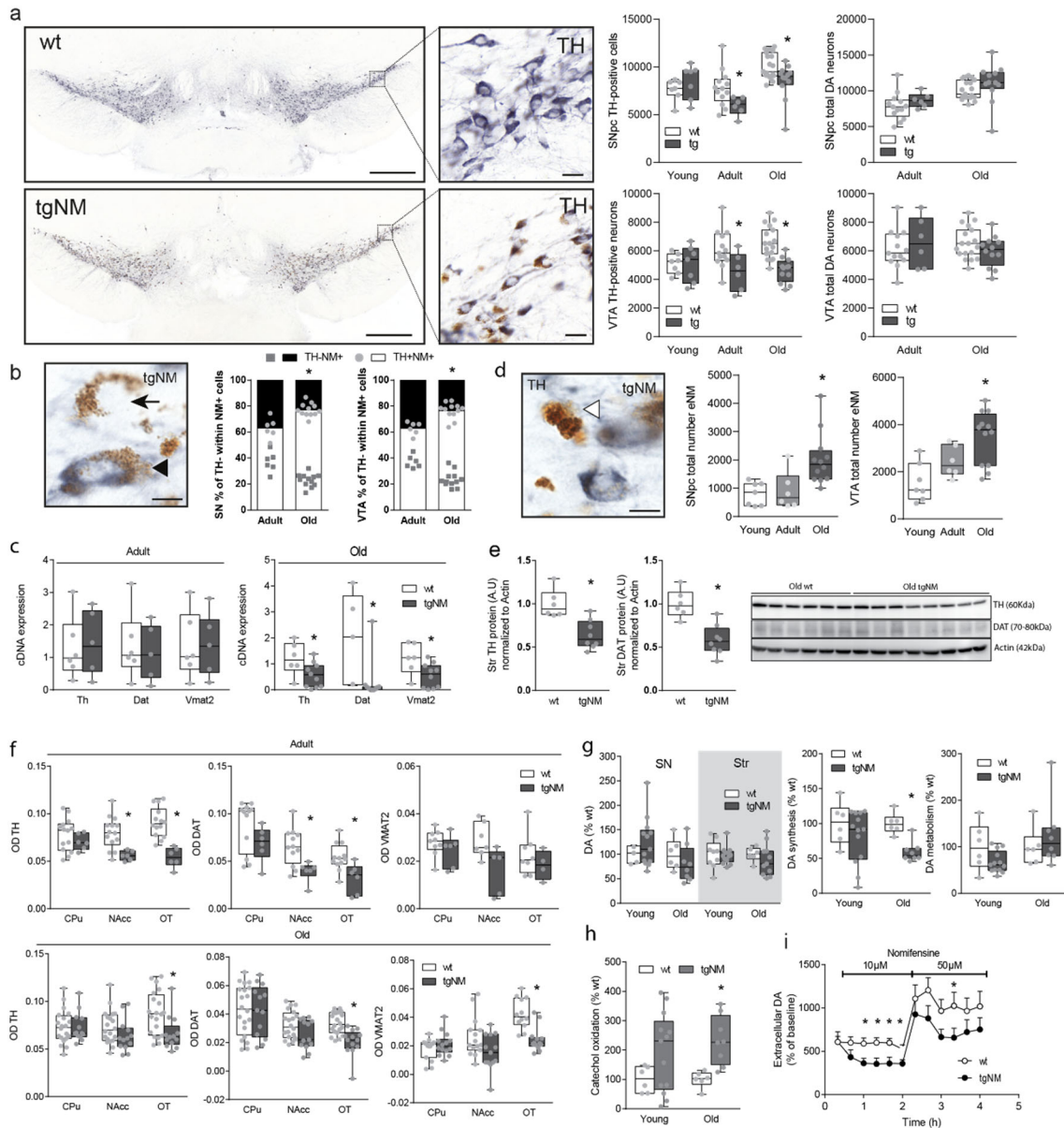


Figure 21. Dopaminergic dysfunction in tgNM mice. **a** *Left*, SNpc and VTA sections immunostained for TH [blue; inset, higher magnification of TH-positive neurons from wt and TgNM mice showing NM (dark brown)]. Scale bars, 500 μ m, 20 μ m (inset). *Right*, Stereological cell counts of SNpc and VTA TH-positive neurons at different ages and of total DA neurons (TH-positive NM-negative + TH-positive NM-positive + TH-negative NM-positive) in adult and old tgNM mice (wt total DA neurons are the same as TH-positive neurons but are represented for comparison). * $p \leq 0.05$ compared to age-matched wt (Mann-Whitney test). SNpc and VTA: Young [n=7(wt), n=7(tgNM)], Adult [n=13(wt), n=6(tgNM)], Old [n=19(wt), n=12(tgNM)]. **b** *Right*, TH immunostained SNpc section showing TH-NM+ cells (arrow) and TH+NM+ cells (arrowhead) in tgNM mice. *Left*, Quantification of the distinct TH-immunoreactive NM-positive neurons in SN and VTA measured as the percentage (%) of each phenotype within the total DA neurons counted in (a). *(TH+NM-), #(TH+NM+), \$(TH-NM+) $p \leq 0.05$ compared to adult (Mann-Whitney test). **c** Expression of DA markers in SN-VTA homogenates by quantitative PCR. * $p \leq 0.05$ compared to age-matched wt (Mann-Whitney test). Young [n=4(wt), n=5(tgNM)], Adult [n=6(wt), n=6(tgNM)], Old [n=6(wt), n=12(tgNM)]. **d** *Right*, TH immunostained SNpc section showing extracellular NM (eNM, white

arrowhead) aggregates in tgNM mice. TH is stained in blue and unstained NM appears as brown. Scale bar, 20 μm . *Left*, Stereological quantification of extracellular NM (eNM) aggregates in tgNM SNpc and VTA regions. $*p \leq 0.05$ compared to young and adult (SN) and compared to young (VTA) (Kruskal Wallis, Dunn's multiple comparison test). SNpc and VTA: Young [n=7(tgNM)], Adult [n=6(tgNM)], Old [n=12(tgNM)]. **e**) Western blot of DA markers (TH and DAT) in striatal protein homogenates from tgNM mice compared to wt littermates. Immunoblot densitometry was normalized to β -actin expression levels. Kilodaltons, kDa; Arbitrary units, A.U. $*p \leq 0.05$ compared wt (Mann-Whitney test). n=6(wt), n=8(tgNM). **f**) Quantification of striatal dopaminergic markers (TH, DAT, VMAT2) by optical densitometry (OD) after immunostaining in adult (top) and old (bottom) tgNM mice compared to wt littermates. $*p \leq 0.05$ compared to age-matched wt (Mann-Whitney test). Adult TH [n=14(wt), n=6(tgNM)], DAT [n=12(wt), n=6 (tgNM)], VMAT [n=7-9(wt), n=4-6 (tgNM)]; Old TH [n=20(wt), n=13(tgNM)], DAT [n=20 (wt), n=13 (tgNM)], VMAT [n=12-15 (wt), n=13-14 (tgNM)]. **g,h**) Ultra-high performance liquid chromatography (UPLC) measurement of DA levels in striatal and SN/VTA homogenates, catechol oxidation, DA synthesis (DA+NE+DOMA+VMA+ 3MT+DOPAC/L-DOPA) and DA metabolism (DOPAC+3MT/DA) in SN/VTA homogenates from tgNM mice compared with wt littermates at young and old ages. $*p \leq 0.05$ compared to age-matched wt (Mann-Whitney test). SN; Young [n=6(wt), n=13(tgNM)], Old [n=6(wt), n=8(tgNM)], Striatum (Str); Young [n=9(wt), n=13(tgNM)], Old [n=6(wt), n=11(tgNM)]. **i**) Striatal DA release in adult tgNM and wt mice measured by in vivo microdialysis in the striatum following nomifensine treatment at different concentrations (10 μM and 50 μM). n=7 (wt), n=7 (tgNM). $*p \leq 0.05$ compared to respective wt (Multiple Mann-Whitney tests). Micromolar, μM .

The reported changes in SN and VTA neuronal bodies were accompanied by reduced expression of DA markers in striatal fibers (i.e. TH, DAT, and VMAT2), as measured by western blot in dissected tissue and by optical densitometry in immunostained histological sections (Fig. 21e,f). While total DA levels were not changed in tgNM, as analyzed by ultra-performance liquid chromatography (UPLC) in striatal and SN-VTA tissue homogenates, these animals exhibited alterations in DA metabolic pathways, including decreased DA synthesis and increased catechol oxidation, the latter producing DA oxidized species acting as NM precursors (Herrera, Muñ Oz, Steinbusch, & Segura-Aguilar, 2017) (Fig. 21g,h). Additionally, we evaluated whether striatal DA release was impaired in tgNM mice by performing in vivo microdialysis. Striatal DA release following chemical stimulation by nomifensine, a NA-DA- reuptake inhibitor, resulted in decreased release of DA in tgNM compared to wt, suggesting a dysfunctional nigrostriatal pathway in tgNM at an adult age (Fig. 21i). All these DA alterations (i.e. decreased TH-immunoreactive neurons in SN and VTA, abundant eNM, decreased TH-immunoreactive fibers and impaired DA release in striatum) concur with the appearance of behavioral alterations at an adult age in tgNM mice.

2.4.3 PD-like neuropathological alterations in SN-VTA from tgNM mice

Neuropathologically, NM-containing SNpc and VTA neurons from tgNM mice exhibited intracellular inclusion bodies as typically seen in PD and aged human brains, including cytoplasmic LB-like inclusions and nuclear MB (Fig. 22a). Similar to humans (Kuusisto et al., 2003a), both LB and MB were immunopositive for p62, a common component of neuropathological inclusions. More than 50% of p62-positive cytoplasmic inclusions were also immunopositive for α -synuclein (Fig. 22a). Inclusion body formation was restricted to melanized neurons and was not observed in wt mice. The number of both LB and MB was less prominent in old tgNM, suggesting that inclusion-containing neurons may be those that preferentially start to degenerate. In agreement with this, the number of neuronal inclusions in PD brains at advanced stages of the disease is much lower than that observed in early PD cases (H. Braak et al., 2003). TgNM mice also exhibited inflammatory changes in the SNpc and VTA, including increased numbers of reactive Iba1-positive microglial cells and GFAP-positive astrocytic cells (Fig. 22b), the first surrounding eNM as it occurs in postmortem PD brains (Ishikawa, 1998; Langston et al., 1999).

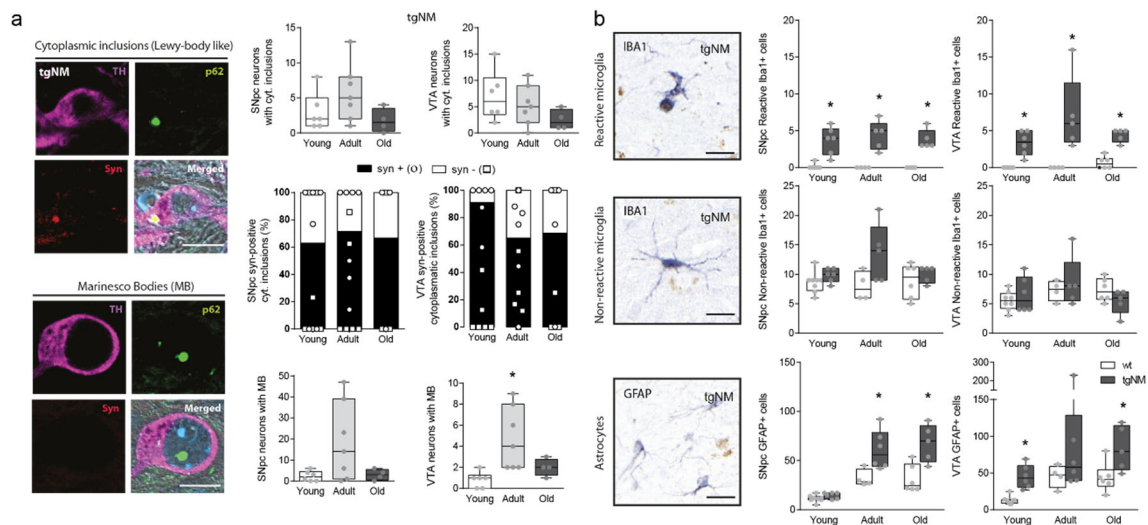


Figure 22. Neuropathological alterations in SN-VTA from tgNM mice. **a**) Representative images of SNpc and VTA sections from tgNM mice exhibiting NM-laden neurons with Lewy Bodies (LB, upper panel) and Marinesco Bodies (MB, lower panel) detected by immunofluorescence with TH (purple), p62 (green) and synuclein (syn) (red). Nuclei are stained with Hoechst (blue) and NM appears as dark grey in the merged image. Photomicrographs correspond to 5- μ m-thick sections. Scale bar, 10 μ m. Quantification of NM-laden neurons with p62-positive total intracytoplasmic (cyt.) Lewy Body-like inclusion bodies (LB) (upper panel) and nuclear Marinesco bodies (MB) (lower panel). n=6 (young tgNM), n=7 (adult tgNM), n=4 (old tgNM) *p<0.05 compared to young (Kruskal Wallis test; Dunn's multiple correction test). Proportion of α -synuclein-positive inclusions in tgNM at different ages (middle panel). Kruskal Wallis not significant. n=7 (young tgNM), n=7 (adult tgNM), n=4 (old tgNM). **b**) *Left*, Representative image of Iba1-

immunohistochemistry (blue), showing reactive (top) and non-reactive (middle) Iba1-positive cells, and GFAP immunohistochemistry (bottom, blue). Scale bar, 20 μ m. *Right*, Quantification of Iba-1 reactive and non-reactive Iba1-positive cells, and GFAP-positive cells in SNpc and VTA sections from tgNM mice and wt littermates at different ages. Young [n=8(wt), n=6(tgNM)], Adult [n=4(wt), n=5 Iba1/6 GFAP (tgNM)], Old [n=6(wt), n=5(tgNM)]. *p \leq 0.05 compared to age-matched wt (Mann-Whitney test).

Overall, our results reveal that progressive NM production in SNpc and VTA from tgNM mice is associated to PD-like DA functional alterations (e.g. phenotypic TH downregulation, impaired DA release, sensorimotor deficits) and neuropathological changes (e.g. LB-like pathology, eNM, neuroinflammation) in the absence of overt neurodegeneration, thus reproducing prodromal/early PD stages.

2.5 Consequences of NM accumulation in noradrenergic LC nucleus

Another major area consistently affected in PD is the LC, a highly melanized region in the pons that constitutes the main source of NA modulation in the brain. The LC is among the earliest sites of LB pathology and its degeneration is postulated to precede SNpc involvement in PD (Betts et al., 2019; H. Braak et al., 2003; Knudsen et al., 2018) and to account for non-motor PD symptoms, including sleep disturbances, anxiety-depression and cognitive decline (Bari, Chokshi, & Schmidt, 2020). Thus, we next examined the consequences of NM buildup in noradrenergic LC neurons.

2.5.1 Behavioral alterations related to noradrenergic dysfunction

First, we assessed the functional integrity of the LC in anxiety-related behavior (open field test), aversive memory (step-down test) and sleep (polysomnography) paradigms. In the open field, adult tgNM mice spent more time and travelled more distance in the periphery than their wt littermates, despite moving at a similar speed, indicative of an anxiety-related behavior (Fig. 23a). In the step-down test, old tgNM animals showed altered memory consolidation of an aversive stimuli (Fig. 23b). TgNM mice descended from the platform before wt animals because they did not remember receiving an electric shock the day before after descending from the platform. This impaired memory consolidation is indicative of a deficit in the LC-amygdala-dependent learning and memory process. Performing polysomnography enabled the characterization of three distinct wake-sleep cycles or vigilance states: (i) paradoxical sleep or REM sleep, which is characterized by a desynchronized cortical activity with muscle atonia; (ii) slow-wave-

sleep, which is characterized by a synchronized cortical activity associated with an immobility; and (iii) wakefulness, which is characterized by a desynchronized cortical activity associated with a high muscle activity (Peyron, Arthaud, Villalba, & Fort, 2020). Adult tgNM mice already exhibited reduced amount of both paradoxical sleep and slow-wave sleep at the expense of wakefulness, indicative of an altered sleep-wake cycle (Fig. 23c). Also, an in-depth analysis of paradoxical sleep or REM sleep evidenced significantly reduced numbers of bouts concomitant with a significant increase of their duration in both adult and old tgNM mice (Fig. 23c), indicative of an irreversible dysregulation of paradoxical sleep ultradian rhythm.

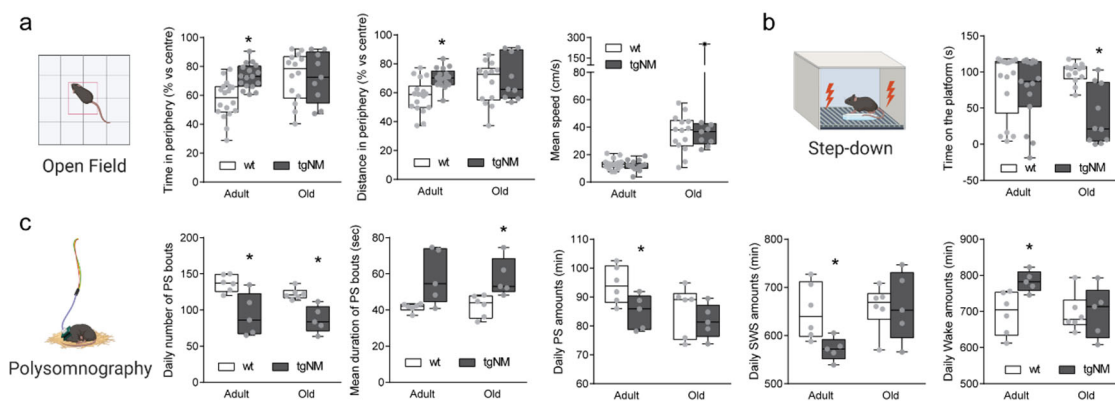


Figure 23. Noradrenergic-related behavior analysis in tgNM mice. a) Open field test; percentage (%) of time spent and distance travelled in the periphery compared with the center of an open field and mean speed during the test. * $p \leq 0.05$ compared to age-matched wt (Mann-Whitney test). Adult [n=18(wt), n=17(tgNM)], Old [n=14(wt), n=9(tgNM)]. **b)** Step down test; time spent on the platform (time second trial-time first trial). * $p \leq 0.05$ compared to age-matched wt (Mann-Whitney test). Adult [n=17(wt), n=15(tgNM)], Old [n=13(wt), n=10(tgNM)]. **c)** Polysomnography; number and mean duration (seconds) of bouts during Paradoxical sleep (PS) state and amounts of the distinct vigilance states (minutes per day) (PS, Slow Wave Sleep [SWS] and Wake). * $p \leq 0.05$ compared to age-matched wt (Mann-Whitney test). Adult [n=7(wt), n=8(tgNM)], Old [n=6(wt), n=5(tgNM)].

2.5.2 Neurodegeneration and PD-like neuropathology in LC from tgNM mice

As performed for midbrain DA neurons, we also performed stereological cell counts of TH-immunoreactive neurons in the LC of tgNM mice. Stereological cell counts revealed a marked reduction of TH-positive cells in the LC of tgNM mice compared to wt littermates already at a pubertal age (1m) (Fig. 23a). In contrast to the SNpc and VTA above, the reduction in TH-positive cells in the LC corresponded to an actual neuronal loss as indicated by stereological cell counts of total noradrenergic LC neurons, including TH-immunopositive and TH-immunonegative melanized neurons (Fig. 24a). We also

found abundant eNM concomitant with cell loss (Fig. 24b). LC neurodegeneration resulted in a significant reduction in total NA levels, already present at a young age, in both LC and its projecting areas such as the prefrontal cortex (PFC), as measured by UPLC in dissected tissue homogenates (Fig. 24c). These animals also exhibited reduced NA synthesis and increased NA metabolism (Fig. 24d), supporting altered NA neurotransmission. As in SNpc and VTA neurons, melanized LC neurons also exhibited p62-positive cytoplasmic inclusions but almost no MB were detected. The highest number of LC cytoplasmic inclusions were found at pubertal ages and decreased afterwards, possibly due to the high degree of neuronal loss in this area with only a few remaining neurons left (Fig. 24e). Most of these inclusions were also immunoreactive for α -synuclein (Fig. 24e). Concomitant to neurodegeneration, tgNM mice LC exhibited marked inflammatory changes from a young age, including microglial activation and astrogliosis (Fig. 24f).

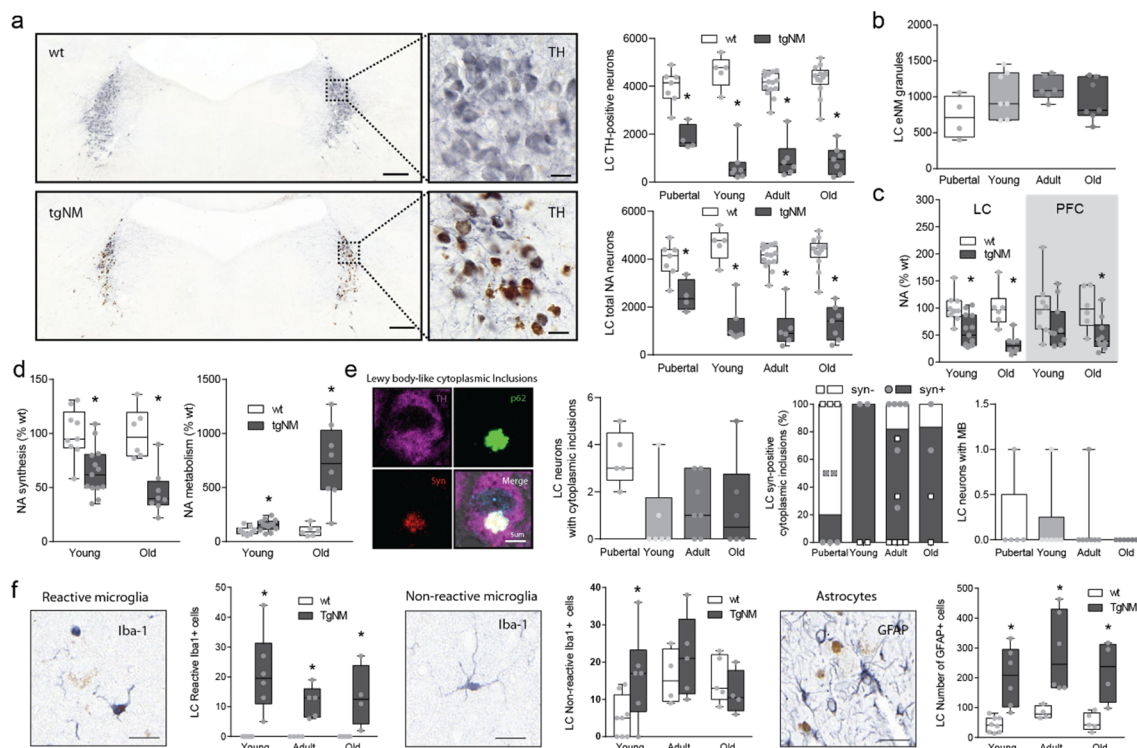


Figure 24. LC neurodegeneration and PD-like neuropathology in tgNM mice. a) Right, LC sections immunostained for TH [grey/blue; inset, higher magnification of TH-positive neurons from wt and tgNM mice showing NM (dark brown)]. Scale bars, 200 μ m, 20 μ m (inset). *Left*, Stereological cell counts of LC TH-positive neurons (upper graph) and total NA neurons (TH-positive NM-negative + TH-positive NM-positive + TH-negative NM-positive) (lower graph) at different ages (in wt animals the number of total NA neurons equals the total number of TH-positive neurons but are represented for comparison). * $p \leq 0.05$ compared to age-matched wt (Mann-Whitney test). Pubertal [n=7 (wt), n=4(tgNM)], Young [n=5 (wt), n=6(tgNM)], Adult [n=14(wt), n=5(tgNM)], Old [n=12(wt), n=7(tgNM)]. **b)** Stereological cell counts of

eNM granules from tgNM mice and wt littermates at different ages. Pubertal [n=7(wt), n=4(tgNM)], Young [n=5 (wt), n=7(tgNM)], Adult [n=14(wt), n=6(tgNM)], Old [n=13(wt), n=7(tgNM)]. Kruskal Wallis test, Dunn's multiple correction test not significant. **c-d**) UPLC measurement of NA (c) levels, NA synthesis (NA/DA) and NA metabolism (DOMA+VMA/NA) (d) in LC and prefrontal cortex (PFC) homogenates from tgNM mice and wt littermates at young and old ages. *p≤0.05 compared to its age-matched wt (Mann-Whitney test). Young LC [n=9(wt), n=13(tgNM)], Old LC [n=6(wt), n=8(tgNM)]. Young PFC [n=9(wt), n=13(tgNM)], Old PFC [n=6(wt), n=10(tgNM)]. **e**) Representative images of LC sections from tgNM mice exhibiting NM-laden neurons with LB-like inclusions detected by immunofluorescence with TH (purple), p62 (green) and α -synuclein (red). Nuclei are stained with Hoechst (blue) and NM appears as dark grey in the merged image. Quantification of NM-laden neurons with p62-positive α -synuclein(syn)-positive/negative total intracytoplasmic inclusion bodies (lewy body-like inclusions, LB) (left), proportions of α -synuclein(syn) reactivity in LC p62-positive inclusions (middle) and p-62 positive nuclear inclusions (marinesco bodies, MB) (*right*). Kruskal Wallis test, Dunn's multiple correction test not significant. n=5 (pubertal tgNM), n=6 (young tgNM), n=7 (adult tgNM), n=6 (old tgNM). **f**) Representative images of tgNM Iba-1 and GFAP immunohistochemistry and quantification of reactive and non-reactive Iba-1-positive cells and GFAP-positive cells. *p≤0.05 compared to age-matched wt (Mann-Whitney test). Young [n=8(wt), n=6(tgNM)], Adult [n=4(wt), n=5(tgNM)], Old [n=5(wt), n=4(tgNM)].

Altogether, our results reveal that tgNM mice exhibit an early and extensive degeneration of the LC (i.e. loss of NA neurons and decreased levels of NA in LC and PFC), linked to non-motor alterations (i.e. anxiety-like behavior, fear-associated memory deficits and sleep disturbances) that precedes nigral DA dysfunction, as it has been proposed to occur in PD.

2.6 Consequences of NM accumulation in cholinergic and serotonergic nuclei

In addition to catecholaminergic pigmented areas, non-pigmented neurons also degenerate in PD, in particular cholinergic neurons from the NBM and PPN (Giguère et al., 2018). These two cholinergic nuclei are vastly connected with the brainstem catecholaminergic areas (French & Muthusamy, 2018; Gratwicke et al., 2013; Mena-Segovia & Bolam, 2017; Tubert, Galtieri, & Surmeier, 2019) (Fig. 25a), and it has been hypothesized that their degeneration in PD may be related to the degeneration of the interconnected melanized neurons from the SNpc, VTA and LC (Bensaid et al., 2016; Szego et al., 2011). We evaluated the integrity of NBM and PPN in tgNM mice and detected a significant decrease in the total number of ChAT-positive neurons in both areas in old tgNM mice (Fig. 25a). However, total acetylcholine (Ach) levels were not decreased in the cortex of old tgNM animals, and they were actually increased in the PPN

itself (Fig. 25b, upper panel). This might be explained by compensatory mechanisms due to the loss of generalized DA innervation since these two neurotransmitters are known to be highly dependent on each other (Lester, Rogers, & Blaha, 2010; Spehlmann & Stahl, 1976).

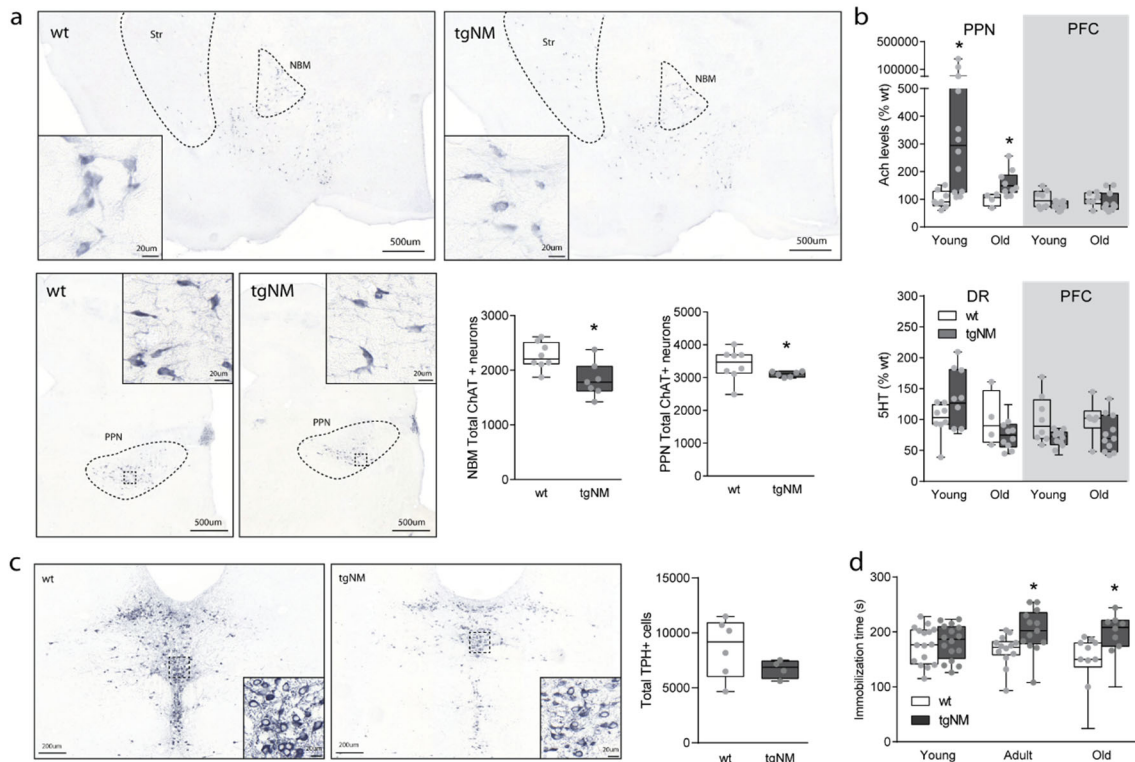


Figure 25. Cholinergic and serotonergic alterations in tgNM mice. **a**) Representative NBM (upper) and PPN (bottom left) sections immunostained for choline acetyltransferase (ChAT). Scale bar 500 μ m, scale bar insets 20 μ m. Bottom right, Stereological cell counts of NBM and PPN ChAT-positive neurons in old wt and tgNM mice. * $p \leq 0.05$ compared to age-matched wt (Mann-Whitney test). NBM [n=8(wt), n=7 (tgNM)] and PPN [n=8(wt), n=6 (tgNM)]. **b**) PPN and prefrontal cortex (PFC) acetylcholine (Ach) levels and DR and PFC serotonin (5HT) levels determined by UPLC in young and old animals. * $p \leq 0.05$ compared to age-matched wt (Mann-Whitney test). Young PPN-DR [n=8 (wt), n=12 (tgNM)], Old PPN-DR [n=4(wt) n=11(tgNM)], Young PFC [n=8(wt), n=13(tgNM)], Old PFC [n=6(wt), n=11(tgNM)]. **c**) Left, Representative dorsal raphe (DR) sections immunostained for tryptophan hydroxylase (TPH). Scale bars represent 200 μ m, Scale bar insets represent 20 μ m. Right, Stereological cell counts of DR TPH-positive neurons and TPH optical densitometry in old wt and tgNM mice. n=6(wt), n=4(tgNM). Mann-Whitney test not significant. **d**) Immobilization time (seconds, s) in the tail suspension test performed in young, adult and old wt and tgNM mice. * $p \leq 0.05$ compared to age-matched wt (Mann-Whitney test). Young [n=16(wt), n=16(tgNM)], Adult [n=15(wt), n=13(tgNM)], Old [n=11(wt), n=11(tgNM)].

Another non-pigmented brain area where variable degrees of cell death have been reported in PD postmortem brains is the one constituted by the different Raphe Nuclei (RN) (Giguère et al., 2018), although the only study using stereological cell counting methods

did not find any cell loss (Cheshire et al., 2015). The RN are the primary source of serotonin (5HT) in the brain, a neurotransmitter that has been linked to anxiety and depression that are common non-motor symptoms affecting 30-35% of PD patients (Aarsland, Páhlhagen, Ballard, Ehrt, & Svenningsson, 2012; Chuquilín-Arista, Álvarez-Avellón, & Menéndez-González, 2020; Miquel-Rio et al., 2022). We assessed the integrity of the dorsal raphe (DR) nucleus in tgNM mice. Stereological assessment of tryptophan hydroxylase (TPH)-positive serotonergic DR neurons did not show statistically-significant differences in old tgNM mice, although these numbers were overall lower than in wt littermates (Fig. 25c). Of note, some TPH-positive DR cells (~3%) contained NM, which is compatible with these neurons being also catecholaminergic, as previously described (McDevitt et al., 2014; Trulson, Cannon, & Raese, 1985). No significant changes were found in 5HT levels in the DR nor in the PFC of tgNM mice by UPLC (Fig. 24b, lower panel). Still, tgNM mice exhibited increased immobilization time in the tail suspension test, indicative of a depressive-like behavior (Cryan, Mombereau, & Vassout, 2005) (Fig. 25d).

Overall, our results show that catecholaminergic deficits linked to NM build-up in tgNM mice are accompanied by structural alterations in two additional cholinergic neuronal groups (PPN and NBM) and by functional alterations that might be linked to serotonergic neuronal groups, which are also affected in PD.

2.7 Consequences of NM accumulation in medullary nuclei

Medullary neuronal groups have also been reported to degenerate in PD brains. Cell loss has been reported in two distinct types of neurons; cholinergic cells from the DMNV (Gai et al., 1992; Halliday et al., 1990) and catecholaminergic NM-containing A2 neurons in DVC (Gai et al., 1993; Halliday et al., 1990; Rajput & Rozdilsky, 1976; C. B. Saper et al., 1991). These pigmented neurons, which are part of the dorsomedial medullary A2 group and present both NA and adrenergic cells, together with the cholinergic neurons of the DMNV provide the major integrative center for the mammalian autonomic nervous system.

2.7.1 PD-like neuropathology in DVC from tgNM mice

We next sought to characterize the viability of DVC medullary pigmented neurons in tgNM mice (Fig 26a). Stereological cell counts of TH-positive, total catecholaminergic neurons and cholinergic neurons (ChAT-positive) in DVC sections showed no consistent

decreases in tgNM mice compared to wt littermates (Fig. 26b). However, only a small percentage (~10%) of TH-positive neurons in the DVC were actually pigmented. This is consistent with the incomplete pigmentation of the catecholaminergic A2 cell group in humans, showing between 15% and 65% of NM-containing cells, depending on the rostrocaudal level (Halliday et al., 1988). Hence, we then evaluated only the pigmented TH-positive neurons and found a significant decrease of these cells with age, as well as in the total number of pigmented DVC neurons (i.e. TH-immunopositive and TH-immunonegative melanized neurons) (Fig. 26c). This was accompanied by extensive eNM and microglial activation, in absence of astrogliosis (Fig. 26d,e). In adult mice, the decreased number of pigmented TH-positive cells mostly represented a loss of the DA phenotype, which is typical of early stages of degeneration. A few LB-like cytoplasmic inclusions were also detected in melanized DVC neurons at early, pubertal ages (1m of age) (Fig. 26f).

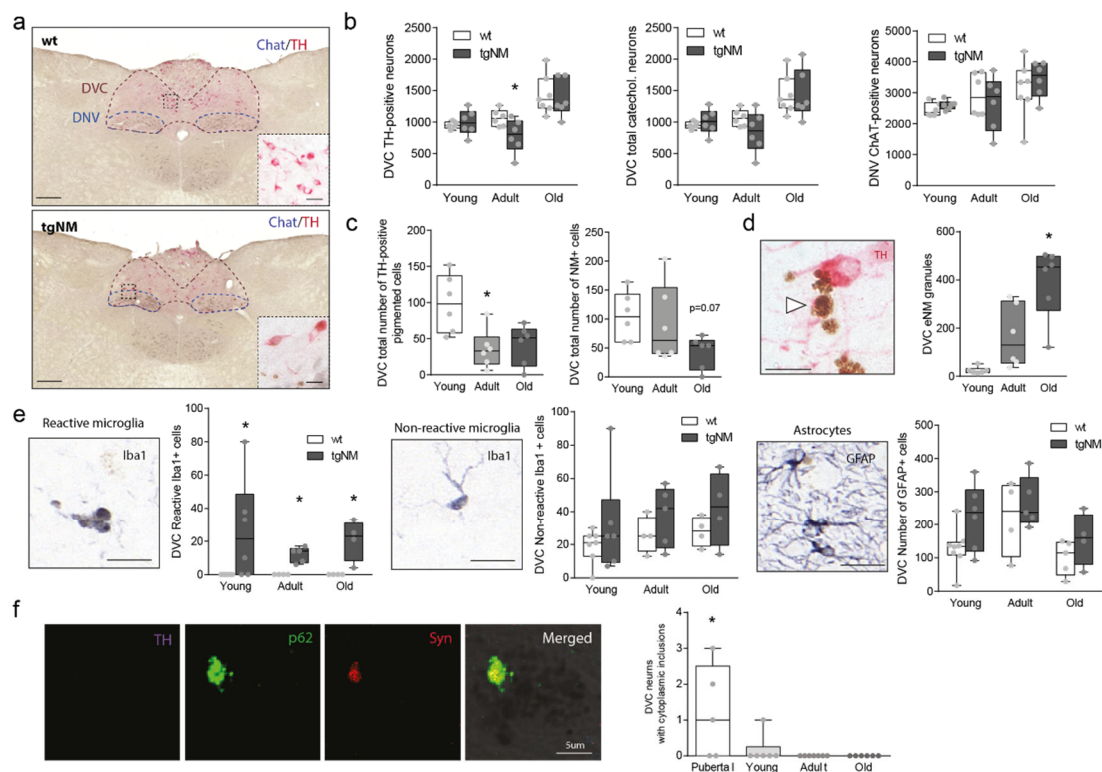


Figure 26. Medullary catecholaminergic nuclei alterations in tgNM mice. **a) Left,** Medullary sections immunostained for tyrosine hydroxylase (TH; ImpactRED-red) and choline acetyltransferase (ChAT; VectorSG-darkblue). Scale bar represents 200 μ m, 10 μ m (insets). **Right,** Representative images of TH-positive (arrow) and TH-negative (black arrowhead) NM-positive neurons and extraneuronal NM granules (eNM, white arrowhead). Scale bar represents 25 μ m. **b)** Stereological cell counts of TH-positive, total catecholaminergic and ChAT-positive cells. * $p \leq 0.05$ compared to age-matched wt (Mann-Whitney test). Young [n=5(TH)/6(ChAT)(wt), n=6(tgNM)], Adult [n=6(wt), n=6(tgNM)], Old [n=7(wt) n=6(tgNM)]. **c)**

Stereological cell counts of DVC pigmented TH-positive neurons and total of DVC pigmented catecholaminergic neurons (including TH-immunopositive and TH-immunonegative melanized neurons). * $p \leq 0.05$ compared to young tgNM (Kruskal Wallis test, Dunn's multiple correction test). $n=6$ (young tgNM), $n=6$ (adult tgNM), $n=6$ (old tgNM). **d**) Stereological quantification of the number of eNM granules in A2 neuronal group in tgNM animals at different ages. * $p \leq 0.05$ compared to young tgNM (Kruskal Wallis test, Dunn's multiple correction test). Young [$n=6$ (tgNM)], Adult [$n=6$ (tgNM)], Old [$n=6$ (tgNM)]. **e**) Representative images and quantification of Iba1-positive reactive and non-reactive cells and GFAP-positive cells in tgNM and wt mice at different ages. * $p \leq 0.05$ compared to age-matched wt (Mann-Whitney test). Young [$n=7$ (Iba1)/8(GFAP)(wt) $n=6$ (tgNM)], Adult [$n=4$ (wt), $n=5$ (tgNM)], Old [$n=4$ (Iba1)/5(GFAP)(wt), $n=4$ (tgNM)]. **f**) Representative image of a cytoplasmic lewy-body like inclusion in a TH-negative neuron (*right*) and quantification of cytoplasmic inclusions in tgNM at different ages. * $p \leq 0.05$ compared to adult and old (Kruskal Wallis test, Dunn's multiple correction test). $n=6$ (young tgNM), $n=7$ (adult tgNM), $n=6$ (old tgNM).

2.7.2 Peripheral alterations associated to medullary brainstem nuclei dysfunction

Considering the reported loss of the DVC A2 pigmented cells with age, we then sought to characterize the behavioral correlates of a diminished catecholaminergic A2 neuronal activity in these animals. The vagus nerve, with its cell bodies in DMNV, innervates most of the major internal organs including the heart, lungs and gastrointestinal tract (Fig. 27a). The sensory input from this organs is conveyed by the A2 neurons that send projections to DMNV to regulate a coordinated response to peripheral stimulus including processing and coordination of cardiovascular and respiratory reflex responses (Zoccal, Furuya, Bassi, Colombari, & Colombari, 2014)

Thus, we assessed the main autonomic parameters (cardiovascular and respiratory) known to be regulated by these brainstem medullary nuclei in tgNM mice. Old tgNM mice showed decreased heart rate, despite no apparent alterations in blood pressure (Fig. 27b-c). These animals also exhibited increased respiratory rate measured by assessing diaphragmatic movements (Fig. 27d). Dysautonomic alterations, in particular cardiovascular and respiratory, are reported to be more frequent causes of death in PD than in age-matched controls (Ben-Shlomo, Marmot, & Ben-Shlomo, 1995; Pinter et al., 2015). We then evaluated life expectancy in tgNM mice and detected a significantly decreased lifespan in these animals compared to their wt counterparts (Fig. 27e).

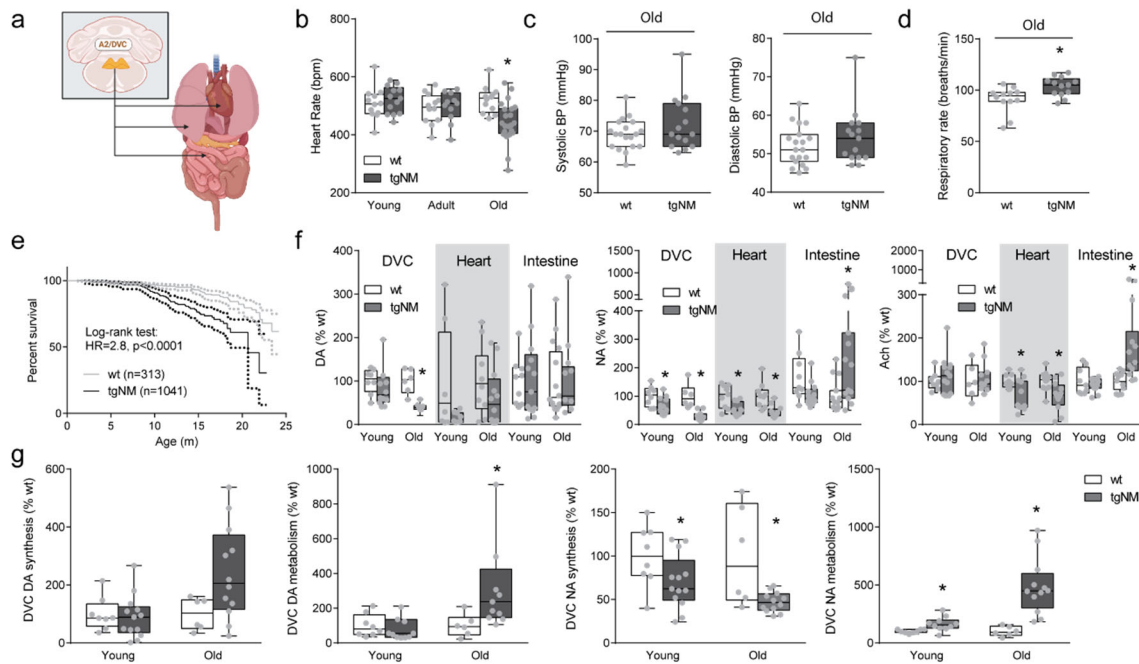


Figure 27. Peripheral alterations in tgNM mice. **a)** Schematic diagram of the peripheral connections with the DVC. **b)** Heart rate measurements of tgNM and wt animals at different ages. * $p \leq 0.05$ compared to age-matched wt (Mann-Whitney test). Young [n=12(wt) n=13(tgNM)], Adult [n=12(wt), n=11(tgNM)], Old [n=12(wt), n=22(tgNM)]. **c)** Systolic and diastolic blood pressure in old mice. n=19(wt), n=15 (tgNM), Mann-Whitney test not significant. **d)** Respiratory rate assessed at an old age. n=12 (wt), n=13(tgNM). * $p \leq 0.05$ compared to age-matched wt (Mann-Whitney test). **e)** Survival analysis of tgNM mice compared with wt littermates. Animals used for experimental purposes are considered as censored and natural deaths are considered as events. $p \leq 0.0001$, Log-rank (Mantel-Cox) (HR= 3.576, 95%CI of ratio 2.317 to 5.519) test and Gehan-Breslow-Wilcoxon (HR= 2.806, 95%CI of ratio 2.330 to 5.487). Total number of followed animals n=1041 (wt), n=313 (tgNM); total number of natural deaths n=57(wt)[5,5%], n=54(tgNM)[17,3%]. **f)** UPLC measurements of the main neurotransmitters (Ach, DA, NA) in tissue homogenates from the DVC and from peripheral organs (heart and intestine). * $p \leq 0.05$ compared to age-matched wt (Mann-Whitney test). Young DVC [n=8(wt), n=13(tgNM)], Old DVC [n=6(wt), n=12(tgNM)]. Young heart [n=9(wt), n=13(tgNM)], Old heart [n=11(wt), n=12(tgNM)]. Young intestines [n=9(wt), n=13(tgNM)], Old intestines [n=17(wt), n=17(tgNM)]. **g)** Catecholamine neurotransmitter synthesis and metabolism in the dorsal medulla. * $p \leq 0.05$ compared to age-matched wt (Mann-Whitney test). Young [n=8 (wt), n=13 (tgNM)], Old [n=6 (wt), n=12 (tgNM)].

These peripheral alterations are thought to be a consequence of deficient autonomic nervous system innervation of the peripheral organs affected. Indeed, decreased cholinergic innervation in the heart is reported in PD and RBD patients (considered prodromal cases of PD) (Horsager et al., 2020; You, Won, Kim, Lee, & Cho, 2021). We then characterized the levels of the main medullary related neurotransmitters (DA, NA, Ach) in medullary nuclei and innervated peripheral organs (Fig. 27f). First, DVC

homogenates showed a reduction of DA and NA but not Ach levels and altered synthesis and metabolism of DA and NA (Fig. 27f-g), which is consistent with the reported loss of catecholaminergic cells and intact numbers of cholinergic cells. Concomitant with the behavioral signs of peripheral autonomic dysfunction, alterations in DA, NA and Ach levels were also detected in vagal-innervated peripheral organs of tgNM mice like the heart and intestines (Fig. 27f). Specifically, levels of DA, NA and Ach were already decreased in heart homogenates from young animals, suggesting an early deficiency of the heart autonomic innervation in tgNM mice. On the contrary, intestines from tgNM showed increased levels of NA and Ach only in old ages, possibly showing a late compensatory mechanism of an altered autonomic innervation.

Overall, in addition to the PD-like alterations in the DVC reported above (i.e. neurodegeneration of melanized neurons, eNM, microgliosis, LB-like inclusions), our results also reveal that tgNM mice recapitulate some of the peripheral autonomic alterations occurring in PD.

RESULTS - CHAPTER 2

RESULTS - CHAPTER 2. TgNM transcriptomic characterization and identification of potential therapeutic targets

1. Transcriptional profiling of anatomically-defined pigmented areas in tgNM mice

After the characterization of a NM-linked pathology in tgNM mice, we next sought to investigate the consequences of progressive NM accumulation in the transcriptomic profile of distinct neuronal groups.

1.1 Sample collection and transcriptomic microarrays

We performed transcriptomic microarrays because of their high coverage of the mouse transcriptome (i. e. >214,000 transcripts) detecting genes, exons, and alternative splicing from both coding RNA and long non-coding RNA (lncRNA) isoforms, and because of its high consistency within different experiments, making them more suitable for comparison between experiments performed in tgNM mice as well as with the large number of transcriptomic microarrays already published in human PD. Also, to overcome the highly heterogeneous cell populations in samples obtained by gross dissection, here we used LCM to isolate anatomically-defined PD-vulnerable catecholaminergic brain regions (SN, VTA and LC) from 10µm frozen brain sections (Fig. 28). Sections were stained with the fast-penetrating stain Histogene that provides good contrast by differential staining of nuclei (blue) and cytoplasm (purple). To correctly identify catecholaminergic areas for microdissection, regions were selected based on consecutive TH immunostained sections (Fig. 28). Catecholaminergic areas (SN, VTA, LC), mainly containing catecholaminergic neurons but also intermingled interneurons and glial cells, were collected from both male and female animals either pigmented (i.e. tgNM) or non-pigmented (i.e. wt) at three different ages across mouse lifespan (3m, 12m and 20m of age), corresponding to different levels of intracellular NM accumulation (n=4-6 mice/group). In contrast to studies in humans, which all accumulate NM with age, tgNM mice allowed us to analyze for the first time the same catecholaminergic brain regions at a given age either in the absence (i.e. wt) or in the presence (i.e. tgNM) of pigmentation.

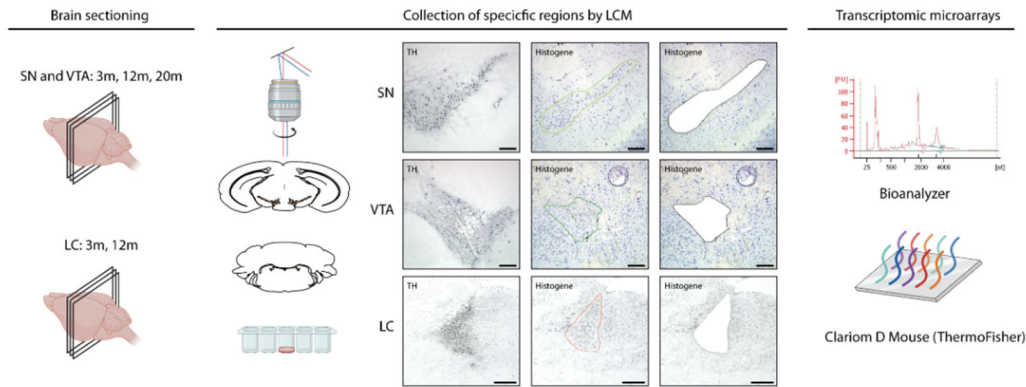


Figure 28. Isolation of histologically-defined PD-vulnerable regions in mice. Schematic representation of the methodological approach used for isolation of anatomically defined specific mouse brain areas. Representative images from SN, VTA and LC TH immunohistochemistry and contiguous Histogene stained sections before and after collection by LCM. RNA was extracted from LCM-collected samples and high-quality RNA was further processed for transcriptomic microarrays. Line represents 200µm. months, m.

To ensure that the RNA quality from microdissected samples was not compromised by the isolation protocol, we performed RNA integrity assessment to all samples. RNA Integrity Number (RIN), a robust and reliable measure of RNA quality (Schroeder et al., 2006), was obtained for all samples and only samples with an acceptable quality ($RIN \geq 5$) were further analyzed for genome-wide transcriptomic changes ($RIN \text{ mean} \pm \text{SD}$ SN= 6.43 ± 0.8 , VTA= 7.01 ± 1.1 , LC= 7.4 ± 0.2) (Fig. 29a). RNA quality did not differ between experimental groups neither correlate with time spent during the LCM collection process, confirming that the protocol for isolating pigmented areas was not compromising RNA quality (Fig. 29b).

After RNA quality assessments, we performed Clariom D transcriptomic microarrays (ThermoFisher, n=90) to obtain transcriptome-wide gene and exon-level data from pigmented (tgNM) and non-pigmented (wt) main catecholaminergic regions. Animal sex was evenly distributed in the different experimental groups to avoid potential bias (Fig. 29c). Microarray expression results confirmed expression of the main catecholaminergic markers in the regions isolated (Pattyn, Goridis, & Brunet, 2000) (Fig. 29d), validating the histological definition of anatomic areas performed.

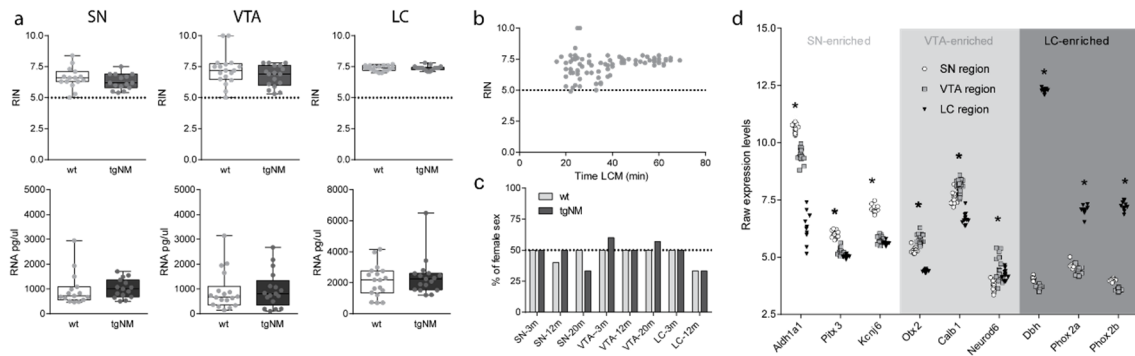


Figure 29. Quality control of collection method and microarray experimental design. a) Bioanalyzer measures of RNA quality (RIN number) and RNA concentration obtained for the different isolated regions. **b)** RNA quality (RIN) correlation with time spent during the LCM collection process (the highest time for LCM collection was considered in pooled samples). Linear regression not significant. **c)** Proportion of female sex in all experimental groups. **d)** Raw expression values of distinct transcripts defining specific neuronal types in microdissected regions from wt animals at 3, 12 and 20m of age for SN and VTA region and at 3, 12m of age in LC region.

Normalization and analysis of the raw data was performed by the Unit of Statistics and Bioinformatics (UEB) from the Vall d'Hebron Research Institute (VHIR). Different outlier detection analyses were performed leading to the exclusion of one sample in the SN microarray dataset while no outliers were detected in the VTA and LC microarrays.

1.2 Differential expression analysis

Differential expression analysis (DEA) between pigmented and non-pigmented areas was performed using the statistical language "R" and the libraries developed for the microarray analysis in the Bioconductor Project (Gentleman et al., 2005). To identify statistically significant differentially expressed genes (DEGs) a threshold of a raw p-value <0.01 and $FC > |1.5|$ was applied for all pigmented regions (Fig. 30a-c, Annex Data Table 2). DEA analysis resulted in a clear regional-dependent pattern of differential expression, being the LC the area with higher number of DEGs followed by VTA and SN (Fig. 30d). Also, there was an increasing number of DEGs with age in all areas, being the oldest age in all areas the one with the highest number of alterations (Fig. 31a). Temporal and regional differences in the amount of DEGs are consistent with the different degrees of NM accumulation in these areas (Fig. 31b), which in turn, correlate with the different degrees of NM-linked pathology described in Chapter 1. Top three most significant DEGs in each area are described in Table 9.

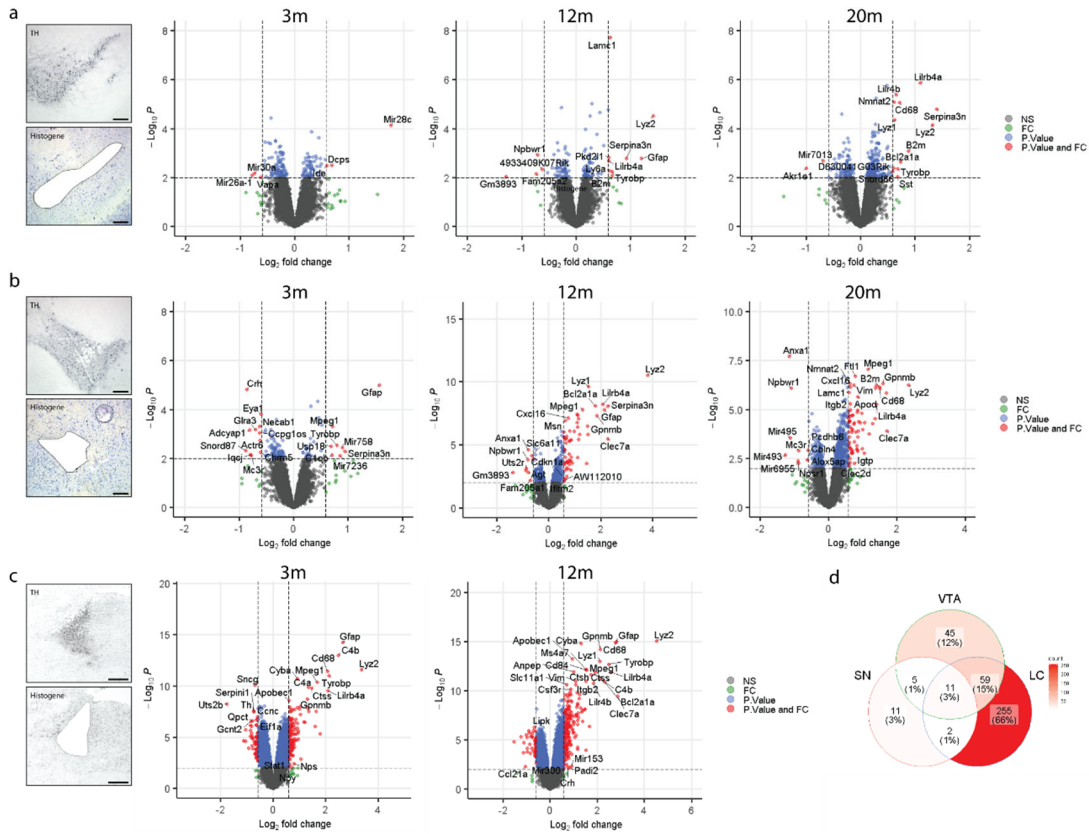


Figure 30. Differential expression analysis (DEA) between pigmented and non-pigmented catecholaminergic nuclei. a-c) Volcano plots showing the statistically significant (raw $p < 0.01$, $FC > |1.5|$, red dots) upregulated and downregulated genes in pigmented and non-pigmented regions compared to non-pigmented regions for each region and age. **d)** Venn diagram showing the overlap between DEGs identified in the three different pigmented brain regions over all ages. Color scale represents the number of genes in that particular region or overlap.

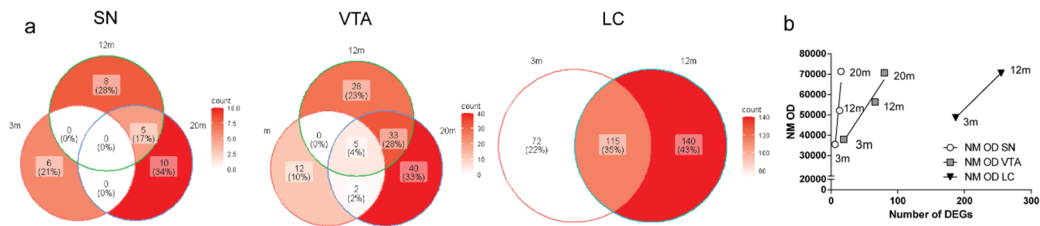


Figure 31. Differentially-expressed genes and NM accumulation. a) Venn diagrams showing the overlap between DEGs identified in the same region at all ages corresponding to increasing degrees of NM accumulation. Color scale represents the number of genes in that particular region or overlap. **b)** Correlation between the number of differentially-expressed genes (DEGs) in a particular region at a particular time and their corresponding level of NM intracellular accumulation (OD) quantified in independent animals.

Region	Age	Gene Symbol	Name	Description	logFC	P.Value	adj.P.Val
SN	3m	Mir28c	mmu-miR-28c	(Predicted targets in miRDB) (1)Ncan, synapse structural plasticity (2)Stk26, predicted to act upstream of or within apoptotic process	1.76	7.258E-05	8.280E-01
		Dcps	Decapping Enzyme, Scavenger	Hydrolyzes cap structures following mRNA degradation by exosome-mediated mRNA decay pathway	0.68	3.095E-03	9.995E-01
		Ide	Insulin Degrading Enzyme	Metallopeptidase that degrades intracellular insulin and other peptides	0.59	3.279E-03	9.995E-01
	12m	Lamc1	Laminin Subunit Gamma 1	Extracellular matrix glycoprotein involved in cellular attachment and migration	0.62	1.930E-08	4.404E-04
		Lyz2	Lysozyme 2	Antimicrobial agent	1.41	3.083E-05	1.005E-01
		Npbwr1	Neuropeptides B And W Receptor 1	G protein-coupled receptor for neuropeptides B and W	-0.70	1.192E-03	9.996E-01
	20m	Lilrb4a	Leukocyte immunoglobulin-like receptor subfamily B member 4A	Inhibitory receptor involved in the down-regulation of the immune response	1.10	1.347E-06	1.962E-02
		Lilr4b	Leukocyte immunoglobulin-like receptor subfamily B member 4	Participates in inflammatory responses and cytotoxicity and limits autoreactivity	0.66	4.169E-06	3.171E-02
		Nmnat2	Nicotinamide Nucleotide Adenylyltransferase 2	Enzyme essential for NADP biosynthetic pathway	0.61	8.457E-06	3.318E-02
	VTA	3m	Gfap	Glial Fibrillary Acidic Protein	Intermediate filament proteins of mature astrocytes	1.58	9.998E-06
Crh			Corticotropin Releasing Hormone	Stimulates the release of adrenocorticotropic hormone from the pituitary gland	-0.86	1.500E-05	1.711E-01
Eya1			EYA Transcriptional Coactivator And Phosphatase 1	Histone phosphatase participating in DNA repair and transcription regulation	-0.60	1.556E-04	7.102E-01
12m		Lyz2	Lysozyme 2	Antimicrobial agent	3.82	3.007E-11	6.861E-07
		Lyz1	Lysozyme 1	Antimicrobial agent	1.54	2.405E-10	2.744E-06
		Lilrb4a	Leukocyte Immunoglobulin Like Receptor B4	Receptor on immune cells that binds to MHC class I molecules on antigen-presenting cells and transduces immune response inhibition	2.09	6.302E-09	4.078E-05
20m		Anxa1	Annexin A1	Participates in innate immune response, antiinflammatory properties	-1.14	1.957E-08	4.465E-04
		Mpeg1	Macrophage Expressed 1	Antimicrobial agent	1.16	8.679E-08	6.601E-04
		Ftl1	Ferritin Light Chain	Light subunit of the ferritin protein, which stores iron in a soluble and nontoxic state	0.79	1.975E-07	9.012E-04
LC	3m	Gfap	Glial Fibrillary Acidic Protein	Intermediate filament proteins of mature astrocytes	2.66	6.002E-15	1.369E-10
		C4b	Complement C4B	Complement factor 4 essential for propagation of the classical complement pathway	2.49	1.041E-13	1.187E-09
		Lyz2	Lysozyme 2	Antimicrobial agent	3.36	2.688E-12	2.044E-08
	12m	Lyz2	Lysozyme 2	Antimicrobial agent	4.52	9.509E-16	9.742E-12
		Gfap	Glial Fibrillary Acidic Protein	Intermediate filament proteins of mature astrocytes	2.83	1.070E-15	9.742E-12
		Cd68	CD68 Molecule	Transmembrane glycoprotein expressed by monocytes participating in phagocytic activities	2.79	1.297E-15	9.742E-12

Table 9. DEGs in pigmented (tgNM) compared to non-pigmented (wt) SN-VTA-LC regions. Top three most significant genes are shown for each comparison. All DEGs are shown in Annex Data Table 2. For mir28c, predicted targets in miRDB are shown. Nicotinamide adenine dinucleotide phosphate, NADP.

1.2.1 Common DEGs between all pigmented regions

Some DEGs were common between the main pigmented areas (11 DEGs, 3%) while the majority were region-specific (Fig. 30d). These common DEGs in all pigmented areas (B2m, Bcl2a1a, CD68, Gfap, Lilr4b, Lilrb4a, Ly6a, Lyz1, Lyz2, Serpina3n, Tyrobp) are mainly specifically expressed in inflammatory cells (microglia/macrophages and astrocytes) and related to neuroinflammatory biological pathways (responses to external stimuli and cytolysis) (Fig. 32a-b). Thus, NM accumulation induces a similar neuroinflammatory activation profile in different brain regions.

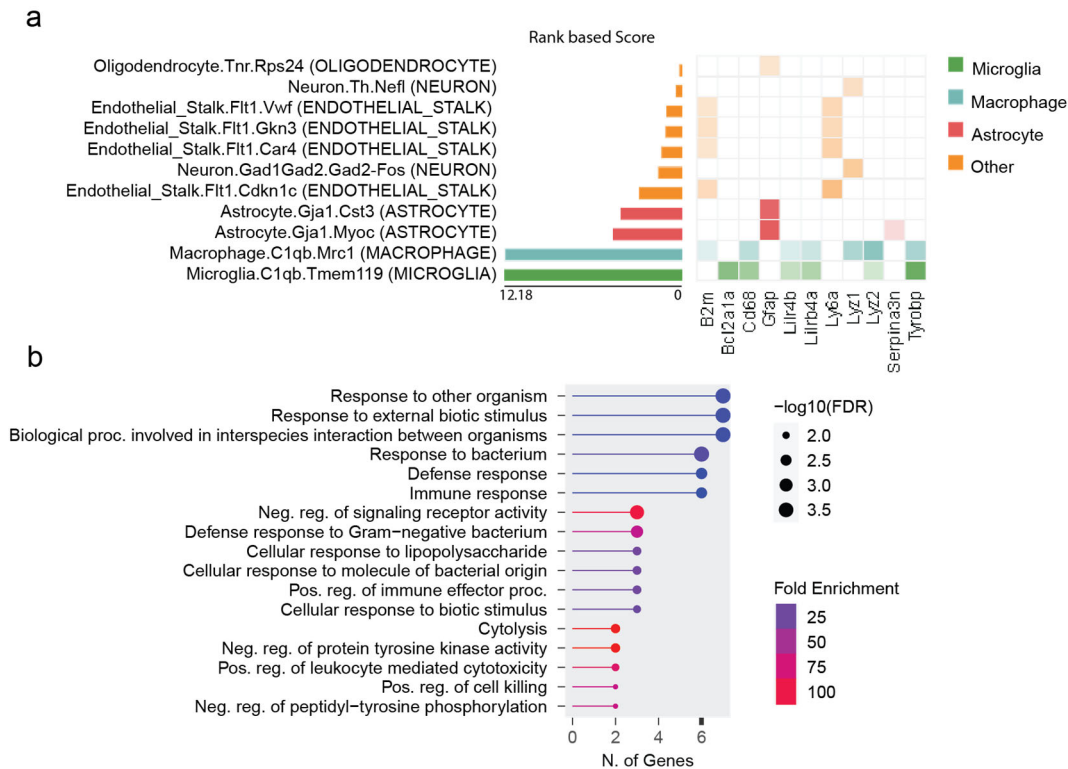


Figure 32. Pan-regional NM-linked transcriptional changes. a) Genes that were differentially expressed in all three areas are related to a neuroinflammatory profile involving myeloid cell lineage specific transcripts (macrophages/microglia), astrocytic transcripts and some endothelial and neuronal transcripts. CellKB (<https://www.cellkb.com/>) gene-rank based score is shown for each gene in the distinct single-cell datasets from the public mouse single-cell dataset from Saunders et al. 2018, Pubmed ID: 30096299. **b)** GO terms enriched in the 11 common DEGs in all pigmented areas obtained with ShinyGO. For each GO term the number of genes overlapping with the pan-regional NM-linked DEGs, the fold enrichment and FDR are shown.

1.2.2 Two-region overlapping DEGs

Only 3 genes with known functions were commonly altered in the two midbrain pigmented regions (SN and VTA) without being altered in LC (Fig. 30d). Also, the three were altered at late ages (12 and 20m). Specifically, these common changes were the downregulation of *Npbwr1* (*Neuropeptide B/W receptor-1*), related to energy homeostasis and neuroendocrine function; the upregulation of *Lamc1* (*Laminin Subunit Gamma 1*), an extracellular matrix protein and the upregulation of *Nmnat2* (*Nicotinamide Nucleotide Adenylyltransferase 2*), essential for NAD biosynthetic pathway and an axonal survival factor.

Regarding the overlap between the midbrain and pontine pigmented structures, VTA and LC regions showed the most abundant overlap within the three pigmented regions with

59 genes (15%) altered in both regions at some age, while only two genes overlapped between SN and LC regions (Fig. 30d).

Within the common genes between the LC and VTA, the most significant in the VTA were mostly related to neuroinflammatory changes and iron homeostasis. Specifically, top common alterations were upregulation of antimicrobial transmembrane pore-forming protein *Mpeg1* (*Macrophage-expressed gene 1*), antigen presentation MHC class I, H2-K1 (*Histocompatibility 2, K1*) and *Ftl1* (*Ferritin light polypeptide 1*) and the altered expression of *Crh* (*Corticotropin Releasing Hormone*) which was downregulated in the VTA and upregulated in the LC. Considering the most significant LC top shared DEGs with VTA, they were all upregulated and related to immune function as well [*C4b* (*Complement C4B*), essential for the classical complement pathway; *Cyba* (*Cytochrome B-245 Alpha Chain*), involved in superoxide production in phagocytes and the glycoprotein *Gpnmb* (*Glycoprotein Nmb*), recently linked associated to PD pathology (Diaz-Ortiz et al., 2022)]. The two DEGs overlapping between SN and LC were the downregulated oxidoreductase activity enzyme *Akr1e1* (*Aldo-Keto Reductase Family 1 Member E1*) and the upregulated *Sst* (*Somatostatin*), which inhibits the secretion of pituitary hormones.

1.2.3 Region-specific DEGs

We identified 11 SN-specific DEGs, 45 VTA-specific DEGs, and 255 LC-specific DEGs. Top SN-specific changes included: (i) at 3m, upregulation of *Mir28c* and *Dcps* (*Decapping Enzyme, Scavenger*), an enzyme that participates in mRNA degradation; (ii) at 12m, upregulation of the cell-cell/matrix interaction protein *Pkd2l1* (*Polycystin-L*); (iii) at 20m, downregulation of *Mir7013* and upregulation of the nucleolar RNA *Snord66* (*Small Nucleolar RNA, C/D Box 66*).

Top VTA-specific changes included: (i) at 3m, downregulation of the DNA repair enzyme *Eya1* (*EYA Transcriptional Coactivator And Phosphatase 1*) and of the neuronal Ca(2+)-binding protein *Necab1* (*N-Terminal EF-Hand Calcium Binding Protein 1*); (ii) at 12m, upregulation of cytoskeleton organizer *Msn* (*Moesin-membrane-organizing extension spike protein*) and of the lysosomal cysteine proteinase *Ctsz* (*Cathepsin Z*); (iii) at 20m, downregulation of anti-inflammatory membrane protein *Anxa1* (*Annexin A1*) and upregulation of the mitochondrial protein *Cmpk2* (*cytidine/uridine monophosphate kinase 2*).

LC-specific top differentially expressed genes included: (i) at 3m, downregulation of a member of the synuclein protein family *Sncg* (*Synuclein Gamma*) and upregulation of mRNA editing enzyme *Apobec1* (*Apolipoprotein B mRNA Editing Enzyme Catalytic Subunit 1*); (ii) at 12m, upregulation of *Apobec1* and of *Slc11a1* (*Solute Carrier Family 11 Member 1*), a divalent transition metal (iron and manganese) transporter.

1.2.4 Non-coding microRNA

We also detected non-coding microRNA (miRNA) being 9 out of 442 in LC, 9 out of 165 in VTA and 4 out of 34 in SN. Remarkably, three out of the six DEGs identified in SN at 3m, before DA dysfunction is detected, were miRNA. This finding highlights their crucial role in the initial consequences of NM accumulation in SN neurons. Interestingly, *Mir692-1* was commonly upregulated in VTA at 12m and 20m and in LC at 3m and 12m. Top predicted targets of *Mir692-1* were cell-adhesion protein *Pcdh20* (*Protocadherin 20*) and mitochondrial protein *Synj2bp* (*Synaptojanin 2 binding protein*) (Annex Data Table 3), pointing to a potential role of these proteins in the NM-linked neuronal dysfunction and neurodegeneration seen in VTA and LC regions.

1.3 Gene set enrichment analysis

Like any other given cellular stimulus, NM accumulation may result in dependent co-regulated expression of complex gene sets that may not be reflected in single gene changes (Yin, Mendoza, Monzon-Sandoval, Urrutia, & Gutierrez, 2021). Thus, our next step was to identify functional gene sets enriched in pigmented areas compared to their equivalent non-pigmented counterparts. For this, we performed Gene set enrichment analysis (GSEA) using all the detected genes ordered by fold change of expression in tgNM compared to wt. GSEA was performed over Gene Ontology (GO) and Reactome Pathways annotation databases.

GSEA analysis yielded statistically significant GO pathways in all regions and ages except in SN at 3m of age. Some of the NM-related biological pathways were common within the top enriched gene sets in all three areas. Neuroinflammation-related pathways were found enriched within the upregulated genes while transcription and RNA processing/translation pathways were enriched within the downregulated genes, among other pathways (Fig. 33). Interestingly, proteasomal and mitochondrial related pathways appeared within the top 10 mostly in the SN (Fig. 33).

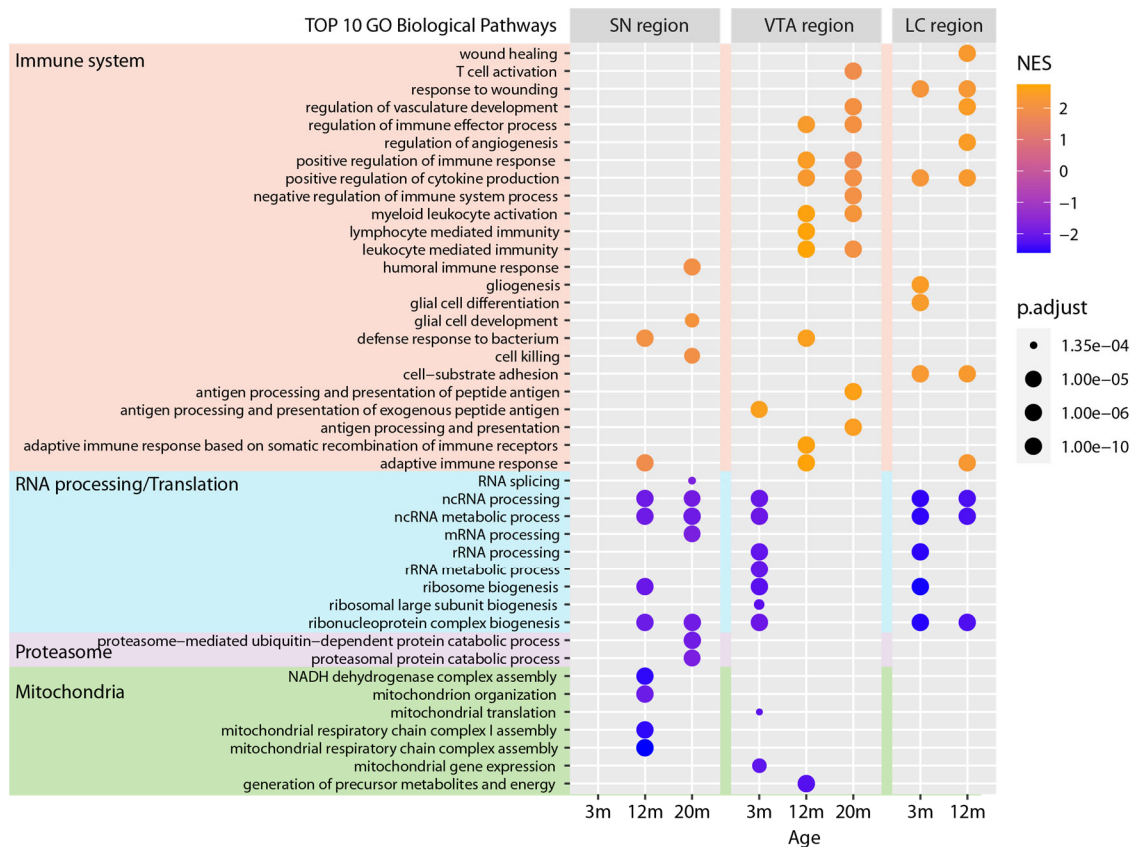


Figure 33. Gene set enrichment analysis with GO database in tgNM compared to wt SN-VTA-LC. Top 10 GO biological pathways (FDR<0.05, ordered by number of genes per GeneSet) enriched in pigmented (tgNM) vs non-pigmented (wt) SN, VTA and LC regions at all ages analyzed (months, m). No statistically significant GO biological pathways were found enriched in SN at 3m from tgNM compared to its age-matched wt.

GSEA analysis with Reactome databases yielded statistically significant pathways in all regions and ages (Fig. 34). Some of the NM-related biological pathways were common with the GO terms, including pathways associated to the immune system, RNA processing/translation and mitochondrial-related pathways. Some other biological categories differed from the GO database, including cell cycle associated pathways

appearing mainly in the LC and SN, metabolism and neurotransmission among others.

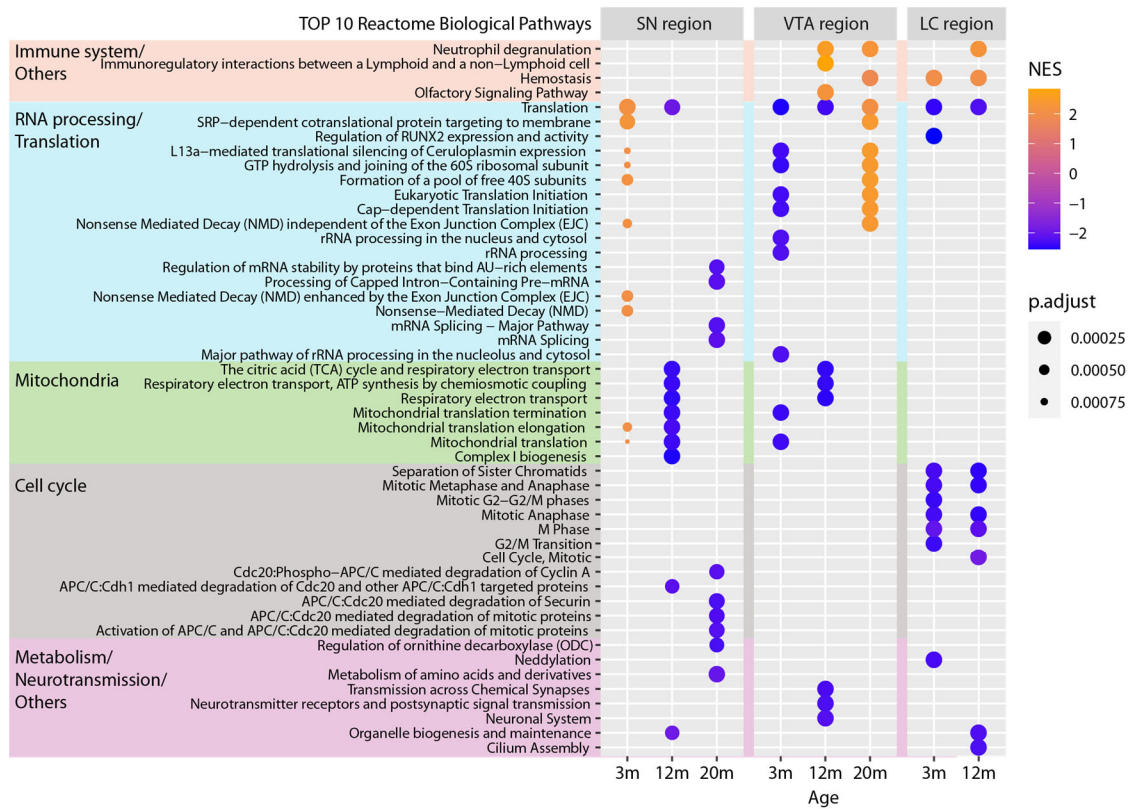


Figure 34. Gene set enrichment analysis with Reactome database in tgNM compared to wt SN-VTA-LC. Top 10 Reactome biological pathways (FDR<0.05, ordered by number of genes per GeneSet) enriched in pigmented (tgNM) vs non-pigmented (wt) SN, VTA and LC regions at all ages analyzed (months, m).

2. Transcriptional profiling of pigmented neurons in tgNM mice

Our transcriptional characterization of pigmented regions led to the identification of neuroinflammatory changes as one of the main consequences of NM accumulation in tgNM brain areas. We then sought to determine if the neuroinflammatory process was due to an overreaction to NM granules released in the extracellular milieu or because of a neuronal-glial direct communication occurring before dysfunction and/or degeneration. Also, we wondered if some neuronal-specific changes might have been masked because of the bulk nature of our previous characterization. For these reasons, we selectively isolated neuronal populations by LCM in order to better characterize the neuronal consequences of NM accumulation.

2.1 Sample collection and microarrays

Considering the extent of neurodegeneration found in the LC region already at pubertal ages (Fig. 24a), we only selected single neurons from SN and VTA regions. Single SN and VTA neurons from both male and female tgNM and wt animals at three different ages were collected (n=4-6/group). Neurons were identified based on their blue-stained cytoplasm together with their characteristic size and shape (Fig. 35a). Since we used a non-specific dye for the isolation procedure, all SN and VTA neuronal subtypes were collected. After microdissection, only RNA samples with acceptable RNA quality (RIN \geq 5) were processed (SN neurons RIN mean \pm SD=6.5 \pm 1, VTA neurons RIN mean \pm SD=6.4 \pm 0.9) (Fig. 35b). After RNA quality assessments, we performed Clariom D transcriptomic microarrays (ThemorFisher, n=62). Male and female animals were evenly distributed in the experimental groups (Fig. 35c). Following the same technical approach as in the regionally-collected samples, validation of the histological identification of SN and VTA neurons was confirmed by the expression levels of the known SN and VTA-enriched transcripts (Fig. 35c).

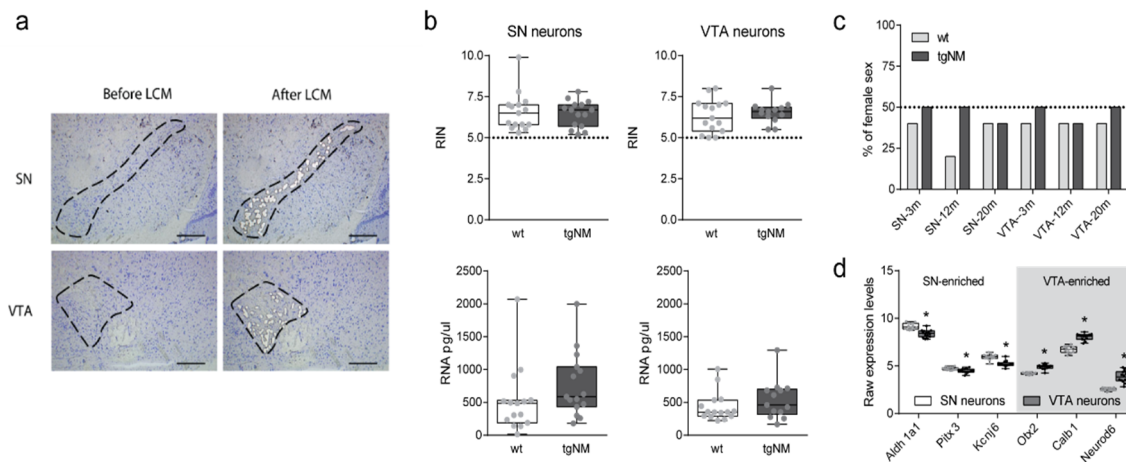
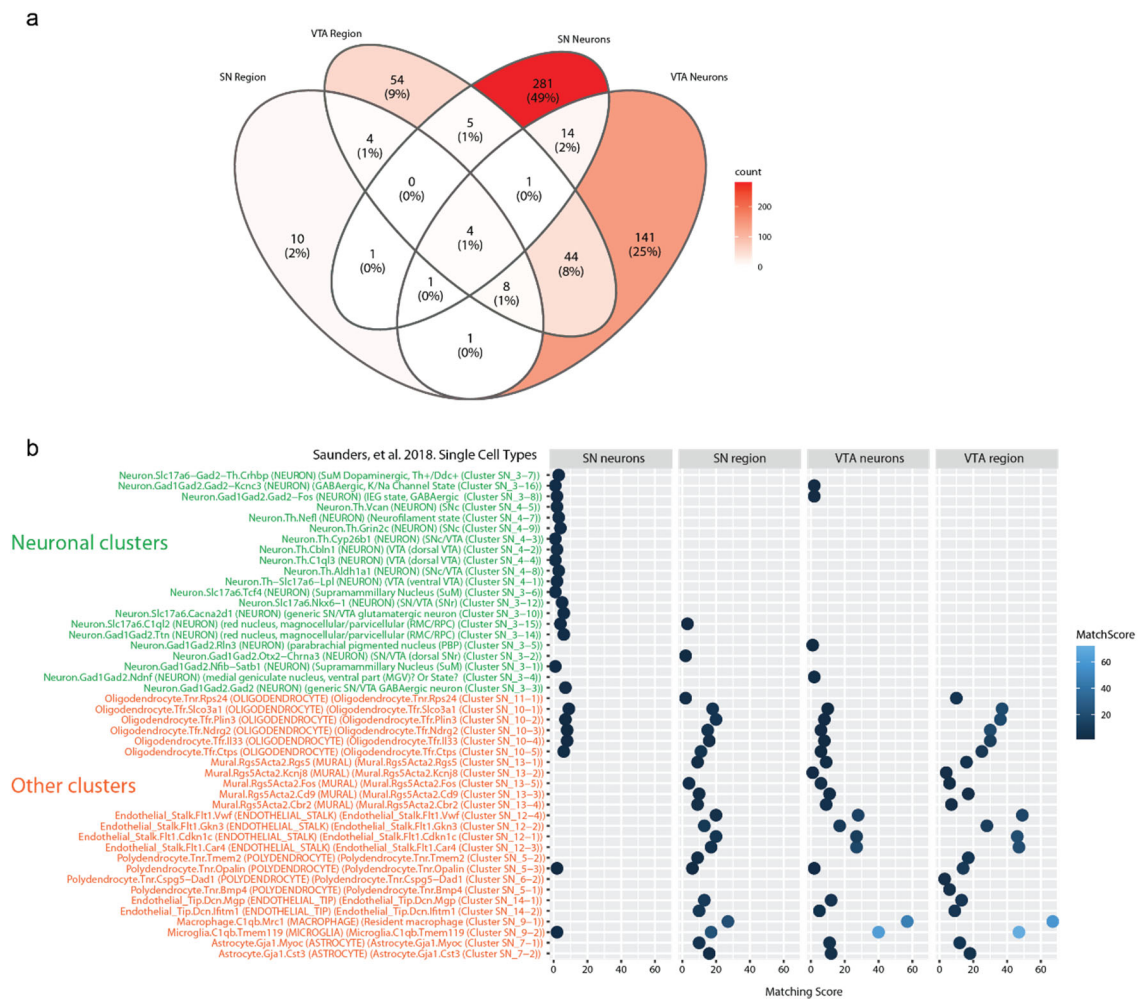


Figure 35. Experimental design and quality control of neuronal-enriched samples. a) Schematic representation of single neurons isolated by LCM. **b)** Bioanalyzer measures of RNA quality (RIN number) and RNA concentration obtained for SN and VTA collected neurons. **c)** Proportion of female sex in all experimental groups. **d)** Raw expression values of SN and VTA neurons of distinct transcripts known to be differentially expressed in SN and VTA neurons. Values represent expression only in wt animals and at all ages assessed (3m, 12m and 20m).

2.2 Differential Expression Analysis

We performed differential expression analysis following the same approach and threshold as in the regionally collected samples. We detected a higher number of DEGs between

tgNM and wt animals in neurons compared to regionally isolated samples (Fig. 36a, Annex Data Table 4). As a confirmation of our neuronal isolation protocol, we assessed the cell type annotation of the main DEGs (<200) using CellKb database, which gathers single-cell datasets for cell type identification. We confirmed an enrichment of neuronal-specific altered transcripts in SN neurons compared to the regionally isolated pigmented areas, though we did not see a major enrichment of neuronal markers in VTA cells (Fig. 36b). These results reveal the consistency of the neuronal enrichment performed by our method, at least for the SN neuronal population. Neuronal-specific datasets are overrepresented in DEGs identified in SN neurons while transcripts typically expressed in immune cell types are found within the DEGs identified in SN region (Fig. 36b).



Regarding SN, with this neuronal-targeted approach we identified a very different transcriptomic profile compared to regionally-collected samples. Only six genes overlapped between the two differently collected samples [6 out of 29 in SN region (21%) and out of 307 (2%) in SN neurons]. The overlapping genes with known function were two genes overlapping at 12m (*Gfap*, *Lyz2*) and two more at 20m (*Akr1e1*, *Nmnat2*). On the other hand, there was a much higher overlap in the VTA between the neuronal and the regional profiles [57 genes overlapped out of 120 (48%) DEGs in region and out of 214 (27%) DEGs in neurons].

As opposed to the regionally-collected samples, here we did not see a pattern of transcriptomic changes in an age-dependent manner since major changes in SN neurons were at 12m, showing a great peak of DEGs (85% of all DEGs in SN neurons), and VTA changes were similar at all ages (Fig. 37). The top three most significant genes are described in Table 10.

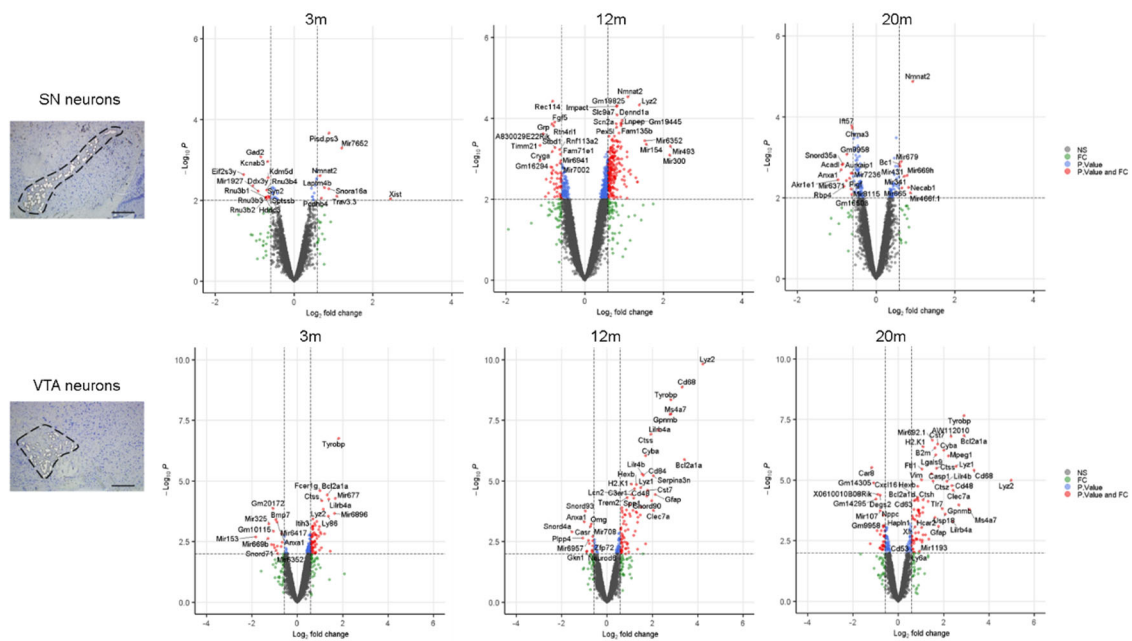


Figure 37. Differential expression analysis between tgNM and wt SNpc and VTA neurons. Schematic representation of single neurons isolated by LCM and volcano plots showing the statistically significant (raw $p < 0.01$, $FC > |1.5|$) upregulated and downregulated genes in red for each region and age.

Region	Age	Gene Symbol	Name	Description	logFC	P.Value	adj.P.Val
SNneurons	3m	Mir1912	Mir1912	(Predicted targets in miRDB) (1)Gnas,signalling (2)Chd6,chromatin remodeling	-2.04	7.29E-05	6.05E-01
		Pisd-ps3	Pisd-ps3	Pseudogene	0.89	2.16E-04	8.97E-01
		Mir7652	Mir7652	(Predicted targets in miRDB) (1) Ppp4r3a,serine/threonine-protein phosphatase (2)Arhgef6, signalling	1.21	5.11E-04	1.00E+00
	12m	Nmnat2	Nicotinamide Nucleotide Adenylyltransferase 2	Enzyme essential for NADP biosynthetic pathway	1.10	2.97E-05	8.41E-02
		Rec114	REC114 Meiotic Recombination Protein	Protein involved in DNA double-strand break formation	-0.81	3.71E-05	8.41E-02
		Lyz2	Lysozyme 2	Antimicrobial agent	1.38	4.69E-05	8.41E-02
	20m	Nmnat2	Nicotinamide Nucleotide Adenylyltransferase 2	Enzyme essential for NADP biosynthetic pathway	0.93	1.33E-05	1.11E-01
		Ift57	Intraflagellar Transport 57	Participates in cilia formation, pro-apoptotic properties	-0.62	1.67E-04	4.09E-01
		Chrna3	Cholinergic Receptor Nicotinic Alpha 3 Subunit	Nicotinic acetylcholine receptor	-0.61	1.92E-04	4.09E-01
VTANEurons	3m	Tyrobp	Transmembrane Immune Signaling Adaptor TYROBP	Transmembrane receptor with a cytoplasmic immunoreceptor tyrosine-based activation motif (ITAM)	1.82	1.74E-07	1.44E-03
		Fcer1g	Fc Epsilon Receptor Ig	Component of the high-affinity immunoglobulin E (IgE) receptor	0.99	2.49E-05	8.99E-02
		Bcl2a1a	BCL2 Related Protein A1	Anti-apoptotic protein, reduces the release of cytochrome c from mitochondria	1.32	3.75E-05	8.99E-02
	12m	Lyz2	Lysozyme 2	Antimicrobial agent	4.21	1.51E-10	1.25E-06
		Cd68	CD68 Molecule	Transmembrane glycoprotein expressed by monocytes participating in phagocytic activities	3.30	1.33E-09	5.54E-06
		Tyrobp	Transmembrane Immune Signaling Adaptor TYROBP	Transmembrane receptor with a cytoplasmic immunoreceptor tyrosine-based activation motif (ITAM)	2.81	4.47E-09	1.24E-05
	20m	Tyrobp	Transmembrane Immune Signaling Adaptor TYROBP	Transmembrane receptor with a cytoplasmic immunoreceptor tyrosine-based activation motif (ITAM)	2.90	2.14E-08	1.78E-04
		Bcl2a1a	BCL2 Related Protein A1	Anti-apoptotic protein, reduces the release of cytochrome c from mitochondria	2.90	1.45E-07	4.41E-04
		AW112010	Long Noncoding RNA AW112010	Predicted to promote mitochondrial biogenesis and differentiation of Tcells	2.33	1.59E-07	4.41E-04

Table 10. Top DEGs in pigmented (tgNM) compared to non-pigmented (wt) SN-VTA neurons. Top three most significant genes are shown for each comparison. All DEGs are shown in Annex Data Table 4. For miRNA, predicted targets in mirDB for the 5 prime arm are shown. Nicotinamide adenine dinucleotide phosphate, NADP.

2.2.1 Common DEGs between SN and VTA neurons

Regarding the neuronal-enriched samples, both DA neuronal subtypes (SN and VTA) showed similar number of DEGs (Fig. 38a). There were 20 common genes between the two subtypes at all ages, representing only a 7% from all SN DEGs and 9% from all VTA DEGs. These common genes were related to the immune system, metabolism of lipids and signaling. Top SN DEGs shared with VTA were upregulation of the NADP biosynthesizing enzyme *Nmat2* (*Nicotinamide Nucleotide Adenylyltransferase 2*) in all three ages and downregulation of the RNA helicase *Ddx3y* (*DEAD-Box Helicase 3 Y-Linked*) at 3m, upregulation of *Lyz2* at 12m and downregulation of the mitochondrial beta-oxidation enzyme *Acadl* (*Acyl-CoA Dehydrogenase Long Chain*) at 20m. Top common genes in VTA were the upregulation of *Lyz2* at all ages, *Nmnat2* at 3m, *CD68* at 12m and 20m.

2.2.2 Subtype-specific DEGs

Considering the differential vulnerability reported in PD postmortem studies in these two DA subtypes, we performed an enrichment analysis with the specific genes found deregulated exclusively in one or another subtype. The SN-specific alterations, consisting on 287 DEGs were related to neurotransmission and vesicle-transport, while VTA-

specific changes, consisting on 194 DEGs, were related mainly to the immune system (Fig. 38b).

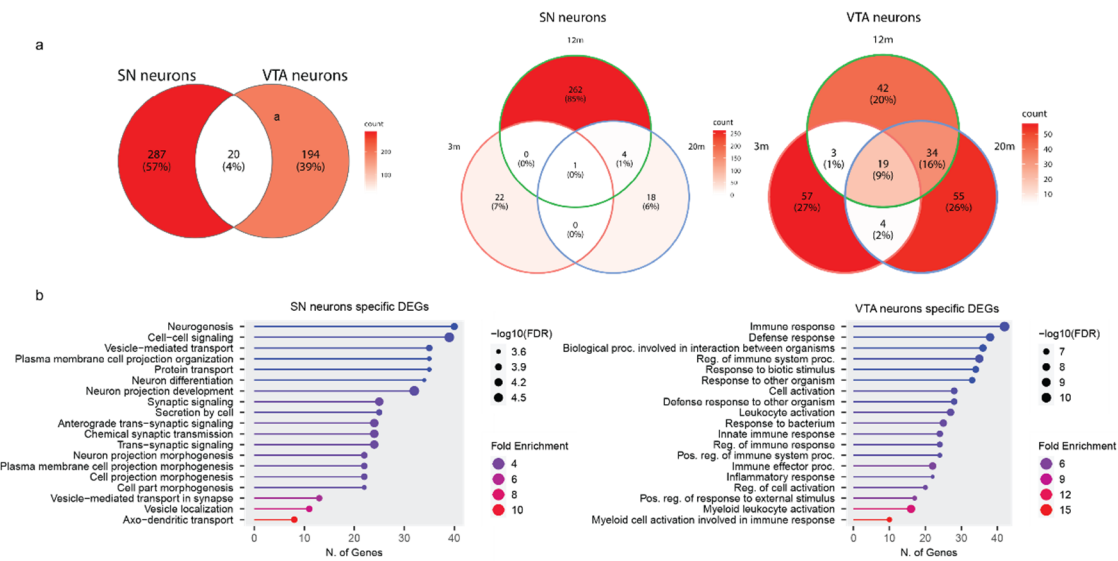


Figure 38. Comparison between SN and VTA neurons specific DEGs. a) Venn diagrams showing the overlap between DEGs in neuronal-enriched samples at different ages. Color scale represents the number of genes in that particular region or overlap. **b)** TOP 19 significant GO biological pathways (FDR<0.05) obtained with ShinyGO in specific SN (a) or VTA (b) neuronal DEGS at all ages.

Top SN-specific DEGs included: (i) at 3m, downregulation of Mir1912 and upregulation of Mir7652; (ii) at 12m, downregulation of Rec114 (*REC114 Meiotic Recombination Protein*), which is involved in DNA double-strand breaks, and upregulation of Impact (*Impact RWD Domain Protein*), a translational regulator that ensures constant high levels of translation upon a variety of stress conditions; (iii) at 20m, downregulation of the proapoptotic protein Ift57 (*Intraflagellar Transport 57*) and nicotinic acetylcholine receptor Chrna3 (*Cholinergic Receptor Nicotinic Alpha 3 Subunit*).

Top VTA-specific DEGs included: (i) at all ages, upregulation of the immunoreceptors Tyrobp (*Transmembrane Immune Signaling Adaptor TYROBP or DAP12*); (ii) at 3m, upregulation of the immunoreceptor Fcer1g (*Fc Epsilon Receptor Ig*); (iii) at 12m, upregulation of the monocytic marker Ms4a7 (*Membrane Spanning 4-Domains A7*); (iv) at 20m, upregulation of antiapoptotic protein Bcl2a1a (*BCL2 Related Protein A1*). Of note, VTA shows a very characteristic immune profile (upregulation of Lyz2, Tyrobp, CD68, Ms4a7, Gpnmb, etc) that arises at 12m and is maintained at 20m (Fig. 37a). This same profile is also observed in the microdissected VTA regions (Fig. 30b). This observation together with the great overlap between VTA neurons and regions (57 genes

out of 120, 48%) (Fig. 36a) and the non-neuronal specific transcripts in these collected VTA neurons (Fig. 36b) suggest that there is a greater abundance of neuroinflammatory cells surrounding neurons in the VTA than in the SN.

2.3 Gene set enrichment analysis

We then performed GSEA to identify biological pathways that change in a coordinated way through the different ages analyzed in the distinct DA subtypes. We performed GSEA using the same two databases (GO and Reactome) as for the regionally-collected samples. The top identified GO terms were related to cell communication, metabolism, RNA processing, and mitochondrial function among others (Fig. 39).

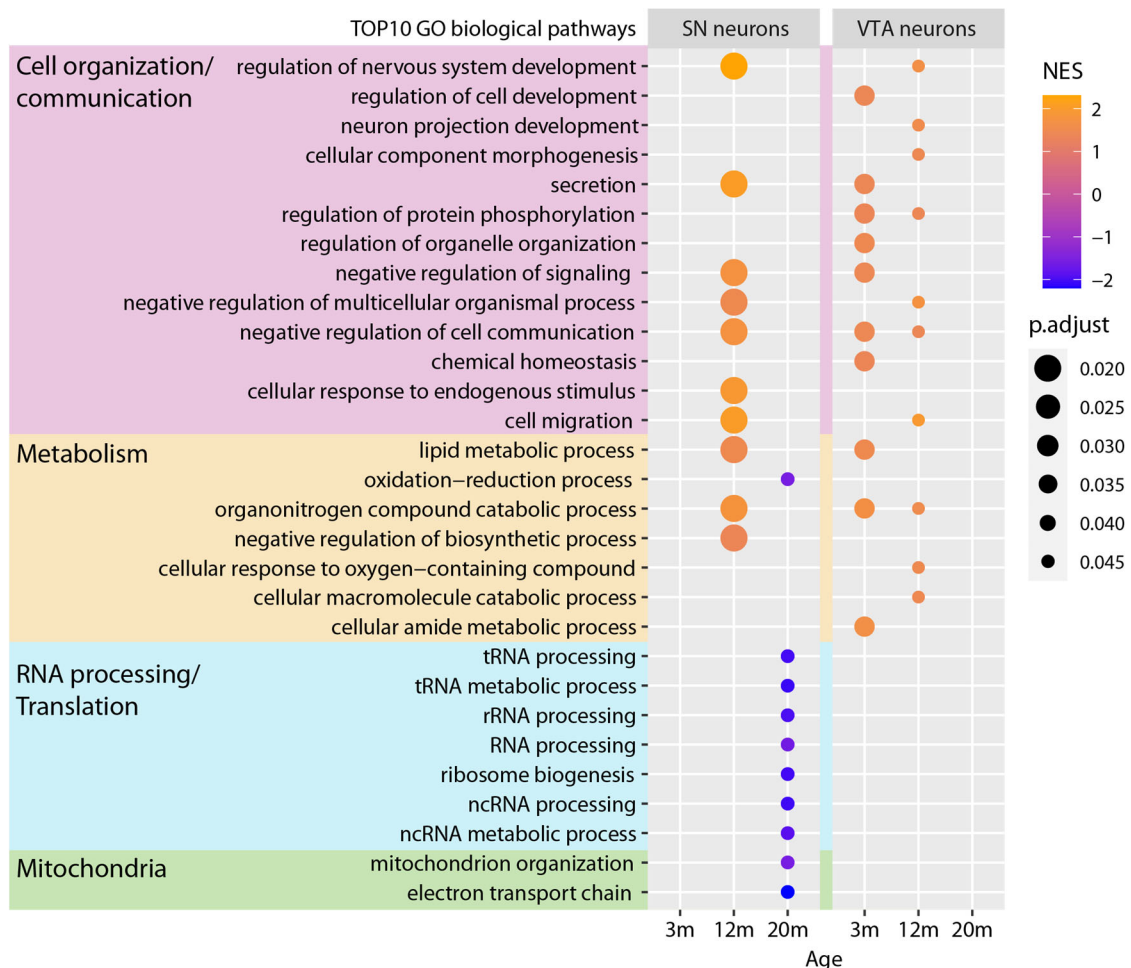


Figure 39. Gene set enrichment analysis with GO database in tgNM compared to wt SN-VTA neurons. Top 10 GO biological pathways (FDR<0.05, ordered by number of genes per GeneSet) enriched in pigmented (tgNM) vs non-pigmented (wt) SN and VTA neurons at all ages analyzed (months, m). No

statistically significant GO biological pathways were found enriched in SN at 3m and VTA at 20m from tgNM compared to its age-matched wt.

Contrary to the Top GO terms, top Reactome pathways showed an enrichment of the immune system (earlier and more pronounced in VTA neurons) (Fig. 40). Also, additional biological categories emerged, including an enrichment in pathways related to membrane trafficking/lipid metabolism, development, cell-cycle, and distinct signaling pathways (Fig. 40).

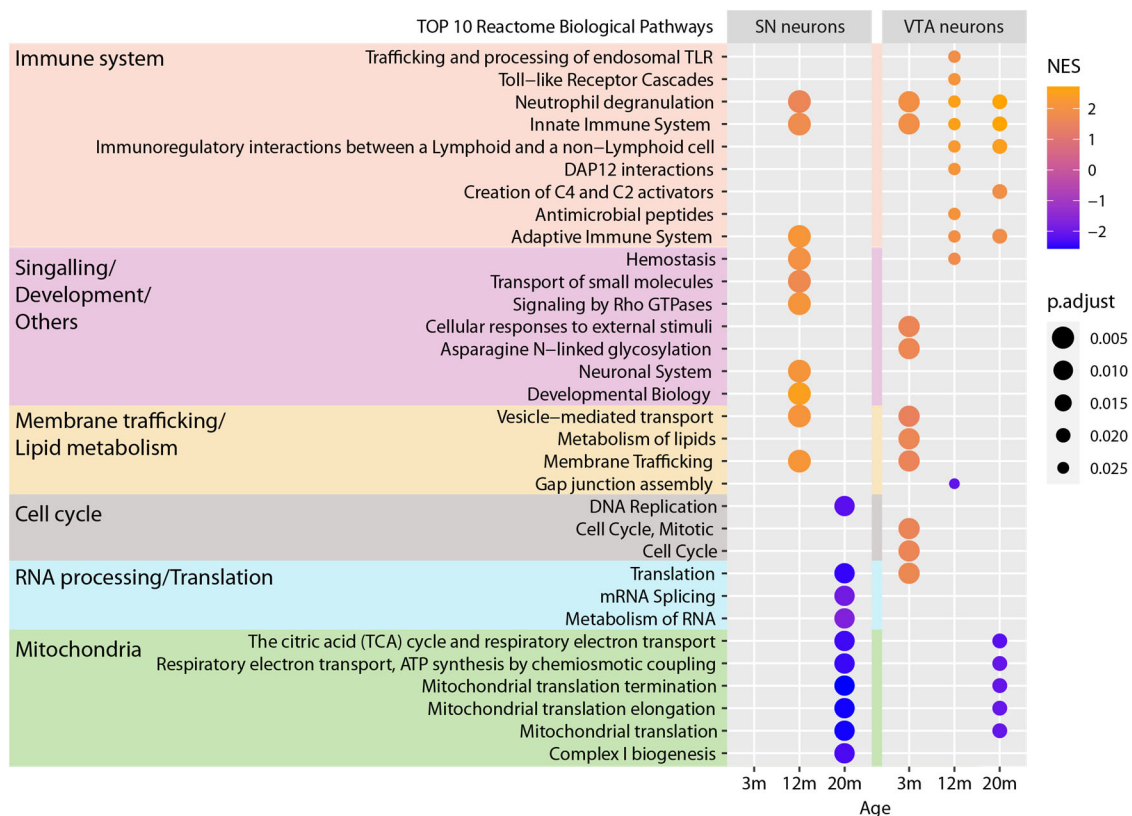


Figure 40. Gene set enrichment analysis with Reactome database in tgNM compared to wt SN-VTA neurons. Top 10 Reactome biological pathways (FDR<0.05, ordered by number of genes per GeneSet) enriched in pigmented (tgNM) vs non-pigmented (wt) SN and VTA neurons at all ages analyzed (months, m). No statistically significant Reactome biological pathways were found enriched in SN at 3m from tgNM compared to its age-matched wt.

Interestingly, the top-enriched GO and Reactome terms in SN neurons at early ages (3m and 12m) DEGs were within the upregulated genes (immune system, cell communication/organization, metabolism) while at old ages (20m) the top GO terms were within the downregulated genes and related to RNA processing/translation and mitochondria (Fig. 39&40). These results support the concept that the dysfunctional

phenotype observed in these pigmented DA neurons at an old age (20m) may be driven by a generalized downregulation of transcriptional activity impacting different biological functions.

3. Differences in the splicing events

Not only differences in transcripts levels but also differences in splicing events might impact cellular phenotypes. Adding another layer of complexity, we also analyzed the splicing events in all the pigmented regions using Transcriptome Analysis Console (TAC) Software. With a statistical significance threshold of $FDR < 0.05$, we only found significant alternative splicing events in the samples collected as regions. The majority of them were found in the LC region, following the same trend as the DEA (SN<VTA<LC) (Fig. 41a-b).

Of note, we identified a significant splicing event in the endogenous Tyr gene, specifically localized in the exon junction spanning second and third exons (TC0700003702.mm.1/Symbol: Tyr/chr7:87,425,270-87,493,411/Strand:-). The Tyr transcript was not differentially expressed in the dataset as a whole but shows a statistically significant difference at the exon level between wt and tgNM (LC: p-value=1.41E-13, FDR=5.32E-09; SN: p-value=1.16E-11, FDR=3.37E-06; VTA: p-value=1.63E-06, FDR=0.07). Alternative splicing events have been reported for Tyr gene in mouse and humans, some of them leading to the loss of Tyr activity and diminished melanization (e.g. in melanomas) (Fryer, Oetting, Brott, & King, 2001; Le Fur, Kelsall, Silvers, & Mintz, 1997; Müller, Ruppert, Schmid, & Schütz, 1988). The further characterization of this splicing event might elucidate a potential role of endogenous Tyr expression (RNA processing) in NM formation in the mouse brain.

GPNMB, which was also differentially expressed in our dataset, was within the top spliced genes and showed a clear alternative splicing in tgNM (SN: p-value=6.60E-05, FDR=0.3016; VTA: p-value=6.65E-08, FDR=0.0126; LC: p-value=1.79E-14, FDR=1.35E-09) (Fig. 41b). This splicing event was a cassette exon type, meaning that an exon between two other exons from the mature mRNA sequence is included to generate a new protein isoform (Cui, Cai, & Stanley, 2017). GPNMB splicing event resulted in higher levels of expression of exon 5 in SN region and exons 5-8 in VTA and LC (Fig. 41c). Splicing events in GPNMB have also been reported in rodents and humans, though

there are still no clear established functional consequences of these alternative spliced transcripts (Chen et al., 2022; Tse et al., 2006).

We also identified a splicing event in the *Lamc2* (laminin, gamma 2) gene in SN and VTA regions (SN: p-value=1.19E-10, FDR=2.31E-05; VTA: p-value=2.45E-10, FDR=6.99E-05), which was not related to a differential expression of the whole transcript in these areas. Specifically, tgNM mice displayed alternative inclusion of the last exon (exon 24) of *Lamc2*, an event that has been described in another pathological context like Myotonic Dystrophy patients (Perfetti et al., 2014). These mRNA processing alterations might be related to the differentially expressed *Lamc1* (highly homologous to *Lamc2*), which is upregulated in SN and VTA regions (SN: logFC=0.62, p-value= 1.9303E-08; VTA: logFC= 0.60, p-value= 1.3395E-06).

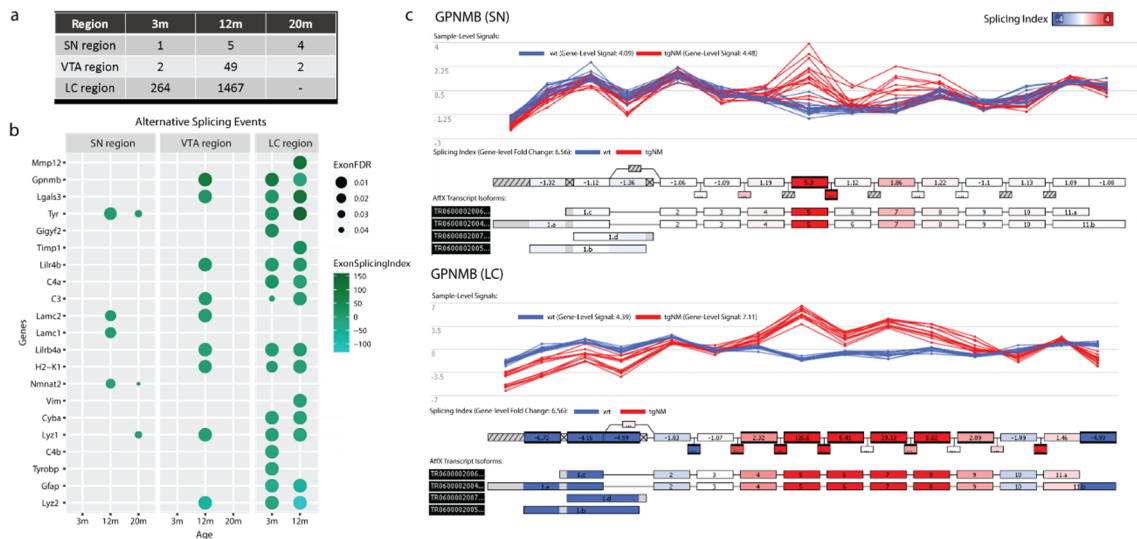


Figure 41. Alternative Splicing events in tgNM pigmented areas. **a)** Number of statistically significant splicing events (FDR≤0.05, Exon Splicing Index≥|2|) detected by TAC software in all the ages and regions. Splicing events were not detected in neuronal-enriched samples. **b)** Top10 significant splicing events (FDR≤0.05, Exon Splicing Index≥|2|) in all regions and ages ordered by Exon Splicing Index for all datasets. Positive splicing index represents higher expression of a specific exon/intron sequence in tgNM than wt, while a negative splicing index represents a higher expression in wt. **c)** Schemes showing GPNMB splicing event in SN region (3+12+20m) (p=6.60E-05, FDR=0.3016) and LC region (3+12m) (LC: p=1.79E-14, FDR=1.35E-09) (TC0600000577.mm.1/Symbol:Gpnmb/chr6:49,036,518-49,058,182/Strand:+).

4. Evidence of the translational value of tgNM mice as a model of human-like NM accumulation

Our group has previously demonstrated that SNpc neurons from PD postmortem brains show higher levels of intracellular NM density than age-matched controls, and that inducing NM accumulation in animal models induces parkinsonian features (Carballo-Carbajal et al., 2019). These results suggested that NM becomes deleterious above a certain threshold of accumulation, potentially participating in the initiation of PD.

In order to assess the resemblance between our NM model and human PD pathology, we next compared tgNM transcriptional profiles at different ages to the publicly available human transcriptomic studies characterizing the expression profiles in postmortem tissue from PD and control subjects. We retrieved 8 studies analyzing postmortem SN from PD and age-matched controls (GSE20163, GSE20164, GSE20292, GSE20333, GSE43490, GSE7621, GSE20141 and GSE24378) and one study analyzing LC in both conditions (GSE34516) from the public database NCBI GEO Datasets. No human transcriptomic studies analyzing specifically VTA region were found (Annex Data Table 5). We then compared the human studies to the corresponding region profiles in tgNM mice (SN and LC) using single-wise correlation analysis (ROAST) (Table 11). The analysis revealed that the late transcriptomic alterations observed in tgNM SN neurons (20m) showed a significant correlation ($p\text{-value}<0.05$) with half of the published human PD transcriptomic studies (4 out of 8) and showed a clear trend of correlation [$p=0.05609$ (GSE20141), $p=0.05959$ (GSE24378)] with two additional studies (Table 11). Interestingly, only the transcriptomic profile from isolated SN neuronal populations showed a statistically significant correlation with postmortem PD SN at 20m of age, which corresponds to the age with the highest levels of NM accumulation in tgNM mice. The sole study available analyzing LC from PD postmortem brains showed a clear correlation with tgNM LC transcriptomic profile already at 3m of age, consistent with the advanced neurodegeneration in both postmortem PD brains and tgNM mice in this area (Table 11&12).

PD postmortem study	Ngenes	tgNM SN region						tgNM SN neurons					
		3m		12m		20m		3m		12m		20m	
		p	FDR	p	FDR	p	FDR	p	FDR	p	FDR	p	FDR
GSE20141_all	135	0.34	0.84	0.52	0.90	0.08	0.48	0.68	0.78	0.22	0.47	0.06	0.09
GSE20163_all	86	0.79	0.91	0.56	0.90	0.38	0.48	0.45	0.75	0.24	0.47	<u>0.03</u>	0.09
GSE20164_all	21	0.90	0.93	0.61	0.90	0.39	0.48	0.27	0.75	0.48	0.53	0.13	0.16
GSE20292_all	289	0.50	0.84	0.51	0.90	0.17	0.48	0.45	0.75	0.27	0.47	<u>0.04</u>	0.09
GSE20333_all	20	0.64	0.84	0.13	0.90	0.14	0.48	0.89	0.91	0.49	0.53	0.38	0.42
GSE24378_all	47	0.30	0.84	0.69	0.90	0.18	0.48	0.16	0.75	0.33	0.47	0.06	0.09
GSE43490_all	375	0.51	0.84	0.76	0.90	0.23	0.48	0.40	0.75	0.33	0.47	<u>0.04</u>	0.09
GSE7621_all	353	0.61	0.84	0.62	0.90	0.31	0.48	0.40	0.75	0.21	0.47	<u>0.03</u>	0.09

Table 11. PD postmortem datasets correlation with tgNM SN at different ages. ROAST analysis comparing tgNM mice SN region (SN region, left; SN neurons, right) to the corresponding human PD transcriptomic signature from postmortem studies. Public GEO datasets used for the analysis include studies analyzing SN bulk dissections (GSE20163, GSE20164, GSE20292, GSE20333, GSE43490 and GSE7621) and LCM isolated SN neurons (GSE20141 and GSE24378) from PD patients compared to healthy controls. Mixed p-values (p) and FDR (up and downregulated DEGs) are shown. $p \leq 0.05$ are highlighted in bold and underlined.

PD postmortem study	Ngenes	tgNM LC region			
		3m		12m	
		p-value	FDR	p-value	FDR
GSE43490_all (LC)	392	<u>1.00E-04</u>	<u>1.00E-04</u>	<u>1.00E-04</u>	<u>1.00E-04</u>

Table 12. PD postmortem datasets correlation with tgNM LC at different ages. ROAST analysis comparing tgNM mice LC region to the corresponding human PD transcriptomic signature from postmortem studies. Public GEO dataset from LC bulk dissection (GSE43490) from PD patients compared to healthy controls was used for the analysis. Mixed p-values (p) and FDR (up and downregulated DEGs) are shown. $p \leq 0.05$ are highlighted in bold and underlined

We then compared the same transcriptomic signatures to PD-associated gene sets from public databases based on experimental data. In this case, 5 out of 7 PD-associated gene sets showed statistically significant correlation with tgNM SN neurons and all of them showed significant correlation with LC region (Table 13&14).

PD-linked dataset	Ngenes	SN region						SN neurons					
		3m		12m		20m		3m		12m		20m	
		p	FDR	p	FDR	p	FDR	p	FDR	p	FDR	p	FDR
ClinVar Gene-Phenotype Associations	2	0.48	0.68	0.77	0.77	0.39	0.54	0.80	0.80	0.35	0.56	0.08	0.08
DISEASES Curated Gene-Disease Association Evidence Scores	29	0.49	0.68	0.64	0.77	0.54	0.54	0.69	0.79	0.71	0.71	<u>0.03</u>	0.06
DISEASES Experimental Gene-Disease Association Evidence Scores	87	0.41	0.68	0.60	0.77	0.50	0.54	0.38	0.79	0.53	0.66	0.07	0.08
GAD Gene-Disease Associations	208	0.53	0.68	0.45	0.77	0.18	0.54	0.38	0.79	0.26	0.56	<u>0.03</u>	0.06
GWAS Catalog SNP-Phenotype Associations	30	0.44	0.68	0.32	0.77	0.44	0.54	0.68	0.79	0.57	0.66	0.05	0.06
GWASdb SNP-Disease Associations	634	0.55	0.68	0.69	0.77	0.36	0.54	0.37	0.79	0.26	0.56	<u>0.04</u>	0.06
High-priority PD genes (PUKAI)	44	0.68	0.68	0.33	0.77	0.27	0.54	0.67	0.79	0.29	0.56	<u>0.02</u>	0.06
PD gene set (PUKAI)	300	0.64	0.68	0.57	0.77	0.24	0.54	0.59	0.79	0.28	0.56	<u>0.04</u>	<u>0.06</u>

Table 13. Gene-lists linked to PD genetically and experimentally. ROAST analysis comparing tgNM mice SN region (left) and SN neurons (right) with PD-related gene sets from different databases. Mixed p-values (p) and FDR (up and downregulated DEGs) are shown. $p \leq 0.05$ are in bold and underlined.¹

PD-linked dataset	Ngenes	tgNM LC region			
		3m		12m	
		p	FDR	p	FDR
GAD Gene-Disease Associations	210	<u>1.00E-04</u>	<u>1.00E-04</u>	<u>1.00E-04</u>	<u>1.00E-04</u>
GWASdb SNP-Disease Associations	660	<u>1.00E-04</u>	<u>1.00E-04</u>	<u>1.00E-04</u>	<u>1.00E-04</u>
DISEASES Experimental Gene-Disease Association Evidence Scores	92	<u>1.00E-04</u>	<u>1.00E-04</u>	<u>1.00E-04</u>	<u>1.00E-04</u>
GWAS Catalog SNP-Phenotype Associations	31	<u>2.00E-04</u>	<u>2.00E-04</u>	<u>3.00E-04</u>	<u>3.33E-04</u>
DISEASES Curated Gene-Disease Association Evidence Scores	27	<u>1.00E-04</u>	<u>1.00E-04</u>	<u>4.00E-04</u>	<u>4.00E-04</u>
High-priority PD genes (PUKAI)	44	<u>1.00E-04</u>	<u>1.00E-04</u>	<u>1.00E-04</u>	<u>1.00E-04</u>
PD gene set (PUKAI)	301	<u>1.00E-04</u>	<u>1.00E-04</u>	<u>2.00E-04</u>	<u>2.40E-04</u>
ClinVar Gene-Phenotype Associations	2	<u>2.66E-01</u>	<u>2.66E-01</u>	<u>4.98E-01</u>	<u>4.98E-01</u>

Table 14. Gene-lists linked to PD genetically and experimentally. ROAST analysis comparing tgNM mice LC region with PD-related gene sets from different databases. Mixed p-values (p) and FDR (up and downregulated DEGs) are shown. $p \leq 0.05$ are in bold and underlined.

¹ SN and LC correlation analysis with PD-associated datasets were done at different times and thus, contain different number of genes.

Recent studies characterizing PD transcriptomic signatures using single-cell RNAseq are able to identify cell-type-specific PD transcriptomic profiles. Also, these studies intend to identify the specific SNpc DA subtypes that are especially vulnerable to the disease. One recent study identified a specific remarkable microglial signature in PD and a specific DA neuronal subtype (CADPS2-high) as specially enriched in PD. In order to compare the microglial profile in our tgNM mice to that reported in PD, we compared the DEGs in microglia from PD postmortem tissue with our dataset from SN region at 20m of age and detected a clear clustering between wt and tgNM animals (Fig. 42a). This suggests that the inflammatory profile in tgNM is highly similar to that found in microglial cells in PD. We then compared the DEGs in DA neurons from this same study with the tgNM SN neurons at 20m. In this case, we did not find a great overlap with the DEG in PD postmortem DA neurons with tgNM SN neurons (only 7 genes were differentially expressed in tgNM SN neurons) (Fig. 42b).

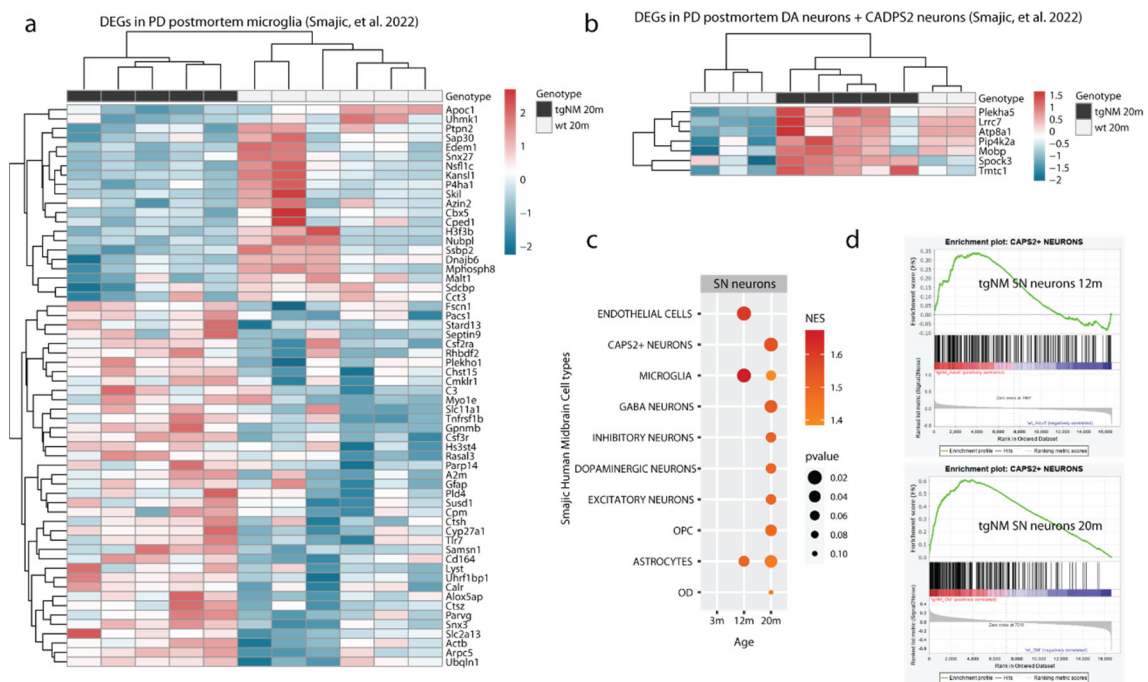


Figure 42. TgNM profiles in relation to single-cell postmortem SN dataset. **a)** Heatmap showing expression values in Z-scored (low to high, blue to red) of DEGs in dataset of SN region at 20m that are reported to be altered in PD postmortem microglia compared to controls in Smajic, et al. 2022 dataset (Smajić, et al., 2022). **b)** Heatmap showing expression values in Z-scores (low to high, blue to red) of DEGs ($p \leq 0.05$) in our dataset of SN neurons at 20m that are reported to be altered in PD DA neurons and CADPS2-positive neurons compared to controls in Smajic, et al, 2022 dataset (Smajić, et al., 2022). Except Plekha5 (DEG in DA neurons) all the other genes are found differentially expressed in CADPS neurons. **c)**

GSEA analysis of the cell groups found in aged midbrain (PD and controls) in our SN neuronal datasets. **d)** GSEA enrichment plot of CAPS2-positive neuronal dataset present in the list of DEG in tgNM compared to wt in SN neurons at 12m and 20m.

To see the enrichment of specific human cell types in the SN with increasing NM levels, we performed GSEA with the whole SN cell types datasets with age. We found a significant enrichment of neuroinflammatory cell transcripts in SN neurons at 12m of age, while at 20m of age there is a significant enrichment of neuronal subtypes and specifically CADPS2+ neurons gene set (Fig. 42c,d). This observation suggests that accumulation of NM increases similarity to aged midbrain inflammatory profiles and neuronal profiles, including the PD-enriched CAPDS2 subtype.

These results suggest that high levels of NM intracellular accumulation (SN at 20m and LC at all ages) induce a transcriptomic signature that correlates with that of PD postmortem brains. Also, tgNM SN neurons appear to concentrate the majority of the DEGs that correlate with postmortem SN PD brains, since a neuronal enrichment is necessary for a statistically significant correlation with postmortem studies. Our results also support the concept that LC degeneration observed in young tgNM mice, as described in Chapter 1, may already be equivalent to advanced stages of PD pathogenesis.

5. Validation of potential NM-related pathways and targets

As shown in Chapter 1, tgNM mice show early and advanced neurodegeneration in LC together with DA neuronal dysfunction concurring with typical PD-like pathology. Thus, the DA system in this model represents an opportunity to understand the mechanisms driving DA dysfunction and consequently identify potential targets, whose modulation might be in time to rescue the undergoing cascade of pathological events. To reliably identify potential therapeutic targets within the tgNM transcriptomic datasets generated and described above, we next performed validation of the main identified biological pathways at transcript and protein levels in the DA dysfunctional areas.

We assessed distinct markers of the identified biological pathways in tgNM pigmented neurons, including the immune system, proteostasis (ALP and proteasome), transcription/translation, and cell cycle in SN and VTA regions. First by qPCR, we confirmed the early neuroinflammatory response in these areas, which was greater in

VTA neurons than in SN neurons (e.g. increases in Tyrobp, Lyz2, Gpnmb, and CD68) and also confirmed the dysregulation of ALP markers (e.g. Extl3, Laptm5, Grn, Hexb, Lamp1 and Parkin) (Fig. 43). Interestingly, in SN neurons we detected early alterations in the expression levels of: (i) Parkin (Prkn), the PD-genetically-linked E3 ubiquitin ligase complex that targets proteins for proteasomal degradation; (ii) Impact, a master regulator of protein synthesis; (iii) Rgl1, a predicted guanine nucleotide exchange factor involved in signal transduction; and (iv) Pttg1, related to chromosome stability and DNA repair (Fig. 43). These alterations occurred in parallel to the first signs of DA dysfunction in this area (i.e. TH- downregulation, deficits in DA release, LB-like inclusions).

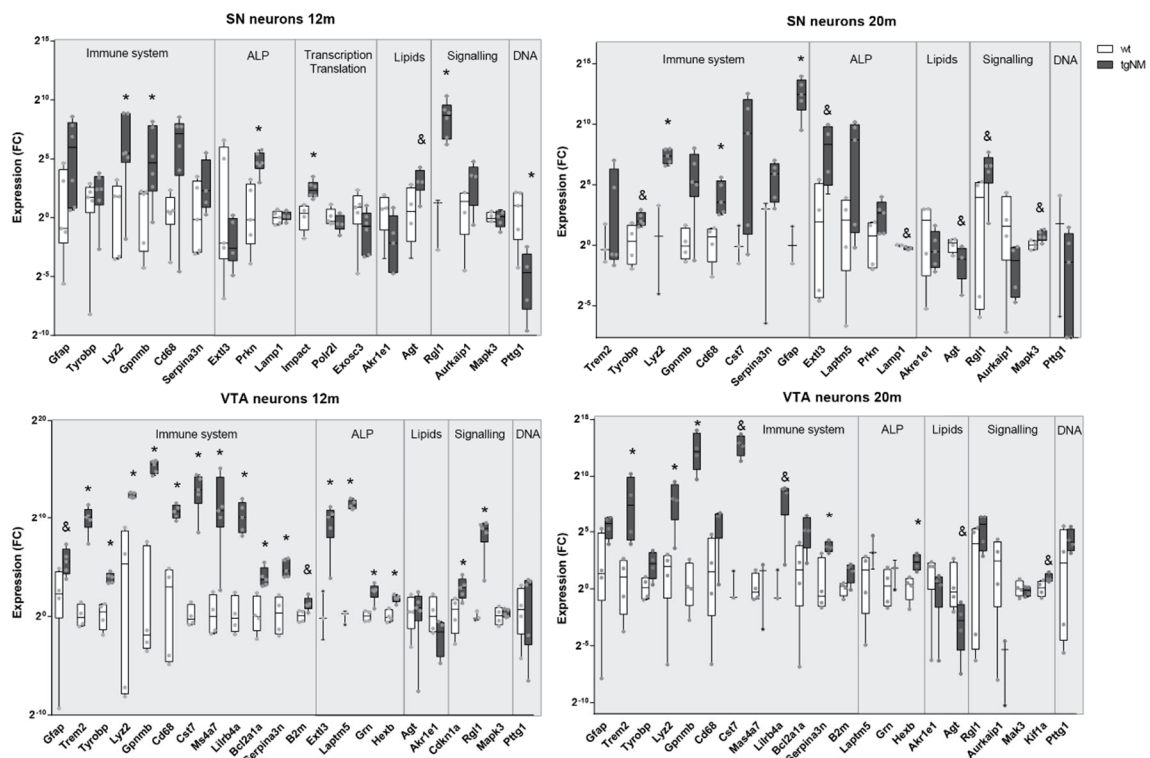


Figure 43. Biological pathway validation at the RNA level. Transcripts from the main biological pathways [Immune system, Autophagy Lysosomal Pathway (ALP)], Transcription and translation, Cell organization and communication (Signaling), and cell cycle or DNA damage (DNA) were assessed by qPCR in SN and VTA neurons from tgNM and wt mice at 12m and 20m of age. Fold changes compared to wt are calculated with the comparative method and normalized with the three less variable genes in the datasets (Ndn, Ppia and Rtn1). * $p \leq 0.05$ compared to age-matched wt (Mann-Whitney test), & $p \leq 0.06$ compared to age-matched wt (Mann-Whitney test). SN12m [n=5(wt) n=6(tgNM)], VTA 12m [n=4(wt), n=5(tgNM)], SN 20m [n=4(wt), n=5(tgNM)], VTA 20m [n=4(wt), n=4(tgNM)].

We then confirmed alterations at the protein level in key players of proteostasis, including increases in key components of the proteasomal system such as ubiquitin and Parkin and decreases in autophagy-related proteins (Lamp1, LCI, LCII, ProCstD, CtsD) (Fig. 44a-

b). These results are consistent with our previous *in vitro* findings in NM-accumulating cells, where clear alterations in the proteostasis mechanisms were reported (Carballo-Carbajal et al., 2019). In addition, some mitochondrial proteins were also decreased (Drp1 and Vdac), consistent with the mitochondrial biological pathway enrichment in downregulated genes at this age in tgNM (Fig. 33 & 34). Upregulation of immune-related markers, such as Iba1, were confirmed, though others like CD68 did not show increased protein levels by WB in vMB homogenates (Fig. 44a-b). Still, we decided to evaluate histologically the expression of CD68, which is indicative of the phagocytic capacity of microglial cells or blood-borne macrophages and has been shown to be increased in PD patients (Doorn et al., 2014). CD68-positive cells were only detected in tgNM animals and absent in wt, confirming the activation of this phagocytic marker by NM accumulation (Fig. 44c). The quantification of CD68-positive cells showed a progressive increase with age of this phagocytic marker in both the SN and the VTA (Fig. 44d), thus following the same trend as the transcriptomic data. These neuroinflammatory changes complement the microgliosis (increased reactive Iba1-positive cells) and astrogliosis (increased GFAP-positive cells) reported in the initial characterization of tgNM mice in Chapter 1.

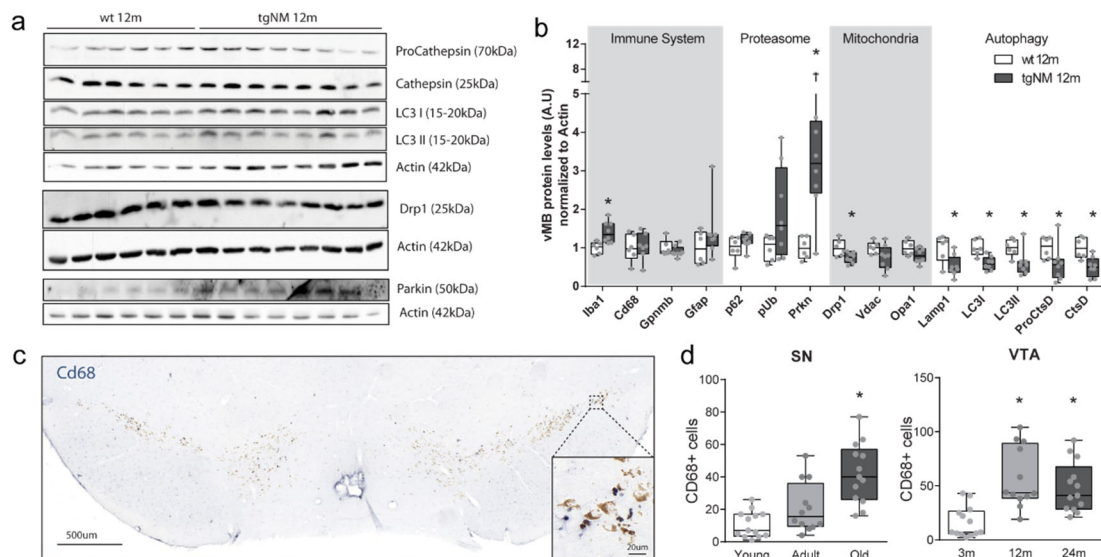


Figure 44. Biological pathway validation at the protein level. a) Representative western blot membranes from the main proteins assessed. **b)** Protein quantification normalized to beta-actin. * $p \leq 0.05$ compared to age-matched wt (Mann-Whitney test). $n=6$ (wt), $n=8$ (tgNM). **c)** Representative CD68 immunostaining in SN of a 20m old tgNM. **d)** Quantification of CD68-positive cells/granules in SN and VTA regions at different ages. * $p \leq 0.05$ compared to 3m (Kruskal Wallis, Dunn's multiple comparisons test). SN and VTA; $n=13$ (3m), $n=12$ (12m), $n=13$ (20m).

Considering the reduction in autophagic protein levels observed in tgNM mice we then sought to evaluate the integrity of the lysosomal function in these animals by measuring enzymatic activities of the main lysosomal enzymes. We performed lysosomal isolation in freshly collected brain tissue, including dissection of the main pigmented areas (i.e. whole vMB, dissected SN-VTA, LC, DVC), from tgNM and wt mice as previously described (Navarro-Romero et al., 2022). The lysosomal enrichment was first confirmed by an increased GBA activity in the enriched fractions compared to total homogenates (Fig. 45a-b). We detected a decrease in GBA activity in DVC isolated lysosomal fractions from tgNM compared to wt animals, while a trend to decreased activity was detected in LC and no change was evident in SN-VTA isolated fractions (Fig. 45c). We did not detect any changes in β -Hexosaminidase (β -Hex) and acid phosphatase (AP) activities. These results report a detectable lysosomal alteration (i.e. GBA activity) in lower brainstem pigmented nuclei but not in midbrain pigmented nuclei. Considering unpublished *in vitro* data generated in the lab showing impaired GBA activity in NM-accumulating cells in culture (data not shown), we envision that further *in vivo* studies evaluating a pure pigmented cell population should be done to better determine lysosomal integrity in NM-accumulating neurons.

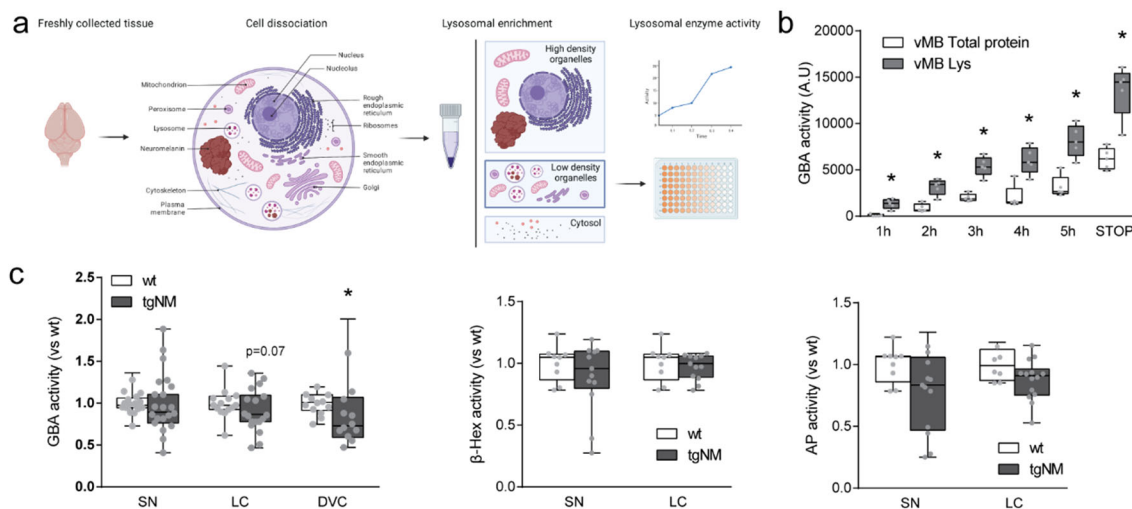


Figure 45. Lysosomal activity in tgNM mice. **a)** Experimental approach for lysosomal activity measurements in lysosomal-enriched samples. **b)** Activity levels detected at different reactions times in total protein homogenates (Total protein) and lysosomal-enriched (Lys) homogenates. * $p \leq 0.05$ compared to total protein (Multiple Mann-Whitney tests). $n=5$ vMB. Arbitrary Units, A.U. **c)** β -Glucocerebrosidase (GBA), β -Hexosaminidase (β -Hex), and acid phosphatase (AP) activities in pigmented brain regions of tgNM at an old age 15-20m. * $p \leq 0.05$ compared to age-matched wt (Mann-Whitney test). GBA activity: SN [($n=24$ (wt), $n=28$ (tgNM))], LC [$n=21$ (wt), $n=28$ (tgNM)], DVC [$n=15$ (wt), $n=15$ (tgNM)]. AP activity: SN

[n=9 (wt), n=13 (tgNM)], LC [n=8(wt), n=14 tgNM]. β -Hex activity: SN [n=9 (wt), n=13 (tgNM)], LC [n=9 (wt), n=13 (tgNM)].

6. Pan-regional neuroinflammatory NM-related genes

With the transcriptomic characterization, we identified 11 genes commonly altered in all pigmented regions related to neuroinflammatory processes. We also noted that there was a clear enrichment of genes known to be related to the described phenotype of disease-associated-microglia (DAM) in the top differentially expressed genes in all areas. DAM genes were initially identified as a gene-network found in microglia isolated from Alzheimer's disease patients, though similar networks seem to participate in multiple other neurodegenerative diseases (Butovsky & Weiner, 2018; Deczkowska et al., 2018; Friedman et al., 2018; Keren-Shaul et al., 2017). Specifically, *Trem2*, which is upregulated in all areas of tgNM, is one of the hub genes in DAM and is essential for the phagocytosis of apoptotic neurons (Hsieh et al., 2009; Takahashi, Rochford, & Neumann, 2005).

We performed a supervised search of known DAM-associated genes (*Tyrobp*, *Trem2*, *Gpnmb*, *Lyz2*, *CD68*, *Lgals3*, *Lilrb4a*, *Axl*, *Apoe*, etc) extracted from different studies characterizing microglial states in disease (Butovsky & Weiner, 2018; Keren-Shaul et al., 2017; Rangaraju et al., 2018). We identified a clear network that is overexpressed in all NM-accumulating areas (Fig. 46a, left panel). Importantly, DAM-associated genes in SN and VTA occurred concomitant to DA dysfunction in these regions, in absence of overt neurodegeneration. These DAM changes were detected in neuronal-enriched samples, implying that these changes might be the consequence of a direct crosstalk with dysfunctional neurons and their immediate extracellular space and/or glial cells in close physical contact. As expected by the high degree of neurodegeneration, we found a clear upregulation of DAM genes already at 3m of age in the LC of tgNM mice. Additionally, we also performed the same search for genes expressed in homeostatic microglia and these were only differentially expressed in VTA and LC, but not in the SN (Fig. 46a, right panel). This observation indicates that while in the VTA and LC there is a general increase in the microglial population together with a phenotypic display of DAM genes, in the SN there is mainly an increase in specific DAM genes, which might be pointing to a very early alteration of the microglial phenotype. These top microglial transcripts were validated by qPCR for SN, VTA and LC regions (Fig. 46b).

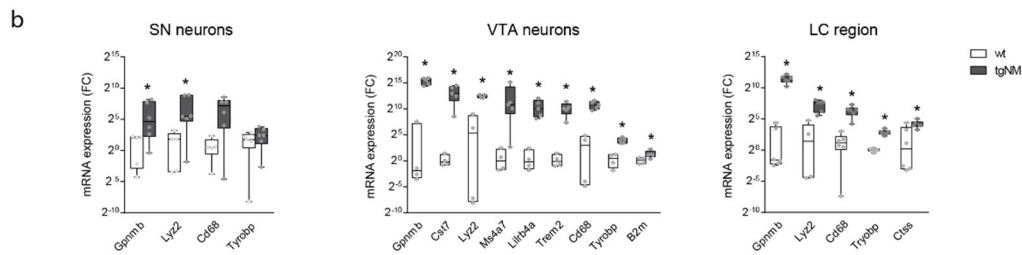
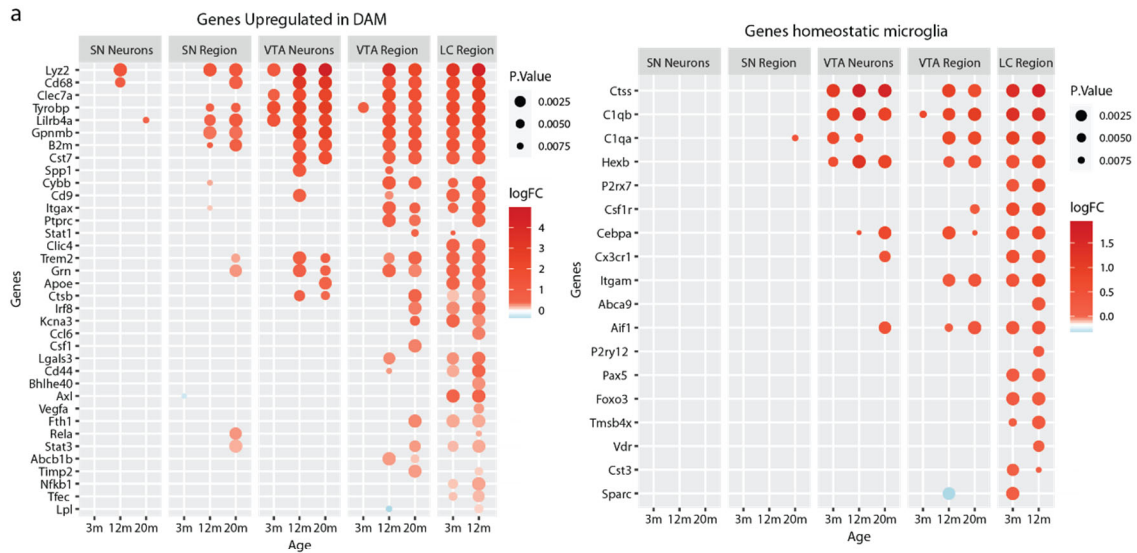


Figure 46. DAM-associated genes increased in all NM-accumulating areas in tgNM. a) Differentially-expressed genes ($p\text{-value} \leq 0.01$) that are known to be upregulated in microglia during the phenoconversion to DAM (right) and genes considered to be markers of homeostatic microglia (left) extracted from (Butovsky & Weiner, 2018; Keren-Shaul et al., 2017; Rangaraju et al., 2018) and shown for all the samples analyzed. Upregulated transcripts are shown in red (positive logFC) and downregulated transcripts are shown in light blue (negative logFC). **b)** Expression of main DAM genes in SN and VTA neurons at 12m (data also presented in Fig. 42 and shown here for comparison) and LC region at 3m validated by qPCR using the comparative method normalized to wt (Fold change, FC) $*p \leq 0.05$, compared to age-matched wt (Mann Whitney test). SN [n=5(wt), n=6(tgNM)], VTA [n=4(wt), n=5(tgNM)], LC [n=6(wt), n=6(tgNM)].

To further characterize the neuroinflammatory profile of tgNM mice we performed a quantitative ELISA for the specific detection of 18 inflammatory cytokines in SN-VTA and LC brain dissections (Fig. 47). We detected increases in IL-1 α (inflammatory) and decreases in IFN lambda (IL-28) (anti-inflammatory) in SN-VTA homogenates in tgNM. Although IL-10 was not significantly altered in tgNM, we detected a positive and negative correlation with IFN lambda (IL-28) and IL-1 α respectively, suggesting an involvement also of IL-10 in the neuroinflammatory reaction detected in tgNM. We also detected a trend to increase of epithelial-cell-derived neutrophil-activating protein (ENA)-78 (CXCL5) in SN, which acts as a neutrophil infiltration chemoattractant (G. N. Liu et al., 2009; Zwijnenburg, De Bie, Roord, Van Der Poll, & Van Furth, 2003)

($p=0.06$ for SN and $p=0.11$ for LC, Mann-Whitney test). Also, ENA-78 levels in tgNM LC correlated positively with IFN α and M-CSF levels, pointing to a potential link with common alterations in these cytokines as well. We did not detect changes in other inflammatory cytokines (e.g. IL-1 β , IL-6, IL-17A, TNF α) except from a trend to increased levels of IL-6 in the SN of tgNM mice.

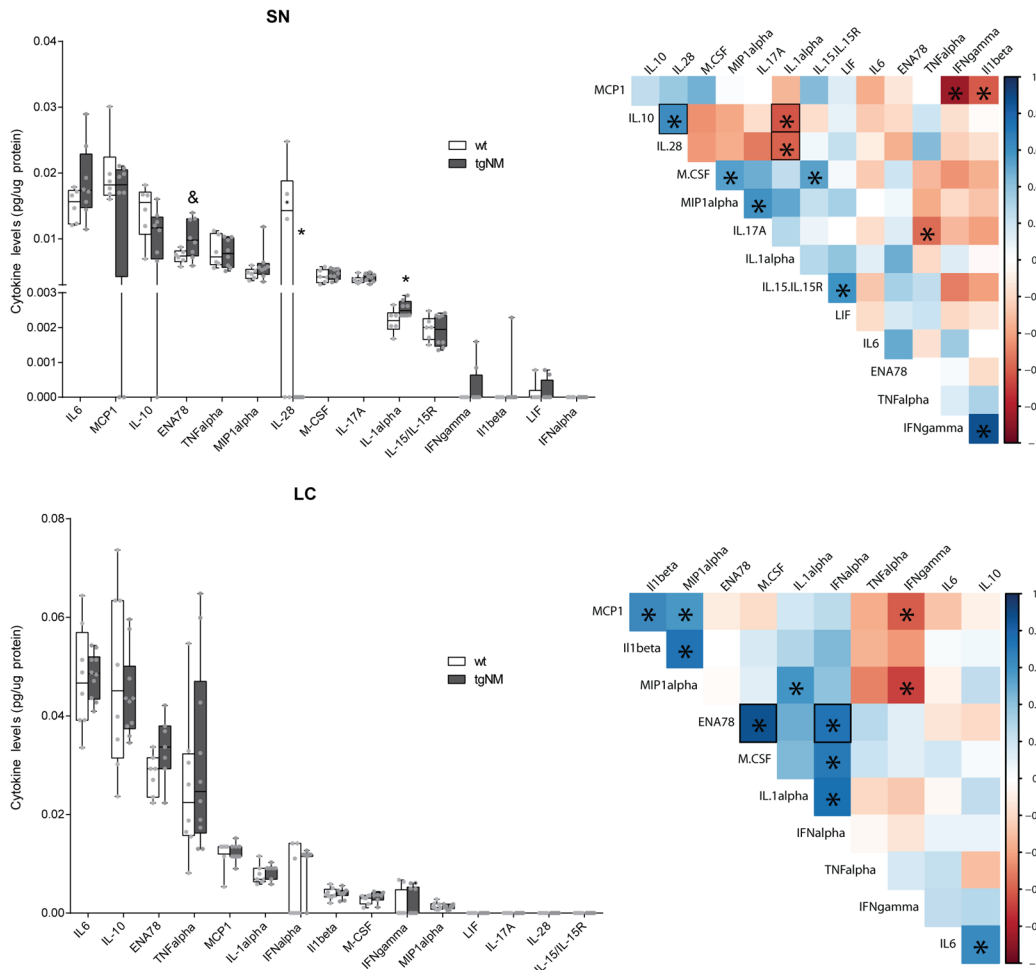


Figure 47. Cytokine profile in pigmented areas of tgNM mice. Left, Cytokine levels (pg/ug protein) in SN at 12m and LC at 3m of age. IL-3, IL-31, G-CSF were not detected in any of the pigmented brain regions (not shown). * $p \leq 0.05$ compared to age-matched wt, & $p \leq 0.06$ compared to age-matched wt (Mann-Whitney test). Right, Correlation matrix of all cytokines. Squared boxes represent the correlation found between the altered cytokines in tgNM with all the others. Colors represent correlation coefficients * $p \leq 0.05$ Spearman correlation.

Since peripheral immunologic alterations have also been shown in PD patients (Qin, Zhang, Cao, Loh, & Cheng, 2016), we hypothesized that peripheral inflammatory changes might also be detected in serum samples of tgNM mice. We assessed the peripheral inflammatory profile of tgNM mice at 12m of age and detected ten out of the eighteen assessed cytokines. We observed a trend to increased levels of G-CSF in serum

of tgNM compared to wt mice (Fig. 48) and a correlation with IL1 α levels, a cytokine that is also increased in tgNM mice SN-VTA (Fig. 48). However, no changes were found in any of the other cytokines assessed. The absence of a clear altered cytokine profile in tgNM mice serums suggest that the ongoing inflammatory processes in the central nervous system in these animals at this age is still highly localized within the brain. Older tgNM animals might show higher levels of systemic inflammatory cytokines and should thus be assessed for the potential identification of inflammatory biomarkers.

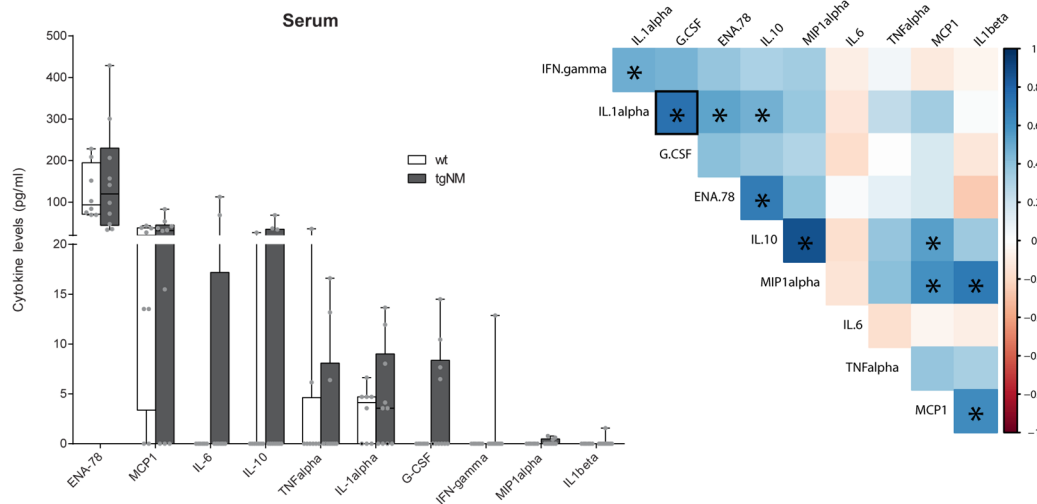


Figure 48. Peripheral neuroinflammatory markers in tgNM mice. a. Cytokine profile assessed in adult tgNM and wt mice. Left, cytokine levels (pg/ml of serum). IL-17A, IFN-alpha, IL-15/IL15R, IL-28, IL-3, M-CSF, LIF, IL-31 were not detected in serum (not shown). Mann-Whitney test not significant. Right, Correlation matrix of all cytokines. Squared box represents correlation of G-CSF, which shows a trend to increase in tgNM mice, with the other cytokines. Colors represent correlation coefficients * $p \leq 0.05$ Spearman correlation. [n=8 (wt), n=10 (tgNM)].

7. GPNMB as a possible NM-linked therapeutic target

When trying to select potential therapeutic targets within the differentially-expressed genes identified between pigmented and non-pigmented mice, GPNMB emerged as a candidate target because of the early/middle age upregulation in all pigmented areas analyzed (i.e. SN, VTA and LC), its reported functions (melanogenic, phagocytic and immune-related) and genetic association to PD.

GPNMB (Glycoprotein nmb) is a type I transmembrane glycoprotein that belongs to the premelanosome protein (PMEL)/NMB family due to its homology to the pMEL17 precursor, a melanocyte-specific protein (Turque et al., 1996; Weterman et al., 1995). It

is expressed in melanocytes where it is essential for the formation of melanosomes (Loftus et al., 2009; P. Zhang et al., 2012). Interestingly, GPNMB locus has been linked to higher PD risk by GWAS studies (Kaiser et al., 2022; Z. hua Liu et al., 2015; Murthy et al., 2017; Pihlstrøm et al., 2013) and it has consistently been shown to be overexpressed in PD postmortem SN (Brendza et al., 2021; Kamath et al., 2022; Moloney, Moskites, Ferrari, Isacson, & Hallett, 2018; Smajić, et al., 2022; Tiklová et al., 2021). GPNMB has been described to play a key role in macroautophagy (recruitment of the autophagy protein LC3 to the phagosome and degradation of phagosomal components) in injured epithelial cells and inflammatory macrophages (Li et al., 2010). Also, it has been proposed to participate in anti-inflammatory processes in the brain (Saade, Araujo de Souza, Scavone, & Kinoshita, 2021). Recently, it has also been related to α -synuclein internalization by neuronal cells (Diaz-Ortiz et al., 2022). However, the exact role of this protein in the pathophysiology of neurologic diseases is still unknown. Additionally, GPNMB has an extracellular domain that can be cleaved by the metalloprotease ADAM10, releasing a soluble extracellular domain (Rose et al., 2010) that has been shown to bind many receptors (Saade et al., 2021). So when GPNMB is in the plasma membrane, this extracellular domain might facilitate therapeutic modulation and when cleaved might be used as a systemic biomarker.

GPNMB expression in tgNM was clearly associated to NM accumulation. It increased over time and it was highly expressed in the LC, followed by the VTA and SN (Fig. 49a), mirroring NM accumulating levels in these areas (LC>VTA>SN) (Fig. 19a). We also found that wt animals did not show any basal expression of GPNMB up to 20m of age by qPCR experiments (MeanCT \pm SD=39.2 \pm 2.5). In tgNM animals, GPNMB expression signal amplification ranged between 36 and 26 CTs [MeanCT \pm SD=25.6 \pm 1.8 (LC), 28.6 \pm 7.4 (VTA), 35.9 \pm 4.2 (SN)]. These results suggest that GPNMB is a NM-dependent transcript whose expression might be induced in response to the progressive accumulation of NM in tgNM mice. We next validated GPNMB overexpression at the protein level by immunohistochemistry and found a clear co-localization with NM (Fig. 49b). We then performed a double immunofluorescence and found no co-localization with TH-positive neurons, suggesting either that GPNMB-positive NM-accumulating neurons have lost their TH phenotype, that they correspond to GPNMB-positive eNM or that GPNMB is expressed in NM granules engulfed by phagocytizing glial cells (Fig. 49c).

Since GPNMB has an extracellular domain (Saade et al., 2021) that can be cleaved, we sought to determine if this could be used as a systemic biomarker in serum samples from tgNM animals at adult (6-8m) and old (16-18m) ages. Our results showed a statistically-significant decrease of GPNMB levels in serum of old tgNM compared to age-matched wt animals (Fig. 49d).

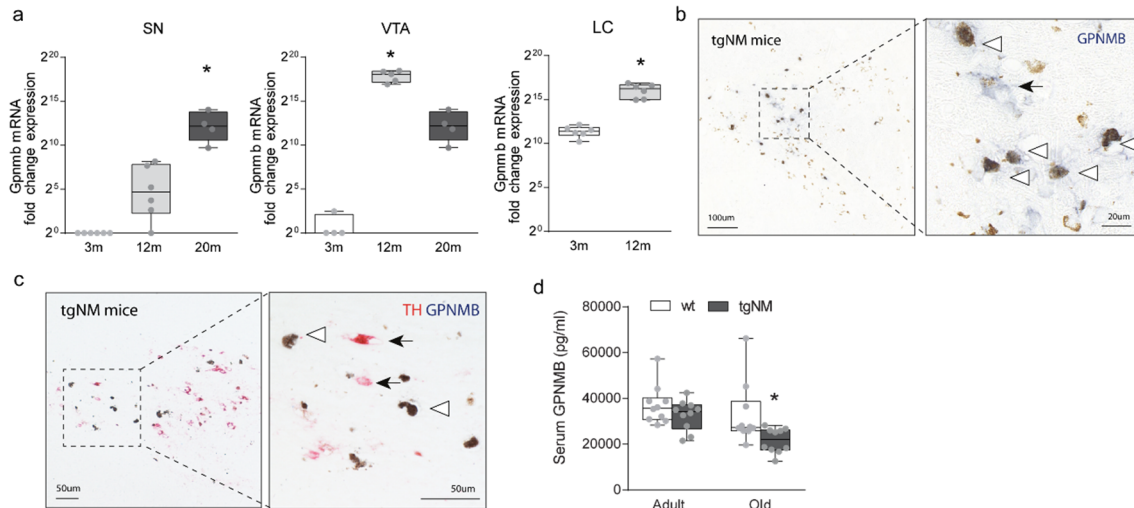


Figure 49. GPNMB expression in tgNM mice. a) Gpnmb expression in SN neurons, VTA neurons and LC region from tgNM mice at different ages. Levels of expression are shown in fold changes compared to wt and normalized to Rtn1, Ppia, and Ndn endogenous reference genes. Almost no expression was detected in wt. (SN and VTA) $*p \leq 0.05$ compared to 3m (Kruskal Wallis, Dunn's multiple comparison test) (LC) $*p \leq 0.05$ compared to 3m (Mann-Whitney test). $n=4-6$ per group. **b)** Representative image of GPNMB immunohistochemistry in 20m old tgNM mice. Normally GPNMB-immunoreactivity is observed co-localizing with NM (arrowheads), sometimes neuronal shapes with faint NM are also visible (arrow). **c)** Representative image of TH and GPNMB double immunohistochemistry in 20m old tgNM mice. No co-localization was found between TH immunoreactivity (arrows) and GPNMB immunoreactivity (arrowheads). **d)** GPNMB levels in serum from adult (6-8m) and old (18-20m) mice determined by ELISA. $*p \leq 0.05$ compared to wt, Mann-Whitney test. Adult [$n=10$ (wt), $n=10$ (tgNM)], Old [$n=10$ (wt), $n=10$ (tgNM)].

We then analyzed the expression of GPNMB in pigmented (SN, LC) and non-pigmented (FC) areas from PD and control subjects (Annex Data Table 6). We first assessed the expression of GPNMB in human cultured melanocytes and confirmed that our expression analysis assay can correctly detect human GPNMB, widely expressed in this cell type (CT mean \pm SD=18.8 \pm 0.7) (Fig. 50a). We then confirmed the expression of GPNMB in human control brains, which was 38 times lower than in human melanocytes (Fig. 50a). We detected an increase in the GPNMB mRNA expression in SN from PD compared to controls, while no difference could be detected in the other pigmented (LC) and non-

pigmented areas (FC) (Fig. 50b). Interestingly, there was a trend for a correlation of GPNMB levels in the SN and PD disease duration (linear regression, $p=0.09$, $R^2=0.34$) (Fig. 50c). We then used the microdissection technique to isolate neuronal tissue from control and PD subjects, including a new cohort of patients as well as some cases from the already characterized population in the bulk analysis (Fig. 50b) and some from another cohort of PD patients (Annex Data Table 6). With this approach, we also confirmed an increased SN GPNMB expression in microdissected neurons from SN PD compared to controls (Fig. 50d). Finally, we validated GPNMB expression in postmortem human control SN at the protein level by immunohistochemistry (Fig. 50e).

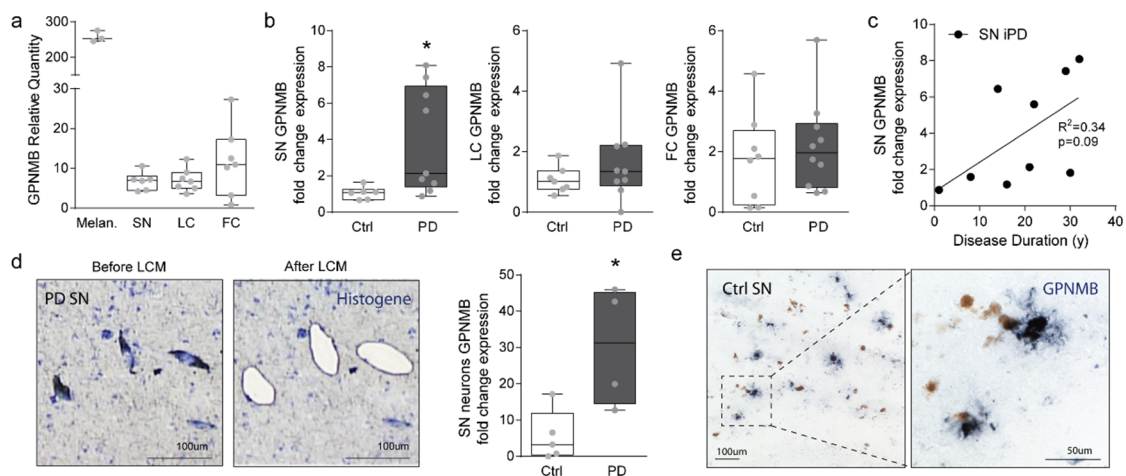


Figure 50. GPNMB expression in PD postmortem SN. **a)** GPNMB expression levels in cultured human melanocytes (melan.) and brain regions from control (Ctrl) human subjects [SN, LC and Frontal Cortex, (FC)]. Relative quantity was calculated using the comparative method and normalizing with the less variable genes in the samples (FO XO1, GOLGA3, HPRT1, and UGGT1). [n=3(melanocyte samples), n=8 (Ctrl brain per region)]. **b)** GPNMB expression levels in two pigmented regions (SN, LC) and one non-pigmented region (FC) in control and PD postmortem tissue. Expression levels are shown as fold changes compared to control subjects previously normalized with endogenous control genes as in d. * $p \leq 0.05$ compared to control (Ctrl), Mann-Whitney test. [n=8 (Ctrl), n=10 (PD)]. Samples with RIN<5 (SN Ctrl n=1, SN PD n=1, LC PD n=1) were excluded. **c)** Correlation analysis between GPNMB levels (fold changes compared to Ctrl) in the SN of PD and disease duration in years post-diagnosis (years, y) (linear regression, $p=0.09$, $R^2=0.34$). Dots represent individual samples. **d) Left,** Images showing the LCM procedure for neuronal isolation from Histogene-stained human PD SN tissue. **Right,** GPNMB expression levels in SN neurons from Ctrl and PD tissue expressed as fold changes compared to Ctrl. $p^* \leq 0.05$ compared to Ctrl. Mann-Whitney test. [n=7 (Ctrl), n=7 (PD)]. Samples with RIN<4 (Ctrl n=2, PD n=2) were excluded. **e)** Representative image of GPNMB immunohistochemistry in postmortem SN tissue from an aged Ctrl subject.

8. GPNMB interplay with NM

Considering all the results above, GPNMB appears as a potential NM-related therapeutic target that might be involved in the pathogenesis of PD. GPNMB has been described to possess multiple functions that could be beneficial in the context of NM-linked pathology, which include the stimulation of melanosome formation in melanocytes (P. Zhang et al., 2012), the anti-inflammatory effect in response to inflammatory stimuli (e.g. colitis, LPS) (Saade et al., 2021), and its essential role in macrophage phagocytosis and lysosomal function (Li et al., 2010; Robinet et al., 2021). In the context of PD, GPNMB has recently been explored in animal models showing inconsistent results depending on the modelling approach. Increased systemic GPNMB expression in transgenic animals is protective in the context of the MPTP neurotoxic PD model (Budge, Neal, Richardson, & Safadi, 2020), while PD models based on α -synuclein (PFF injection into striatum, AAV-A53T α -synuclein injection into SNpc), remain unaffected by the knockout of GPNMB (Brendza et al., 2021).

To understand the possible role of GPNMB in NM-accumulating pathology, we induced AAV-mediated overexpression of human GPNMB in the SNpc of the NM-accumulating AAV-TYR mouse model (Carballo-Carbajal et al., 2019). AAV-TYR model of NM accumulation, as described in our previous work (Carballo-Carbajal et al., 2019), exhibits an earlier and steeper NM accumulation compared to tgNM mice and the pigmentation is restricted to the SNpc, which enables the assessment of a nigral-restricted therapeutic approach. Additionally, the unilateral accumulation of NM enables an easily recognizable motor phenotype with a simple asymmetry test that is associated to a marked nigrostriatal degeneration. In this context, we hypothesized that GPNMB overexpression will modulate NM formation/accumulation and/or PD-like features (i.e. DA cell death, LB-like inclusion body formation, motor symptoms) in the AAV-TYR NM-accumulating mouse model of PD.

We first performed a pilot study to confirm that our injected AAV-GPNMB viral vector was indeed expressing GPNMB in the SNpc of injected mice. In particular, we observed that AAV-induced GPNMB overexpression was confined to DA neurons (TH-positive cells) and not microglia (Iba-1-positive cells) (Fig. 51a). We also confirmed that there was no DA fiber loss in the striatum by AAV-GPNMB injection, ruling out a possible toxic effect associated to AAV-mediated GPNMB overexpression *per se* (Fig. 51b).

Then, AAV-GPNMB and AAV-TYR were injected either in combination or separately above the SNpc of 10-weeks-old mice (n=8 per group and age, for a total of 48 animals) (Fig. 51c). We first performed a motor behavioral assessment with the asymmetry test, which consists on assessing how many times the animals use the contralateral forepaw to step up in a glass cylinder. At 4m post-injection (pi), TYR expressing mice exhibited a reduced use of the contralateral forepaw, while mice expressing both TYR and GPNMB maintained the balanced use of both forepaws (~50%) (Fig. 51d). This was associated with an attenuation of nigrostriatal denervation by GPNMB in NM-producing animals (Fig. 51e). While preliminary, these initial results suggest that GPNMB overexpression may exert a protective effect on NM-linked PD-like pathology.

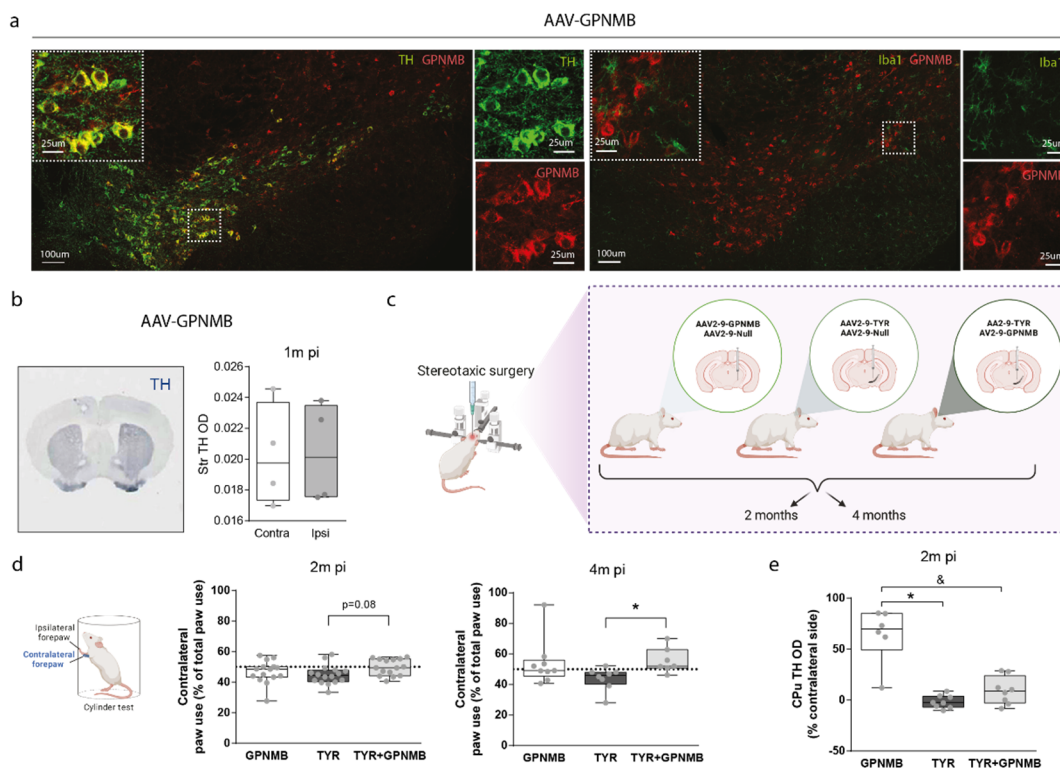


Figure 51. GPNMB overexpression attenuates NM-linked deficits. **a)** Co-localization of GPNMB overexpression in TH-positive cells in the SNpc of AAV-GPNMB-injected mice. No co-localization of GPNMB with Iba-1 positive cells was detected. n=4 AAV-GPNMB injected mice. **b)** Optical densitometry (OD) of striatal TH immunohistochemistry in AAV-GPNMB injected mice. Ipsi, Ipsilateral. Contra, Contralateral. n=4 AAV-GPNMB injected mice. **c)** Schematic diagram of the experimental design for the overexpression of GPNMB and/or TYR by stereotaxic surgery in the mouse SNpc. **d)** Behavioral assessment of motor alterations (asymmetry cylinder test) in AAV-TYR and AAV-TYR+AAV-GPNMB-injected mice at 2 and 4 months (m) post-injection (pi). 2m pi [n=15 (AAV-GPNMB), n=16 (AAV-TYR), n=15 (AAV-TYR+AAV-GPNMB)] 4m pi [n=9 (AAV-GPNMB), n=8(AAV-TYR) n=7 (AAV-TYR+AAV-GPNMB)]. * $p \leq 0.05$ compared to AAV-TYR injected mice (Kruskal Wallis, Dunn's multiple comparison test). **e)** Optical densitometry (OD) of striatal TH immunohistochemistry in AAV-GPNMB and

AAV-TYR and AAV-TYR+AAV-GPNMB injected mice shown as percentage of contralateral side (%). * $p \leq 0.05$ compared to AAV-GPNMB injected mice, & $p \leq 0.06$ compared to AAV-GPNMB injected mice (Kruskal Wallis, Dunn's multiple comparisons test). n=6 (AAV-GPNMB), n=8 (AAV-TYR), n=8 (AAV-TYR+GPNMB).

The remaining characterization of SNpc neuropathology (e.g. NM levels, SNpc stereological cell counts, number of eNM, neuroinflammation) are currently ongoing. The results from these experiments will enable the identification of a potential role of GPNMB in modulating NM levels and PD-related pathology.

DISCUSSION

DISCUSSION

In the present work, we have generated an experimental *in vivo* model of age-dependent production and intracellular accumulation of human-like NM within PD-vulnerable catecholaminergic neuronal groups. Our results support the concept that modelling human continuous age-dependent brain-wide pigmentation in mice is sufficient to ultimately trigger a progressive PD-like phenotype with motor and non-motor deficits, affecting multiple neuronal systems in the brain and peripheral organs and to induce a PD-like transcriptomic profile. Finally, the NM-associated target GPNMB is identified as a new potential therapeutic agent for PD.

1. Generation of a new TYR-expressing NM-accumulating model of PD

1.1 TYR overexpression in mice

First of all, the generation of a transgenic mouse model overexpressing an exogenous protein deserves special attention to the effects of the protein overexpression itself. TYR possesses a double-edge synthesizing property. On the one hand, TYR has catecholamine-synthesizing activity (Rios et al., 1999), which may lead to higher DA levels and consequently higher DA-oxidation and DA-induced toxicity. On the other hand, the oxidizing capacity of TYR may also remove excess amounts of cytosolic DA into the formation of NM granules, which can in turn prevent progressive cell damage. These two sides of the same coin cannot be independently investigated, since TYR participates in different steps of the same process. Our data suggests that TYR is not producing an excess of cytosolic DA since DA levels are not changed in tgNM mice. Also, other studies modulating TYR expression suggest a potential protective role of the expression of Tyr in mice. Tyr null mice show aggravated methamphetamine-induced DA neurotoxicity (Miyazaki et al., 2006) and inhibition of TYR in catecholaminergic cells *in vitro* induces cell death (Higashi, Asanuma, Miyazaki, & Ogawa, 2000). These results suggest that TYR expression *per se* is not neurotoxic and it is hypothesized that TYR exerts its protective role by generating NM. However, our results in AAV-TYR overexpressing rodents (Carballo-Carbajal et al., 2019) and in tgNM mice indicate that NM can impact negatively in cellular homeostasis leading to neuronal dysfunction and neurodegeneration when exceeding a particular threshold of intracellular accumulation.

In line with this, the decrease of intracellular NM levels in AAV-TYR rats after boosting lysosomal exocytosis without modulating oxidative TYR capacity results in a protective effect in these animals (Carballo-Carbajal et al., 2019). These observations support the notion that the etiopathogenic factor underlying PD-like features in tgNM mice is the NM accumulation and not the expression of TYR *per se*.

1.2 Modelling brain pigmentation distribution and accumulation

Pigmentation in the human brain occurs at varying degrees in all catecholaminergic nuclei (A1-A14) and the most highly pigmented nuclei are midbrain areas SN/A9 and VTA/A10, pontine area LC/A6 and medullary area DVC/A2 (Bogerts, 1981; C. Saper & Petit, 1982). In tgNM mice, pigmentation occurs at varying degrees in all catecholaminergic nuclei, as in the human brain, being these same three nuclei detected by simple macroscopic observation in a clarified tgNM mouse brain. The intensity of NM granules in NM-producing mice indicated a progressive age-dependent and caudorostral ascending pattern of NM accumulation, reaching higher levels of pigmentation earlier in the medulla and pons than in midbrain nuclei. These results are consistent with studies evaluating NM content in human pigmented nuclei, which showed age-dependent NM accumulation with higher levels of pigmentation earlier in the LC than in the SN (Fedorow et al., 2006; L. Zecca et al., 2004).

1.3 Dopaminergic dysfunction

Degeneration of SNpc neurons and the motor alterations resulting from depletion of DA input into the striatum currently constitute the cardinal symptoms of the disease and the basis for a clinical diagnosis. Studies evaluating the neighboring VTA integrity suggest that it is a relatively spared population, compared to the SNpc. However, a total of 5 studies have analyzed cell death in the VTA and the one that used stereological cell counting reported a cell loss of 31% in three PD cases compared to three controls (Giguère et al., 2018; McRitchie et al., 1997). In tgNM mice, progressive age-dependent NM accumulation resulted in DA dysfunction detectable at an adult age (i.e. TH phenotypic loss, decreased fiber density and impaired DA release in the striatum), although no actual significant cell loss was detected up to old ages (20m). In contrast to the above mentioned studies assessing cell death in postmortem PD tissue, we did not detect a special resistance of VTA cells to dysfunction in tgNM mice. Indeed, we detected a slightly higher degree of vulnerability in VTA cells including: i) higher loss of TH fibers in the VTA- projection areas of the striatum (nucleus accumbens [NAcc] and olfactory tubercle [OT]) (Chapter

1, Fig. 21), ii) higher numbers of eNM (Chapter 1, Fig. 21), and iii) higher gene expression changes (Chapter 2, Fig. 30d). This might be due to the fact that in VTA, neurons exhibit a major portion of their cytoplasm occupied by NM compared to the SNpc (mean NM occupied cell area; VTA 3m: 34.4%, VTA 12m: 46.8%, VTA 20m: 51.8% vs SN 3m: 28.1%, SN 12m: 37.8%, SN 20m: 35.5%), which is also in line with our observation that VTA cells show a smaller cell area than SN cells. However, this is not reported in other studies that show similar cell areas between SN and VTA neurons (Bucci et al., 2017). Another possibility is that the specific physiology of VTA cells determines a higher vulnerability than SNpc cells to cope with a similar amount of induced NM in tgNM mice. However, this is not the case in human PD, where there is a lower degree of cell loss in the VTA than in the SNpc. This difference could be explained by specific species differences, or by the fact that in humans not all VTA cells are pigmented and levels of NM accumulation per cell might be different than in SNpc cells. In summary, tgNM mice does not show a specific higher vulnerability of SN cells compared to VTA cells, as reported in most human PD postmortem studies. Still, both DA subpopulations showed decreased DA function at old ages in tgNM mice compared with wt littermates.

DA dysfunction in tgNM mice resulted in early signs of behavioral alterations, including fine motor and balance alterations, olfactory deficits and altered audible vocalizations. All these features are common symptoms that are usually present in humans before an overt parkinsonism is diagnosed. Slight motor abnormalities like reduced arm swing, changes in walking patterns, stiffness, tremor, or bradykinesia usually precede a PD diagnosis, although these patterns are highly unspecific, as they are also present in 15% to 95% of the elderly population (D. Berg et al., 2013; Louis & Bennett, 2007). Unlike mild parkinsonism, olfactory dysfunction is considerably more specific and one of the most common and earliest non-motor symptoms of PD, being present in approximately 90% of early-stage PD cases (Doty, 2012). Also, voice and speech disorders are frequent in individuals with PD and are suggested to appear early in the course of the diseases (Dashtipour, Tafreshi, Lee, & Crawley, 2018; Grant et al., 2014; Ho, Ianssek, Marigliani, Bradshaw, & Gates, 1998; Skodda, Grönheit, Mancinelli, & Schlegel, 2013). Here we found that NM-producing mice start showing audible vocalization deficits at young ages, preceding olfactory dysfunction and fine motor alterations which both appear at adult ages, thus replicating sensorimotor prodromal symptoms occurring years before clinical diagnosis in humans.

1.4 Noradrenergic neurodegeneration

The LC represents the major NA brain nucleus and is the second major area affected in PD, showing consistent neurodegeneration in PD postmortem studies (ranging from “some” to 94%) (Giguère et al., 2018). Symptoms associated with the depletion of NA innervation due to LC neurodegeneration consist in both motor and non-motor alterations, which include sleep disorders, anxiety, depression, cognitive alterations and autonomic dysfunction (Breton-Provencher, Drummond, & Sur, 2021; Delaville et al., 2011; Samuels & Szabadi, 2008). In tgNM mice, the LC showed high levels of NM accumulation already at young ages resulting in a clear deficit of the NA system in these animals (i.e. early LC neurodegeneration and NA depletion in the PFC). The decreased NA tone due to the great loss of LC neurons might be contributing to the already mentioned motor and non-motor behavioral alterations found in adult tgNM mice. Considering that the LC is recognized as a major wakefulness-promoting nucleus (Samuels & Szabadi, 2008), its neurodegeneration and the reduced NA tone in the projection areas might lead to the alterations detected in the sleep-wake cycle. Also, LC activity participates in anxiety-like behaviors and in encoding fear-related memories through its NA innervation of the amygdala (McCall et al., 2017), thus explaining the altered encoding of aversive stimuli observed in tgNM mice. Finally, LC projections also control the autonomic nervous system (Samuels & Szabadi, 2008), potentially contributing to the autonomic dysfunction (i.e. abnormal heart rate and respiratory rate) observed in tgNM mice compared with wt littermates.

1.5 Medullary nuclei alterations

Neurodegeneration in the medullary nuclei has also been shown in PD postmortem studies. Most of the studies assessed cell loss using catecholaminergic specific markers (TH/PNMT immunostaining or pigmentation) (Gai et al., 1993; Halliday et al., 1990; Rajput & Rozdilsky, 1976; C. B. Saper et al., 1991). As reported in humans (Halliday et al., 1988), we found that not all catecholaminergic cells in this cell group are pigmented in tgNM mouse brains. In humans, the pigmentation above the level of the obex (where the fourth ventricle becomes the central canal) is 15%, while below this level, increases to 65% reaching 85% in the most caudal sections. Interestingly, as in humans, we detected most of the DVC pigmented cells in tgNM mice below the obex, although a detailed quantitative study of the pigmentation gradient along the different caudorostral levels should be conducted in tgNM to confirm this observation. The reasons for the incomplete

pigmentation of these cell groups remain unknown. This could be explained by the fact that these cells are a mix of different catecholaminergic subtypes expressing different neurotransmitter types. This would be supported by the absence of NM in adrenergic cells (PNMT-positive) as described by Halliday and colleagues (Halliday et al., 1988). A careful examination of the molecular determinants that drive this selective pigmentation (e.g. differences in neurotransmitters, expression levels of Tyr or TH, antioxidant capacity) might reveal interesting facts in relation to the processes of NM formation in the human and rodent brain.

Although not all catecholaminergic DVC cells are pigmented, quantification of pigmented cells in tgNM mice revealed high levels of intracellular NM accumulation already at early ages, which were comparable to those reached in young LC. The high levels of NM accumulation in pigmented cells concurred with decreased numbers of pigmented DVC catecholaminergic neurons in adult and old mice compared with young tgNM mice. In contrast, the adjacent non-pigmented ChAT-positive cholinergic neurons were not affected. This observation is not consistent with the reduced number of DMNV cells reported in postmortem PD studies. However, these studies are not totally comparable because cell death in PD subjects was evaluated using Nissl staining (Eadie, 1963; Gai et al., 1992). The only study using ChAT-immunostaining evaluated cases suffering from other synucleopathies (Benarroch et al., 2006) (Introduction, Table 3).

The DVC is considered the major processing center for ascending visceral information, receiving input from heart, lungs, intestines and kidneys (Champagnat et al., 2001; Critchley & Harrison, 2013). Because of its role in processing sensory information from vital autonomic functions, autonomic dysfunction has been described in association with lesions in these nuclei (Martín-Gallego et al., 2016; Pyatigorskaya et al., 2016). Autonomic alterations in PD are highly prevalent (80% of PD patients) and include, among others, orthostatic hypotension, constipation, urogenital dysfunction, sleep disorders, respiratory and cardiovascular dysfunction, which may even lead to the patient's death (Gonçalves et al., 2021; Poewe et al., 2017). Considering the alterations found in tgNM medullary nuclei, we assessed possible peripheral dysfunction in these animals (i.e. cardiovascular and respiratory). Old NM-producing mice showed alterations in heart and respiratory rates, suggesting a failure to maintain cardio-respiratory homeostasis in accordance to the DVC role as a critical brainstem cardiorespiratory control center (Michael Spyer & Gourine, 2009). While highly prevalent in early PD, we

did not find signs of constipation in tgNM mice using a standard intestinal transit time test (data not shown), although we are currently performing additional studies using alternative methods. Still, we found significant changes in the levels of key neurotransmitters (i.e. NA and Ach) in different visceral organs (i.e. heart and intestines), suggesting an inappropriate function of the autonomic nervous system in NM-producing mice.

1.6 Cholinergic and serotonergic alterations

In addition, we aimed to assess the condition of cholinergic and serotonergic populations, which are also at risk in PD. Some studies evaluating cell loss in the main cholinergic nuclei of the brain reported consistent neurodegeneration in the PPN (average 41%) and in the NBM (“some” to 72%), while studies evaluating the serotonergic RN show conflicting results (Giguère et al., 2018). Cholinergic degeneration in the PPN has been linked to gait and balance disturbances (Pahapill & Lozano, 2000; Rinne, Ma, Lee, Collan, & Røyttä, 2008) and cholinergic cell loss in the NBM has been linked to cognitive impairment (Schulz, Pagano, Fernández Bonfante, Wilson, & Politis, 2018). Although cell loss in serotonergic RN in PD is a matter of debate, alterations in the integrity of the serotonergic terminals have been reported in PD (i.e. decreased PET functional imaging studies and decreased serotonergic metabolites) (Politis & Loane, 2011). In tgNM mice, we also found alterations in non-catecholaminergic non-pigmented brain nuclei. Old NM-producing mice showed decreased number of cholinergic neurons in both the PPN and NBM. Despite the decreased cholinergic neurons in the PPN, we detected a significant increase in the total Ach levels in this area. This result might indicate a compensatory mechanism of the cholinergic system to the decreased DA innervation in tgNM mice, since these two neurotransmitters are highly dependent on each other (König et al., 2019; McKinley et al., 2019; Spehlmann & Stahl, 1976). Indeed, PPN and SN are reciprocally innervated (French & Muthusamy, 2018) and normal activity of DA neuronal systems are critically dependent on cholinergic innervation of the PPN (Lester et al., 2010), which might be overstimulated due to the DA dysfunction in the SN.

On the other hand, no significant changes in serotonin levels nor in the number of cells in the serotonergic DR were found in NM-producing mice up to 20m of age, although these numbers were overall lower than in wt littermates. Interestingly, we found significant depressive-like behaviors in adult and old tgNM mice. Depressive-like behaviors are usually linked to alterations in the serotonergic system, but can also arise

from other neurotransmitter systems (Belujon & Grace, 2017; Moncrieff et al., 2022; Moret & Briley, 2011). Indeed, other known depression-linked pathways are altered in tgNM, such as the DA mesolimbic pathway or the general NA brain innervation.

1.7 PD-like neuropathological hallmarks

Importantly, tgNM mice reproduce the main PD neuropathological hallmarks in pigmented brain areas. First, the well-known observation of TH-phenotypic loss seen in aged healthy individuals, PD and ILBD subjects (Chu & Kordower, 2007; Huynh et al., 2021; Milber et al., 2012) is also detected in all pigmented neuronal groups analyzed in tgNM mice.

Second, neuroinflammatory changes are highly prevalent in pigmented areas from tgNM mouse brains. This is consistent with the fact that neuroinflammatory changes are highly localized within NM accumulating areas in the human PD brain (Cebrián et al., 2014; E. C. Hirsch & Hunot, 2009), and that some changes have also been reported in pigmented areas from non-diseased aged brains (Beach et al., 2007; Korzhevskii et al., 2021). Moreover, we found neuroinflammation (microgliosis and astrogliosis) in all pigmented nuclei (SN, VTA, LC, DVC), even in those without overt neurodegeneration. Specifically, Iba-1-positive cells were found to be surrounding eNM. The results shown here suggest that the neuroinflammatory changes found in postmortem brains may start prior to overt neurodegeneration and be linked to the presence of incipient extracellular NM.

Third, classical LB in PD present in pigment-containing neurons occur in close physical association with NM (E. Braak et al., 2001), and MB are intranuclear inclusions that increase with age and are exclusively found in NM-filled neurons (Yuen & Baxter, 1963). TgNM mice showed consistent MB and LB-like inclusion bodies in NM-filled neurons, while these were absent or rarely found in wt animals. The largest amount of LB were found in the SN and VTA regions, which do not show overt neurodegeneration, while these inclusions were rarely seen in the LC and DVC, in which neurodegeneration is fully established. Also, the largest number of inclusions were found at the onset of cell dysfunction/neurodegeneration in the different brain areas analyzed. These observations suggest that cells containing inclusion are the ones that degenerate in tgNM mice. This is consistent with our previous observations in AAV-TYR rats, in which inclusion body formation peaked before the onset of neurodegeneration (Carballo-Carbajal et al., 2019).

Still, some considerations must be taken into account when comparing the quantifications of inclusions in the different tgNM mice pigmented areas: (i) pigmented cell density differences: DVC catecholaminergic cell density is lower than in the SNpc (Bucci et al., 2017) and even less when considering only the pigmented cells (~10%) where these inclusions are exclusively found; (ii) neurodegeneration differences: LC shows already overt neurodegeneration at 1m of age, so the inclusion-formation period, which in the SNpc occurs in parallel to cell dysfunction, might happen at earlier ages not analyzed; (iii) NM-accumulation rate differences: the more progressive nature of NM accumulation in SN might be predisposing this cell type to higher levels of inclusion formation than in other areas like LC and DVC, where higher levels of NM are reported earlier.

Also there seems to be a link between high NM levels and LB-like pathology (i.e. DVC and LC at early ages, SN and VTA at early and late ages). In this context, the caudorostral gradient of LB-pathology reported in some PD brains (H. Braak et al., 2003) could be linked to a caudorostral gradient of increasing intracellular NM levels promoting LB-like pathology. Indeed, it has been reported that α -synuclein redistributes to the NM pigment in early stages of PD and becomes entrapped within NM granules, which may predispose melanized neurons to precipitate α -synuclein around pigment-associated lipids under oxidative conditions, such as those linked to NM formation (Fasano et al., 2003; Halliday et al., 2005; Zucca et al., 2018). Still, Braak staging does not apply to all PD patients since some of them do not show LB in medullary nuclei (Kalaitzakis et al., 2008). Indeed, Braak model has recently been reformulated in a proposed new scheme in which two distinct subtypes of PD would exist; one showing first α -synuclein pathology in the body (body-first), and then spreading consecutively in the typical order of pathology DVC > LC > SN, and the other one showing first α -synuclein pathology in the brain (brain-first), and then intracerebral spreading of pathology depending on the disease onset site (Borghammer et al., 2022; Borghammer & Van Den Berge, 2019; Van Den Berge & Ulusoy, 2022). Further studies in tgNM evaluating gut pathology and studies in humans addressing the levels of NM in different brain areas in PD subjects fitting each subtype will be necessary to fully understand the complexity of PD pathophysiology.

Finally, NM-producing mice exhibit a decreased lifespan compared to non-pigmented wt mice. Although no cause of death could be confirmed by autopsy, the general autonomic dysregulation in tgNM mice may explain the higher probability of a sudden death in these animals (Mutch, Calder, Crawford, Stewart, & Besson, 1990). Indeed, alterations in the

respiratory and cardiovascular systems are reported as more frequent death causes in PD patients than in age-matched controls (Ben-Shlomo et al., 1995; Pinter et al., 2015). Additionally, some PD patients suffer from a sudden death termed as Sudden Unexpected Death in Parkinson's Disease (SUDPAR), without any apparent cause of death determined by autopsy (Matsumoto et al., 2014; Scorza, Fiorini, Scorza, & Finsterer, 2018).

1.8 Relevance of tgNM as a new PD model

The results presented here show that NM accumulation in the murine brain leads to the main neuropathological hallmarks of PD, but also, of brain aging (i.e. neuroinflammation, inclusion-body formation, alterations in several neurotransmitter systems [DA/NE/Ach] and NM-specific neurodegeneration). These have major consequences in brain and body functions. Indeed, typical motor and non-motor symptoms present in PD and also seen in the aged population (i.e. fine motor alterations, sleep alterations, anxiety and depressive-like disorders, cognitive dysfunction, autonomic alterations). Overall, tgNM mice represent a new valuable mouse model for PD research, recapitulating both early motor and non-motor features of the disease, and contributes to our understanding of PD pathophysiology and of brain aging. Specifically, this new mouse model represents a step forward since it enables the PD research community to:

1. *Model PD by reproducing an aging-related physiologic feature of the human brain.* Most animal models of PD so far replicated individual pathogenic features and provided important insights in testing particular hypothesis (e.g. genetic mutations, exogenous toxins, α -synuclein aggregates). Here, we model a physiologic human feature that is present in all human beings in an age-related manner (i.e. NM accumulation in the brain). Understanding the factors that influence age-dependent brain pigmentation in humans is a question that remains to be solved.
2. *Characterize multisystemic effects in PD.* None of the previous animal models available reproduced at once the main features seen in humans and thus limited our understanding of how various events coincide and influence each other in PD. The animal model presented here mirrors the biological complexity of a multisystem condition such as PD, affecting a myriad of brain neurotransmission systems and tissues in the body and leading to motor, non-motor and peripheral alterations. Thus, this model represents an opportunity to study how imbalances

in catecholaminergic PD vulnerable groups affect other neurotransmitter systems in the brain and how this affects body functions.

3. *Explore the prodromal phase of PD.* In tgNM mice, LC neurodegeneration precedes SN dysfunction leading to NA deficits preceding DA alterations. This model supports the hypothesis that LC neurodegeneration could occur before SNpc neurodegeneration in PD as it has been reported for RBD patients (Knudsen et al., 2018), which are considered to be prodromal cases of PD since different studies indicate that within 15 years nearly all RBD patients will develop a synucleinopathy, including PD (Iranzo et al., 2013).
4. *Replicate the therapeutic window of prodromal PD.* The appearance of prodromal symptoms (e.g. olfaction, sleep alterations, mild motor symptoms, autonomic dysfunction) in tgMN mice coincides with the beginning of DA neuronal dysfunction in the absence of SN cell death. Thus, this model allows a therapeutic window in which mild prodromal symptoms can be detected but the SNpc is dysfunctional without overt neurodegeneration. Studying the markers of this prodromal phase is essential to identify new biomarkers categorizing populations at risk for developing PD and to identify and test new therapeutic agents acting at this initial phases of the disease (Fig. 52).
5. *Characterize early neuroinflammatory changes.* Our results point to neuroinflammation as an early event occurring prior to cellular dysfunction in SN and VTA regions. This model thus enables a further characterization of the neuroinflammatory profile before the onset of neuronal dysfunction/neurodegeneration.
6. *Characterize LB formation.* LB are rarely seen in PD models and tgNM mice represent an opportunity to characterize the different steps and modulators of the LB-formation process, as well as the regional differences in LB-formation and their pathological implications.

tgNM mice prodromal PD

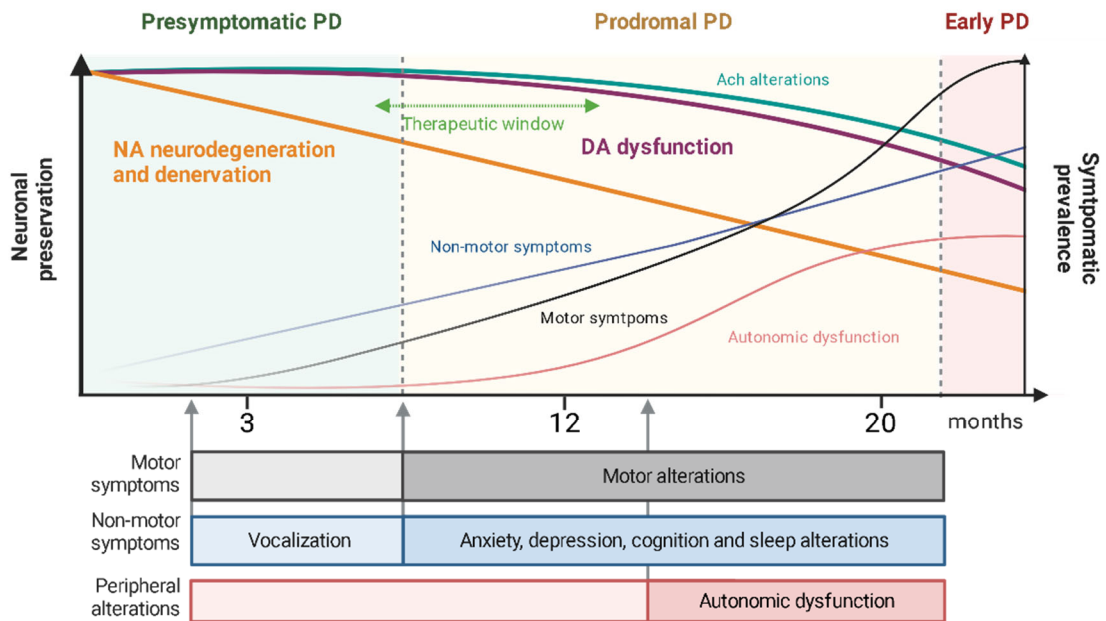


Figure 52. Schematic evolution of the prodromal phase modelled by tgNM mice. TgNM mice model a prodromal phase of PD in which neurodegeneration in the SNpc is not established and motor and non-motor symptoms (i.e. vocalization deficits, anxiety-related behavior, depressive-like symptoms, learning deficits, and sleep alterations) can already be detected. This phase represents a therapeutic window in which disease-modifying agents can be identified and tested for therapeutic efficacy.

2. Transcriptomic characterization of the effects of progressive NM accumulation in neurons

2.1 Characterization of progressively pigmented distinct regions

We have specifically isolated anatomically defined brain regions in both wt and NM-accumulating mice using a rapid staining that enables an acceptable RNA quality for posterior transcriptomic analyses. The number of DEGs identified followed a regional and age-dependent pattern similar to that of NM accumulation levels and neuropathological features (Chapter 1), which suggests that these changes are linked to pigment accumulation. In line with this, LC analyses displayed the highest degree of transcriptomic changes possibly reflecting the high degree of neurodegeneration found in this area, followed by VTA, which seems to show a slightly higher degree of vulnerability than SN in these animals, as discussed above (Discussion, Section 1.3).

2.2 TOP individual DEGs

The most significant DEGs in the majority of the comparisons performed were neuroinflammatory-related transcripts. In the LC, the top 3 DEGs for both ages (3m and 12m) were related to the generalized neuroinflammatory profile (e.g. *Gfap*, *C4b*, *Lyz2*, *CD68*). These top DEGs are consistent with the high degree of astrogliosis (increased GFAP-positive cells) and microgliosis (increased *Iba1* and *CD68*-positive cells) observed in this area at these ages (Chapter 1, Fig. 24f&data not shown). The results from the transcriptomic analyses allowed an in-depth characterization and thus a better understanding of the neuroinflammatory response. Specifically, *C4b* has been recently reported to opsonize microglia debris that are later phagocytized and degraded by astrocytes (Zhou et al., 2022). Also, the highly expressed *Lyz2* suggests the presence of a DAM-related microglial subtype (Keren-Shaul et al., 2017), long before neurodegeneration has been established in this area.

The VTA also showed major neuroinflammatory changes (e.g. *Lyz1*, *Lyz2*, *Gfap*, *Lilrb4a*, *Anxa1*, and *Mpeg1*). All of them were upregulated, except a downregulation of the anti-inflammatory protein *Anxa1* at late stages (20m). The changes observed point to DAM-type microgliosis and to astrogliosis. Interestingly, *Lilrb4a* is expressed in monocytes, macrophages, dendritic and plasma cells and its family of proteins bind to MHC I molecules on antigen-presenting cells (J. Liu et al., 2020). Thus, altered *Lilrb4a* expression might be related to the reported expression of MHC I by pigmented neurons in

the SN and LC (Cebrián et al., 2014). In line with this, we also detect increased $\beta 2m$, a component of the MCHI, in tgNM mice VTA neurons at 20m of age. Other top deregulated genes in early VTA changes were related to neuroendocrine function (i.e. Crh), DNA repair (i.e. Eya1) and in late VTA changes to iron homeostasis (i.e. Ftl1). In the neuronal-enriched approach we detected increased transcripts in VTA neurons related to immune response (e.g. Tyrobp, Lyz2, Fcer1g, CD68) and cell survival (i.e. Bcl2a1a). Some but not all of these top genes have been related to PD pathology, so we will discuss their possible relevance in a PD context:

Crh (Corticotropin Releasing Hormone) is released specifically by VTA neurons in response to stress (B. Wang et al., 2005) and Crh receptor antagonists inhibit striatal DA release (Bagosi, Jászberényi, Bujdosó, & Telegdy, 2006). Thus, the early downregulation of the Crh transcript in the VTA (Chapter 1, Table 9) might be related to the later DA dysfunction observed in these cells at 12m and 20m of age. Indeed, decreased Crh-immunoreactivity has been described in the cerebral cortex of PD patients and in other neurodegenerative diseases (De Souza, Whitehouse, Price, & Vale, 1987; Whitehouse et al., 1987). Crh receptors are normally expressed throughout the brain, including the mesolimbic DA pathway, and Crh system has been extensively linked to the regulation of the stress response, anxiety and mood disorders (Aubry, 2013; Dedic et al., 2019). A further characterization of Crh peptides in the different tgNM mouse brain regions involved directly in the hypothalamus pituitary axis would be interesting for an in-depth characterization of the altered stress-response described in these animals.

Eya1 (EYA Transcriptional Coactivator And Phosphatase 1) is a protein phosphatase that stimulates DNA repair mechanisms by regulating histone H2AX phosphorylation and thus avoiding DNA damage-dependent pro-apoptotic factors (Nowsheen et al., 2018; W. Wong, 2009). Recently, a common variant in EYA1 has been linked to essential tremor, and other DNA repair gene variants (i.e. APE1, XRCC1, and XRCC3) have been linked with increased PD risk. In this context, the early downregulation of this pro-repair factor might be inducing a pathological effect on VTA cells.

Ftl1 (Ferritin light polypeptide 1) stores iron in a soluble, non-toxic form. The late upregulation of Ftl1 seen in VTA might be pointing to a dysregulation of iron homeostasis at this age, which is highly relevant considering the iron-scavenging properties of NM. In fact, mutations in the ferritin light chain gene (FTL1) lead to excessive iron accumulation in the brain causing an adult-onset movement disorder known as neuroferritinopathy (N.

Kumar, Rizek, & Jog, 2016). Considering that Ftl1 serum levels in these patients are low, it would be interesting to assess Ftl1 as a potential new peripheral biomarker.

Bcl2a1a, a cell survival factor, hasn't been directly related to human PD but its upregulation already at 3m of age in VTA cells might reflect an effort to maintain cellular function, since expression of Bcl2 overexpression protects DA neurons to apoptotic insults (Van der Heide & Smidt, 2013).

In SN, only a few neuroinflammatory genes appeared within the top three DEGs (i.e. upregulation of *Lyz2*, *Lilrb4a* and *Lilr4b*). Apart from these neuroinflammatory changes, other top deregulated genes were related to cell signaling (i.e. *Ide*, *Npbwr1*), RNA metabolism (i.e. *Dcps*), metabolism and neuronal survival (i.e. *Nmat2*), and extracellular matrix (i.e. *Lamc1*). SN-neuronal enriched samples enabled the identification of other new top DEGs: (i) at 3m of age, altered expression of miRNA (*Mir1912*, *Mir7652*) and pseudogene *pisd-ps3*; (ii) at 12m, a downregulation of *Rec114*, which participates in double-strand DNA breaks (R. Kumar et al., 2018); (iii) at 20m, a downregulation of the intraflagellar transport protein (*ift57*), or *Hippi*, which has been shown to form a complex with caspase 8 (Gervais et al., 2002) and to act as a transcriptional regulator of different caspases (Majumder, Choudhury, Banerjee, Lahiri, & Bhattacharyya, 2007), and a downregulation of the nicotinic receptor *Chrna3*. Some but not all of these top genes have been related to PD pathology, so we will discuss their possible relevance in a PD context:

Ide is a metallopeptidase involved in the degradation of insulin and other β -sheet proteins that was found upregulated in SN at 3m. Interestingly, it has been found to block α -synuclein amyloid formation *in vitro* (Sharma et al., 2015). The upregulation of this enzyme might be related to the increased aggregate formation (LB-like inclusions) observed in this region in tgNM mice at 12m (Chapter 1, Fig. 22a).

Dcps (Decapping Enzyme, Scavenger) degrades short mRNA fragments that have undergone prior processing by the exosome (Fuchs, Wurm, Neu, & Sprangers, 2020). Alterations in the mRNA decapping pathway have recently been reported in human neurons harboring familial synucleinopathy mutations (iPSC-derived and in postmortem brain) (Hallacli et al., 2022). Considering that the mRNA metabolism gene sets have been repeatedly identified in the biological pathway analyses performed, the early deregulation of this gene might be crucial in displaying the phenotype of tgNM mice and deserves further characterization.

Lamc1 (Laminin Subunit Gamma 1), upregulated in SN region at 12m, is an extracellular matrix glycoprotein and a key component of the basal membrane predominantly synthesized by brain microvascular endothelial cells, pericytes, and astrocytes (Nguyen, Bix, & Yao, 2021). Basal lamina actively regulates BBB integrity and an abnormal BBB has been extensively reported in PD patients (Nguyen et al., 2021). Also, injections of laminin mimetic nanofibers reduce striatal injury and enhance recovery in the 6-OHDA PD model (Sever et al., 2016). Thus, the increase observed in Lamc1 expression might be reflecting a change in the basal lamina and BBB functionality in tgNM, which deserves further study.

Npbwr1, the receptor for neuropeptide B (NPB) and neuropeptide W (NPW), was found downregulated in the SN at 20m. The functions of NPB and NPW neuropeptides are still poorly characterized. However, some studies assessing the pharmacological effects of NPB/NPW when injected intracerebroventricularly in rodents point to its relation to stress, body temperature, body weight and heart rate (Sakurai, 2013). All of these are of importance in the context of PD non-motor symptomatology and in some of the features displayed by tgNM mice.

Nmnat2, an essential enzyme for Nicotinamide adenine dinucleotide phosphate (NADP) synthesis, was found upregulated at 20m. Nmnat2 participates in neuronal survival and maintenance of healthy axons by delaying Wallerian axon degeneration (Tang, 2019), and we thus speculate that it might be upregulated in tgNM mice in response to neuronal stress.

Chrna3 is a nicotinic cholinergic receptor widely expressed in the nigrostriatal system and whose expression is reduced in the SN of PD and DLB cases by [3H]nicotine binding measurements on postmortem tissue (Perry et al., 1995). Considering that nicotine consumption (i.e. smoking) reduces the risk for developing PD, the downregulation of nicotinic receptors in the SN at 20m might represent an interesting new candidate for disease modification in tgNM mice.

All the targets discussed here point to novel potentially interesting pathways to be explored as underlying mechanisms of LC neurodegeneration and SN/VTA dysfunction described in tgNM mice (Chapter 1).

2.3 NM-related biological pathways

Considering that genes behave in an interdependent fashion within complex gene regulatory networks, we complemented our study with gene set enrichment analyses in pigmented areas (i.e. tgNM mice) compared to the same areas in absence of pigment (i.e. wt littermates).

Interestingly, we detected neuroinflammatory changes as the main altered pathways but also altered translation/transcription, proteasome and mitochondria-related pathways (Chapter 2, Fig. 33&34). Additionally, we identified cell cycle-related pathways as one of the main altered biological categories in the LC and in the SN in the analyses with the Reactome database (Chapter 2, Fig. 34). In the LC, these gene sets might be related to the extensive cell loss in this area while in the SN it might be reflecting early changes in cell cycle stability and major changes in proteasomal degradation, which are linked to cell cycle pathways or DNA-damage signals. Indeed, in the SN, these pathways included genes that coded for proteasomal proteins involved in the degradation of cell cycle proteins (e.g. Psmc4, Psmb7, Psma2, Psmc2) and Pttg1, a regulatory protein involved in many biological functions, including microtubule nucleation, p53-induced cell death and DNA repair (Bernal et al., 2002; Moreno-Mateos et al., 2011). Also, in the neuronal-enriched samples we identified again pathways linked to neuroinflammatory, RNA processing and mitochondrial functions, but also alterations in cell-organization, membrane trafficking and lipid metabolism-related pathways.

An interesting common feature in the different GSEA analyses performed for neuronal-enriched samples is that during early and adult ages, the top alterations were mostly upregulation of biological functions (e.g. immune system, signaling, membrane trafficking) while in old tgNM, top alterations were related to the downregulation of cellular functions (e.g. RNA processing/translation, mitochondrial function) (Chapter 2, Fig. 39&40). This observation might be pointing to the current hypothesis that DA cells experience a broad decrease of cellular functions (i.e. catecholamine synthesis, translation, transcription, mitochondrial function) before actual neurodegeneration is manifested, which establishes a therapeutic window for a possible functional recovery of these cells before neurodegeneration.

2.4 Translational value of the NM-induced transcriptomic profile identified in tgNM mice

The transcriptomic profile identified in SN neuronal-enriched samples correlated with the one described in human SN postmortem studies (Chapter 2, Table 11). This observation strengthens the suitability of tgNM mice as a translational model for PD research. Also, the comparison of our datasets with the recently published snRNAseq study in PD SN (Smajić, et al., 2022) leads to the formulation of new hypotheses. For example, that the CADPS2 neuronal phenotype might be modelled by age-dependent NM accumulation in SN neurons. Also, that microglial DEGs in PD are modelled by NM-accumulation. In order to better address these questions and to characterize the cell-specific individual molecular profile of distinct subtypes of NM-containing catecholaminergic neurons and other neuronal and glial populations, we plan to perform snRNAseq experiments in tgNM mice, which will enable a more direct comparison of tgNM mice transcriptomic profile with the growing number of snRNAseq studies performed in postmortem PD brain tissue (Adams et al., 2022; Kamath et al., 2022; Q. Wang et al., 2022).

2.5 Splicing events

We reported statistically significant splicing events occurring in all three pigmented regions when analyzed as whole regions while no significant splicing events were detected in neuronal-enriched samples. This might be explained by higher alterations of splicing events in non-neuronal cells or by an additional statistical power for detection due to higher levels of expression in regional samples of a specific transcript. For example, we detected statistically-significant splicing events with a restrictive threshold ($FDR < 0.05$) in Tyr in SN, VTA and LC regions but not in neurons, although a trend was also observed in VTA neurons (raw p-value= $3.11E-05$). Interestingly, we detected a highly significant alternative splicing event in the GPNMB transcript consisting on the inclusion of exon 5. The higher expression of exon 5 within the GPNMB transcript in tgNM compared to wt was also detected in neuronal-enriched samples from SN ($p=0.0016$) and VTA ($p=1.97E-05$). Interestingly, exon 5 is localized within the amyloidogenic region of GPNMB, detected also in its homologue PMEL, the removal of which leads to abrogated amyloid formation (Hee, Mitchell, Liu, & Leonhardt, 2017) (Fig. 53). This alternative splicing event might be linked to the potential role of GPNMB in amyloidogenic NM nucleation, an idea that has also been suggested by others (Zucca et al., 2018).

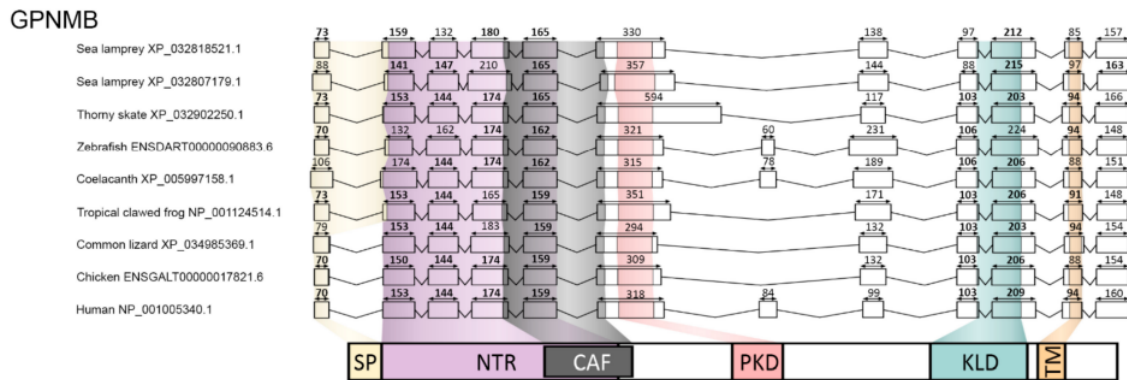


Figure 53. The intron-exon architecture of GPNMB in relation to protein domains. Schematic representation of gene family orthologs showing exons (boxes, to scale) and separated by introns (lines, not to scale). Nucleotides coding for different protein domains are color-coded: signal peptide (yellow), N-terminal region (NTR; purple), core amyloid fragment (CAF; black) polycystic kidney domain (PKD; red), repeat domain (RPT; blue), kringle-like domain (KLD; green), transmembrane domain (TM; orange). Numbers above the exons denote exon length in basepairs. From (Chrystal et al., 2021).

2.6 Validation of the main NM-related candidates and biological pathways

In order to identify potential new therapeutic targets, we validated some of the main markers of the altered biological pathways reported at the protein level. For instance, Parkin protein levels were increased in SN-VTA dissections from tgNM mice at 12m of age (Chapter 2, Fig. 44). Parkin, which is genetically linked to PD, is a multiprotein E3 ubiquitin ligase that targets substrate protein for proteasomal degradation. Parkin increases in tgNM might be related to several reported pathological processes occurring in tgNM mice: (i) mitochondrial dysfunction, since Parkin together with Pink1, has been extensively linked to quality control of healthy mitochondria (Vázquez-Vélez et al., 2021); (ii) inflammation, since Parkin has also been associated to exacerbated inflammasome activation in immune cells (Mouton-Liger et al., 2018); (iii) LB-like inclusion formation, since Parkin has been described to localize to LB (Schlossmacher et al., 2002), to ubiquitinate α -synuclein (Shimura et al., 2001), and PD patients carrying Parkin loss-of-function mutation do not show LB pathology (Schneider & Alcalay, 2017); (iv) NM formation, since Parkin has recently been associated to increased NM formation and has been shown to co-localize with NM pigment in control human SN neurons (Tokarew et al., 2021). The importance and relevance of this finding will be further explored in a new collaboration that we have established with Professor Michael G.

Schlossmacher (Ottawa Hospital Research Institute, Canada). Additionally, markers from the autophagic and lysosomal pathway (i.e. Lamp1, LC3, CtsD), which are highly linked to NM formation and accumulation, were also found decreased in tgNM mice (Chapter 2, Fig. 44). These findings are consistent with the altered proteostasis that was also extensively described in the *in vitro* model of NM accumulation (Carballo-Carbajal et al., 2019). These results strengthen the hypothesis that continuous buildup of NM within autophagosomes ultimately exhausts the autophagic capacity of the cell, leading to a general failure of proteostasis and subsequent dysfunction and degeneration of NM-laden cells. Consistent with this, we detected decreased activity of the lysosomal enzyme GBA in tgNM mice LC and DVC brain homogenates. However, no changes were detected in SN-VTA samples. We did not detect changes in any of the other lysosomal enzymes assessed (i.e. β -hexosaminidase and acid phosphatase). These results do not exclude defective function of lysosomal enzymes specifically in catecholaminergic neurons since whole brain dissections were analyzed and hence, lysosomes from different cell types were also included. Further studies evaluating a pure pigmented cell population (e.g. with cell sorting) should be done to better determine lysosomal integrity in NM-accumulating neurons. We also detected decreased levels of the mitochondrial protein Drp1 (Dynamin 1 like) (Chapter 2, Fig. 44), which participates in mitochondrial fission, in agreement with the alteration in mitochondrial-related pathways detected within the top altered gene sets in SN and VTA regions (Chapter 2, Fig. 33-34&39-40). Finally, alterations in the phagocytic microglial marker CD68 were also validated by immunohistochemistry, confirming the phagocytic phenotype of the microgliosis shown in Chapter 1.

2.7 DAM profile

We detected a pan-regional microglial reaction to NM that was observed in all pigmented regions. These changes were highly similar to the phenotype known as DAM, which has been observed in multiple neurodegenerative diseases (Friedman et al., 2018). Microglia has been reported to transition to a DAM phenotype in response to neurodegeneration-associated molecular patterns, which include apoptotic bodies of dying neurons, myelin debris, lipid degradation products and extracellular protein aggregates (Deczkowska et al., 2018).

The activation of the DAM phenotype is thought to be initially protective and directed to phagocytize and contain the sensed damage. Indeed, mutations in key players of this pathway are known to produce microglial defects and neurological disorders. For

example, homozygous loss-of-function mutations in TREM2, or its required adaptor for trafficking and signaling Tyrobp/DAP12, cause the Nasu-Hakola disease, a rare disease involving neurodegeneration of the white matter that resembles frontotemporal dementia (Song & Colonna, 2018). Also, loss-of-function mutations in the essential myeloid lineage growth factor receptor CSF1R, which interacts with TREM2-Tyrobp receptor (Hu et al., 2021), lead to adult-onset leukodystrophy with neuroaxonal spheroids and pigmented glia (Konno, Kasanuki, Ikeuchi, Dickson, & Wszolek, 2018). Interestingly, this disorder is pathologically characterized by pigmented macrophages that are CD68-positive and contain brown granular pigments (Konno et al., 2018). The alterations in these two disorders might be pointing to a similar etiopathogenic mechanism, since CSF1R and Tyrobp/DAP12 have been reported to signal via common downstream pathways (Konishi & Kiyama, 2020; Song & Colonna, 2018). In the context of PD animal models, TREM2 stimulation in microglia was shown to induce cytoskeleton reorganization and increased phagocytosis of apoptotic neurons (Takahashi et al., 2005). Also, a recent study overexpressing TREM2 specifically in microglia showed inhibition of apoptosis in DA neurons and improved motor symptoms in the MPTP mouse model (W. Huang et al., 2021). However, another study showed no effects of Tyrobp deficiency in MPTP-induced cell death (Kinugawa et al., 2013). Although not fully established, these studies suggest a beneficial effect of Trem2-Tyrobp/DAP12 pathway (i.e. clearance of apoptotic neurons and behavioral improvements) in the context of PD models. Thus, in tgNM mice, the reported increase in this pathway (i.e. increased Trem2, Tyrobp) might be reflecting the effort of microglia to engulf and degrade harmful stimuli, including extracellular debris like eNM (Fig. 54).

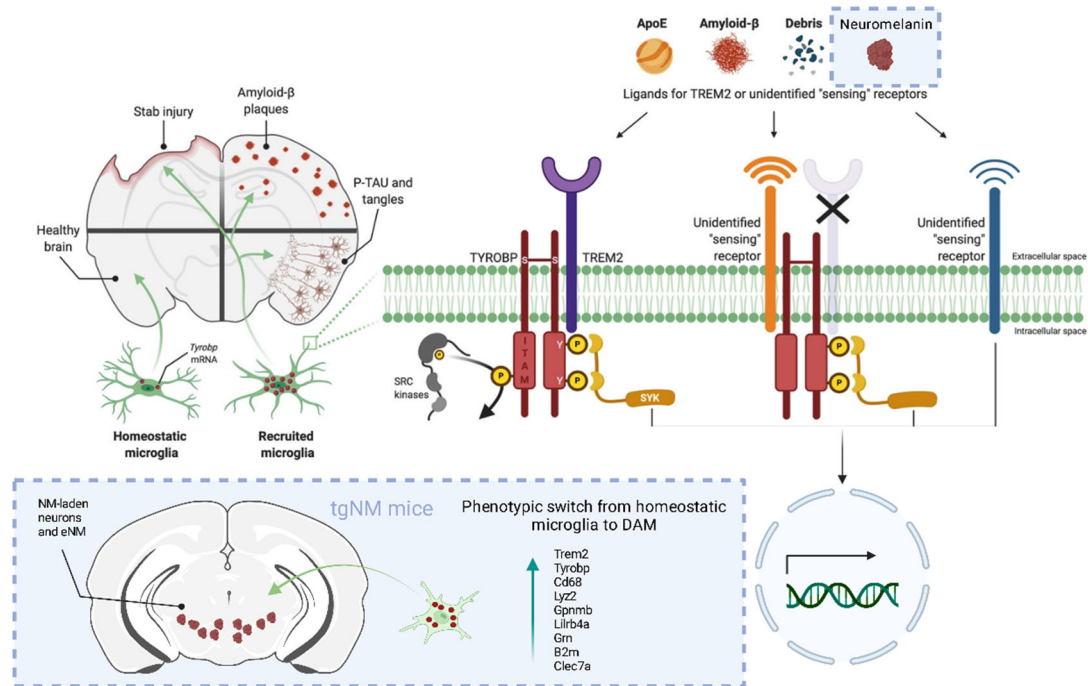


Figure 54. Proposed shared mechanism between microglial activation in tgNM mice with other neurodegenerative diseases. *Left*, In response to penetrating stab injury or accumulation of amyloid beta ($A\beta$) deposits or misfolded TAU, (or in the proposed scenario by this PhD thesis, NM-laden neurons or eNM), Tyrobp transcription is upregulated in microglia, thereby marking these cells as “recruited microglia”. *Right*, Multiple alternative signaling pathways can be considered: Ligand signaling is initiated by APOE, $A\beta$, debris, (or in the proposed scenario by this PhD thesis, NM-laden neurons or eNM) at sensing receptors and leads to phosphorylation of the tyrosine residues in the cytoplasmic immunoreceptor phosphotyrosine-based activation motif (ITAM) of TYROBP by SRC kinases and the recruitment of SYK. Genes upregulated in tgNM are shown next to the blue arrow. APOE, apolipoprotein E; DAM, disease-associated microglia; ITAM, immunoreceptor tyrosine-based activation motif; SYK, spleen tyrosine kinase; TREM2, triggering receptor expressed on myeloid cells-2; TYROBP, tyrosine kinase binding protein. Figure adapted from (Audrain et al., 2021).

Interestingly, these DAM genes were found in neurodegenerated areas like the LC but also in dysfunctional areas without overt neurodegeneration like SN and VTA. This might be related to the high number of eNM detected in the different pigmented regions, which is known to induce a pro-inflammatory profile in glial cells *in vivo* and *in vitro* (Wilms et al., 2003; W. Zhang et al., 2011). However, neuroinflammatory genes were also detected when neuronal-enriched samples were analyzed. The latter observation has two possible explanations: (i) the neuronal cytoplasm expresses immune-related transcripts or (ii) immune cells are increased around melanized neurons compared to non-melanized neurons (i.e. forming cell-to-cell contacts or in the immediate extracellular environment).

The increase in microglia-neuron contacts and even microglial ramifications penetrating DA neuronal somas has been shown in the 6-OHDA PD animal model (Virgone-Carlotta et al., 2013). We thus propose a scenario in which the induction of the DAM phenotype is stimulated by the release of eNM granules and/or incipient release of neuronal contents to the extracellular milieu, as it has been proposed for other neuronal components in other neurodegenerative diseases (Fig. 54).

2.8 Neuroinflammatory cytokines

We also characterized the neuroinflammatory cytokine profile in tgNM brain and serum samples. We detected increased levels of IL-1 α in SN-VTA brain homogenates of tgNM mice. IL-1 α has recently been shown to induce A1 phenotype in astrocytes, a phenotype that induces neuronal death (Liddel et al., 2017). Indeed, the complement component 3 (C3), one of the most characteristic and highly upregulated genes in A1 astrocytes, is increased in PD postmortem brains (Liddel et al., 2017) and also in tgNM animals (VTA and LC regions). The increase in IL-1 α cytokine levels in SN-VTA brain homogenates and the increased C3 transcript expression in pigmented tgNM brain regions suggest that the astrogliosis reported in Chapter 1 might be driven by an A1-type profile, similar to that reported in PD postmortem brains (Liddel et al., 2017). We also detected decreases of IFN type III or gamma (also known as IL-28) in SN-VTA dissected tissues. The type III are a group of anti-viral cytokines that act mainly in mucosal epithelial tissues (Wack, Terczyńska-Dyla, & Hartmann, 2015). Recently, type III interferons have been linked to neuroinflammation by maintaining autoreactive T-cell effector function and limiting recovery in a murine model of multiple sclerosis (Manivasagam et al., 2022). TgNM mice also showed a trend to increased ENA-78 levels in both SN-VTA and LC brain homogenates. Although ENA-78 changes have not been described in the context of PD, ENA-78 seems to possess neutrophil chemotactic properties that could be relevant in the context of PD. For example, in bacterial meningitis, ENA-78 is increased in the cerebrospinal fluid where it is involved in the recruitment of neutrophils to the brain (Zwijnenburg et al., 2003).

Finally, we detected minor changes of G-CSF in serum samples from tgNM mice. G-CSF regulates the production of circulating blood cells by the bone marrow and is already used for the treatment of neutropenia in humans (Tsai et al., 2017). This finding is interesting considering that G-CSF has been suggested to be neuroprotective in PD. In a phase 1 clinical trial, G-CSF was administered in early-stage PD patients, resulting in a slower

reduction of the striatal DA PET signal and in unchanged motor scores after 2 years of follow-up (Tsai et al., 2017).

2.9 GPNMB as a new NM-related biomarker or therapeutic target

After the genome-wide transcriptomic profiles of NM-accumulating cells performed in tgNM mice, we focused in one of the genes identified as a new potential therapeutic target of interest, the glycoprotein GPNMB.

GPNMB (Glycoprotein nmb) is a type I transmembrane glycoprotein that belongs to the premelanosome protein (PMEL)/NMB family due to its homology to the pMEL17 precursor, a melanocyte-specific protein (Turque et al., 1996; Weterman et al., 1995). It has been reported to be essential for the formation of melanosomes in melanocytes (Loftus et al., 2009; P. Zhang et al., 2012), promote lipogenesis in adipocytes (XM et al., 2019), stimulate phagocytosis in kidney-epithelial cells and macrophages (Li et al., 2010), promote eosinophil maturation (SM et al., 2017) and inhibit T cell activation (J.-S. Chung et al., 2007), among others. In the recent years, evidences show that GPNMB is overexpressed in numerous neurological disorders. Upregulation of GPNMB has been reported in postmortem brain tissue and CSF of Alzheimer's disease (Hüttenrauch et al., 2018; Satoh, Kino, Yanaizu, Ishida, & Saito, 2019), brain tissue and CSF of frontotemporal dementia patients (M. Huang et al., 2020), peri-infarct region in brain cerebral ischemia–reperfusion injury (Nakano et al., 2014) and CSF from amyotrophic lateral sclerosis (Oeckl et al., 2020; Zhu et al., 2019).

In the context of PD, genomic variants within the locus of GPNMB have consistently been reported to confer a higher risk for developing PD (Z. hua Liu et al., 2015; Nalls et al., 2014; Pihlstrøm et al., 2013). Specifically, these genomic variants translate to an increased brain expression of GPNMB in individuals carrying the predisposing allele (Murthy et al., 2017). Indeed, recent studies show consistent upregulation of GPNMB in human PD postmortem SN tissue and plasma (Brendza et al., 2021; Diaz-Ortiz et al., 2022; Kamath et al., 2022; Moloney et al., 2018; Smajić, et al., 2022; Tiklová et al., 2021). These observations lead to the idea of a potential pathologic effect of GPNMB overexpression. In line with this, a recent *in vitro* study showed that GPNMB is necessary for the internalization of α -synuclein and development of α -synuclein pathology (Diaz-

Ortiz et al., 2022). However, evidences from *in vivo* models show that GPNMB might act as a protective factor (Budge et al., 2020).

Overall, GPNMB represents an interesting potential new therapeutic target to explore in the context of NM-accumulating PD models because of its genetic association to PD and because of its potential functions (e.g. autophagy, melanogenesis, immune system).

We first validated the upregulation of the GPNMB protein by immunohistochemistry in tgNM mice SN and VTA neurons in biological replicates. Next, considering that GPNMB has an extracellular domain that can be cleaved and released (Rose et al., 2010), we also assessed GPNMB levels in serum samples from tgNM mice. We detected decreased levels of GPNMB in old tgNM mice compared to wt. This observation is opposed to the reported increased levels of GPNMB in PD serum samples (Diaz-Ortiz et al., 2022). The latter study also reports a positive correlation between GPNMB plasma levels and motor scores. The discordance between these findings and our results in tgNM mice might have different explanations. First, differences in the epitope detected, since we used different ELISA kits, which might be leading to different results. Second, differences in animal species, since, although mouse *Gpnmb* shares a considerable homology with human GPNMB (70.9% homology), the differences between species could lead to changes in GPNMB function and processing. For instance, mouse *Gpnmb* could be retained in the brain while human GPNMB might be released in peripheral biofluids. This hypothesis is supported by the observation that the murine *Gpnmb* is secreted as a membrane-bound fragment and not as a soluble ectodomain (Ripoll, Irvine, Ravasi, Sweet, & Hume, 2007). Third, differences in the PD disease stage assessed, since tgNM mice mimic a prodromal phase whereas the PD patients analyzed in this study were assessed at a mean of 7 years post-diagnosis.

We also confirmed the previously published increased GPNMB expression in PD brains by qPCR and the expression of GPNMB protein in postmortem SN tissue by immunohistochemistry. Additionally, we described that GPNMB levels in SN from PD patients showed a trend to correlate with disease duration ($p=0.09$, $R^2=0.34$). This correlation was not found in another study that reported no correlation of SN GPNMB levels with disease duration, Braak stage, neuronal loss, or eNM (Moloney et al., 2018). Still, as indicated above, a recent study showed correlation of GPNMB plasma levels with motor scores (Diaz-Ortiz et al., 2022), suggesting that GPNMB is somehow related to the progression of PD pathology.

Another important aspect is that the cell-type expression of GPNMB is still not clearly defined. The majority of studies point to a microglial GPNMB expression. Two recent snRNAseq studies characterizing postmortem PD SN identify GPNMB as a marker of a subset of microglial cells upregulated in PD (Kamath et al., 2022; Smajić, et al., 2022). However, while histochemical studies showing increased GPNMB protein expression in PD tissue performed double immunostaining in order to co-localize its expression in specific cell types showed co-localization with Iba1, they also reported “*occasional low expression in large objects the size of DA neurons but typically lacking neuromelanin*” (Brendza et al., 2021). Here, we detected increased expression of GPNMB in LCM-isolated NM-laden SN neurons from PD cases compared to controls. This is consistent with another study also reporting increases in GPNMB expression in LCM-isolated NM-positive cells from PD postmortem brains (Tiklová et al., 2021). However, it must be considered that long postmortem intervals, together with the specific LCM protocol used, could impact RNA quality and affect gene expression results. Thus, additional studies in order to clearly identify GPNMB expression in PD DA neurons would be required.

To investigate the exact role of GPNMB in NM-induced pathology, we overexpressed human GPNMB using an AAV co-injected in the SNpc with an AAV-TYR to induce NM-dependent pathology in mice as previously described (Carballo-Carbajal et al., 2019). We have already identified that AAV-mediated overexpression of GPNMB is localized within TH-positive cells and preliminary results indicate it might exert a neuroprotective effect in the context of the AAV-TYR model. This preliminary observation would be consistent with the protective effect reported in toxic models of PD (Budge et al., 2020) The results from these experiments will elucidate the potential role of GPNMB in the modulation of NM induced pathology.

GPNMB has now become a hot topic in PD research because of its recent link to α -synuclein neuronal internalization (Diaz-Ortiz et al., 2022; Pizarro Galleguillos, Mohamed, & Periñan, 2022) and is regarded as a potential therapeutic target holding great promise by different funding agencies and pharmaceutical companies.

2.10 Relevance of the transcriptomic characterization in tgNM animals

All these results show that NM accumulation in the murine brain leads to transcriptomic changes that reproduce alterations in biological pathways known to participate in PD and

in some other pathways that have rarely been explored in the context of PD etiopathogenesis. The targets reported here and the correlation with PD postmortem studies enable the identification of interesting new lines of research to understand their role in NM-induced pathology. Consistent with this, we have selected GPNMB as a potential new therapeutic target that we are now modulating in a NM-producing animal model. Specifically, the transcriptomic results reported here may represent a new step forward in:

1. *Identification of new NM-induced biological pathways and targets.* NM accumulation has been long suspected to act as a vulnerability factor for PD. Transcriptomic alterations found in NM-laden neurons mean a step forward in the definition of a vulnerable subtype and the identification of the molecular fingerprints that dictate it.
2. *Translational transcriptomic profile.* High levels of NM accumulation in mouse SN neurons lead to transcriptomic alterations that correlate with gene expression profiles from PD postmortem SN. This identification strengthens the translational value of the reported transcriptomic profiles and in turn, of the tgNM model itself. Accordingly, we expect that the targets identified in these animals would have a potential therapeutic value.
3. *GPNMB identification as a new therapeutic target.* GPNMB has recently gained interest in PD research because of its genetic link to PD and its overexpression in PD postmortem brains. Here we found that NM accumulation induces GPNMB overexpression, thus identifying GPNMB as a new NM-induced putative therapeutic target.

CONCLUSIONS

CONCLUSIONS

Chapter 1 – Aim 1

1. Human and mouse tyrosinase are expressed at low levels in the brain.
2. The tgNM mouse model generated reproduces the regional distribution (A1-A16) and age-dependent accumulation of NM in the human brain.
3. TgNM mice show motor and non-motor behavioral alterations including peripheral autonomic dysfunction, thus reproducing prodromal PD symptomatology.
4. Modelling human brain pigmentation in mice affects multiple neuronal systems in the brain including the dopaminergic, noradrenergic, cholinergic and serotonergic systems.
5. LC noradrenergic neurodegeneration precedes SN and VTA dopaminergic dysfunction in tgNM mice.
6. TgNM mice show typical neuropathological PD-like features in pigmented brain areas (i.e. MB, LB-like inclusions, microgliosis and astrogliosis).

Chapter 2 – Aim 2

1. The main pigmented brain areas and neurons in tgNM mice show transcriptomic changes linked to cellular homeostatic processes, including cell communication, neurotransmission, metabolism, transcription/translation, proteostasis and mitochondrial function.
2. The transcriptomic analysis performed allows the identification of splicing events in genes like TYR and GPNMB, which could have important implications for their functions.
3. The transcriptional profiles of tgNM mice SN neurons and LC region correlate with human PD postmortem studies and PD-linked datasets.
4. Disease associated microglial (DAM) genes are upregulated in the main pigmented catecholaminergic areas and correlate with a microglial reactive phenotype.
5. GPNMB is among the most upregulated genes in NM-accumulating areas and preliminary results show a protective effect of GPNMB overexpression in NM-accumulating models, in accordance to its potential as a therapeutic target for PD.

REFERENCES

REFERENCES

- Aarsland, D., Pålhlagen, S., Ballard, C. G., Ehrt, U., & Svenningsson, P. (2012). Depression in Parkinson disease - Epidemiology, mechanisms and management. *Nature Reviews Neurology*, *8*(1), 35–47. <https://doi.org/10.1038/NRNEUROL.2011.189>
- Abbott, R. D., Nelson, J. S., Ross, G. W., Uyehara-Lock, J. H., Tanner, C. M., Masaki, K. H., ... Petrovitch, H. (2017). Marinesco Bodies and Substantia Nigra Neuron Density in Parkinson's Disease. *Neuropathology and Applied Neurobiology*, *43*(7), 621. <https://doi.org/10.1111/NAN.12419>
- Adams, L., Kyung Song, M., Tanaka, Y., & Kim, Y.-S. (2022). Single-nuclei paired multiomic analysis of young, aged, and Parkinson's disease human midbrain reveals age-associated glial changes and their contribution to Parkinson's disease. *medRxiv*. <https://doi.org/10.1101/2022.01.18.22269350>
- Agarwal, D., Sandor, C., Volpato, V., Caffrey, T. M., Monzón-Sandoval, J., Bowden, R., ... Webber, C. (2020). A single-cell atlas of the human substantia nigra reveals cell-specific pathways associated with neurological disorders. *Nature Communications* *2020 11:1*, *11*(1), 1–11. <https://doi.org/10.1038/s41467-020-17876-0>
- Aguila, J., Cheng, S., Kee, N., Cao, M., Wang, M., Deng, Q., & Hedlund, E. (2021). Spatial RNA Sequencing Identifies Robust Markers of Vulnerable and Resistant Human Midbrain Dopamine Neurons and Their Expression in Parkinson's Disease. *Frontiers in Molecular Neuroscience*, *14*, 134. <https://doi.org/10.3389/FNMOL.2021.699562/BIBTEX>
- Alarcón-Arís, D., Pavia-Collado, R., Miquel-Rio, L., Coppola-Segovia, V., Ferrés-Coy, A., Ruiz-Bronchal, E., ... Bortolozzi, A. (2020). Anti- α -synuclein ASO delivered to monoamine neurons prevents α -synuclein accumulation in a Parkinson's disease-like mouse model and in monkeys. *EBioMedicine*, *59*. <https://doi.org/10.1016/J.EBIOM.2020.102944>
- Alarcón-Arís, D., Recasens, A., Galofré, M., Carballo-Carbajal, I., Zacchi, N., Ruiz-Bronchal, E., ... Bortolozzi, A. (2018). Selective α -Synuclein Knockdown in Monoamine Neurons by Intranasal Oligonucleotide Delivery: Potential Therapy for Parkinson's Disease. *Molecular Therapy*, *26*(2), 550. <https://doi.org/10.1016/J.YMTHE.2017.11.015>
- Aubry, J. M. (2013). CRF system and mood disorders. *Journal of Chemical Neuroanatomy*, *54*, 20–24. <https://doi.org/10.1016/J.JCHEMNEU.2013.09.003>
- Audrain, M., Haure-Mirande, J. V., Mleczko, J., Wang, M., Griffin, J. K., St George-Hyslop, P. H., ... Ehrlich, M. E. (2021). Reactive or transgenic increase in microglial TYROBP reveals a TREM2-independent TYROBP–APOE link in wild-type and Alzheimer's-related mice. *Alzheimer's & Dementia*, *17*(2), 149–163. <https://doi.org/10.1002/ALZ.12256>
- Avery, M. C., & Krichmar, J. L. (2017). Neuromodulatory systems and their interactions: A review of models, theories, and experiments. *Frontiers in Neural Circuits*, *11*, 108. <https://doi.org/10.3389/FNCIR.2017.00108/BIBTEX>
- Bagosi, Z., Jászberényi, M., Bujdosó, E., & Telegdy, G. (2006). The Effects of Corticotropin-Releasing Factor and the Urocortins on Striatal Dopamine Release Induced by Electrical Stimulation—An in vitro Superfusion Study. *Neurochemical Research* *2006 31:2*, *31*(2), 209–213. <https://doi.org/10.1007/S11064-005-9010-X>
- Banati, R. B., Daniel, S. E., & Blunt, S. B. (1998). Glial pathology but absence of apoptotic nigral neurons in long-standing Parkinson's disease. *Movement Disorders : Official Journal of the Movement Disorder Society*, *13*(2), 221–227. <https://doi.org/10.1002/MDS.870130205>
- Bari, B. A., Chokshi, V., & Schmidt, K. (2020). Locus coeruleus-norepinephrine: basic functions and insights into Parkinson's disease. *Neural Regeneration Research*, *15*(6), 1006. <https://doi.org/10.4103/1673-5374.270297>
- Barker, R. A. (2020). Parkinson's disease as a preventable pandemic. *The Lancet Neurology*, *19*(10), 813. [https://doi.org/10.1016/s1474-4422\(20\)30302-1](https://doi.org/10.1016/s1474-4422(20)30302-1)
- Bastías-Candia, S., Zolezzi, J. M., & Inestrosa, N. C. (2019). Revisiting the Paraquat-Induced Sporadic

- Parkinson's Disease-Like Model. *Molecular Neurobiology*, 56(2), 1044–1055.
<https://doi.org/10.1007/S12035-018-1148-Z/TABLES/2>
- Beach, T. G., Sue, L. I., Walker, D. G., Lue, L. F., Connor, D. J., Caviness, J. N., ... Adler, C. H. (2007). Marked microglial reaction in normal aging human substantia nigra: correlation with extraneuronal neuromelanin pigment deposits. *Acta Neuropathologica*, 114(4), 419–424.
<https://doi.org/10.1007/s00401-007-0250-5>
- Beach, T. G., Walker, D. G., Sue, L. I., Newell, A., Adler, C. C., & Joyce, J. N. (2004). Substantia nigra Marinesco bodies are associated with decreased striatal expression of dopaminergic markers. *Journal of Neuropathology and Experimental Neurology*, 63(4), 329–337.
<https://doi.org/10.1093/JNEN/63.4.329>
- Belujon, P., & Grace, A. A. (2017). Dopamine System Dysregulation in Major Depressive Disorders. *International Journal of Neuropsychopharmacology*, 20(12), 1036.
<https://doi.org/10.1093/IJNP/PYX056>
- Benarroch, E. E., Schmeichel, A. M., Sandroni, P., Low, P. A., & Parisi, J. E. (2006). Involvement of vagal autonomic nuclei in multiple system atrophy and Lewy body disease. *Neurology*, 66(3), 378–383. <https://doi.org/10.1212/01.WNL.0000196638.98781.BB>
- Bensaid, M., Michel, P. P., Clark, S. D., Hirsch, E. C., & François, C. (2016). Role of pedunculopontine cholinergic neurons in the vulnerability of nigral dopaminergic neurons in Parkinson's disease. *Experimental Neurology*, 275, 209–219. <https://doi.org/10.1016/j.expneurol.2015.11.004>
- Ben-Shlomo, Y., Marmot, M. G., & Ben-Shlomo, Y. (1995). Survival and cause of death in a cohort of patients with parkinsonism: possible clues to aetiology? *Neurosurgery, and Psychiatry*, 58, 293–299. <https://doi.org/10.1136/jnnp.58.3.293>
- Berg, D., Borghammer, P., Fereshtehnejad, S. M., Heinzl, S., Horsager, J., Schaeffer, E., & Postuma, R. B. (2021). Prodromal Parkinson disease subtypes - key to understanding heterogeneity. *Nature Reviews. Neurology*, 17(6), 349–361. <https://doi.org/10.1038/S41582-021-00486-9>
- Berg, D., Godau, J., Seppi, K., Behnke, S., Liepelt-Scarfone, I., Lerche, S., ... Poewe, W. (2013). The PRIPS study: screening battery for subjects at risk for Parkinson's disease. *European Journal of Neurology*, 20(1), 102–108. <https://doi.org/10.1111/J.1468-1331.2012.03798.X>
- Berg, D., Postuma, R. B., Adler, C. H., Bloem, B. R., Chan, P., Dubois, B., ... Deuschl, G. (2015). MDS research criteria for prodromal Parkinson's disease. *Movement Disorders*, 30(12), 1600–1611.
<https://doi.org/10.1002/MDS.26431>
- Bernal, J. A., Luna, R., Espina, Á., Lázaro, I., Ramos-Morales, F., Romero, F., ... Pintor-Toro, J. A. (2002). Human securin interacts with p53 and modulates p53-mediated transcriptional activity and apoptosis. *Nature Genetics*, 32(2), 306–311. <https://doi.org/10.1038/NG997>
- Betts, M. J., Kirilina, E., Otaduy, M. C. G., Ivanov, D., Acosta-Cabronero, J., Callaghan, M. F., ... Hämmerer, D. (2019). Locus coeruleus imaging as a biomarker for noradrenergic dysfunction in neurodegenerative diseases. *Brain*, 142(9), 2558. <https://doi.org/10.1093/BRAIN/AWZ193>
- Binder, M. D., Hirokawa, N., & Windhorst, U. (2008). Dorsal Vagal Complex (DVC). *Encyclopedia of Neuroscience*, 998–999. https://doi.org/10.1007/978-3-540-29678-2_1597/COVER
- Birkmayer, W., & Hornykiewicz, O. (1962). Der L-Dioxyphenylalanin (=L-DOPA)-Effekt beim Parkinson-Syndrom des Menschen: Zur Pathogenese und Behandlung der Parkinson-Akinese. *Archiv Für Psychiatrie Und Nervenkrankheiten Vereinigt Mit Zeitschrift Für Die Gesamte Neurologie Und Psychiatrie*, 203(5), 560–574. <https://doi.org/10.1007/BF00343235>
- Björklund, A., & Dunnett, S. B. (2007). Dopamine neuron systems in the brain: an update. *Trends in Neurosciences*, 30(5), 194–202. <https://doi.org/10.1016/j.tins.2007.03.006>
- Blesa, J., Phani, S., Jackson-Lewis, V., & Przedborski, S. (2012). Classic and New Animal Models of Parkinson's Disease. *Journal of Biomedicine and Biotechnology*, 2012.
<https://doi.org/10.1155/2012/845618>
- Blesa, J., & Przedborski, S. (2014). Parkinson's disease: Animal models and dopaminergic cell

- vulnerability. *Frontiers in Neuroanatomy*, 8(DEC), 155.
<https://doi.org/10.3389/FNANA.2014.00155/BIBTEX>
- Bloem, B. R., Okun, M. S., & Klein, C. (2021). Parkinson's disease. *The Lancet*, 397(10291), 2284–2303.
[https://doi.org/10.1016/S0140-6736\(21\)00218-X](https://doi.org/10.1016/S0140-6736(21)00218-X)
- Bnirri, & Rullrin. (1983). Histochemical Observations On Rodent Brain Melanin', *IO*, 847–851.
 Retrieved from <https://eurekamag.com/pdf.php?pdf=005577648>
- Bogerts, B. (1981). A brainstem atlas of catecholaminergic neurons in man, using melanin as a natural marker. *Journal of Comparative Neurology*, 197(1), 63–80. <https://doi.org/10.1002/cne.901970106>
- Bohnen, N. I., Yarnall, A. J., Weil, R. S., Moro, E., Moehle, M. S., Borghammer, P., ... Albin, R. L. (2022). Cholinergic system changes in Parkinson's disease: emerging therapeutic approaches. *The Lancet Neurology*, 21(4), 381–392. [https://doi.org/10.1016/S1474-4422\(21\)00377-X](https://doi.org/10.1016/S1474-4422(21)00377-X)
- Borghammer, P., Just, M. K., Horsager, J., Skjærbæk, C., Raunio, A., Kok, E. H., ... Van Den Berge, N. (2022). A postmortem study suggests a revision of the dual-hit hypothesis of Parkinson's disease. *Npj Parkinson's Disease* 2022 8:1, 8(1), 1–11. <https://doi.org/10.1038/s41531-022-00436-2>
- Borghammer, P., & Van Den Berge, N. (2019). Brain-First versus Gut-First Parkinson's Disease: A Hypothesis. *Journal of Parkinson's Disease*, 9(Suppl 2), S281. <https://doi.org/10.3233/JPD-191721>
- Borrageiro, G., Haylett, W., Seedat, S., Kuivaniemi, H., & Bardien, S. (2017). A review of genome-wide transcriptomics studies in Parkinson's disease. *European Journal of Neuroscience*, 47(1), 1–16.
<https://doi.org/10.1111/EJN.13760>
- Bossers, K., Meerhoff, G., Balesar, R., Van Dongen, J. W., Kruse, C. G., Swaab, D. F., & Verhaagen, J. (2009). Analysis of gene expression in Parkinson's disease: Possible involvement of neurotrophic support and axon guidance in dopaminergic cell death. *Brain Pathology*, 19(1), 91–107.
<https://doi.org/10.1111/J.1750-3639.2008.00171.X>
- Bové, J., Prou, D., Perier, C., & Przedborski, S. (2005). Toxin-Induced Models of Parkinson's Disease. *NeuroRx*, 2(3), 484. <https://doi.org/10.1602/NEURORX.2.3.484>
- Braak, E., Sandmann-Keil, D., Rüb, U., Gai, W. P., de Vos, R. A., Steur, E. N., ... Braak, H. (2001). alpha-synuclein immunopositive Parkinson's disease-related inclusion bodies in lower brain stem nuclei. *Acta Neuropathologica*, 101(3), 195–201. Retrieved from <http://www.ncbi.nlm.nih.gov/pubmed/11307617>
- Braak, H., Tredici, K., Rüb, U., de Vos, R. A. I., Jansen Steur, E. N. H., & Braak, E. (2003). Staging of brain pathology related to sporadic Parkinson's disease. *Neurobiology of Aging*, 24(2), 197–211.
[https://doi.org/10.1016/S0197-4580\(02\)00065-9](https://doi.org/10.1016/S0197-4580(02)00065-9)
- Brendza, R., Lin, H., Stark, K., Foreman, O., Tao, J., Pierce, A., ... Friedman, B. A. (2021). Genetic ablation of Gpnmb does not alter synuclein-related pathology. *Neurobiology of Disease*, 159, 105494. <https://doi.org/10.1016/J.NBD.2021.105494>
- Breton-Provencher, V., Drummond, G. T., & Sur, M. (2021). Locus Coeruleus Norepinephrine in Learned Behavior: Anatomical Modularity and Spatiotemporal Integration in Targets. *Frontiers in Neural Circuits*, 15, 46. <https://doi.org/10.3389/FNCIR.2021.638007/BIBTEX>
- Briggs, C. E., Wang, Y., Kong, B., Woo, T. U. W., Iyer, L. K., & Sonntag, K. C. (2015). Midbrain dopamine neurons in Parkinson's disease exhibit a dysregulated miRNA and target-gene network. *Brain Research*, 1618, 111. <https://doi.org/10.1016/J.BRAINRES.2015.05.021>
- Brochard, V., Combadière, B., Prigent, A., Laouar, Y., Perrin, A., Beray-Berthet, V., ... Hunot, S. (2009). Infiltration of CD4+ lymphocytes into the brain contributes to neurodegeneration in a mouse model of Parkinson disease. *The Journal of Clinical Investigation*, 119(1), 182–192.
<https://doi.org/10.1172/JCI36470>
- Brown, R. E., & Wong, A. A. (2007). The influence of visual ability on learning and memory performance in 13 strains of mice. *Learning & Memory*, 14(3), 134.
<https://doi.org/10.1101/LM.473907>
- Bucci, D., Busceti, C. L., Calierno, M. T., Di Pietro, P., Madonna, M., Biagioni, F., ... Fornai, F. (2017).

- Systematic Morphometry of Catecholamine Nuclei in the Brainstem. *Frontiers in Neuroanatomy*, 0, 98. <https://doi.org/10.3389/FNANA.2017.00098>
- Budge, K. M., Neal, M. L., Richardson, J. R., & Safadi, F. F. (2020). Transgenic Overexpression of GPNMB Protects Against MPTP-Induced Neurodegeneration. *Molecular Neurobiology* 2020 57:7, 57(7), 2920–2933. <https://doi.org/10.1007/S12035-020-01921-6>
- Burke, R. E., Dauer, W. T., & Vonsattel, J. P. G. (2008). A Critical Evaluation of The Braak Staging Scheme for Parkinson's Disease. *Annals of Neurology*, 64(5), 485. <https://doi.org/10.1002/ANA.21541>
- Burke, R. E., & O'Malley, K. (2013). Axon Degeneration in Parkinson's Disease. *Experimental Neurology*, 246, 72. <https://doi.org/10.1016/J.EXPNEUROL.2012.01.011>
- Bush, W. D., Garguilo, J., Zucca, F. A., Albertini, A., Zecca, L., Edwards, G. S., ... Simon, J. D. (2006). The surface oxidation potential of human neuromelanin reveals a spherical architecture with a pheomelanin core and a eumelanin surface. *Proceedings of the National Academy of Sciences of the United States of America*, 103(40), 14785–14789. <https://doi.org/10.1073/PNAS.0604010103/ASSET/2650CC78-ADD1-4198-9380-7266659B85B3/ASSETS/GRAPHIC/ZPQ04006-3608-M02.JPEG>
- Butovsky, O., & Weiner, H. L. (2018). Microglial signatures and their role in health and disease. *Nature Reviews Neuroscience* 2018 19:10, 19(10), 622–635. <https://doi.org/10.1038/s41583-018-0057-5>
- Cabello, C. R., Thune, J. J., Pakkenberg, H., & Pakkenberg, B. (2002). Ageing of substantia nigra in humans: cell loss may be compensated by hypertrophy. *Neuropathology and Applied Neurobiology*, 28(4), 283–291. <https://doi.org/10.1046/J.1365-2990.2002.00393.X>
- Cantuti-Castelvetri, I., Keller-McGandy, C., Bouzou, B., Asteris, G., Clark, T. W., Frosch, M. P., & Standaert, D. G. (2007). Effects of Gender on Nigral Gene Expression and Parkinson Disease. *Neurobiology of Disease*, 26(3), 606. <https://doi.org/10.1016/J.NBD.2007.02.009>
- Carballo-Carbajal, I., Laguna, A., Romero-Giménez, J., Cuadros, T., Bové, J., Martínez-Vicente, M., ... Vila, M. (2019). Brain tyrosinase overexpression implicates age-dependent neuromelanin production in Parkinson's disease pathogenesis. *Nature Communications*, 10(1), 973. <https://doi.org/10.1038/s41467-019-08858-y>
- Cebrián, C., Zucca, F. A., Mauri, P., Steinbeck, J. A., Studer, L., Scherzer, C. R., ... Sulzer, D. (2014). MHC-I expression renders catecholaminergic neurons susceptible to T-cell-mediated degeneration. *Nature Communications*, 5(1), 3633. <https://doi.org/10.1038/ncomms4633>
- Champagnat, J., Fortin, G., Jungbluth, S., Abadie, V., Chatonnet, F., Dominquez-Del-Toro, E., & Guimaraes, L. (2001). Information processing at the nucleus tractus solitarii and respiratory rhythm generation. *Respiratory Research* 2001 2:1, 2(1), 1–2. <https://doi.org/10.1186/RR97>
- Charcot, J.-M. (1872). De la paralysie agitante. In Oeuvres Complètes (t 1) Leçons sur les maladies du système nerveux. *A Delahaye, Paris*, 155–188. <https://doi.org/10.1101/CSHPERSPECT.A008862>
- Chaudhuri, K. R., Healy, D. G., & Schapira, A. H. V. (2006). Non-motor symptoms of Parkinson's disease: diagnosis and management. *The Lancet Neurology*, 5(3), 235–245. [https://doi.org/10.1016/S1474-4422\(06\)70373-8](https://doi.org/10.1016/S1474-4422(06)70373-8)
- Chaudhuri, K. R., & Schapira, A. H. (2009). Non-motor symptoms of Parkinson's disease: dopaminergic pathophysiology and treatment. *The Lancet Neurology*, 8(5), 464–474. [https://doi.org/10.1016/S1474-4422\(09\)70068-7](https://doi.org/10.1016/S1474-4422(09)70068-7)
- Chen, G.-J., Yan, S.-S., Zhang, J.-H., Zhang, J., Isaac, |, Deng, B., & Rong He, |. (2022). The alternative 3' splice site of GPNMB may promote neuronal survival after neonatal hypoxic-ischemic encephalopathy injury. *Ibrain*, 8(3), 302–313. <https://doi.org/10.1002/IBRA.12056>
- Cheshire, P., Ayton, S., Bertram, K. L., Ling, H., Li, A., Mclean, C., ... Williams, D. R. (2015). Serotonergic markers in Parkinson's disease and levodopa-induced dyskinesias. *Movement Disorders : Official Journal of the Movement Disorder Society*, 30(6), 796–804. <https://doi.org/10.1002/MDS.26144>

- Choong, C. J., & Mochizuki, H. (2022). Neuropathology of α -synuclein in Parkinson's disease. *Neuropathology*, 42(2), 93–103. <https://doi.org/10.1111/NEUP.12812>
- Chrystal, P. W., Footz, T., Hodges, E. D., Jensen, J. A., Walter, M. A., & Allison, W. T. (2021). Functional Domains and Evolutionary History of the PMEL and GPNMB Family Proteins. *Molecules* 2021, Vol. 26, Page 3529, 26(12), 3529. <https://doi.org/10.3390/MOLECULES26123529>
- Chu, Y., & Kordower, J. H. (2007). Age-associated increases of α -synuclein in monkeys and humans are associated with nigrostriatal dopamine depletion: Is this the target for Parkinson's disease? *Neurobiology of Disease*, 25(1), 134–149. <https://doi.org/10.1016/J.NBD.2006.08.021>
- Chung, E. J., Cho, H. J., Hur, D. Y., Kim, Y. S., Lee, K. H., & Kim, S. J. (2022). One Autopsy Proved Neocortical Lewy Body Disease Without the Involvement of the Olfactory Bulb and Brainstem. *Journal of Korean Medical Science*, 37(23). <https://doi.org/10.3346/JKMS.2022.37.E195>
- Chung, J.-S., Sato, K., Dougherty, I. I., Cruz, P. D., Jr, & Ariizumi, K. (2007). DC-HIL is a negative regulator of T lymphocyte activation. *Blood*, 109(10), 4320. <https://doi.org/10.1182/BLOOD-2006-11-053769>
- Chuquilín-Arista, F., Álvarez-Avellón, T., & Menéndez-González, M. (2020). Prevalence of Depression and Anxiety in Parkinson Disease and Impact on Quality of Life: A Community-Based Study in Spain. *Journal of Geriatric Psychiatry and Neurology*, 33(4), 207–213. <https://doi.org/10.1177/0891988719874130>
- Connolly, B. S., & Lang, A. E. (2014). Pharmacological Treatment of Parkinson Disease: A Review. *JAMA*, 311(16), 1670–1683. <https://doi.org/10.1001/JAMA.2014.3654>
- Cotzias, G. C., Papavasiliou, P. S., & Gellene, R. (1969). Modification of Parkinsonism — Chronic Treatment with L-Dopa. <http://dx.doi.org/10.1056/NEJM196902132800701>, 280(7), 337–345. <https://doi.org/10.1056/NEJM196902132800701>
- Critchley, H. D., & Harrison, N. A. (2013). Visceral Influences on Brain and Behavior. *Neuron*, 77(4), 624–638. <https://doi.org/10.1016/J.NEURON.2013.02.008>
- Croisier, E., Moran, L. B., Dexter, D. T., Pearce, R. K. B., & Graeber, M. B. (2005). Microglial inflammation in the parkinsonian substantia nigra: Relationship to alpha-synuclein deposition. *Journal of Neuroinflammation*, 2(1), 1–8. <https://doi.org/10.1186/1742-2094-2-14/FIGURES/2>
- Cryan, J. F., Mombereau, C., & Vassout, A. (2005). The tail suspension test as a model for assessing antidepressant activity: Review of pharmacological and genetic studies in mice. *Neuroscience and Biobehavioral Reviews*, 29(4–5), 571–625. <https://doi.org/10.1016/J.NEUBIOREV.2005.03.009>
- Cui, Y., Cai, M., & Stanley, H. E. (2017). Comparative Analysis and Classification of Cassette Exons and Constitutive Exons. *BioMed Research International*, 2017. <https://doi.org/10.1155/2017/7323508>
- Damier, P., Hirsch, E. C., Zhang, P., Agid, Y., & Javoy-Agid, F. (1993). Glutathione peroxidase, glial cells and Parkinson's disease. *Neuroscience*, 52(1), 1–6. [https://doi.org/10.1016/0306-4522\(93\)90175-F](https://doi.org/10.1016/0306-4522(93)90175-F)
- Dashtipour, K., Tafreshi, A., Lee, J., & Crawley, B. (2018). Speech disorders in Parkinson's disease: pathophysiology, medical management and surgical approaches. <https://doi.org/10.2217/nmt-2018-0021>, 8(5), 337–348. <https://doi.org/10.2217/NMT-2018-0021>
- Davis, J., Maillet, M., Miano, J. M., & Molkentin, J. D. (2012). Lost in Transgenesis: A Users guide for Genetically Manipulating the Mouse in Cardiac Research. *Circulation Research*, 111(6), 761. <https://doi.org/10.1161/CIRCRESAHA.111.262717>
- Dawson, T. M., Golde, T. E., & Lagier-Tourenne, C. (2018). Animal models of neurodegenerative diseases. *Nature Neuroscience* 2018 21:10, 21(10), 1370–1379. <https://doi.org/10.1038/S41593-018-0236-8>
- De Souza, E. B., Whitehouse, P. J., Price, D. L., & Vale, W. W. (1987). Abnormalities in Corticotropin-releasing Hormone (CRH) in Alzheimer's Disease and Other Human Disorders. *Annals of the New York Academy of Sciences*, 512(1), 237–247. <https://doi.org/10.1111/J.1749-6632.1987.TB24964.X>

- Decressac, M., Mattsson, B., Lundblad, M., Weikop, P., & Björklund, A. (2012). Progressive neurodegenerative and behavioural changes induced by AAV-mediated overexpression of α -synuclein in midbrain dopamine neurons. *Neurobiology of Disease*, *45*(3), 939–953. <https://doi.org/10.1016/J.NBD.2011.12.013>
- Deczkowska, A., Keren-Shaul, H., Weiner, A., Colonna, M., Schwartz, M., & Amit, I. (2018). Disease-Associated Microglia: A Universal Immune Sensor of Neurodegeneration. *Cell*, *173*(5), 1073–1081. <https://doi.org/10.1016/J.CELL.2018.05.003>
- Dedic, N., Kühne, C., Gomes, K. S., Hartmann, J., Ressler, K. J., Schmidt, M. V., & Deussing, J. M. (2019). Deletion of CRH From GABAergic Forebrain Neurons Promotes Stress Resilience and Dampens Stress-Induced Changes in Neuronal Activity. *Frontiers in Neuroscience*, *13*, 986. <https://doi.org/10.3389/FNINS.2019.00986/BIBTEX>
- Del Rey, N. L. G., Quiroga-Varela, A., Garbayo, E., Carballo-Carbajal, I., Fernández-Santiago, R., Monje, M. H. G., ... Blesa, J. (2018). Advances in Parkinson's Disease: 200 Years Later. *Frontiers in Neuroanatomy*, *12*. <https://doi.org/10.3389/FNANA.2018.00113>
- Delaville, C., de Deurwaerdère, P., & Benazzouz, A. (2011). Noradrenaline and Parkinson's disease. *Frontiers in Systems Neuroscience*, *5*(MAY 2011). <https://doi.org/10.3389/FNSYS.2011.00031>
- Deng, W., McLaughlin, S. L., & Klinke, D. J. (2017). Quantifying spontaneous metastasis in a syngeneic mouse melanoma model using real time PCR. *The Analyst*, *142*(16), 2945. <https://doi.org/10.1039/C7AN00623C>
- Diaz-Ortiz, M. E., Seo, Y., Posavi, M., Cordon, M. C., Clark, E., Jain, N., ... Chen-Plotkin, A. S. (2022). GPNMB confers risk for Parkinson's disease through interaction with α -synuclein. *Science*, *377*(6608). https://doi.org/10.1126/SCIENCE.ABK0637/SUPPL_FILE/SCIENCE.ABK0637_DATA_S1.ZIP
- Dickson, D. W., Uchikado, H., Fujishiro, H., & Tsuboi, Y. (2010). Evidence in favor of Braak staging of Parkinson's disease. *Movement Disorders*, *25*(S1), S78–S82. <https://doi.org/10.1002/MDS.22637>
- Dijkstra, A. A., Ingrassia, A., De Menezes, R. X., Van Kesteren, R. E., Rozemuller, A. J. M., Heutink, P., & Van De Berg, W. D. J. (2015). Evidence for Immune Response, Axonal Dysfunction and Reduced Endocytosis in the Substantia Nigra in Early Stage Parkinson's Disease. *PloS One*, *10*(6). <https://doi.org/10.1371/JOURNAL.PONE.0128651>
- Ding, S. L., Royall, J. J., Sunkin, S. M., Ng, L., Facer, B. A. C., Lesnar, P., ... Lein, E. S. (2016). Comprehensive cellular-resolution atlas of the adult human brain. *The Journal of Comparative Neurology*, *524*(16), 3127–3481. <https://doi.org/10.1002/CNE.24080>
- Doorn, K. J., Moors, T., Drukarch, B., van de Berg, W. D. J., Lucassen, P. J., & van Dam, A. M. (2014). Microglial phenotypes and toll-like receptor 2 in the substantia nigra and hippocampus of incidental Lewy body disease cases and Parkinson's disease patients. *Acta Neuropathologica Communications*, *2*(1). <https://doi.org/10.1186/S40478-014-0090-1>
- Dorsey, E. R., & Bloem, B. R. (2018). The Parkinson pandemic - A call to action. *JAMA Neurology*, *75*(1), 9–10. <https://doi.org/10.1001/JAMANEUROL.2017.3299>
- Dorsey, E. R., Sherer, T., Okun, M. S., & Bloem, B. R. (2018). The Emerging Evidence of the Parkinson Pandemic. *Journal of Parkinson's Disease*, *8*, 3–8. <https://doi.org/10.3233/JPD-181474>
- Doty, R. L. (2012). Olfactory dysfunction in Parkinson disease. *Nature Reviews Neurology* *2012* *8*:6, *8*(6), 329–339. <https://doi.org/10.1038/nrneurol.2012.80>
- Double, K. L., Rowe, D. B., Carew-Jones, F. M., Hayes, M., Chan, D. K. Y., Blackie, J., ... Halliday, G. M. (2009). Anti-melanin antibodies are increased in sera in Parkinson's disease. *Experimental Neurology*, *217*(2), 297–301. <https://doi.org/10.1016/j.expneurol.2009.03.002>
- Double, K. L., Zecca, L., Costi, P., Mauer, M., Griesinger, C., Ito, S., ... Gerlach, M. (2000). Structural characteristics of human substantia nigra neuromelanin and synthetic dopamine melanins. *Journal of Neurochemistry*, *75*(6), 2583–2589. Retrieved from <http://www.ncbi.nlm.nih.gov/pubmed/11080212>

- Duke, D. C., Moran, L. B., Kalaitzakis, M. E., Deprez, M., Dexter, D. T., Pearce, R. K. B., & Graeber, M. B. (2006). Transcriptome analysis reveals link between proteasomal and mitochondrial pathways in Parkinson's disease. *Neurogenetics*, 7(3), 139–148. <https://doi.org/10.1007/s10048-006-0033-5>
- Dumitriu, A., Golji, J., Labadorf, A. T., Gao, B., Beach, T. G., Myers, R. H., ... Latourelle, J. C. (2016). Integrative analyses of proteomics and RNA transcriptomics implicate mitochondrial processes, protein folding pathways and GWAS loci in Parkinson disease. *BMC Medical Genomics*, 9(1). <https://doi.org/10.1186/S12920-016-0164-Y>
- Durrenberger, P. F., Grünblatt, E., Fernando, F. S., Monoranu, C. M., Evans, J., Riederer, P., ... Dexter, D. T. (2012). Inflammatory pathways in Parkinson's disease; A BNE microarray study. *Parkinson's Disease*. <https://doi.org/10.1155/2012/214714>
- Eadie, M. J. (1963). The pathology of certain medullary nuclei in parkinsonism. *Brain*, 86(4), 781–792. <https://doi.org/10.1093/BRAIN/86.4.781>
- Ehringer, H., & Hornykiewicz, O. (1960). Verteilung Von Noradrenalin Und Dopamin (3-Hydroxytyramin) Im Gehirn Des Menschen Und Ihr Verhalten Bei Erkrankungen Des Extrapyramidalen Systems. *Klinische Wochenschrift* 1960 38:24, 38(24), 1236–1239. <https://doi.org/10.1007/BF01485901>
- Elstner, M., Morris, C. M., Heim, K., Bender, A., Mehta, D., Jaros, E., ... Prokisch, H. (2011). Expression analysis of dopaminergic neurons in Parkinson's disease and aging links transcriptional dysregulation of energy metabolism to cell death. *Acta Neuropathologica*, 122(1), 75–86. <https://doi.org/10.1007/s00401-011-0828-9>
- Espay, A. J., Lewitt, P. A., & Kaufmann, H. (2014). Norepinephrine deficiency in Parkinson's disease: The case for noradrenergic enhancement. *Movement Disorders*, 29(14), 1710–1719. <https://doi.org/10.1002/MDS.26048>
- Fasano, M., Giraud, S., Coha, S., Bergamasco, B., & Lopiano, L. (2003). Residual substantia nigra neuromelanin in Parkinson's disease is cross-linked to alpha-synuclein. *Neurochemistry International*, 42(7), 603–606. Retrieved from <http://www.ncbi.nlm.nih.gov/pubmed/12590943>
- Fedorow, H., Halliday, G. M., Rickert, C. H., Gerlach, M., Riederer, P., & Double, K. L. (2006). Evidence for specific phases in the development of human neuromelanin. *Neurobiology of Aging*, 27(3), 506–512. <https://doi.org/10.1016/j.neurobiolaging.2005.02.015>
- Fedorow, H., Tribl, F., Halliday, G., Gerlach, M., Riederer, P., & Double, K. L. (2005). Neuromelanin in human dopamine neurons: Comparison with peripheral melanins and relevance to Parkinson's disease. *Progress in Neurobiology*, 75(2), 109–124. <https://doi.org/10.1016/j.pneurobio.2005.02.001>
- Feigin, V. L., Nichols, E., Alam, T., Bannick, M. S., Beghi, E., Blake, N., ... Vos, T. (2019). Global, regional, and national burden of neurological disorders, 1990–2016: a systematic analysis for the Global Burden of Disease Study 2016. *The Lancet Neurology*, 18(5), 459–480. [https://doi.org/10.1016/S1474-4422\(18\)30499-X](https://doi.org/10.1016/S1474-4422(18)30499-X)
- Fénelon, G., & Walusinski, O. (2021). The landmark contributions of Paul Blocq, Georges Marinesco, and Édouard Brissaud in Parkinson's disease. *Revue Neurologique*, 177(10), 1214–1220. <https://doi.org/10.1016/J.NEUROL.2021.02.386>
- Fenichel, G. M., & Bazelon, M. (1968). Studies on neuromelanin: II. Melanin in the brainstems of infants and children. *Neurology*, 18(8), 817–820. <https://doi.org/10.1212/WNL.18.8.817>
- Fernández, A., Hayashi, M., Garrido, G., Montero, A., Guardia, A., Suzuki, T., & Montoliu, L. (2021). Genetics of non-syndromic and syndromic oculocutaneous albinism in human and mouse. *Pigment Cell & Melanoma Research*, 34(4), 786–799. <https://doi.org/10.1111/PCMR.12982>
- Finlay, J. B., Liu, X., Ermel, R. W., & Adamson, T. W. (2015). Maternal Weight Gain as a Predictor of Litter Size in Swiss Webster, C57BL/6J, and BALB/cJ mice. *Journal of the American Association for Laboratory Animal Science : JAALAS*, 54(6), 694. Retrieved from <http://pmc/articles/PMC4671784/>
- Foley, J. M., & Banter, D. (1958). On the Nature of Pigment Granules in the Cells of the Locus Coeruleus and Substantia Nigra. *Journal of Neuropathology & Experimental Neurology*, 17(4), 586–598.

<https://doi.org/10.1097/00005072-195810000-00005>

- Forno, L. S., Langston, J. W., DeLanney, L. E., Irwin, I., & Ricaurte, G. A. (1986). Locus ceruleus lesions and eosinophilic inclusions in MPTP-treated monkeys. *Annals of Neurology*, 20(4), 449–455. <https://doi.org/10.1002/ANA.410200403>
- French, I. T., & Muthusamy, K. A. (2018). A Review of the Pedunculo-pontine Nucleus in Parkinson's Disease. *Frontiers in Aging Neuroscience*, 10(APR). <https://doi.org/10.3389/FNAGI.2018.00099>
- Friedman, B. A., Srinivasan, K., Ayalon, G., Meilandt, W. J., Lin, H., Huntley, M. A., ... Hansen, D. V. (2018). Diverse Brain Myeloid Expression Profiles Reveal Distinct Microglial Activation States and Aspects of Alzheimer's Disease Not Evident in Mouse Models. *Cell Reports*, 22(3), 832–847. <https://doi.org/10.1016/j.celrep.2017.12.066>
- Fryer, J. P., Oetting, W. S., Brott, M. J., & King, R. A. (2001). Alternative Splicing of the Tyrosinase Gene Transcript in Normal Human Melanocytes and Lymphocytes. *Journal of Investigative Dermatology*, 117(5), 1261–1265. <https://doi.org/10.1046/J.0022-202X.2001.01549.X>
- Fuchs, A. L., Wurm, J. P., Neu, A., & Sprangers, R. (2020). Molecular basis of the selective processing of short mRNA substrates by the DcpS mRNA decapping enzyme. *Proceedings of the National Academy of Sciences of the United States of America*, 117(32), 19237–19244. <https://doi.org/10.1073/PNAS.2009362117/-/DCSUPPLEMENTAL>
- Funayama, M., Nishioka, K., Li, Y., & Hattori, N. (2022). Molecular genetics of Parkinson's disease: Contributions and global trends. *Journal of Human Genetics* 2022, 1–6. <https://doi.org/10.1038/s10038-022-01058-5>
- Gai, W. P., Blumbergs, P. C., Geffen, L. B., & Blessing, W. W. (1992). Age-related loss of dorsal vagal neurons in Parkinson's disease. *Neurology*, 42(11), 2106–2111. <https://doi.org/10.1212/WNL.42.11.2106>
- Gai, W. P., Geffen, L. B., Denoroy, L., & Blessing, W. W. (1993). Loss of C1 and C3 epinephrine-synthesizing neurons in the medulla oblongata in parkinson's disease. *Annals of Neurology*, 33(4), 357–367. <https://doi.org/10.1002/ANA.410330405>
- Galiano-Landeira, J., Torra, A., Vila, M., & Bové, J. (2020). CD8 T cell nigral infiltration precedes synucleinopathy in early stages of Parkinson's disease. *Brain*, 143(12), 3717–3733. <https://doi.org/10.1093/BRAIN/AWAA269>
- Gálvez-Jiménez, N. A. (2007). Parkinson's Disease. *Neurobiology of Disease*, 51–67. <https://doi.org/10.1016/B978-012088592-3/50007-4>
- Gegg, M. E., Burke, D., Heales, S. J. R., Cooper, J. M., Hardy, J., Wood, N. W., & Schapira, A. H. V. (2012). Glucocerebrosidase deficiency in substantia nigra of parkinson disease brains. *Annals of Neurology*, 72(3), 455–463. <https://doi.org/10.1002/ANA.23614>
- Gentleman, R., Carey, V. J., Huber, W., Irizarry, R. A., & Dudoit, S. (2005). *Bioinformatics and Computational Biology Solutions Using R and Bioconductor*. New York, NY: Springer New York. <https://doi.org/10.1007/0-387-29362-0>
- German, D. C., Walker, B. S., Manaye, ' K, Smith, W. K., Woodward, D. J., & North', A. J. (1988). The Human Locus Coeruleus: Computer Reconstruction of Cellular Distribution. *The Journal of Neuroscience*, 8(5), 1778–1788.
- Gervais, F. G., Singaraja, R., Xanthoudakis, S., Gutekunst, C. A., Leavitt, B. R., Metzler, M., ... Nicholson, D. W. (2002). Recruitment and activation of caspase-8 by the Huntingtin-interacting protein Hip-1 and a novel partner Hippi. *Nature Cell Biology*, 4(2), 95–105. <https://doi.org/10.1038/NCB735>
- Giguère, N., Nanni, S. B., & Trudeau, L. E. (2018, June 19). On cell loss and selective vulnerability of neuronal populations in Parkinson's disease. *Frontiers in Neurology*. Frontiers Media S.A. <https://doi.org/10.3389/fneur.2018.00455>
- Glaab, E., & Schneider, R. (2015). Comparative pathway and network analysis of brain transcriptome changes during adult aging and in Parkinson's disease. *Neurobiology of Disease*, 74, 1–13.

<https://doi.org/10.1016/J.NBD.2014.11.002>

- Goetz, C. G. (2011). The History of Parkinson's Disease: Early Clinical Descriptions and Neurological Therapies. *Cold Spring Harbor Perspectives in Medicine*, 1(1). <https://doi.org/10.1101/CSHPERSPECT.A008862>
- Gómez-Isla, T., Hollister, R., West, H., Mui, S., Growdon, J. H., Petersen, R. C., ... Hyman, B. T. (1997). Neuronal loss correlates with but exceeds neurofibrillary tangles in Alzheimer's disease. *Annals of Neurology*, 41(1), 17–24. <https://doi.org/10.1002/ANA.410410106>
- Gonçalves, V. C., Cuenca-Bermejo, L., Fernandez-Villalba, E., Martin-Balbuena, S., da Silva Fernandes, M. J., Scorza, C. A., & Herrero, M. T. (2021). Heart Matters: Cardiac Dysfunction and Other Autonomic Changes in Parkinson's Disease. *Neuroscientist*. <https://doi.org/10.1177/1073858421990000>
- Gonzalez-Sepulveda, M., Compte, J., Cuadros, T., Nicolau, A., Guillard-Sirieix, C., Peñuelas, N., ... Vila, M. (2022). In vivo reduction of age-dependent neuromelanin accumulation mitigates features of Parkinson's disease. *bioRxiv*, 2022.08.08.503142. <https://doi.org/10.1101/2022.08.08.503142>
- Gonzalez-Sepulveda, M., Laguna, A., Carballo-Carbajal, I., Galiano-Landeira, J., Romero-Gimenez, J., Cuadros, T., ... Vila, M. (2020). Validation of a reversed phase UPLC-MS/MS method to determine dopamine metabolites and oxidation intermediates in neuronal differentiated SH-SY5Y cells and brain tissue. *ACS Chemical Neuroscience*, 11(17), 2679–2687. <https://doi.org/10.1021/ACSCHEMNEURO.0C00336>
- Götz, M. E., Double, K., Gerlach, M., Youdim, M. B. H., & Riederer, P. (2006). The Relevance of Iron in the Pathogenesis of Parkinson's Disease. *Annals of the New York Academy of Sciences*, 1012(1), 193–208. <https://doi.org/10.1196/ANNALS.1306.017>
- Grall-Bronnec, M., Victorri-Vigneau, C., Donnio, Y., Leboucher, J., Rousselet, M., Thiabaud, E., ... Challet-Bouju, G. (2018). Dopamine Agonists and Impulse Control Disorders: A Complex Association. *Drug Safety*, 41(1), 19. <https://doi.org/10.1007/S40264-017-0590-6>
- Grant, L. M., Richter, F., Miller, J. E., White, S. A., Fox, C. M., Zhu, C., ... Ciucci, M. R. (2014). Vocalization deficits in mice over-expressing alpha-synuclein, a model of pre-manifest Parkinson's disease. *Behavioral Neuroscience*, 128(2), 110–121. <https://doi.org/10.1037/A0035965>
- Gratwicke, J., Kahan, J., Zrinzo, L., Hariz, M., Limousin, P., Foltynie, T., & Jahanshahi, M. (2013). The nucleus basalis of Meynert: A new target for deep brain stimulation in dementia? *Neuroscience and Biobehavioral Reviews*, 37(10), 2676–2688. <https://doi.org/10.1016/J.NEUBIOREV.2013.09.003>
- Greggio, E., Bergantino, E., Carter, D., Ahmad, R., Costin, G.-E., Hearing, V. J., ... Cookson, M. R. (2005). Tyrosinase exacerbates dopamine toxicity but is not genetically associated with Parkinson's disease. *Journal of Neurochemistry*, 93(1), 246–256. <https://doi.org/10.1111/j.1471-4159.2005.03019.x>
- Grotemeyer, A., McFleder, R. L., Wu, J., Wischhusen, J., & Ip, C. W. (2022). Neuroinflammation in Parkinson's Disease – Putative Pathomechanisms and Targets for Disease-Modification. *Frontiers in Immunology*, 13, 2301. <https://doi.org/10.3389/FIMMU.2022.878771/BIBTEX>
- Grünblatt, E., Mandel, S., Jacob-Hirsch, J., Zeligson, S., Amariglio, N., Rechavi, G., ... Youdim, M. B. H. (2004). Gene expression profiling of parkinsonian substantia nigra pars compacta; alterations in ubiquitin-proteasome, heat shock protein, iron and oxidative stress regulated proteins, cell adhesion/cellular matrix and vesicle trafficking genes. *Journal of Neural Transmission*, 111(12), 1543–1573. <https://doi.org/10.1007/s00702-004-0212-1>
- Hallacli, E., Kayatekin, C., Nazeen, S., Wang, X. H., Sheinkopf, Z., Sathyakumar, S., ... Khurana, V. (2022). The Parkinson's disease protein alpha-synuclein is a modulator of processing bodies and mRNA stability. *Cell*, 185(12), 2035–2056.e33. <https://doi.org/10.1016/J.CELL.2022.05.008>
- Halliday, G. M., Fedorow, H., Rickert, C. H., Gerlach, M., Riederer, P., & Double, K. L. (2006). Evidence for specific phases in the development of human neuromelanin. *Journal of Neural Transmission*, 113(6), 721–728. <https://doi.org/10.1007/s00702-006-0449-y>
- Halliday, G. M., Li, Y. W., Blumbergs, P. C., Joh, T. H., Cotton, R. G. H., Howe, P. R. C., ... Geffen, L.

- B. (1990). Neuropathology of immunohistochemically identified brainstem neurons in Parkinson's disease. *Annals of Neurology*, 27(4), 373–385. <https://doi.org/10.1002/ana.410270405>
- Halliday, G. M., Li, Y. W., Joh, T. H., Cotton, R. G. H., Howe, P. R. C., Geffen, L. B., & Blessing, W. W. (1988). Distribution of monoamine-synthesizing neurons in the human medulla oblongata. *Journal of Comparative Neurology*, 273(3), 301–317. <https://doi.org/10.1002/CNE.902730303>
- Halliday, G. M., Ophof, A., Broe, M., Jensen, P. H., Kettle, E., Fedorow, H., ... Double, K. L. (2005). - Synuclein redistributes to neuromelanin lipid in the substantia nigra early in Parkinson's disease. *Brain*, 128(11), 2654–2664. <https://doi.org/10.1093/brain/awh584>
- Hare, D., Ayton, S., Bush, A., & Lei, P. (2013). A delicate balance: Iron metabolism and diseases of the brain. *Frontiers in Aging Neuroscience*, 5(JUL), 34. <https://doi.org/10.3389/FNAGI.2013.00034/BIBTEX>
- Hauser, M. A., Li, Y. J., Xu, H., Nouredine, M. A., Shao, Y. S., Gullans, S. R., ... Vance, J. M. (2005). Expression profiling of substantia nigra in Parkinson disease, progressive supranuclear palsy, and frontotemporal dementia with parkinsonism. *Archives of Neurology*, 62(6), 917–921. <https://doi.org/10.1001/ARCHNEUR.62.6.917>
- Hee, J. S., Mitchell, S. M., Liu, X., & Leonhardt, R. M. (2017). Melanosomal formation of PMEL core amyloid is driven by aromatic residues. *Scientific Reports 2017 7:1*, 7(1), 1–15. <https://doi.org/10.1038/srep44064>
- Heinzel, S., Berg, D., Gasser, T., Chen, H., Yao, C., & Postuma, R. B. (2019). Update of the MDS research criteria for prodromal Parkinson's disease. *Movement Disorders*, 34(10), 1464–1470. <https://doi.org/10.1002/MDS.27802>
- Henderson-Smith, A., Corneveaux, J. J., De, M., Cuyugan, L., Liang, W. S., Huentelman, M., ... Dunckley, T. L. (2016). Next-generation profiling to identify the molecular etiology of Parkinson dementia. *Neurol Genet*, 2, 75. <https://doi.org/10.1212/NXG.0000000000000075>
- Herrera, A., Muñ Oz, P., Steinbusch, H. W. M., & Segura-Aguilar, J. (2017). Are Dopamine Oxidation Metabolites Involved in the Loss of Dopaminergic Neurons in the Nigrostriatal System in Parkinson's Disease? <https://doi.org/10.1021/acschemneuro.7b00034>
- Higashi, Y., Asanuma, M., Miyazaki, I., & Ogawa, N. (2000). Inhibition of tyrosinase reduces cell viability in catecholaminergic neuronal cells. *Journal of Neurochemistry*, 75(4), 1771–1774. <https://doi.org/10.1046/J.1471-4159.2000.0751771.X>
- Hirsch, E. C., & Hunot, S. (2009). Neuroinflammation in Parkinson's disease: a target for neuroprotection? *The Lancet Neurology*, 8(4), 382–397. [https://doi.org/10.1016/S1474-4422\(09\)70062-6](https://doi.org/10.1016/S1474-4422(09)70062-6)
- Hirsch, E., Graybiel, A. M., & Agid, Y. A. (1988). Melanized dopaminergic neurons are differentially susceptible to degeneration in Parkinson's disease. *Nature*, 334(6180), 345–348. <https://doi.org/10.1038/334345a0>
- Ho, A. K., Ianssek, R., Marigliani, C., Bradshaw, J. L., & Gates, S. (1998). Speech impairment in a large sample of patients with Parkinson's disease. *Behavioural Neurology*, 11(3), 131–137. <https://doi.org/10.1155/1999/327643>
- Horsager, J., Andersen, K. B., Knudsen, K., Skjærbæk, C., Fedorova, T. D., Okkels, N., ... Borghammer, P. (2020). Brain-first versus body-first Parkinson's disease: a multimodal imaging case-control study. *Brain*, 143(10), 3077–3088. <https://doi.org/10.1093/BRAIN/AWAA238>
- Hsieh, C. L., Koike, M., Spusta, S. C., Niemi, E. C., Yenari, M., Nakamura, M. C., & Seaman, W. E. (2009). A Role for TREM2 Ligands in the Phagocytosis of Apoptotic Neuronal Cells by Microglia. *Journal of Neurochemistry*, 109(4), 1144. <https://doi.org/10.1111/J.1471-4159.2009.06042.X>
- Hu, B., Duan, S., Wang, Z., Li, X., Zhou, Y., Zhang, X., ... Zheng, H. (2021). Insights Into the Role of CSF1R in the Central Nervous System and Neurological Disorders. *Frontiers in Aging Neuroscience*, 13, 807. <https://doi.org/10.3389/FNAGI.2021.789834/BIBTEX>
- Huang, M., Modeste, E., Dammer, E., Merino, P., Taylor, G., Duong, D. M., ... Kukar, T. (2020).

- Network analysis of the progranulin-deficient mouse brain proteome reveals pathogenic mechanisms shared in human frontotemporal dementia caused by GRN mutations. *Acta Neuropathologica Communications*, 8(1), 163. <https://doi.org/10.1186/s40478-020-01037-x>
- Huang, W., Lv, Q., Xiao, Y., Zhong, Z., Hu, B., Yan, S., ... Lu, G. (2021). Triggering Receptor Expressed on Myeloid Cells 2 Protects Dopaminergic Neurons by Promoting Autophagy in the Inflammatory Pathogenesis of Parkinson's Disease. *Frontiers in Neuroscience*, 15. <https://doi.org/10.3389/FNINS.2021.745815>
- Hüttenrauch, M., Ogorek, I., Klafki, H., Otto, M., Stadelmann, C., Weggen, S., ... Wirths, O. (2018). Glycoprotein NMB: a novel Alzheimer's disease associated marker expressed in a subset of activated microglia. *Acta Neuropathologica Communications*, 6(1), 108. <https://doi.org/10.1186/s40478-018-0612-3>
- Huynh, B., Fu, Y., Kirik, D., Shine, J. M., & Halliday, G. M. (2021). Comparison of Locus Coeruleus Pathology with Nigral and Forebrain Pathology in Parkinson's Disease. *Movement Disorders*, 36(9), 2085–2093. <https://doi.org/10.1002/MDS.28615>
- Ikemoto, K., Nagatsu, I., Ito, S., King, R. A., Nishimura, A., & Nagatsu, T. (1998). Does tyrosinase exist in neuromelanin-pigmented neurons in the human substantia nigra? *Neuroscience Letters*, 253(3), 198–200. [https://doi.org/10.1016/S0304-3940\(98\)00649-1](https://doi.org/10.1016/S0304-3940(98)00649-1)
- Iranzo, A., Tolosa, E., Gelpi, E., Molinuevo, J. L., Valldeoriola, F., Serradell, M., ... Santamaria, J. (2013). Neurodegenerative disease status and post-mortem pathology in idiopathic rapid-eye-movement sleep behaviour disorder: An observational cohort study. *The Lancet Neurology*, 12(5), 443–453. [https://doi.org/10.1016/S1474-4422\(13\)70056-5](https://doi.org/10.1016/S1474-4422(13)70056-5)
- Irizarry, R. A., Hobbs, B., Collin, F., Beazer-Barclay, Y. D., Antonellis, K. J., Scherf, U., & Speed, T. P. (2003). Exploration, normalization, and summaries of high density oligonucleotide array probe level data. *Biostatistics (Oxford, England)*, 4(2), 249–264. <https://doi.org/10.1093/biostatistics/4.2.249>
- Ishikawa, A. (1998). Clinical and neuropathological aspects of autosomal recessive juvenile parkinsonism. *Journal of Neurology, Supplement*, 245(3). <https://doi.org/10.1007/PL00007745>
- Ito, S., & Wakamatsu, K. (2008). Chemistry of Mixed Melanogenesis—Pivotal Roles of Dopaquinone†. *Photochemistry and Photobiology*, 84(3), 582–592. <https://doi.org/10.1111/J.1751-1097.2007.00238.X>
- Itzev, D. E., Ovtscharoff, W. A., Marani, E., & Usunoff, K. G. (2002). Neuromelanin-containing, catecholaminergic neurons in the human brain: Ontogenetic aspects, development and aging. *Biomedical Reviews*, 13, 39–47. <https://doi.org/10.14748/BMR.V13.116>
- Jellinger, K. A. (2003a). Neuropathological spectrum of synucleinopathies. *Movement Disorders*, 18(SUPPL. 6). <https://doi.org/10.1002/MDS.10557>
- Jellinger, K. A. (2003b). α -Synuclein pathology in Parkinson's and Alzheimer's disease brain: incidence and topographic distribution—a pilot study. *Acta Neuropathologica* 2003 106:3, 106(3), 191–202. <https://doi.org/10.1007/S00401-003-0725-Y>
- Jellinger, K., Kienzl, E., Rumpelmair, G., Riederer, P., Stachelberger, H., Ben-Shachar, D., & Youdim, M. B. H. (1992). Iron-Melanin Complex in Substantia Nigra of Parkinsonian Brains: An X-Ray Microanalysis. *Journal of Neurochemistry*, 59(3), 1168–1171. <https://doi.org/10.1111/J.1471-4159.1992.TB08362.X>
- Kaiser, S., Zhang, L., Mollenhauer, B., Jacob, J., Longerich, S., Del-Aguila, J., ... Serrano-Fernandez, P. (2022). Parkinson's disease causality and heterogeneity: a proteogenomic view. *medRxiv*, 2022.03.09.22272131. <https://doi.org/10.1101/2022.03.09.22272131>
- Kalaitzakis, M. E., Graeber, M. B., Gentleman, S. M., & Pearce, R. K. B. (2008). The dorsal motor nucleus of the vagus is not an obligatory trigger site of Parkinson's disease: a critical analysis of alpha-synuclein staging. *Neuropathology and Applied Neurobiology*, 34(3), 284–295. <https://doi.org/10.1111/J.1365-2990.2007.00923.X>
- Kamath, T., Abdulraouf, A., Burris, S. J., Langlieb, J., Gazestani, V., Nadaf, N. M., ... Macosko, E. Z.

- (2022). Single-cell genomic profiling of human dopamine neurons identifies a population that selectively degenerates in Parkinson's disease. *Nature Neuroscience* 2022 25:5, 25(5), 588–595. <https://doi.org/10.1038/s41593-022-01061-1>
- Kastner, A., Hirsch, E. C., Lejeune, O., Javoy-Agid, F., Rascol, O., & Agid, Y. (1992). Is the Vulnerability of Neurons in the Substantia Nigra of Patients with Parkinson's Disease Related to Their Neuromelanin Content? *Journal of Neurochemistry*, 59(3), 1080–1089. <https://doi.org/10.1111/j.1471-4159.1992.tb08350.x>
- Keo, A., Mahfouz, A., Ingrassia, A. M. T., Meneboo, J. P., Villenet, C., Mutez, E., ... Reinders, M. J. T. (2020). Transcriptomic signatures of brain regional vulnerability to Parkinson's disease. *Communications Biology* 2020 3:1, 3(1), 1–12. <https://doi.org/10.1038/s42003-020-0804-9>
- Keren-Shaul, H., Spinrad, A., Weiner, A., Matcovitch-Natan, O., Dvir-Szternfeld, R., Ulland, T. K., ... Amit, I. (2017). A Unique Microglia Type Associated with Restricting Development of Alzheimer's Disease. *Cell*, 169(7), 1276–1290.e17. <https://doi.org/10.1016/J.CELL.2017.05.018/ATTACHMENT/63D76284-8C53-4D00-93AA-E1E70B1AE6DE/MMC7.XLSX>
- Kim, W., Lee, Y., McKenna, N. D., Yi, M., Simunovic, F., Wang, Y., ... Sonntag, K. C. (2014). miR-126 contributes to Parkinson disease by dysregulating IGF-1/PI3K signaling: miRNAs and IGF-1 signaling in Parkinson disease. *Neurobiology of Aging*, 35(7), 1712. <https://doi.org/10.1016/J.NEUROBIOLAGING.2014.01.021>
- Kinugawa, K., Monnet, Y., Béchade, C., Alvarez-Fischer, D., Hirsch, E. C., Bessis, A., & Hunot, S. (2013). DAPI2 and CD11b contribute to the microglial-induced death of dopaminergic neurons in vitro but not in vivo in the MPTP mouse model of Parkinson's disease. *Journal of Neuroinflammation*, 10. <https://doi.org/10.1186/1742-2094-10-82>
- Klingelhoefer, L., & Reichmann, H. (2017). Parkinson's disease as a multisystem disorder. *Journal of Neural Transmission* 2017 124:6, 124(6), 709–713. <https://doi.org/10.1007/S00702-017-1692-0>
- Knudsen, K., Fedorova, T. D., Hansen, A. K., Sommerauer, M., Otto, M., Svendsen, K. B., ... Borghammer, P. (2018). In-vivo staging of pathology in REM sleep behaviour disorder: a multimodality imaging case-control study. *The Lancet. Neurology*, 17(7), 618–628. [https://doi.org/10.1016/S1474-4422\(18\)30162-5](https://doi.org/10.1016/S1474-4422(18)30162-5)
- König, M., Berlin, B., Schwab, K., Frahm, S., Theuring, F., Wischik, C. M., ... Klein, J. (2019). Increased Cholinergic Response in α -Synuclein Transgenic Mice (h- α -synL62). *ACS Chemical Neuroscience*, 10(4), 1915–1922. https://doi.org/10.1021/ACSCHMNEURO.8B00274/ASSET/IMAGES/MEDIUM/CN-2018-00274C_0006.GIF
- Konishi, H., & Kiyama, H. (2020). Non-pathological roles of microglial TREM2/DAP12: TREM2/DAP12 regulates the physiological functions of microglia from development to aging. *Neurochemistry International*, 141, 104878. <https://doi.org/10.1016/J.NEUINT.2020.104878>
- Konno, T., Kasanuki, K., Ikeuchi, T., Dickson, D. W., & Wszolek, Z. K. (2018). CSF1R-related leukoencephalopathy: A major player in primary microgliopathies. *Neurology*, 91(24), 1092. <https://doi.org/10.1212/WNL.0000000000006642>
- Konnova, E. A., & Swanberg, M. (2018). Animal Models of Parkinson's Disease. *Exon Publications*, 83–106. <https://doi.org/10.15586/CODONPUBLICATIONS.PARKINSONSDISEASE.2018.CH5>
- Kordower, J. H., Olanow, C. W., Dodiya, H. B., Chu, Y., Beach, T. G., Adler, C. H., ... Bartus, R. T. (2013). Disease duration and the integrity of the nigrostriatal system in Parkinson's disease. *Brain : A Journal of Neurology*, 136(Pt 8), 2419–2431. <https://doi.org/10.1093/brain/awt192>
- Korzhevskii, D. E., Kirik, O. V., Guselnikova, V. V., Tsyba, D. L., Fedorova, E. A., & Grigorev, I. P. (2021). Changes in cytoplasmic and extracellular neuromelanin in human substantia nigra with normal aging. *European Journal of Histochemistry : EJH*, 65(Suppl 1), 3283. <https://doi.org/10.4081/EJH.2021.3283>
- Kowall, N. W., Hantraye, P., Brouillet, E., Beal, M. F., McKee, A. C., & Ferrante, R. J. (2000). MPTP induces alpha-synuclein aggregation in the substantia nigra of baboons. *NeuroReport*, 11(1), 211–

213. <https://doi.org/10.1097/00001756-200001170-00041>

- Kumar, N., Rizek, P., & Jog, M. (2016). Neuroferritinopathy: Pathophysiology, Presentation, Differential Diagnoses and Management. *Tremor and Other Hyperkinetic Movements*, 6(0), 355. <https://doi.org/10.5334/TOHM.317>
- Kumar, R., Oliver, C., Brun, C., Juarez-Martinez, A. B., Tarabay, Y., Kadlec, J., & De Massy, B. (2018). Mouse REC114 is essential for meiotic DNA double-strand break formation and forms a complex with MEI4. *Life Science Alliance*, 1(6). <https://doi.org/10.26508/LSA.201800259>
- Kumar, T. R., Larson, M., Wang, H., McDermott, J., & Bronshteyn, I. (2009). Transgenic mouse technology: principles and methods. *Methods in Molecular Biology (Clifton, N.J.)*, 590, 335–362. https://doi.org/10.1007/978-1-60327-378-7_22
- Kumaran, R., & Cookson, M. R. (2015). Pathways to Parkinsonism Redux: convergent pathobiological mechanisms in genetics of Parkinson's disease. *Human Molecular Genetics*, 24(R1), R32. <https://doi.org/10.1093/HMG/DDV236>
- Kuusisto, E., Parkkinen, L., & Alafuzoff, I. (2003a). Morphogenesis of Lewy bodies: dissimilar incorporation of alpha-synuclein, ubiquitin, and p62. *Journal of Neuropathology and Experimental Neurology*, 62(12), 1241–1253. <https://doi.org/10.1093/JNEN/62.12.1241>
- Kuusisto, E., Parkkinen, L., & Alafuzoff, I. (2003b). Morphogenesis of Lewy Bodies: Dissimilar Incorporation of-Synuclein, Ubiquitin, and p62. *Journal of Neuropathology and Experimental Neurology*, 62(12). Retrieved from <https://academic.oup.com/jnen/article/62/12/1241/2610054>
- Langston, J. W., Forno, L. S., Tetrud, J., Reeves, A. G., Kaplan, J. A., & Karluk, D. (1999). Evidence of active nerve cell degeneration in the substantia nigra of humans years after 1-methyl-4-phenyl-1,2,3,6-tetrahydropyridine exposure. *Annals of Neurology*, 46(4), 598–605. Retrieved from <http://www.ncbi.nlm.nih.gov/pubmed/10514096>
- Le Fur, N., Kelsall, S. R., Silvers, W. K., & Mintz, B. (1997). Selective increase in specific alternative splice variants of tyrosinase in murine melanomas: A projected basis for immunotherapy. *Proceedings of the National Academy of Sciences of the United States of America*, 94(10), 5332–5337. <https://doi.org/10.1073/PNAS.94.10.5332/ASSET/C0AEDC98-CCBE-4BC9-BCF3-E0A15766EB0D/ASSETS/GRAPHIC/PQ1070863003.JPEG>
- Lemos-Amado, F., Domingues, P., Ferrer-Correia, A., Remião, F., Milhazes, N., Borges, F., ... Bastos, M. L. (2001). Electrospray tandem mass spectrometry of aminochromes. *Rapid Communications in Mass Spectrometry*, 15(24), 2466–2471. <https://doi.org/10.1002/rcm.498>
- Lester, D. B., Rogers, T. D., & Blaha, C. D. (2010). Acetylcholine–Dopamine Interactions in the Pathophysiology and Treatment of CNS Disorders. *CNS Neuroscience & Therapeutics*, 16(3), 137. <https://doi.org/10.1111/J.1755-5949.2010.00142.X>
- Li, B., Castano, A. P., Hudson, T. E., Nowlin, B. T., Lin, S.-L., Bonventre, J. V., ... Duffield, J. S. (2010). The melanoma-associated transmembrane glycoprotein Gpnmb controls trafficking of cellular debris for degradation and is essential for tissue repair. *The FASEB Journal*, 24(12), 4767–4781. <https://doi.org/10.1096/FJ.10-154757>
- Liddelw, S. A., Guttenplan, K. A., Clarke, L. E., Bennett, F. C., Bohlen, C. J., Schirmer, L., ... Barres, B. A. (2017). Neurotoxic reactive astrocytes are induced by activated microglia. *Nature*, 541(7638), 481. <https://doi.org/10.1038/NATURE21029>
- Lillie, R. D. (1957). Metal reduction reaction of the melanins: histochemical studies. <http://dx.doi.org/10.1177/5.4.325>, 5(4), 325–333. <https://doi.org/10.1177/5.4.325>
- Liu, G. N., Shi, H. Z., Xie, Z. H., Shen, H. H., Huang, H. Q., Deng, J. M., ... Wu, Y. B. (2009). Epithelial neutrophil-activating peptide-78 recruits neutrophils into pleural effusion. *European Respiratory Journal*, 34(1), 184–190. <https://doi.org/10.1183/09031936.00111908>
- Liu, J., Wu, Q., Shi, J., Guo, W., Jiang, X., Zhou, B., & Ren, C. (2020). LILRB4, from the immune system to the disease target. *Am J Transl Res*, 12(7), 3149–3166. Retrieved from www.ajtr.org
- Liu, Z. hua, Guo, J. feng, Li, K., Wang, Y. qin, Kang, J. feng, Wei, Y., ... Tang, B. sha. (2015). Analysis

- of several loci from genome-wide association studies in Parkinson's disease in mainland China. *Neuroscience Letters*, 587, 68–71. <https://doi.org/10.1016/j.neulet.2014.12.027>
- Loftus, S. K., Antonellis, A., Matera, I., Renaud, G., Baxter, L. L., Reid, D., ... Pavan, W. J. (2009). Gpnmb is a Melanoblast-Expressed, MITF-Dependent Gene. *Pigment Cell & Melanoma Research*, 22(1), 99. <https://doi.org/10.1111/J.1755-148X.2008.00518.X>
- Louis, E. D., & Bennett, D. A. (2007). Mild Parkinsonian signs: An overview of an emerging concept. *Movement Disorders*, 22(12), 1681–1688. <https://doi.org/10.1002/MDS.21433>
- Lubbe, S. J., Escott-Price, V., Brice, A., Gasser, T., Pittman, A. M., Bras, J., ... International Parkinson's Disease Genomics Consortium. (2016). Rare variants analysis of cutaneous malignant melanoma genes in Parkinson's disease. *Neurobiology of Aging*, 48, 222.e1-222.e7. <https://doi.org/10.1016/j.neurobiolaging.2016.07.013>
- Luk, K. C., Kehm, V., Carroll, J., Zhang, B., O'Brien, P., Trojanowski, J. Q., & Lee, V. M. Y. (2012). Pathological α -synuclein transmission initiates Parkinson-like neurodegeneration in nontransgenic mice. *Science (New York, N.Y.)*, 338(6109), 949–953. <https://doi.org/10.1126/SCIENCE.1227157>
- Ma, S. Y., R oytt a, M., Collan, Y., & Rinne, J. O. (1999). Unbiased morphometrical measurements show loss of pigmented nigral neurones with ageing. *Neuropathology and Applied Neurobiology*, 25(5), 394–399. <https://doi.org/10.1046/J.1365-2990.1999.00202.X>
- Mai, J. K., & Paxinos, G. (2012). The Human Nervous System. *The Human Nervous System*. <https://doi.org/10.1016/C2009-0-02721-4>
- Majumder, P., Choudhury, A., Banerjee, M., Lahiri, A., & Bhattacharyya, N. P. (2007). Interactions of HIPPI, a molecular partner of Huntingtin interacting protein HIP1, with the specific motif present at the putative promoter sequence of the caspase-1, caspase-8 and caspase-10 genes. *The FEBS Journal*, 274(15), 3886–3899. <https://doi.org/10.1111/J.1742-4658.2007.05922.X>
- Manaye, K. F., McIntire, D. D., Mann, D. M. A., & German, D. C. (1995). Locus coeruleus cell loss in the aging human brain: A non-random process. *Journal of Comparative Neurology*, 358(1), 79–87. <https://doi.org/10.1002/CNE.903580105>
- Manivasagam, S., Williams, J. L., Vollmer, L. L., Bollman, B., Bartleson, J. M., Ai, S., ... Klein, R. S. (2022). Targeting IFN- λ Signaling Promotes Recovery from Central Nervous System Autoimmunity. *Journal of Immunology (Baltimore, Md. : 1950)*, 208(6), 1341–1351. <https://doi.org/10.4049/JIMMUNOL.2101041>
- Mann, D. M. A., & Yates, P. O. (1974). Lipoprotein pigments-their relationship to ageing in the human nervous system: II. The melanin content of pigmented nerve cells. *Brain*, 97(1), 489–498. <https://doi.org/10.1093/BRAIN/97.1.489>
- Mann, D. M. A., & Yates, P. O. (1979). The effects of ageing on the pigmented nerve cells of the human locus caeruleus and substantia nigra. *Acta Neuropathologica*, 47(2), 93–97. <https://doi.org/10.1007/BF00717030>
- Mann, D. M. A., & Yates, P. O. (1983). Possible role of neuromelanin in the pathogenesis of Parkinson's disease. *Mechanisms of Ageing and Development*, 21(2), 193–203. [https://doi.org/10.1016/0047-6374\(83\)90074-X](https://doi.org/10.1016/0047-6374(83)90074-X)
- Mari, M., Tooze, S. A., & Reggiori, F. (2011). The puzzling origin of the autophagosomal membrane. *FL1000 Biology Reports*, 3(1). <https://doi.org/10.3410/B3-25>
- Mariani, E., Frabetti, F., Tarozzi, A., Pelleri, M. C., Pizzetti, F., & Casadei, R. (2016). Meta-Analysis of Parkinson's Disease Transcriptome Data Using TRAM Software: Whole Substantia Nigra Tissue and Single Dopamine Neuron Differential Gene Expression. *PLOS ONE*, 11(9), e0161567. <https://doi.org/10.1371/journal.pone.0161567>
- Marsden, C. D. (1961). Pigmentation in the nucleus substantiae nigrae of mammals. *Journal of Anatomy*, 95(Pt 2), 256–261. Retrieved from <http://www.ncbi.nlm.nih.gov/pubmed/13767161>
- Mart n-Gallego, A., Andrade-Andrade, I., Dawid-Milner, M. S., Dom nguez-P ez, M., Romero-Moreno, L., Gonz lez-Garc a, L., ... Arr ez-S nchez, M. A. (2016). Autonomic dysfunction elicited by a

- medulla oblongata injury after fourth ventricle tumor surgery in a pediatric patient. *Autonomic Neuroscience: Basic and Clinical*, 194, 52–57. <https://doi.org/10.1016/J.AUTNEU.2015.12.002>
- Matsumoto, H., Sengoku, R., Saito, Y., Kakuta, Y., Murayama, S., & Imafuku, I. (2014). Sudden death in Parkinson's disease: A retrospective autopsy study. *Journal of the Neurological Sciences*, 343(1–2), 149–152. <https://doi.org/10.1016/J.JNS.2014.05.060>
- Matsushita, N., Okada, H., Yasoshima, Y., Takahashi, K., Kiuchi, K., & Kobayashi, K. (2002). Dynamics of tyrosine hydroxylase promoter activity during midbrain dopaminergic neuron development. *Journal of Neurochemistry*, 82(2), 295–304. Retrieved from <http://www.ncbi.nlm.nih.gov/pubmed/12124430>
- McCall, J. G., Siuda, E. R., Bhatti, D. L., Lawson, L. A., McElligott, Z. A., Stuber, G. D., & Bruchas, M. R. (2017). Locus coeruleus to basolateral amygdala noradrenergic projections promote anxiety-like behavior. *eLife*, 6. <https://doi.org/10.7554/ELIFE.18247>
- McDevitt, R. A., Tiran-Cappello, A., Shen, H., Balderas, I., Britt, J. P., Marino, R. A. M., ... Bonci, A. (2014). Serotonergic versus Nonserotonergic Dorsal Raphe Projection Neurons: Differential Participation in Reward Circuitry. *Cell Reports*, 8(6), 1857–1869. <https://doi.org/10.1016/J.CELREP.2014.08.037>
- McGeer, P. L., Itagaki, S., Boyes, B. E., & McGeer, E. G. (1988). Reactive microglia are positive for HLA-DR in the substantia nigra of Parkinson's and Alzheimer's disease brains. *Neurology*, 38(8), 1285–1285. <https://doi.org/10.1212/WNL.38.8.1285>
- McGeer, P. L., McGeer, E. G., & Suzuki, J. S. (1977). Aging and Extrapyramidal Function. *Archives of Neurology*, 34(1), 33–35. <https://doi.org/10.1001/ARCHNEUR.1977.00500130053010>
- McKeith, I. G., Dickson, D. W., Lowe, J., Emre, M., O'Brien, J. T., Feldman, H., ... Yamada, M. (2005). Diagnosis and management of dementia with Lewy bodies: Third report of the DLB consortium. *Neurology*, 65(12), 1863–1872. <https://doi.org/10.1212/01.WNL.0000187889.17253.B1>
- McKinley, J. W., Shi, Z., Kawikova, I., Hur, M., Bamford, I. J., Sudarsana Devi, S. P., ... Bamford, N. S. (2019). Dopamine Deficiency Reduces Striatal Cholinergic Interneuron Function in Models of Parkinson's Disease. *Neuron*, 103(6), 1056–1072.e6. <https://doi.org/10.1016/J.NEURON.2019.06.013/ATTACHMENT/DAEC4344-2522-41C2-8042-26F7FA37DD2B/MMC1.PDF>
- McRitchie, D. A., Cartwright, H. R., & Halliday, G. M. (1997). Specific A10 Dopaminergic Nuclei in the Midbrain Degenerate in Parkinson's Disease. *Experimental Neurology*, 144(1), 202–213. <https://doi.org/10.1006/exnr.1997.6418>
- Mena-Segovia, J., & Bolam, J. P. (2017). Rethinking the Pedunculo-pontine Nucleus: From Cellular Organization to Function. *Neuron*, 94(1), 7–18. <https://doi.org/10.1016/J.NEURON.2017.02.027>
- Michael Spyer, K., & Gourine, A. V. (2009). Chemosensory pathways in the brainstem controlling cardiorespiratory activity. *Philosophical Transactions of the Royal Society B: Biological Sciences*, 364(1529), 2603–2610. <https://doi.org/10.1098/RSTB.2009.0082>
- Miklossy, J., Doudet, D. D., Schwab, C., Yu, S., McGeer, E. G., & McGeer, P. L. (2006). Role of ICAM-1 in persisting inflammation in Parkinson disease and MPTP monkeys. *Experimental Neurology*, 197(2), 275–283. <https://doi.org/10.1016/J.EXPNEUROL.2005.10.034>
- Milber, J. M., Noorigian, J. V., Morley, J. F., Petrovitch, H., White, L., Ross, G. W., & Duda, J. E. (2012). Lewy pathology is not the first sign of degeneration in vulnerable neurons in Parkinson disease. *Neurology*, 79(24), 2307. <https://doi.org/10.1212/WNL.0B013E318278FE32>
- Miquel-Rio, L., Alarcón-Arís, D., Torres-López, M., Còppola-Segovia, V., Pavia-Collado, R., Paz, V., ... Bortolozzi, A. (2022). Human α -synuclein overexpression in mouse serotonin neurons triggers a depressive-like phenotype. Rescue by oligonucleotide therapy. *Translational Psychiatry*, 12(1). <https://doi.org/10.1038/S41398-022-01842-Z>
- Miranda, M., Botti, D., Bonfigli, A., Ventura, T., & Arcadi, A. (1984). Tyrosinase-like activity in normal human substantia nigra. *General Pharmacology*, 15(6), 541–544. Retrieved from <http://www.ncbi.nlm.nih.gov/pubmed/6441736>

- Mirza, B., Hadberg, H., Thomsen, P., & Moos, T. (1999). The absence of reactive astrocytosis is indicative of a unique inflammatory process in Parkinson's disease. *Neuroscience*, *95*(2), 425–432. [https://doi.org/10.1016/S0306-4522\(99\)00455-8](https://doi.org/10.1016/S0306-4522(99)00455-8)
- Miyazaki, I., Asanuma, M., Diaz-Corrales, F. J., Fukuda, M., Kitaichi, K., Miyoshi, K., & Ogawa, N. (2006). Methamphetamine-induced dopaminergic neurotoxicity is regulated by quinone formation-related molecules. *The FASEB Journal*, *20*(3), 571–573. <https://doi.org/10.1096/FJ.05-4996FJE>
- Moloney, E. B., Moskites, A., Ferrari, E. J., Isacson, O., & Hallett, P. J. (2018). The glycoprotein GPNMB is selectively elevated in the substantia nigra of Parkinson's disease patients and increases after lysosomal stress. *Neurobiology of Disease*, *120*, 1–11. <https://doi.org/10.1016/j.nbd.2018.08.013>
- Moncrieff, J., Cooper, R. E., Stockmann, T., Amendola, S., Hengartner, M. P., & Horowitz, M. A. (2022). The serotonin theory of depression: a systematic umbrella review of the evidence. *Molecular Psychiatry* *2022*, 1–14. <https://doi.org/10.1038/s41380-022-01661-0>
- Mootha, V. K., Lindgren, C. M., Eriksson, K. F., Subramanian, A., Sihag, S., Lehar, J., ... Groop, L. C. (2003). PGC-1 α -responsive genes involved in oxidative phosphorylation are coordinately downregulated in human diabetes. *Nature Genetics* *2003 34:3*, *34*(3), 267–273. <https://doi.org/10.1038/ng1180>
- Moran, L. B., Duke, D. C., Deprez, M., Dexter, D. T., Pearce, R. K. B., & Graeber, M. B. (2006). Whole genome expression profiling of the medial and lateral substantia nigra in Parkinson's disease. *Neurogenetics*, *7*(1), 1–11. <https://doi.org/10.1007/s10048-005-0020-2>
- Moreno-Mateos, M. A., Espina, Á. G., Torres, B., Gámez Del Estal, M. M., Romero-Franco, A., Ríos, R. M., & Pintor-Toro, J. A. (2011). PTTG1/securin modulates microtubule nucleation and cell migration. *Molecular Biology of the Cell*, *22*(22), 4302–4311. <https://doi.org/10.1091/MBC.E10-10-0838/ASSET/IMAGES/LARGE/4302FIG10.JPEG>
- Moret, C., & Briley, M. (2011). The importance of norepinephrine in depression. *Neuropsychiatric Disease and Treatment*, *7*(Suppl 1), 9. <https://doi.org/10.2147/NDT.S19619>
- Morrison, J. H., & Hof, P. R. (1997). Life and Death of Neurons in the Aging Brain. *Science*, *278*(5337), 412–419. <https://doi.org/10.1126/SCIENCE.278.5337.412>
- Mouton-Liger, F., Rosazza, T., Sepulveda-Diaz, J., Jeang, A., Hassoun, S. M., Claire, E., ... Corti, O. (2018). Parkin deficiency modulates NLRP3 inflammasome activation by attenuating an A20-dependent negative feedback loop. *Glia*, *66*(8), 1736–1751. <https://doi.org/10.1002/GLIA.23337>
- Müller, G., Ruppert, S., Schmid, E., & Schütz, G. (1988). Functional analysis of alternatively spliced tyrosinase gene transcripts. *The EMBO Journal*, *7*(9), 2723–2730. <https://doi.org/10.1002/J.1460-2075.1988.TB03126.X>
- Murakami, K., Wakamatsu, K., Nakanishi, Y., Takahashi, H., Sugiyama, S., & Ito, S. (2008). Serum levels of pigmentation markers are elevated in patients undergoing hemodialysis. *Blood Purification*, *25*(5–6), 483–489. <https://doi.org/10.1159/000112516>
- Murer, M. G., Dziewczapolski, G., Menalled, L. B., García, M. C., Agid, Y., Gershanik, O., & Raisman-Vozari, R. (1998). Chronic levodopa is not toxic for remaining dopamine neurons, but instead promotes their recovery, in rats with moderate nigrostriatal lesions. *Annals of Neurology*, *43*(5), 561–575. <https://doi.org/10.1002/ana.410430504>
- Murthy, M. N., Blauwendraat, C., Guelfi, S., Hardy, J., Lewis, P. A., & Trabzuni, D. (2017). Increased brain expression of GPNMB is associated with genome wide significant risk for Parkinson's disease on chromosome 7p15.3. *Neurogenetics*, *18*(3), 121–133. <https://doi.org/10.1007/s10048-017-0514-8>
- Mutch, W. J., Calder, S. A., Crawford, J. R., Stewart, L., & Besson, J. A. O. (1990). Mortality and causes of death in idiopathic Parkinson's disease: results from the Aberdeen whole population study. *Scottish Medical Journal*, *35*(6), 173–175. <https://doi.org/10.1177/003693309003500605>
- Myall, D. J., Pitcher, T. L., Pearson, J. F., Dalrymple-Alford, J. C., Anderson, T. J., & Macaskill, M. R. (2017). Parkinson's in the oldest old: Impact on estimates of future disease burden.

- Nagatsu, T., Nakashima, A., Ichinose, H., & Kobayashi, K. (2019). Human tyrosine hydroxylase in Parkinson's disease and in related disorders. *Journal of Neural Transmission*, 126(4), 397–409. <https://doi.org/10.1007/S00702-018-1903-3>
- Nakano, Y., Suzuki, Y., Takagi, T., Kitashoji, A., Ono, Y., Tsuruma, K., ... Hara, H. (2014). Glycoprotein nonmetastatic melanoma protein B (GPNMB) as a novel neuroprotective factor in cerebral ischemia-reperfusion injury. *Neuroscience*, 277, 123–131. <https://doi.org/10.1016/j.neuroscience.2014.06.065>
- Nalls, M. A., Pankratz, N., Lill, C. M., Do, C. B., Hernandez, D. G., Saad, M., ... Singleton, A. B. (2014). Large-scale meta-analysis of genome-wide association data identifies six new risk loci for Parkinson's disease. *Nature Genetics*, 46(9), 989. <https://doi.org/10.1038/NG.3043>
- Navarro-Romero, A., Fernandez-Gonzalez, I., Riera, J., Montpeyo, M., Albert-Bayo, M., Lopez-Royo, T., ... Martinez-Vicente, M. (2022). Lysosomal lipid alterations caused by glucocerebrosidase deficiency promote lysosomal dysfunction, chaperone-mediated-autophagy deficiency, and alpha-synuclein pathology. *Npj Parkinson's Disease* 2022 8:1, 8(1), 1–15. <https://doi.org/10.1038/s41531-022-00397-6>
- Nguyen, B., Bix, G., & Yao, Y. (2021). Basal lamina changes in neurodegenerative disorders. *Molecular Neurodegeneration*, 16(1), 1–25. <https://doi.org/10.1186/S13024-021-00502-Y/TABLES/5>
- Nowsheen, S., Aziz, K., Luo, K., Deng, M., Qin, B., Yuan, J., ... Lou, Z. (2018). ZNF506-dependent positive feedback loop regulates H2AX signaling after DNA damage. *Nature Communications* 2018 9:1, 9(1), 1–11. <https://doi.org/10.1038/s41467-018-05161-0>
- Obeso, J. A., Stamelou, M., Goetz, C. G., Poewe, W., Lang, A. E., Weintraub, D., ... Stoessl, A. J. (2017). Past, Present, and Future of Parkinson's Disease: A Special Essay on the 200th Anniversary of the Shaking Palsy. *Movement Disorders : Official Journal of the Movement Disorder Society*, 32(9), 1264. <https://doi.org/10.1002/MDS.27115>
- Odh, G., Carstam, R., Paulson, J., Wittbjør, A., Rosengren, E., & Rorsman, H. (1994). Neuromelanin of the Human Substantia Nigra: A Mixed-Type Melanin. *Journal of Neurochemistry*, 62(5), 2030–2036. <https://doi.org/10.1046/J.1471-4159.1994.62052030.X>
- Oeckl, P., Weydt, P., Thal, D. R., Weishaupt, J. H., Ludolph, A. C., & Otto, M. (2020). Proteomics in cerebrospinal fluid and spinal cord suggests UCHL1, MAP2 and GPNMB as biomarkers and underpins importance of transcriptional pathways in amyotrophic lateral sclerosis. *Acta Neuropathologica*, 139(1), 119–134. <https://doi.org/10.1007/s00401-019-02093-x>
- Ohm, D. T., Peterson, C., Lobrovich, R., Cousins, K. A. Q., Gibbons, G. S., McMillan, C. T., ... Irwin, D. J. (2020). Degeneration of the locus coeruleus is a common feature of tauopathies and distinct from TDP-43 proteinopathies in the frontotemporal lobar degeneration spectrum. *Acta Neuropathologica*, 140(5), 675. <https://doi.org/10.1007/S00401-020-02210-1>
- Okunoye, O., Marston, L., Walters, K., & Schrag, A. (2022). Change in the incidence of Parkinson's disease in a large UK primary care database. *Npj Parkinson's Disease* 2022 8:1, 8(1), 1–7. <https://doi.org/10.1038/s41531-022-00284-0>
- Olanow, C. W., Kieburtz, K., & Katz, R. (2017). Clinical approaches to the development of a neuroprotective therapy for PD. *Experimental Neurology*, 298, 246–251. <https://doi.org/10.1016/J.EXPNEUROL.2017.06.018>
- Olanow, C. W., Kieburtz, K., & Schapira, A. H. V. (2008). Why have we failed to achieve neuroprotection in Parkinson's disease? *Annals of Neurology*, 64(SUPPL. 2). <https://doi.org/10.1002/ANA.21461>
- Oliveras-Salvá, M., Van Der Perren, A., Casadei, N., Stroobants, S., Nuber, S., D'Hooge, R., ... Baekelandt, V. (2013). RAAV2/7 vector-mediated overexpression of alpha-synuclein in mouse substantia nigra induces protein aggregation and progressive dose-dependent neurodegeneration. *Molecular Neurodegeneration*, 8(1), 1–14. <https://doi.org/10.1186/1750-1326-8-44/FIGURES/6>
- Orr, C. F., Rowe, D. B., Mizuno, Y., Mori, H., & Halliday, G. M. (2005). A possible role for humoral

- immunity in the pathogenesis of Parkinson's disease. *Brain*, 128(11), 2665–2674.
<https://doi.org/10.1093/BRAIN/AWH625>
- Ou, Z., Pan, J., Tang, S., Duan, D., Yu, D., Nong, H., & Wang, Z. (2021). Global Trends in the Incidence, Prevalence, and Years Lived With Disability of Parkinson's Disease in 204 Countries/Territories From 1990 to 2019. *Frontiers in Public Health*, 9, 1994.
<https://doi.org/10.3389/FPUH.2021.776847/BIBTEX>
- Ouchi, Y., Yoshikawa, E., Sekine, Y., Futatsubashi, M., Kanno, T., Ogusu, T., & Torizuka, T. (2005). Microglial activation and dopamine terminal loss in early Parkinson's disease. *Annals of Neurology*, 57(2), 168–175. <https://doi.org/10.1002/ANA.20338>
- Pahapill, P. A., & Lozano, A. M. (2000). The pedunculopontine nucleus and Parkinson's disease. *Brain : A Journal of Neurology*, 123 (Pt 9)(9), 1767–1783. <https://doi.org/10.1093/BRAIN/123.9.1767>
- Parent, M., & Parent, A. (2010). Substantia nigra and Parkinson's disease: A brief history of their long and intimate relationship. *Canadian Journal of Neurological Sciences*, 37(3), 313–319.
<https://doi.org/10.1017/S0317167100010209>
- Parkinson, J. (1817). "An Essay on the Shaking Palsy." *Sherwood, Neely, & Jones, London*.
- Parkkinen, L., Kauppinen, T., Pirttilä, T., Autere, J. M., & Alafuzoff, I. (2005). α -Synuclein pathology does not predict extrapyramidal symptoms or dementia. *Annals of Neurology*, 57(1), 82–91.
<https://doi.org/10.1002/ANA.20321>
- Parkkinen, L., O'Sullivan, S. S., Collins, C., Petrie, A., Holton, J. L., Revesz, T., & Lees, A. J. (2011). Disentangling the relationship between lewy bodies and nigral neuronal loss in Parkinson's disease. *Journal of Parkinson's Disease*, 1(3), 277–286. <https://doi.org/10.3233/JPD-2011-11046>
- Pattyn, A., Goridis, C., & Brunet, J.-F. (2000). Specification of the Central Noradrenergic Phenotype by the Homeobox Gene Phox2b. <https://doi.org/10.1006/mcne.1999.0826>
- Paumier, K. L., Luk, K. C., Manfredsson, F. P., Kanaan, N. M., Lipton, J. W., Collier, T. J., ... Sortwell, C. E. (2015). Intrastratial injection of pre-formed mouse α -synuclein fibrils into rats triggers α -synuclein pathology and bilateral nigrostriatal degeneration. *Neurobiology of Disease*, 82, 185–199.
<https://doi.org/10.1016/J.NBD.2015.06.003>
- Perfetti, A., Greco, S., Fasanaro, P., Bugiardini, E., Cardani, R., Garcia Manteiga, J. M., ... Martelli, F. (2014). Genome Wide Identification of Aberrant Alternative Splicing Events in Myotonic Dystrophy Type 2. *PLOS ONE*, 9(4), e93983. <https://doi.org/10.1371/JOURNAL.PONE.0093983>
- Periñán, M. T., Brolin, K., Bandres-Ciga, S., Blauwendraat, C., Klein, C., Gan-Or, Z., ... Noyce, A. (2022). Effect Modification between Genes and Environment and Parkinson's Disease Risk. *Annals of Neurology*. <https://doi.org/10.1002/ANA.26467>
- Perry, E. K., Morris, C. M., Court, J. A., Cheng, A., Fairbairn, A. F., McKeith, I. G., ... Perry, R. H. (1995). Alteration in nicotine binding sites in Parkinson's disease, Lewy body dementia and Alzheimer's disease: Possible index of early neuropathology. *Neuroscience*, 64(2), 385–395.
[https://doi.org/10.1016/0306-4522\(94\)00410-7](https://doi.org/10.1016/0306-4522(94)00410-7)
- Pey, P., Pearce, R. K. B., Kalaitzakis, M. E., Griffin, W. S. T., & Gentleman, S. M. (2014). Phenotypic profile of alternative activation marker CD163 is different in Alzheimer's and Parkinson's disease. *Acta Neuropathologica Communications*, 2(1), 1–14. <https://doi.org/10.1186/2051-5960-2-21/FIGURES/6>
- Peyron, C., Arthaud, S., Villalba, M., & Fort, P. E. (2020). Defining and measuring paradoxical (REM) sleep in animal models of sleep disorders. *Current Opinion in Physiology*, 15, 203–209.
<https://doi.org/10.1016/j.cophys.2020.03.008i>
- Pihlström, L., Axelsson, G., Björnará, K. A., Dizdar, N., Fardell, C., Forsgren, L., ... Toft, M. (2013). Supportive evidence for 11 loci from genome-wide association studies in Parkinson's disease. *Neurobiology of Aging*, 34(6), 1708.e7-1708.e13.
<https://doi.org/10.1016/j.neurobiolaging.2012.10.019>
- Pinter, B., Diem-Zangerl, A., Wenning, G. K., Scherfler, C., Obergerner, W., Seppi, K., & Poewe, W.

- (2015). Mortality in Parkinson's disease: A 38-year follow-up study. *Movement Disorders*, 30(2), 266–269. <https://doi.org/10.1002/MDS.26060>
- Pizarro Galleguillos, B. M., Mohamed, W., & Periñan, M. T. (2022). The Glycoprotein GPNMB: A Secret Ingredient for Understanding Parkinson's Disease Etiology? *Movement Disorders*. <https://doi.org/10.1002/MDS.29264>
- Plum, S., Steinbach, S., Attems, J., Keers, S., Riederer, P., Gerlach, M., ... Marcus, K. (2016). Proteomic characterization of neuromelanin granules isolated from human substantia nigra by laser-microdissection. *Scientific Reports* 2016 6:1, 6(1), 1–8. <https://doi.org/10.1038/srep37139>
- Poe, G. R., Foote, S., Eschenko, O., Johansen, J. P., Bouret, S., Aston-Jones, G., ... Sara, S. J. (2020). Locus coeruleus: a new look at the blue spot. *Nature Reviews Neuroscience*, 21(11), 644–659. <https://doi.org/10.1038/S41583-020-0360-9>
- Poewe, W., Seppi, K., Tanner, C. M., Halliday, G. M., Brundin, P., Volkman, J., ... Lang, A. E. (2017). Parkinson disease. *Nature Reviews Disease Primers*, 3, 17013. <https://doi.org/10.1038/nrdp.2017.13>
- Politis, M., & Loane, C. (2011). Serotonergic Dysfunction in Parkinson's Disease and Its Relevance to Disability. *The Scientific World Journal*, 11, 1726. <https://doi.org/10.1100/2011/172893>
- Polymeropoulos, M. H., Lavedan, C., Leroy, E., Ide, S. E., Dehejia, A., Dutra, A., ... Nussbaum, R. L. (1997). Mutation in the α -synuclein gene identified in families with Parkinson's disease. *Science*, 276(5321), 2045–2047. <https://doi.org/10.1126/science.276.5321.2045>
- Pringsheim, T., Jette, N., Frolkis, A., & Steeves, T. D. L. (2014). The prevalence of Parkinson's disease: A systematic review and meta-analysis. *Movement Disorders*, 29(13), 1583–1590. <https://doi.org/10.1002/mds.25945>
- Pyatigorskaya, N., Mongin, M., Valabregue, R., Yahia-Cherif, L., Ewencyk, C., Poupon, C., ... Lehéricy, S. (2016). Medulla oblongata damage and cardiac autonomic dysfunction in Parkinson disease. *Neurology*, 87(24), 2540–2545. <https://doi.org/10.1212/WNL.0000000000003426>
- Qin, X. Y., Zhang, S. P., Cao, C., Loh, Y. P., & Cheng, Y. (2016). Aberrations in Peripheral Inflammatory Cytokine Levels in Parkinson Disease: A Systematic Review and Meta-analysis. *JAMA Neurology*, 73(11), 1316–1324. <https://doi.org/10.1001/JAMANEUROL.2016.2742>
- Rajput, A. H., & Rozdilsky, B. (1976). Dysautonomia in Parkinsonism: a clinicopathological study. *Journal of Neurology, Neurosurgery, and Psychiatry*, 39(11), 1092–1100. <https://doi.org/10.1136/JNNP.39.11.1092>
- Ranganathan, P., & Pramesh, C. S. (2012). Censoring in survival analysis: Potential for bias. *Perspectives in Clinical Research*, 3(1), 40. <https://doi.org/10.4103/2229-3485.92307>
- Rangaraju, S., Dammer, E. B., Raza, S. A., Rathakrishnan, P., Xiao, H., Gao, T., ... Levey, A. I. (2018). Identification and therapeutic modulation of a pro-inflammatory subset of disease-associated-microglia in Alzheimer's disease. *Molecular Neurodegeneration*, 13(1), 1–25. <https://doi.org/10.1186/S13024-018-0254-8/FIGURES/10>
- Riley, B. E., Gardai, S. J., Emig-Agius, D., Bessarabova, M., Ivliev, A. E., Schüle, B., ... Johnston, J. A. (2014). Systems-Based Analyses of Brain Regions Functionally Impacted in Parkinson's Disease Reveals Underlying Causal Mechanisms. *PLOS ONE*, 9(8), e102909. <https://doi.org/10.1371/JOURNAL.PONE.0102909>
- Rinne, J. O., Ma, S. Y., Lee, M. S., Collan, Y., & Røyttä, M. (2008). Loss of cholinergic neurons in the pedunculopontine nucleus in Parkinson's disease is related to disability of the patients. *Parkinsonism & Related Disorders*, 14(7), 553–557. <https://doi.org/10.1016/J.PARKRELDIS.2008.01.006>
- Rios, M., Habecker, B., Sasaoka, T., Eisenhofer, G., Tian, H., Landis, S., ... Roffler-Tarlov, S. (1999). Catecholamine synthesis is mediated by tyrosinase in the absence of tyrosine hydroxylase. *The Journal of Neuroscience: The Official Journal of the Society for Neuroscience*, 19(9), 3519–3526. <https://doi.org/10.1523/JNEUROSCI.19-09-03519.1999>
- Ripoll, V. M., Irvine, K. M., Ravasi, T., Sweet, M. J., & Hume, D. A. (2007). Gpnmb Is Induced in

Macrophages by IFN- γ and Lipopolysaccharide and Acts as a Feedback Regulator of Proinflammatory Responses. *The Journal of Immunology*, 178(10), 6557–6566. <https://doi.org/10.4049/JIMMUNOL.178.10.6557>

- Robinet, P., Ritchey, B., Lorkowski, S. W., Alzayed, A. M., DeGeorgia, S., Schodowski, E., ... Smith, J. D. (2021). Quantitative trait locus mapping identifies the Gpnmb gene as a modifier of mouse macrophage lysosome function. *Scientific Reports*, 11(1), 10249. <https://doi.org/10.1038/S41598-021-89800-5>
- Rose, A. A. N., Annis, M. G., Dong, Z., Pepin, F., Hallett, M., Park, M., & Siegel, P. M. (2010). ADAM10 Releases a Soluble Form of the GPNMB/Osteoactivin Extracellular Domain with Angiogenic Properties. *PLoS ONE*, 5(8). <https://doi.org/10.1371/JOURNAL.PONE.0012093>
- Rudow, G., O'Brien, R., Savonenko, A. V., Resnick, S. M., Zonderman, A. B., Pletnikova, O., ... Troncoso, J. C. (2008). Morphometry of the human substantia nigra in ageing and Parkinson's disease. *Acta Neuropathologica*, 115(4), 461–470. <https://doi.org/10.1007/s00401-008-0352-8>
- S.Y. Ma, B.J. Ciliax, G. Stebbins, S. Jaffar, J.N. Joyce, E.J. Cochran, J., ... E.J. Mufson. (1999). Dopamine transporter-immunoreactive neurons decrease with age in the human substantia nigra - Ma - 1999 - Journal of Comparative Neurology - Wiley Online Library. *The Journal of Comparative Neurology*, 409, 25–37. Retrieved from [https://onlinelibrary.wiley.com/doi/10.1002/\(SICI\)1096-9861\(19990621\)409:1%3C25::AID-CNE3%3E3.0.CO;2-E](https://onlinelibrary.wiley.com/doi/10.1002/(SICI)1096-9861(19990621)409:1%3C25::AID-CNE3%3E3.0.CO;2-E)
- Saade, M., Araujo de Souza, G., Scavone, C., & Kinoshita, P. F. (2021). The Role of GPNMB in Inflammation. *Frontiers in Immunology*, 12, 1687. <https://doi.org/10.3389/FIMMU.2021.674739/XML/NLM>
- Sacchini, S., Arbelo, M., Bombardi, C., Fernández, A., Cozzi, B., Bernaldo De Quirós, Y., & Herráez, P. (2018). Locus coeruleus complex of the family Delphinidae. *Scientific Reports*, 8(1). <https://doi.org/10.1038/S41598-018-23827-Z>
- Sacchini, S., Fernández, A., Mompeó, B., Ramírez, R., Arbelo, M., Holgersen, U., ... Andrada, M. (2022). Toothed Whales Have Black Neurons in the Blue Spot. *Veterinary Sciences*, 9(10). <https://doi.org/10.3390/VETSCI9100525>
- Sakurai, T. (2013). NPBWR1 and NPBWR2: Implications in Energy Homeostasis, Pain, and Emotion. *Frontiers in Endocrinology*, 4(MAR). <https://doi.org/10.3389/FENDO.2013.00023>
- Samuels, E. R., & Szabadi, E. (2008). Functional Neuroanatomy of the Noradrenergic Locus Coeruleus: Its Roles in the Regulation of Arousal and Autonomic Function Part I: Principles of Functional Organisation. *Current Neuropharmacology*, 6(3), 235. <https://doi.org/10.2174/157015908785777229>
- Sanghera, M. K., Zamora, J. L., & German, D. C. (1995). Calbindin-D28k-containing Neurons in the Human Hypothalamus: Relationship to Dopaminergic Neurons. *Neurodegeneration*, 4(4), 375–381. <https://doi.org/10.1006/NEUR.1995.0045>
- Saper, C. B., Sorrentino, D. M., German, D. C., & Lacalle, S. De. (1991). Medullary catecholaminergic neurons in the normal human brain and in Parkinson's disease. *Annals of Neurology*, 29(6), 577–584. <https://doi.org/10.1002/ANA.410290602>
- Saper, C., & Petit, C. (1982). Correspondence of melanin-pigmented neurons in human brain with A1-A14 catecholamine cell groups. *Brain: A Journal of Neurology*, 105(Pt 1), 87–101. <https://doi.org/10.1093/BRAIN/105.1.87>
- Sasaki, M., Shibata, E., Tohyama, K., Takahashi, J., Otsuka, K., Tsuchiya, K., ... Sakai, A. (2006). Neuromelanin magnetic resonance imaging of locus ceruleus and substantia nigra in Parkinson's disease. *NeuroReport*, 17(11), 1215–1218. <https://doi.org/10.1097/01.WNR.0000227984.84927.A7>
- Satoh, J. ichi, Kino, Y., Yanaizu, M., Ishida, T., & Saito, Y. (2019). Microglia express GPNMB in the brains of Alzheimer's disease and Nasu-Hakola disease. *Intractable and Rare Diseases Research*, 8(2), 120–128. <https://doi.org/10.5582/irdr.2019.01049>
- Saunders, A., Macosko, E. Z., Wysoker, A., Goldman, M., Krienen, F. M., de Rivera, H., ... McCarroll,

- S. A. (2018). Molecular Diversity and Specializations among the Cells of the Adult Mouse Brain. *Cell*, 174(4), 1015–1030.e16. <https://doi.org/10.1016/J.CELL.2018.07.028>
- Schapira, A. H. V., Chaudhuri, K. R., & Jenner, P. (2017). Non-motor features of Parkinson disease. *Nature Reviews Neuroscience* 2017 18:7, 18(7), 435–450. <https://doi.org/10.1038/nrn.2017.62>
- Scherer, H. J. (1939). Melanin pigmentation of the substantia nigra in primates. *The Journal of Comparative Neurology*, 71(1), 91–98. <https://doi.org/10.1002/cne.900710106>
- Schlossmacher, M. G., Frosch, M. P., Gai, W. P., Medina, M., Sharma, N., Forno, L., ... Kosik, K. S. (2002). Parkin Localizes to the Lewy Bodies of Parkinson Disease and Dementia with Lewy Bodies. *The American Journal of Pathology*, 160(5), 1655. [https://doi.org/10.1016/S0002-9440\(10\)61113-3](https://doi.org/10.1016/S0002-9440(10)61113-3)
- Schneider, S. A., & Alcalay, R. N. (2017). Neuropathology of genetic synucleinopathies with parkinsonism: Review of the literature. *Movement Disorders*, 32(11), 1504–1523. <https://doi.org/10.1002/MDS.27193>
- Schroeder, A., Mueller, O., Stocker, S., Salowsky, R., Leiber, M., Gassmann, M., ... Ragg, T. (2006). The RIN: an RNA integrity number for assigning integrity values to RNA measurements. *BMC Molecular Biology*, 7, 3. <https://doi.org/10.1186/1471-2199-7-3>
- Schulz, J., Pagano, G., Fernández Bonfante, J. A., Wilson, H., & Politis, M. (2018). Nucleus basalis of Meynert degeneration precedes and predicts cognitive impairment in Parkinson's disease. *Brain*, 141(5), 1501. <https://doi.org/10.1093/BRAIN/AWY072>
- Scorza, F. A., Fiorini, A. C., Scorza, C. A., & Finsterer, J. (2018). Cardiac abnormalities in Parkinson's disease and Parkinsonism. *Journal of Clinical Neuroscience*, 53, 1–5. <https://doi.org/10.1016/J.JOCN.2018.04.031>
- Seppi, K., Weintraub, D., Coelho, M., Perez-Lloret, S., Fox, S. H., Katzenschlager, R., ... Sampaio, C. (2011). The Movement Disorder Society Evidence-Based Medicine Review Update: Treatments for the Non-Motor Symptoms of Parkinson's Disease. *Movement Disorders : Official Journal of the Movement Disorder Society*, 26(0 3), S42. <https://doi.org/10.1002/MDS.23884>
- Sever, M., Turkyilmaz, M., Sevinc, C., Cakir, A., Ocalan, B., Cansev, M., ... Tekinay, A. B. (2016). Regenerative effects of peptide nanofibers in an experimental model of Parkinson's disease. *Acta Biomaterialia*, 46, 79–90. <https://doi.org/10.1016/J.ACTBIO.2016.09.011>
- Sharma, S. K., Chorell, E., Steneberg, P., Vernersson-Lindahl, E., Edlund, H., & Wittung-Stafshede, P. (2015). Insulin-degrading enzyme prevents α -synuclein fibril formation in a nonproteolytical manner. *Scientific Reports*, 5. <https://doi.org/10.1038/SREP12531>
- Shibata, E., Sasaki, M., Tohyama, K., Kanbara, Y., Otsuka, K., Ehara, S., & Sakai, A. (2006). Age-related Changes in Locus Ceruleus on Neuromelanin Magnetic Resonance Imaging at 3 Tesla. *Magnetic Resonance in Medical Sciences*, 5(4), 197–200. <https://doi.org/10.2463/MRMS.5.197>
- Shimura, H., Schlossmacher, M. G., Hattori, N., Frosch, M. P., Trockenbacher, A., Schneider, R., ... Selkoe, D. J. (2001). Ubiquitination of a New Form of α -Synuclein by Parkin from Human Brain: Implications for Parkinson's Disease. *Science*, 293(5528), 263–269. <https://doi.org/10.1126/SCIENCE.1060627>
- Sian-Hülsmann, J., Mandel, S., Youdim, M. B. H., & Riederer, P. (2011). The relevance of iron in the pathogenesis of Parkinson's disease. *Journal of Neurochemistry*, 118(6), 939–957. <https://doi.org/10.1111/J.1471-4159.2010.07132.X>
- Simunovic, F., Yi, M., Wang, Y., Macey, L., Brown, L. T., Krichevsky, A. M., ... Sonntag, K. C. (2009). Gene expression profiling of substantia nigra dopamine neurons: further insights into Parkinson's disease pathology. *Brain*, 132(7), 1795–1809. <https://doi.org/10.1093/brain/awn323>
- Singh, V. K., & Seed, T. M. (2021). How necessary are animal models for modern drug discovery? *Expert Opinion on Drug Discovery*, 16(12), 1391–1397. <https://doi.org/10.1080/17460441.2021.1972255>
- Skodda, S., Grönheit, W., Mancinelli, N., & Schlegel, U. (2013). Progression of voice and speech

- impairment in the course of Parkinson's disease: A longitudinal study. *Parkinson's Disease*. <https://doi.org/10.1155/2013/389195>
- SM, H., JH, K., BK, K., TG, U., HJ, K., HH, L., ... IY, C. (2017). GPNMB promotes proliferation of developing eosinophils. *Journal of Biochemistry*, *162*(2), 85–91. <https://doi.org/10.1093/JB/MVX002>
- Smajić, S., Smajić, S., Prada-Medina, C. A., Landoulsi, Z., Ghelfi, J., Delcambre, S., ... Spielmann, M. (2022). Single-cell sequencing of human midbrain reveals glial activation and a Parkinson-specific neuronal state. *Brain*, *145*(3), 964–978. <https://doi.org/10.1093/BRAIN/AWAB446>
- Smyth, G. K. (2004). Linear models and empirical bayes methods for assessing differential expression in microarray experiments. *Statistical Applications in Genetics and Molecular Biology*, *3*(1). <https://doi.org/10.2202/1544-6115.1027/MACHINEREADABLECITATION/RIS>
- Song, W. M., & Colonna, M. (2018). The Microglial Response to Neurodegenerative Disease. *Advances in Immunology*, *139*, 1–50. <https://doi.org/10.1016/BS.AI.2018.04.002>
- Spehlmann, R., & Stahl, S. M. (1976). DOPAMINE ACETYLCHOLINE IMBALANCE IN PARKINSON'S DISEASE. Possible Regenerative Overgrowth of Cholinergic Axon Terminals. *The Lancet*, *307*(7962), 724–726. [https://doi.org/10.1016/S0140-6736\(76\)93095-6](https://doi.org/10.1016/S0140-6736(76)93095-6)
- Spencer, S., Saper, C. B., Joh, T., Reis, D. J., Goldstein, M., & Raese, J. D. (1985). Distribution of catecholamine-containing neurons in the normal human hypothalamus. *Brain Research*, *328*(1), 73–80. [https://doi.org/10.1016/0006-8993\(85\)91324-1](https://doi.org/10.1016/0006-8993(85)91324-1)
- Spillantini, M. G., Schmidt, M. L., Lee, V. M. Y., Trojanowski, J. Q., Jakes, R., & Goedert, M. (1997). Alpha-synuclein in Lewy bodies. *Nature*, *388*(6645), 839–840. <https://doi.org/10.1038/42166>
- Stokholm, M. G., Iranzo, A., Østergaard, K., Serradell, M., Otto, M., Svendsen, K. B., ... Pavese, N. (2017). Assessment of neuroinflammation in patients with idiopathic rapid-eye-movement sleep behaviour disorder: a case-control study. *The Lancet Neurology*, *16*(10), 789–796. [https://doi.org/10.1016/S1474-4422\(17\)30173-4](https://doi.org/10.1016/S1474-4422(17)30173-4)
- Subramanian, A., Tamayo, P., Mootha, V. K., Mukherjee, S., Ebert, B. L., Gillette, M. A., ... Mesirov, J. P. (2005). Gene set enrichment analysis: a knowledge-based approach for interpreting genome-wide expression profiles. *Proceedings of the National Academy of Sciences of the United States of America*, *102*(43), 15545–15550. <https://doi.org/10.1073/PNAS.0506580102>
- Sukhorukova, E. G., Alekseeva, O. S., & Korzhevsky, D. E. (2014). Catecholaminergic neurons of mammalian brain and neuromelanin. *Journal of Evolutionary Biochemistry and Physiology*, *50*(5), 383–391. <https://doi.org/10.1134/S0022093014050020>
- Sulzer, D., Bogulavsky, J., Larsen, K. E., Behr, G., Karatekin, E., Kleinman, M. H., ... Zecca, L. (2000). Neuromelanin biosynthesis is driven by excess cytosolic catecholamines not accumulated by synaptic vesicles. *Proceedings of the National Academy of Sciences*, *97*(22), 11869–11874. <https://doi.org/10.1073/pnas.97.22.11869>
- Sulzer, D., Cassidy, C., Horga, G., Kang, U. J., Fahn, S., Casella, L., ... Zecca, L. (2018). Neuromelanin detection by magnetic resonance imaging (MRI) and its promise as a biomarker for Parkinson's disease. *Npj Parkinson's Disease* *2018 4:1*, *4*(1), 1–13. <https://doi.org/10.1038/s41531-018-0047-3>
- Sulzer, D., Mosharov, E., Tallozy, Z., Zucca, F. A., Simon, J. D., & Zecca, L. (2008). Neuronal pigmented autophagic vacuoles: lipofuscin, neuromelanin, and ceroid as macroautophagic responses during aging and disease. *Journal of Neurochemistry*, *106*(1), 24–36. <https://doi.org/10.1111/j.1471-4159.2008.05385.x>
- Sulzer, D., & Surmeier, D. J. (2013). Neuronal vulnerability, pathogenesis, and Parkinson's disease. *Movement Disorders*, *28*(6), 715–724. <https://doi.org/10.1002/mds.25187>
- Surmeier, D. J., Obeso, J. A., & Halliday, G. M. (2017). Selective neuronal vulnerability in Parkinson disease. *Nature Reviews. Neuroscience*, *18*(2), 101. <https://doi.org/10.1038/NRN.2016.178>
- Surmeier, D. J., & Sulzer, D. (2013). The pathology roadmap in Parkinson disease. *Prion*, *7*(1), 85. <https://doi.org/10.4161/PRI.23582>

- Szego, É. M., Gerhardt, E., Outeiro, T. F., Kermer, P., Arancibia, S., Tapia-Arancibia, L., & al., et. (2011). Dopamine-depletion and increased α -synuclein load induce degeneration of cortical cholinergic fibers in mice. *Journal of the Neurological Sciences*, 310(1–2), 90–95. <https://doi.org/10.1016/j.jns.2011.06.048>
- Takahashi, K., Rochford, C. D. P., & Neumann, H. (2005). Clearance of apoptotic neurons without inflammation by microglial triggering receptor expressed on myeloid cells-2. *The Journal of Experimental Medicine*, 201(4), 647–657. <https://doi.org/10.1084/JEM.20041611>
- Tang, B. L. (2019). Why is NMNAT Protective against Neuronal Cell Death and Axon Degeneration, but Inhibitory of Axon Regeneration? *Cells 2019, Vol. 8, Page 267*, 8(3), 267. <https://doi.org/10.3390/CELLS8030267>
- Thakur, P., Breger, L. S., Lundblad, M., Wan, O. W., Mattsson, B., Luk, K. C., ... Björklund, A. (2017). Modeling Parkinson's disease pathology by combination of fibril seeds and α -synuclein overexpression in the rat brain. *Proceedings of the National Academy of Sciences of the United States of America*, 114(39), E8284–E8293. https://doi.org/10.1073/PNAS.1710442114/SUPPL_FILE/PNAS.201710442SI.PDF
- Tief, K., Schmidt, A., & Beermann, F. (1998). New evidence for presence of tyrosinase in substantia nigra, forebrain and midbrain. *Brain Research. Molecular Brain Research*, 53(1–2), 307–310. Retrieved from <http://www.ncbi.nlm.nih.gov/pubmed/9473705>
- Tiklová, K., Gillberg, L., Volakakis, N., Lundén-Miguel, H., Dahl, L., Serrano, G. E., ... Perlmann, T. (2021). Disease Duration Influences Gene Expression in Neuromelanin-Positive Cells From Parkinson's Disease Patients. *Frontiers in Molecular Neuroscience*, 14. <https://doi.org/10.3389/FNMOL.2021.763777/FULL>
- Tokarew, J. M., El-Kodsi, D. N., Lengacher, N. A., Fehr, T. K., Nguyen, A. P., Shutinoski, B., ... Hayter, B. (2021). Age-associated insolubility of parkin in human midbrain is linked to redox balance and sequestration of reactive dopamine metabolites. *Acta Neuropathologica*, 141, 725–754. <https://doi.org/10.1007/s00401-021-02285-4>
- Tribl, F., Arzberger, T., Riederer, P., & Gerlach, M. (2007). Tyrosinase is not detected in human catecholaminergic neurons by immunohistochemistry and Western blot analysis. *Journal of Neural Transmission, Supplementa*, (72), 51–55. https://doi.org/10.1007/978-3-211-73574-9_8/COVER
- Trulson, M. E., Cannon, M. S., & Raese, J. D. (1985). Identification of dopamine-containing cell bodies in the dorsal and median raphe nuclei of the rat brain using tyrosine hydroxylase immunochemistry. *Brain Research Bulletin*, 15(2), 229–234. [https://doi.org/10.1016/0361-9230\(85\)90142-X](https://doi.org/10.1016/0361-9230(85)90142-X)
- Tsai, S. T., Chu, S. C., Liu, S. H., Pang, C. Y., Hou, T. W., Lin, S. Z., & Chen, S. Y. (2017). Neuroprotection of Granulocyte Colony-Stimulating Factor for Early Stage Parkinson's Disease. *Cell Transplantation*, 26(3), 409. <https://doi.org/10.3727/096368916X694247>
- Tse, K. F., Jeffers, M., Pollack, V. A., McCabe, D. A., Shadish, M. L., Khramtsov, N. V., ... LaRochelle, W. J. (2006). CR011, a fully human monoclonal antibody-auristatin E conjugate, for the treatment of melanoma. *Clinical Cancer Research*, 12(4), 1373–1382. <https://doi.org/10.1158/1078-0432.CCR-05-2018>
- Tubert, C., Galtieri, D., & Surmeier, D. J. (2019). The pedunclopontine nucleus and Parkinson's disease. *Neurobiology of Disease*, 128, 3–8. <https://doi.org/10.1016/J.NBD.2018.08.017>
- Turque, N., Denhez, F., Martin, P., Planque, N., Bailly, M., Bègue, A., ... Saule, S. (1996). Characterization of a new melanocyte-specific gene (QNR-71) expressed in v-myc-transformed quail neuroretina. *EMBO Journal*, 15(13), 3338–3350. <https://doi.org/10.1002/J.1460-2075.1996.TB00699.X>
- Ungerstedt, U. (1968). 6-hydroxy-dopamine induced degeneration of central monoamine neurons. *European Journal of Pharmacology*, 5(1), 107–110. [https://doi.org/10.1016/0014-2999\(68\)90164-7](https://doi.org/10.1016/0014-2999(68)90164-7)
- Usunoff, K. G., Itzev, D. E., Ovtcharoff, W. A., & Marani, E. (2002). Neuromelanin in the human brain: A review and atlas of pigmented cells in the substantia nigra. *Archives of Physiology and Biochemistry*, 110(4), 257–369. <https://doi.org/10.1076/APAB.110.4.257.11827>

- Van Den Berge, N., & Ulusoy, A. (2022). Animal models of brain-first and body-first Parkinson's disease. *Neurobiology of Disease*, 163. <https://doi.org/10.1016/J.NBD.2021.105599>
- Van der Heide, L. P., & Smidt, M. P. (2013). The BCL2 code to dopaminergic development and Parkinson's disease. *Trends in Molecular Medicine*, 19(4), 211–216. <https://doi.org/10.1016/J.MOLMED.2013.02.003>
- Vázquez-Vélez, G. E., Zoghbi, H. Y., & Duncan, D. (2021). Annual Review of Neuroscience Parkinson's Disease Genetics and Pathophysiology. <https://doi.org/10.1146/annurev-neuro-100720>
- Vijayashankar, N., & Brody, H. (1979). A quantitative study of the pigmented neurons in the nuclei locus coeruleus and subcoeruleus in man as related to aging. *Journal of Neuropathology and Experimental Neurology*, 38(5), 490–497. <https://doi.org/10.1097/00005072-197909000-00004>
- Vila, M., Laguna, A., & Carballo-Carbajal, I. (2019). Intracellular crowding by age-dependent neuromelanin accumulation disrupts neuronal proteostasis and triggers Parkinson disease pathology. *Autophagy*, 15(11), 2028–2030. <https://doi.org/10.1080/15548627.2019.1659621>
- Vila, M., Vukosavic, S., Jackson-Lewis, V., Neystat, M., Jakowec, M., & Przedborski, S. (2000). α -Synuclein Up-Regulation in Substantia Nigra Dopaminergic Neurons Following Administration of the Parkinsonian Toxin MPTP. *Journal of Neurochemistry*, 74(2), 721–729. <https://doi.org/10.1046/J.1471-4159.2000.740721.X>
- Virgone-Carlotta, A., Uhlrich, J., Akram, M. N., Ressenkoff, D., Chrétien, F., Domenget, C., ... Touret, M. (2013). Mapping and kinetics of microglia/neuron cell-to-cell contacts in the 6-OHDA murine model of Parkinson's disease. *Glia*, 61(10), 1645–1658. <https://doi.org/10.1002/GLIA.22546>
- Wack, A., Terczyńska-Dyla, E., & Hartmann, R. (2015). Guarding the frontiers: the biology of type III interferons. *Nature Immunology* 2015 16:8, 16(8), 802–809. <https://doi.org/10.1038/ni.3212>
- Wang, B., Shaham, Y., Zitzman, D., Azari, S., Wise, R. A., & You, Z. B. (2005). Cocaine experience establishes control of midbrain glutamate and dopamine by corticotropin-releasing factor: a role in stress-induced relapse to drug seeking. *The Journal of Neuroscience: The Official Journal of the Society for Neuroscience*, 25(22), 5389–5396. <https://doi.org/10.1523/JNEUROSCI.0955-05.2005>
- Wang, Q., Wang, M., Choi, I., Ho, L., Farrell, K., Beaumont, K. G., ... Yue, Z. (2022). Single-cell transcriptomic atlas of the human substantia nigra in Parkinson's disease. *bioRxiv*, 2022.03.25.485846. <https://doi.org/10.1101/2022.03.25.485846>
- Welch, J. D., Kozareva, V., Ferreira, A., Vanderburg, C., Martin, C., & Macosko, E. Z. (2019). Single-Cell Multi-omic Integration Compares and Contrasts Features of Brain Cell Identity. *Cell*, 177(7), 1873–1887.e17. <https://doi.org/10.1016/j.cell.2019.05.006>
- West, M. J., Coleman, P. D., Flood, D. G., & Troncoso, J. C. (1994). Differences in the pattern of hippocampal neuronal loss in normal ageing and Alzheimer's disease. *Lancet (London, England)*, 344(8925), 769–772. [https://doi.org/10.1016/S0140-6736\(94\)92338-8](https://doi.org/10.1016/S0140-6736(94)92338-8)
- Weterman, M. A. J., Ajubi, N., van Dinter, I. M. R., Degen, W. G. J., van Muijen, G. N. P., Ruiter, D. J., & Bloemers, H. P. J. (1995). nmb, a novel gene, is expressed in low-metastatic human melanoma cell lines and xenografts. *International Journal of Cancer*, 60(1), 73–81. <https://doi.org/10.1002/ijc.2910600111>
- Whitehouse, P. J., Cathala, F., Zweig, R. M., Singer, H. S., Castaigne, P., Kuhar, M. J., ... De Souza, E. B. (1987). Reductions in corticotropin releasing factor-like immunoreactivity in cerebral cortex in Alzheimer's disease, Parkinson's disease, and progressive supranuclear palsy. *Neurology*, 37(6), 905–905. <https://doi.org/10.1212/WNL.37.6.905>
- Wilms, H., Rosenstiel, P., Sievers, J., Deuschl, G., Zecca, L., & Lucius, R. (2003). Activation of microglia by human neuromelanin is NF-kappaB dependent and involves p38 mitogen-activated protein kinase: implications for Parkinson's disease. *The FASEB Journal: Official Publication of the Federation of American Societies for Experimental Biology*, 17(3), 500–502. <https://doi.org/10.1096/FJ.02-0314FJE>
- Wong, W. (2009). Repair or Die. *Science Signaling*, 2(65). <https://doi.org/10.1126/SCISIGNAL.265EC126>

- Wong, Y. C., Luk, K., Purtell, K., Burke Nanni, S., Stoessl, A. J., Trudeau, L. E., ... Volpicelli-Daley, L. A. (2019). Neuronal vulnerability in Parkinson disease: Should the focus be on axons and synaptic terminals? *Movement Disorders*, *34*(10), 1406–1422. <https://doi.org/10.1002/MDS.27823>
- Wu, D., Lim, E., Vaillant, F., Asselin-Labat, M. L., Visvader, J. E., & Smyth, G. K. (2010). ROAST: Rotation gene set tests for complex microarray experiments. *Bioinformatics*, *26*(17), 2176–2182. <https://doi.org/10.1093/bioinformatics/btq401>
- Xing, Y., Sapuan, A., Dineen, R. A., & Auer, D. P. (2018). Life span pigmentation changes of the substantia nigra detected by neuromelanin-sensitive MRI. *Movement Disorders*, *33*(11), 1792–1799. <https://doi.org/10.1002/MDS.27502>
- XM, G., YF, L., J, L., JQ, W., J, W., JQ, W., ... BL, S. (2019). Gpnmb secreted from liver promotes lipogenesis in white adipose tissue and aggravates obesity and insulin resistance. *Nature Metabolism*, *1*(5), 570–583. <https://doi.org/10.1038/S42255-019-0065-4>
- Xu, Y., Stokes, A. H., Freeman, W. M., Kumer, S. C., Vogt, B. A., & Vrana, K. E. (1997). Tyrosinase mRNA is expressed in human substantia nigra. *Brain Research. Molecular Brain Research*, *45*(1), 159–162. Retrieved from <http://www.ncbi.nlm.nih.gov/pubmed/9105685>
- Ye, J., Coulouris, G., Zaretskaya, I., Cutcutache, I., Rozen, S., & Madden, T. L. (2012). Primer-BLAST: a tool to design target-specific primers for polymerase chain reaction. *BMC Bioinformatics*, *13*(1), 134. <https://doi.org/10.1186/1471-2105-13-134/FIGURES/5>
- Yin, W., Mendoza, L., Monzon-Sandoval, J., Urrutia, A. O., & Gutierrez, H. (2021). Emergence of co-expression in gene regulatory networks. *PLoS ONE*, *16*(4). <https://doi.org/10.1371/JOURNAL.PONE.0247671>
- You, S., Won, K. S., Kim, K. T., Lee, H. W., & Cho, Y. W. (2021). Cardiac autonomic dysfunction is associated with severity of rem sleep without atonia in isolated rem sleep behavior disorder. *Journal of Clinical Medicine*, *10*(22), 5414. <https://doi.org/10.3390/JCM10225414/S1>
- Yuan, X., Tian, Y., Liu, C., & Zhang, Z. (2022). Environmental factors in Parkinson's disease: New insights into the molecular mechanisms. *Toxicology Letters*, *356*, 1–10. <https://doi.org/10.1016/J.TOXLET.2021.12.003>
- Yuen, P., & Baxter, D. W. (1963). The morphology of Marinesco bodies (paranucleolar corpuscles) in the melanin-pigmented nuclei of the brain-stem. *J. Neurol. Neurosurg. Psychiatr*, *26*, 178.
- Zecca, L., Fariello, R., Riederer, P., Sulzer, D., Gatti, A., & Tampellini, D. (2002). The absolute concentration of nigral neuromelanin, assayed by a new sensitive method, increases throughout the life and is dramatically decreased in Parkinson's disease. *FEBS Letters*, *510*(3), 216–220. [https://doi.org/10.1016/S0014-5793\(01\)03269-0](https://doi.org/10.1016/S0014-5793(01)03269-0)
- Zecca, L., Shima, T., Stroppolo, A., Goj, C., Battiston, G. A., Gerbasi, R., ... Swartz, H. M. (1996). Interaction of neuromelanin and iron in substantia nigra and other areas of human brain. *Neuroscience*, *73*(2), 407–415. [https://doi.org/10.1016/0306-4522\(96\)00047-4](https://doi.org/10.1016/0306-4522(96)00047-4)
- Zecca, L., Stroppolo, A., Gatti, A., Tampellini, D., Toscani, M., Gallorini, M., ... Zucca, F. A. (2004). The role of iron and copper molecules in the neuronal vulnerability of locus coeruleus and substantia nigra during aging. *PNAS*, *101*, 9843–9848. Retrieved from www.pnas.org/cgi/doi/10.1073/pnas.0403495101
- Zecca, L., Wilms, H., Geick, S., Claasen, J. H., Brandenburg, L. O., Holzknacht, C., ... Lucius, R. (2008). Human neuromelanin induces neuroinflammation and neurodegeneration in the rat substantia nigra: implications for Parkinson's disease. *Acta Neuropathologica* *2008* *116*:1, *116*(1), 47–55. <https://doi.org/10.1007/S00401-008-0361-7>
- Zecca, L., Zucca, F. A., Wilms, H., & Sulzer, D. (2003). Neuromelanin of the substantia nigra: a neuronal black hole with protective and toxic characteristics. *Trends in Neurosciences*, *26*(11), 578–580. <https://doi.org/10.1016/j.tins.2003.08.009>
- Zhang, P., Liu, W., Zhu, C., Yuan, X., Li, D., Gu, W., ... Gao, T. (2012). Silencing of GPNMB by siRNA Inhibits the Formation of Melanosomes in Melanocytes in a MITF-Independent Fashion. *PLoS ONE*, *7*(8). <https://doi.org/10.1371/JOURNAL.PONE.0042955>

- Zhang, W., Phillips, K., Wielgus, A. R., Liu, J., Albertini, A., Zucca, F. A., ... Zecca, L. (2011). Neuromelanin Activates Microglia and Induces Degeneration of Dopaminergic Neurons: Implications for Progression of Parkinson's Disease. *Neurotoxicity Research*, *19*(1), 63–72. <https://doi.org/10.1007/s12640-009-9140-z>
- Zhang, X. T., Wei, K. J., Chen, Y. Y., Shi, Z. C., Liu, L. K., Li, J., ... Ji, W. (2018). Molecular cloning and expression analysis of tyr and tyrp1 genes in normal and albino yellow catfish *Tachysurus fulvidraco*. *Journal of Fish Biology*, *92*(4), 979–998. <https://doi.org/10.1111/JFB.13556>
- Zhang, Y., James, M., Middleton, F. A., & Davis, R. L. (2005). Transcriptional analysis of multiple brain regions in Parkinson's disease supports the involvement of specific protein processing, energy metabolism, and signaling pathways, and suggests novel disease mechanisms. *American Journal of Medical Genetics - Neuropsychiatric Genetics*, *137 B*(1), 5–16. <https://doi.org/10.1002/AJMG.B.30195>
- Zhou, T., Li, Y., Li, X., Zeng, F., Rao, Y., He, Y., ... Peng, B. (2022). Microglial debris is cleared by astrocytes via C4b-facilitated phagocytosis and degraded via RUBICON-dependent noncanonical autophagy in mice. *Nature Communications* *2022 13:1*, *13*(1), 1–22. <https://doi.org/10.1038/s41467-022-33932-3>
- Zhu, S., Wuolikainen, A., Wu, J., Öhman, A., Wingsle, G., Moritz, T., ... Trupp, M. (2019). Targeted Multiple Reaction Monitoring Analysis of CSF Identifies UCHL1 and GPNMB as Candidate Biomarkers for ALS. *Journal of Molecular Neuroscience*, *69*(4), 643–657. <https://doi.org/10.1007/s12031-019-01411-y>
- Zoccal, D. B., Furuya, W. I., Bassi, M., Colombari, D. S. A., & Colombari, E. (2014). The nucleus of the solitary tract and the coordination of respiratory and sympathetic activities. *Frontiers in Physiology*, *5 JUN*, 238. <https://doi.org/10.3389/FPHYS.2014.00238/BIBTEX>
- Zucca, F. A., Basso, E., Cupaioli, F. A., Ferrari, E., Sulzer, D., Casella, L., & Zecca, L. (2014). Neuromelanin of the Human Substantia Nigra: An Update. *Neurotoxicity Research*, *25*(1), 13–23. <https://doi.org/10.1007/s12640-013-9435-y>
- Zucca, F. A., Vanna, R., Cupaioli, F. A., Bellei, C., De Palma, A., Di Silvestre, D., ... Zecca, L. (2018). Neuromelanin organelles are specialized autolysosomes that accumulate undegraded proteins and lipids in aging human brain and are likely involved in Parkinson's disease. *Npj Parkinson's Disease* *2018 4:1*, *4*(1), 1–23. <https://doi.org/10.1038/s41531-018-0050-8>
- Zwijnenburg, P. J. G., De Bie, H. M. A., Roord, J. J., Van Der Poll, T., & Van Furth, A. M. (2003). Chemotactic activity of CXCL5 in cerebrospinal fluid of children with bacterial meningitis. *Journal of Neuroimmunology*, *145*(1–2), 148–153. <https://doi.org/10.1016/J.JNEUROIM.2003.09.013>

ANNEX

ANNEX

Annex Data Table 1. Human sample information for TYR expression determination in SN postmortem tissue.

CASE	Gender	Age at death (years)	PMI (hours)	Clinical diagnosis	Braak PD Staging
Control-1	F	91	8	No neurological disease	0-No LB
Control-2	M	83	13	No neurological disease	0-No LB
Control-3	F	86	4	Acute stroke	0-No LB
Control-4	F	90	12.25	Acute stroke	0-No LB
Control-5	M	58	5	Hepatic encephalopathy	0-No LB
Control-6	M	76	11.5	No neurological disease	0-No LB
Control-7	F	70	14	ELA stage I	0-No LB
Control-8	M	70	4.5	Vascular Encephalopathy	0-No LB

Annex Data Table 2. DEGs ($p < 0.01$, $FC > |1.5|$) in tgNM mice NM-containing regions compared to wt non pigmented regions.

Gene Symbol	Entrez	logFC	AveExpr	t	P.Value	adj.P.Val	Region	Age
Mir28c	100628567	1.76268573	5.85450893	4.74746501	7.2581E-05	0.82800461	SN	3m
Dcps	69305	0.67949922	6.90877145	3.2761432	0.00309541	0.99947216	SN	3m
Ide	15925	0.59226793	7.92192247	3.25275245	0.00327878	0.99947216	SN	3m
Mir30a	387225	-0.73582867	4.45660614	-2.96198201	0.00663669	0.99947216	SN	3m
Mir26a-1	387218	-0.77535795	5.44260804	-2.88451385	0.00797959	0.99947216	SN	3m
Vapa	30960	-0.62269934	8.81311359	-2.81109803	0.00948728	0.99947216	SN	3m
Lamc1	226519	0.62288281	6.0434513	8.10368594	1.9303E-08	0.00044042	SN	12m
Lyz2	17105	1.41366322	5.53218309	5.07899534	3.083E-05	0.10048722	SN	12m
Npbwr1	226304	-0.70317562	6.21916652	-3.65822621	0.00119226	0.99961717	SN	12m
Pkd2l1	329064	0.59496575	5.19670126	3.57460827	0.00147204	0.99961717	SN	12m
Gfap	14580	1.19934957	8.37201182	3.52808322	0.0016545	0.99961717	SN	12m
Serpina3n	20716	0.92252906	7.0846216	3.52801412	0.00165479	0.99961717	SN	12m
Lilrb4a	14728	0.59709981	4.36634033	3.43307456	0.00209813	0.99961717	SN	12m
4933409K07Rik	108816	-0.62200345	6.50996303	-3.12812236	0.00444662	0.99961717	SN	12m

Ly6a	110454	0.60542232	6.32298113	3.05656927	0.0052881	0.99961717	SN	12m
Tyrobp	22177	0.657253	7.38433337	3.02506549	0.00570516	0.99961717	SN	12m
Fam205a2	545611	-0.73276533	6.27898239	-2.94957118	0.00683629	0.99961717	SN	12m
B2m	12010	0.6596845	8.69441938	2.86080673	0.00843967	0.99961717	SN	12m
Gm3893	100042539	-1.28415521	6.76418428	-2.82381542	0.00920812	0.99961717	SN	12m
Lilrb4a	14728	1.09790668	4.36634033	6.31368774	1.3472E-06	0.01961916	SN	20m
Lilr4b	14727	0.65609902	3.68887245	5.86228951	4.1695E-06	0.03171038	SN	20m
Nmnat2	226518	0.61473957	9.16687451	5.58347224	8.4571E-06	0.03318414	SN	20m
Cd68	12514	0.71260174	5.72877699	5.57116188	8.7265E-06	0.03318414	SN	20m
Serpina3n	20716	1.39676843	7.0846216	5.34264155	1.5652E-05	0.05101668	SN	20m
Lyz1	17110	0.6276083	4.65256402	4.94435109	4.3635E-05	0.11061872	SN	20m
Lyz2	17105	1.32632549	5.53218309	4.76610208	6.9166E-05	0.14346242	SN	20m
B2m	12010	0.87592184	8.69441938	3.79925955	0.00083381	0.51416473	SN	20m
Mir7013	102465613	-0.68404838	6.01489418	-3.43986276	0.00206293	0.6611702	SN	20m
Bcl2a1a	12044	0.73204776	5.5810373	3.40179246	0.00226807	0.67464407	SN	20m
D630041G03Rik	320749	0.60534981	5.91804646	3.15692143	0.00414561	0.67464407	SN	20m
Akr1e1	56043	-0.99912857	7.37563137	-3.15175058	0.00419817	0.67464407	SN	20m
Tyrobp	22177	0.68131324	7.38433337	3.13639247	0.0043581	0.67464407	SN	20m
Snord66	100217430	0.59283858	5.22522491	3.04476946	0.00544077	0.67464407	SN	20m
Sst	20604	0.67813331	7.0190992	2.82749388	0.00912884	0.68115462	SN	20m
Gfap	14580	1.58018342	8.5269113	5.20904575	9.9981E-06	0.17109581	VTA	3m
Crh	12918	-0.85641877	4.95330349	-5.07151864	1.4998E-05	0.17109581	VTA	3m
Eya1	14048	-0.59530359	5.48679745	-4.27028128	0.00015564	0.71021524	VTA	3m
Necab1	69352	-0.62212306	8.31741474	-3.87105078	0.00048529	0.99995207	VTA	3m
Mpeg1	17476	0.71484925	4.31445887	3.86789534	0.00048962	0.99995207	VTA	3m
Gla3	110304	-0.69234213	6.40650626	-3.76066814	0.00066116	0.99995207	VTA	3m
Adcyap1	11516	-0.80765962	5.72663451	-3.75385363	0.00067384	0.99995207	VTA	3m
Ccpg1os	546143	-0.62310265	6.07729933	-3.64801617	0.000904	0.99995207	VTA	3m
Actr6	67019	-0.61374496	6.74463367	-3.39700939	0.00179466	0.99995207	VTA	3m
Tyrobp	22177	0.79765303	7.64560056	3.22733379	0.00282456	0.99995207	VTA	3m
Usp18	24110	0.68821199	4.42521504	3.18241512	0.00318013	0.99995207	VTA	3m
Mir758	791071	0.89408065	5.85850293	3.13724359	0.00358047	0.99995207	VTA	3m
Snord87	266793	-0.87535514	3.025718	-3.03544484	0.00466536	0.99995207	VTA	3m
Serpina3n	20716	0.94225144	6.97987324	3.00058323	0.0051037	0.99995207	VTA	3m

Chrm5	213788	-0.60235542	6.34981527	-2.98148565	0.00536004	0.99995207	VTA	3m
Iqej	208426	-0.79237172	6.57567803	-2.88241633	0.0068965	0.99995207	VTA	3m
Mc3r	17201	-0.77611027	6.57862427	-2.87212584	0.00707792	0.99995207	VTA	3m
C1qb	12260	0.70766933	5.86680631	2.86519033	0.0072027	0.99995207	VTA	3m
Mir7236	102465713	0.85115548	3.27623699	2.8376434	0.007719	0.99995207	VTA	3m
Lyz2	17105	3.81922521	6.22742111	9.76058674	3.0072E-11	6.8613E-07	VTA	12m
Lyz1	17110	1.54012585	4.90226508	8.95639793	2.4049E-10	2.7436E-06	VTA	12m
Lilrb4a	14728	2.08985151	4.63552492	7.7529683	6.3018E-09	4.078E-05	VTA	12m
Bcl2a1a	12044	1.80380696	5.5191133	7.67733235	7.7831E-09	4.078E-05	VTA	12m
Serpina3n	20716	2.27727769	6.97987324	7.62794587	8.9367E-09	4.078E-05	VTA	12m
Mpeg1	17476	1.30390277	4.31445887	7.42092767	1.5998E-08	5.2917E-05	VTA	12m
Gfap	14580	2.13870047	8.5269113	7.41572097	1.6235E-08	5.2917E-05	VTA	12m
H2-K1	14972	1.09119377	6.77969864	7.13862553	3.5656E-08	0.00010169	VTA	12m
Cybb	13058	1.11465511	3.87275414	7.06318344	4.4233E-08	0.00011164	VTA	12m
Gpnmb	93695	1.85749757	4.70326283	7.02792166	4.8931E-08	0.00011164	VTA	12m
Cxcl16	66102	0.74736844	5.1463004	6.88894955	7.2921E-08	0.00015125	VTA	12m
Ms4a7	109225	1.1472959	3.36294865	6.8563032	8.0106E-08	0.00015231	VTA	12m
Msn	17698	0.63080113	6.22853554	6.73470764	1.1377E-07	0.00019968	VTA	12m
Lcn2	16819	1.08863336	4.32117832	6.60910676	1.6368E-07	0.00026676	VTA	12m
Tyrobp	22177	1.49942435	7.64560056	6.38127067	3.1761E-07	0.0004831	VTA	12m
Mmp12	17381	1.123847	3.32000202	6.30712393	3.9439E-07	0.0005624	VTA	12m
Cyba	13057	0.80594909	6.27697559	6.06931812	7.9154E-07	0.00099795	VTA	12m
Ctss	13040	0.98363286	7.67465839	6.05488001	8.2581E-07	0.00099795	VTA	12m
Anpep	16790	0.58969033	4.41459099	6.01114256	9.3904E-07	0.00107125	VTA	12m
Cd68	12514	1.51029192	5.93360802	5.86395931	1.4478E-06	0.00152215	VTA	12m
C3	12266	1.19311246	4.51427214	5.85932979	1.4677E-06	0.00152215	VTA	12m
Ms4a6c	73656	0.70120043	3.8279926	5.73005527	2.1482E-06	0.00201597	VTA	12m
H2-Q5	15016	0.59204939	5.66405065	5.68755739	2.4351E-06	0.00213687	VTA	12m
Clec7a	56644	2.27513176	5.22922367	5.59946371	3.1579E-06	0.00251296	VTA	12m
Ifi207	226691	0.62042889	3.41375011	5.5861018	3.2849E-06	0.00251296	VTA	12m
Ptpre	19264	0.66998366	3.59749989	5.58411518	3.3042E-06	0.00251296	VTA	12m
Lilr4b	14727	1.14374661	3.70462309	5.56636111	3.482E-06	0.00256274	VTA	12m
Ctsz	64138	0.87674473	6.84551093	5.51298894	4.0762E-06	0.0029063	VTA	12m
Casp1	12362	0.83662632	3.31624495	5.48554555	4.4202E-06	0.00305607	VTA	12m

Cd84	12523	0.79495504	3.95255678	5.43830869	5.0817E-06	0.00322984	VTA	12m
Vim	22352	0.66280447	6.14381743	5.35206118	6.5554E-06	0.003936	VTA	12m
Bcl2a1d	12047	0.58602144	3.0170174	4.94031995	2.2068E-05	0.01118918	VTA	12m
Rac2	19354	0.62622729	5.578384	4.9093812	2.417E-05	0.01128082	VTA	12m
Anxa1	16952	-0.79045366	5.33080347	-4.90858261	2.4227E-05	0.01128082	VTA	12m
Ftl1	14325	0.60211171	7.41115421	4.82720945	3.0768E-05	0.01376459	VTA	12m
Mir692-1	751529	0.79014144	7.40958532	4.63667166	5.3751E-05	0.02189958	VTA	12m
Slc6a11	243616	-0.64215747	10.0151795	-4.53096404	7.3155E-05	0.02781827	VTA	12m
A2m	232345	0.86361832	4.73080568	4.464383	8.8779E-05	0.03320612	VTA	12m
C3ar1	12267	0.63518612	4.07212225	4.45556968	9.108E-05	0.03351728	VTA	12m
B2m	12010	1.11789639	8.65206162	4.41295465	0.00010306	0.03674173	VTA	12m
Slc25a18	71803	-0.60210446	8.41700067	-4.3329137	0.00012992	0.04359139	VTA	12m
Npbwr1	226304	-0.79923664	7.44080144	-4.30301557	0.00014163	0.04544248	VTA	12m
Ch25h	12642	0.77060222	4.31674253	4.25058107	0.00016472	0.05011027	VTA	12m
Olfrl11	545205	0.85823186	3.53752456	4.19713879	0.00019206	0.0553023	VTA	12m
C1qa	12259	0.80709552	7.4771031	4.19590911	0.00019274	0.0553023	VTA	12m
Ifi30	65972	0.67430142	5.22628604	4.13239721	0.0002312	0.06205879	VTA	12m
Itgax	16411	0.71715925	4.1783386	4.1244189	0.00023653	0.06275234	VTA	12m
S100a6	20200	0.70913486	4.01933392	4.0994598	0.00025401	0.06511783	VTA	12m
C4a	625018	0.89954351	6.50097841	4.09225594	0.00025929	0.06573182	VTA	12m
Cebpa	12606	0.62492109	4.86103593	4.07210314	0.00027462	0.06810628	VTA	12m
C4b	12268	1.44803447	7.47788605	4.03024162	0.00030937	0.0746415	VTA	12m
Ctsc	13032	0.60126149	4.58230879	3.98891998	0.00034788	0.08099211	VTA	12m
Cd48	12506	0.7956621	4.17663428	3.98313493	0.00035363	0.08149966	VTA	12m
Lgals1	16852	0.6936967	6.81352748	3.76827753	0.00064726	0.12841725	VTA	12m
Uts2r	217369	-0.86101681	3.9603987	-3.7118404	0.00075744	0.14030138	VTA	12m
Cst7	13011	0.73633014	4.33531626	3.69738157	0.00078847	0.14277577	VTA	12m
C1qb	12260	0.84822386	5.86680631	3.61232094	0.00099758	0.16695504	VTA	12m
Tgm1	21816	0.62286775	4.39495912	3.5922795	0.00105416	0.1705072	VTA	12m
Fam205a2	545611	-0.88249861	5.79348568	-3.59136347	0.00105682	0.1705072	VTA	12m
Agt	11606	-0.78240026	8.05910247	-3.47694627	0.00144519	0.20515617	VTA	12m
Gm3893	100042539	-1.38192341	6.35262075	-3.4616401	0.00150659	0.20981016	VTA	12m
Fcer1g	14127	0.69073129	5.68574724	3.21073657	0.00295128	0.30060859	VTA	12m
Cdkn1a	12575	0.60836074	6.23831176	3.01303238	0.00494288	0.39724155	VTA	12m

AW112010	107350	0.62621349	3.71328166	2.97635795	0.00543091	0.40911154	VTA	12m
Fam205a1	433698	-0.71662275	5.38176613	-2.92168075	0.00624365	0.43299436	VTA	12m
Ifitm2	80876	0.60804632	5.4625421	2.84980928	0.00748685	0.44965944	VTA	12m
Anxa1	16952	-1.14273461	5.33080347	-7.34970199	1.9568E-08	0.00044646	VTA	20m
Mpeg1	17476	1.15842192	4.31445887	6.82848589	8.6791E-08	0.00066008	VTA	20m
Ftl1	14325	0.78815087	7.41115421	6.54444907	1.9749E-07	0.00090117	VTA	20m
Gpmb	93695	1.59608784	4.70326283	6.25460819	4.5985E-07	0.00113027	VTA	20m
Nmnat2	226518	0.63311423	8.64776069	6.23891974	4.8145E-07	0.00113027	VTA	20m
Lyz2	17105	2.34053191	6.22742111	6.19526496	5.4709E-07	0.00113027	VTA	20m
Vim	22352	0.73895579	6.14381743	6.18014634	5.7187E-07	0.00113027	VTA	20m
Tyropb	22177	1.39712287	7.64560056	6.15831457	6.0966E-07	0.00113027	VTA	20m
Cxcl16	66102	0.63988111	5.1463004	6.10888853	7.0475E-07	0.00113027	VTA	20m
B2m	12010	1.4932203	8.65206162	6.10515163	7.1252E-07	0.00113027	VTA	20m
Bcl2a1a	12044	1.37635643	5.5191133	6.06730544	7.9623E-07	0.00113027	VTA	20m
Npbwr1	226304	-1.08746372	7.44080144	-6.06396896	8.0407E-07	0.00113027	VTA	20m
Cd68	12514	1.50401454	5.93360802	6.04820836	8.4215E-07	0.00113027	VTA	20m
Lamc1	226519	0.59742911	5.6459539	5.89037286	1.3395E-06	0.00169791	VTA	20m
Serpina3n	20716	1.68975324	6.97987324	5.86218552	1.4554E-06	0.00174773	VTA	20m
Apod	11815	0.86029089	9.80881732	5.72067502	2.2085E-06	0.00251944	VTA	20m
Itgb2	16414	0.6381388	4.92124262	5.44477041	4.9857E-06	0.0047397	VTA	20m
Lilrb4a	14728	1.40843924	4.63552492	5.41172047	5.4967E-06	0.0050165	VTA	20m
Rac2	19354	0.64176967	5.578384	5.21097054	9.9415E-06	0.00872405	VTA	20m
Mir692-1	751529	0.85302005	7.40958532	5.18448243	1.075E-05	0.00875932	VTA	20m
Bcl2a1d	12047	0.58993705	3.0170174	5.15100421	1.1865E-05	0.00933497	VTA	20m
Lyz1	17110	0.8464503	4.90226508	5.09827545	1.3861E-05	0.01020147	VTA	20m
Cst7	13011	0.97567188	4.33531626	5.07422996	1.4879E-05	0.01054307	VTA	20m
Cmpk2	22169	0.60070007	6.20971395	4.99120631	1.9E-05	0.01060756	VTA	20m
Klk6	19144	0.71791383	7.55450269	4.98912737	1.9116E-05	0.01060756	VTA	20m
Cd84	12523	0.703512	3.95255678	4.98468202	1.9368E-05	0.01060756	VTA	20m
Ctsh	13036	0.62121388	5.970528	4.92208476	2.3284E-05	0.01180554	VTA	20m
Ifit3	15959	0.58764438	4.30058317	4.87225329	2.6956E-05	0.01255167	VTA	20m
Mir5123	100628614	1.36335884	3.69167953	4.84199472	2.9461E-05	0.01344363	VTA	20m
Trim30d	209387	0.60919268	3.93527233	4.75678673	3.7825E-05	0.01568378	VTA	20m
Anxa3	11745	0.62723475	4.9462707	4.74574611	3.9068E-05	0.01568378	VTA	20m

Anln	68743	0.59226467	6.59904994	4.73881748	3.9869E-05	0.01568378	VTA	20m
A2m	232345	0.88204978	4.73080568	4.72255861	4.1813E-05	0.01590149	VTA	20m
C1qb	12260	1.06352335	5.86680631	4.69102271	4.5856E-05	0.01641404	VTA	20m
Ifitm3	66141	0.59255566	5.59930765	4.69033406	4.5948E-05	0.01641404	VTA	20m
Lilr4b	14727	0.93036377	3.70462309	4.68963463	4.6042E-05	0.01641404	VTA	20m
Tlr7	170743	0.75814113	3.57562193	4.66901394	4.8904E-05	0.0169059	VTA	20m
Gfap	14580	1.29503839	8.5269113	4.65083272	5.1573E-05	0.01730412	VTA	20m
Ms4a7	109225	0.7469378	3.36294865	4.62321056	5.5906E-05	0.01796536	VTA	20m
C3ar1	12267	0.62181196	4.07212225	4.51758123	7.606E-05	0.02230683	VTA	20m
Ctsz	64138	0.68164342	6.84551093	4.43931402	9.5479E-05	0.02649294	VTA	20m
Ifit1	15957	1.00629382	4.30469576	4.41323665	0.00010298	0.02764176	VTA	20m
Lcn2	16819	0.69987628	4.32117832	4.4007537	0.00010677	0.02832651	VTA	20m
Usp18	24110	0.86505097	4.42521504	4.35786424	0.00012088	0.02965605	VTA	20m
Clec7a	56644	1.70660171	5.22922367	4.35027507	0.00012356	0.02986393	VTA	20m
C1qa	12259	0.80134282	7.4771031	4.31483458	0.00013688	0.03176121	VTA	20m
Ctss	13040	0.67640939	7.67465839	4.3124771	0.00013781	0.03176121	VTA	20m
Ephx1	13849	0.59145136	7.66980678	4.30484596	0.00014088	0.0318794	VTA	20m
A330049N07Rik	327768	1.18859881	5.35711824	4.23761742	0.00017098	0.03612084	VTA	20m
H2-K1	14972	0.60791349	6.77969864	4.11906991	0.00024018	0.04385478	VTA	20m
Fcgr1g	14127	0.85499793	5.68574724	4.11628338	0.00024209	0.04385478	VTA	20m
Mir495	751522	-1.1242189	5.35821306	-4.07317761	0.00027378	0.04713535	VTA	20m
Cd48	12506	0.75440845	4.17663428	3.91153801	0.00043299	0.06226911	VTA	20m
Ctla2b	13025	0.61821815	4.52457527	3.88779225	0.00046296	0.06412304	VTA	20m
Fcgr2b	14130	0.59101993	3.75991486	3.80108728	0.00059055	0.07403285	VTA	20m
Ly6c2	100041546	0.82482105	7.75120669	3.73590992	0.00070839	0.07922821	VTA	20m
St6galnac3	20447	0.60914537	5.88445764	3.68546199	0.00081498	0.08478479	VTA	20m
Fcgr3	14131	0.64732828	5.81696459	3.63872299	0.00092751	0.09166085	VTA	20m
Mir1912	100526529	0.98414346	6.92352631	3.61828227	0.00098132	0.09376255	VTA	20m
Lgals1	16852	0.64165393	6.81352748	3.61009618	0.00100371	0.09438503	VTA	20m
Cxcr4	12767	0.834623	4.40211908	3.60168115	0.00102724	0.09488871	VTA	20m
Scrg1	20284	0.84316943	5.81069411	3.57737851	0.00109823	0.0985857	VTA	20m
Pcdhb6	93877	-0.59311948	5.11861727	-3.55122651	0.00117991	0.10314513	VTA	20m
Ly6a	110454	0.69910006	6.21365647	3.5475514	0.00119185	0.10379115	VTA	20m
Mc3r	17201	-0.87634395	6.57862427	-3.53306826	0.00124005	0.10634322	VTA	20m

Ly86	17084	0.85456295	5.7482397	3.50439565	0.00134107	0.11006424	VTA	20m
Cdkn1a	12575	0.67885329	6.23831176	3.48227614	0.00142438	0.1136318	VTA	20m
AW112010	107350	0.70159554	3.71328166	3.45377643	0.0015391	0.11823599	VTA	20m
Ctla2a	13024	0.69631873	5.91564558	3.42821358	0.00164952	0.12151383	VTA	20m
Mgp	17313	1.04824985	5.18906163	3.42272375	0.00167421	0.12151383	VTA	20m
Rs5-8s1	790956	0.66902513	9.22141259	3.41968409	0.00168803	0.12151383	VTA	20m
Mir493	100124466	-1.25806585	7.0311217	-3.34011862	0.00209142	0.13441663	VTA	20m
C3	12266	0.62791187	4.51427214	3.19381615	0.00308604	0.16885142	VTA	20m
Cbln4	228942	-0.61328799	6.2580796	-3.1076981	0.00386777	0.19050394	VTA	20m
Mir6955	102466210	-0.89285711	5.31793095	-3.06686793	0.00430101	0.20375651	VTA	20m
Gbp7	229900	0.61971534	5.14366186	3.0033185	0.00506794	0.21817014	VTA	20m
Npsr1	319239	-0.8764837	4.59762703	-2.98209904	0.00535162	0.2243662	VTA	20m
Igtp	16145	0.76275613	4.82402604	2.9576035	0.00569773	0.2300835	VTA	20m
Alox5ap	11690	0.60288508	5.85861425	2.93094618	0.00609831	0.23907057	VTA	20m
Clec2d	93694	0.60280371	4.72448906	2.84561395	0.00756615	0.2651757	VTA	20m
Gfap	14580	2.65758829	9.58255376	13.6672543	6.0017E-15	1.3693E-10	LC	3m
C4b	12268	2.4861364	7.73936843	12.304037	1.0407E-13	1.1873E-09	LC	3m
Lyz2	17105	3.35895519	7.03153528	10.8631689	2.688E-12	2.0443E-08	LC	3m
Cd68	12514	2.07029217	6.94442005	10.7331695	3.6502E-12	2.0821E-08	LC	3m
Tyrobp	22177	2.13078214	8.3209597	10.3068221	1.011E-11	4.6135E-08	LC	3m
Cyba	13057	0.91930261	7.23141694	10.0362227	1.9537E-11	7.4294E-08	LC	3m
Mpeg1	17476	1.67680594	5.14017314	9.71713474	4.301E-11	1.4019E-07	LC	3m
Sncg	20618	-0.69664232	11.3909303	-9.45548902	8.2966E-11	2.3662E-07	LC	3m
C4a	625018	1.32925776	6.94315648	9.29827818	1.2366E-10	3.1348E-07	LC	3m
Ctss	13040	1.46109689	8.49509081	9.19322672	1.6174E-10	3.6902E-07	LC	3m
Lilrb4a	14728	2.08097353	5.46165604	8.96167981	2.9378E-10	6.0936E-07	LC	3m
Gpnmb	93695	1.30229282	5.9171108	8.27381789	1.8024E-09	3.4269E-06	LC	3m
Apobec1	11810	0.60634203	5.25235833	8.12016543	2.7251E-09	4.7828E-06	LC	3m
Uts2b	224065	-1.75782471	8.15124808	-7.85886704	5.5412E-09	9.0305E-06	LC	3m
Ms4a7	109225	1.03652037	4.26833616	7.62516264	1.0526E-08	1.3305E-05	LC	3m
Gpam	14732	0.61702123	7.3759425	7.61596807	1.0797E-08	1.3305E-05	LC	3m
Apod	11815	0.93252901	8.9668162	7.5446102	1.3151E-08	1.5003E-05	LC	3m
Lyz1	17110	1.29409931	6.34911727	7.51052753	1.4453E-08	1.5703E-05	LC	3m
Cd84	12523	0.99935711	4.57210783	7.44345076	1.7411E-08	1.6891E-05	LC	3m

Ptprb	19263	0.65789531	6.47041274	7.43617161	1.7767E-08	1.6891E-05	LC	3m
Igfbp5	16011	0.81701476	8.80517231	7.38289912	2.0607E-08	1.8084E-05	LC	3m
Atp1b2	11932	0.73889155	8.917414	7.35135856	2.2501E-08	1.9015E-05	LC	3m
Th	21823	-0.74914347	11.7918332	-7.27930733	2.7519E-08	2.2014E-05	LC	3m
Bcl2a1a	12044	1.63526432	6.14800716	7.2549875	2.9457E-08	2.2014E-05	LC	3m
C1qb	12260	1.36238737	6.80260502	7.23343545	3.129E-08	2.2014E-05	LC	3m
Anpep	16790	0.63880912	5.38836294	7.23167177	3.1445E-08	2.2014E-05	LC	3m
Man2b1	17159	0.67186004	8.0815004	7.22722467	3.184E-08	2.2014E-05	LC	3m
Serpini1	20713	-0.72656709	9.27601877	-7.21316463	3.312E-08	2.2225E-05	LC	3m
Ctsh	13036	1.0425653	6.68763361	6.99435592	6.1329E-08	3.7818E-05	LC	3m
Ccnc	51813	-0.59704911	8.28874505	-6.80203928	1.0581E-07	6.1902E-05	LC	3m
Nfia	18027	0.59659833	7.20119315	6.76043763	1.1911E-07	6.6285E-05	LC	3m
Gjc3	118446	0.71386234	7.94000536	6.70706296	1.3869E-07	7.3432E-05	LC	3m
Ctsc	13032	0.60893679	5.59047562	6.69975936	1.4161E-07	7.3432E-05	LC	3m
Sash1	70097	0.62602836	7.84043363	6.67451012	1.522E-07	7.6595E-05	LC	3m
Agtr1a	11607	-0.6041294	6.76035011	-6.66941851	1.5443E-07	7.6595E-05	LC	3m
Itpkb	320404	0.86337758	7.85696152	6.62234142	1.7667E-07	8.1295E-05	LC	3m
Adora1	11539	0.65790231	7.50547073	6.61698763	1.794E-07	8.1295E-05	LC	3m
Slc1a2	20511	0.71229957	8.84170084	6.61249998	1.8172E-07	8.1295E-05	LC	3m
Clic4	29876	0.60336072	7.43641266	6.56922182	2.0569E-07	8.1631E-05	LC	3m
Cd9	12527	0.67225251	7.80037964	6.56129206	2.1041E-07	8.1631E-05	LC	3m
Eif1a	13664	-0.63198947	7.73883369	-6.56033737	2.1099E-07	8.1631E-05	LC	3m
Phyhd1	227696	0.65895013	7.26371701	6.55252786	2.1577E-07	8.2048E-05	LC	3m
Qpct	70536	-0.79555266	9.34953606	-6.48020128	2.6552E-07	9.7712E-05	LC	3m
Gent2	14538	-0.83399835	7.86723613	-6.45485062	2.8558E-07	0.00010268	LC	3m
Lilr4b	14727	1.17560076	4.74746731	6.42736106	3.0907E-07	0.00010525	LC	3m
Laptm5	16792	0.69205955	6.25101019	6.39747394	3.3682E-07	0.00010879	LC	3m
Ifitm2	80876	0.81897925	6.33164939	6.39570661	3.3854E-07	0.00010879	LC	3m
C3ar1	12267	1.21303189	4.90094889	6.36272999	3.7226E-07	0.00011325	LC	3m
Fcer1g	14127	0.91593105	6.44410744	6.30371877	4.4128E-07	0.00012745	LC	3m
Tnr	21960	0.71686164	7.3969493	6.24827187	5.1788E-07	0.00013764	LC	3m
Hacd3	57874	-0.6357636	8.82964829	-6.19993063	5.9552E-07	0.00014769	LC	3m
Prelp	116847	0.77207217	7.25726178	6.18815549	6.1615E-07	0.00014955	LC	3m
Slc31a1	20529	-0.64266266	7.53847223	-6.15633418	6.7556E-07	0.00016028	LC	3m

Gabbr2	242425	0.59465547	9.25392198	6.15336245	6.814E-07	0.00016028	LC	3m
Hsd17b2	15486	-0.86285568	7.80167702	-6.12903283	7.3112E-07	0.00016577	LC	3m
Trpm3	226025	0.69674143	7.19178096	6.11141967	7.6938E-07	0.00017043	LC	3m
Plxdc2	67448	0.70709915	7.4886004	6.07405307	8.5737E-07	0.00017532	LC	3m
B2m	12010	1.60376007	9.37812206	6.06998771	8.6753E-07	0.00017532	LC	3m
Hspb3	56534	-0.82954709	6.51087337	-6.06758598	8.7359E-07	0.00017532	LC	3m
9530091C08Rik	320440	0.71028729	5.78402534	6.06156188	8.8898E-07	0.00017637	LC	3m
Glr1	14654	0.63292833	7.41313523	6.02775434	9.8057E-07	0.00018593	LC	3m
Mobp	17433	0.81088274	8.66807524	5.97571962	1.1404E-06	0.00019863	LC	3m
C1qa	12259	0.91645637	7.84430879	5.93086778	1.2991E-06	0.00021795	LC	3m
Hepacam	72927	0.64124448	7.75515965	5.89985039	1.4217E-06	0.00023169	LC	3m
Fcgr3	14131	0.70641824	6.82266634	5.82222431	1.7818E-06	0.00026581	LC	3m
Magea13	75352	-1.05438425	6.78288302	-5.81434407	1.8232E-06	0.00026665	LC	3m
Slc14a1	108052	0.81485552	8.05862975	5.80172568	1.8914E-06	0.00027141	LC	3m
Gch1	14528	-0.85310727	9.09786384	-5.76284841	2.1181E-06	0.00029246	LC	3m
Serping1	12258	0.58777234	6.30172765	5.74935014	2.203E-06	0.00029246	LC	3m
Flt1	14254	0.63313904	7.12637617	5.74592003	2.2252E-06	0.00029246	LC	3m
C1qc	12262	0.62569735	6.42329166	5.73255539	2.3135E-06	0.00029378	LC	3m
Vim	22352	0.60311533	7.1676994	5.73224439	2.3156E-06	0.00029378	LC	3m
Cst7	13011	0.94526675	5.04571578	5.72839716	2.3417E-06	0.00029425	LC	3m
Plce1	74055	0.72955986	6.91854837	5.6765417	2.7237E-06	0.00032536	LC	3m
Pitpnc1	71795	0.61812087	7.55024935	5.65395803	2.9091E-06	0.00033749	LC	3m
Lrig1	16206	0.59040339	7.43453522	5.63694591	3.057E-06	0.00034529	LC	3m
Ntsr2	18217	0.60555869	8.87939459	5.61534974	3.2558E-06	0.00035886	LC	3m
Lipk	240633	-0.59764447	4.99846018	-5.56802076	3.7378E-06	0.000393	LC	3m
Lcat	16816	0.96531896	8.02218641	5.55988102	3.8276E-06	0.00039804	LC	3m
Prkce	18754	0.61482868	7.29425818	5.54251621	4.0265E-06	0.00040811	LC	3m
Slit1	20562	0.60196604	7.68363904	5.54116629	4.0424E-06	0.00040811	LC	3m
Nmur2	216749	-0.81657369	7.05032826	-5.53610594	4.1026E-06	0.00040981	LC	3m
Sdc4	20971	0.60444806	7.92852739	5.53521963	4.1132E-06	0.00040981	LC	3m
Csflr	12978	0.69695459	6.92784838	5.52558234	4.2305E-06	0.00041544	LC	3m
Clec7a	56644	1.78248837	5.84474282	5.51220629	4.3989E-06	0.00042507	LC	3m
Casp1	12362	0.88154956	4.34379773	5.50133575	4.5407E-06	0.00043135	LC	3m
Mcts1	68995	-0.59406791	6.71241782	-5.49592568	4.613E-06	0.00043135	LC	3m

Antxr1	69538	0.77385511	6.83609463	5.47380432	4.9207E-06	0.00045119	LC	3m
Shc3	20418	0.82595208	8.00540328	5.47071246	4.9653E-06	0.00045119	LC	3m
Zfp361l	12192	0.60653091	7.50065519	5.45344144	5.222E-06	0.0004618	LC	3m
Nckap1l	105855	0.65261854	5.57220629	5.43962785	5.4369E-06	0.00047164	LC	3m
Rnf122	68867	0.59859567	5.55413927	5.43901198	5.4467E-06	0.00047164	LC	3m
S100a1	20193	0.62271515	8.37617559	5.37651964	6.5368E-06	0.00051491	LC	3m
Fxyd1	56188	0.70437974	9.49062139	5.37610437	6.5447E-06	0.00051491	LC	3m
Calb2	12308	0.636073	9.86069835	5.32156512	7.6743E-06	0.00055764	LC	3m
Ovgp1	12659	-0.85957633	8.55783029	-5.31254561	7.8791E-06	0.00057045	LC	3m
Chrna4	11438	0.5937223	7.21582653	5.30602864	8.0305E-06	0.00057617	LC	3m
Grm1	14816	0.59080189	6.67922974	5.30300822	8.1016E-06	0.00057633	LC	3m
Tnfaip8l3	244882	-0.80426275	6.54004201	-5.30155017	8.1361E-06	0.0005765	LC	3m
Ddc	13195	-0.66167154	9.75389224	-5.26256671	9.1168E-06	0.00062219	LC	3m
Tm4sf1	17112	-0.65012052	7.58843849	-5.24331551	9.6438E-06	0.00063744	LC	3m
Calr3	73316	-0.63313987	6.80671575	-5.2384134	9.7828E-06	0.00063772	LC	3m
Crim1	50766	0.60344797	8.14222218	5.18852323	1.1316E-05	0.0006997	LC	3m
Rbm11	224344	-0.62246665	7.04786564	-5.18348017	1.1484E-05	0.0007036	LC	3m
Rgs9	19739	-0.59239774	9.87406503	-5.15970183	1.2309E-05	0.00073519	LC	3m
Chodl	246048	-0.80744352	8.9921807	-5.15013495	1.2657E-05	0.0007494	LC	3m
Maoa	17161	-0.7858054	11.2556516	-5.13468372	1.3241E-05	0.00076872	LC	3m
H2-K1	14972	0.81650248	7.74916453	5.09946957	1.4673E-05	0.00082257	LC	3m
Ly86	17084	0.95272274	6.03241989	5.09393723	1.4912E-05	0.00082894	LC	3m
Cryab	12955	0.69814318	8.63838308	5.05716317	1.66E-05	0.00089116	LC	3m
Trf	22041	0.5951282	9.20185094	5.05412895	1.6747E-05	0.00089696	LC	3m
Ttyh2	117160	0.61669839	9.03412254	5.04325735	1.7287E-05	0.00091537	LC	3m
Sst	20604	0.77077075	9.70261388	5.00596807	1.9271E-05	0.00096074	LC	3m
Cd48	12506	0.88806965	4.8978693	4.98743463	2.034E-05	0.00100154	LC	3m
Kcnd2	16508	0.6939617	9.3484545	4.98527232	2.0469E-05	0.00100217	LC	3m
Plcl2	224860	0.60893185	7.35081217	4.98217197	2.0654E-05	0.00100694	LC	3m
Calcr	12311	-0.64110377	10.0152293	-4.96768615	2.1544E-05	0.00103267	LC	3m
Ifitm3	66141	0.83396365	6.57619073	4.963409	2.1814E-05	0.00103762	LC	3m
Chrb3	108043	-1.12571184	9.58160403	-4.94949416	2.2716E-05	0.00106125	LC	3m
Tm4sf4	229302	-1.05238427	6.43703311	-4.94260133	2.3177E-05	0.0010748	LC	3m
ErbB4	13869	0.61363619	7.29176303	4.94017863	2.3341E-05	0.00107802	LC	3m

Cd38	12494	0.67477481	7.06289146	4.91600585	2.5042E-05	0.0011421	LC	3m
Cybrd1	73649	0.70607927	6.97940281	4.91488333	2.5124E-05	0.0011421	LC	3m
Slc18a2	214084	-0.72489123	11.4192142	-4.91069448	2.5432E-05	0.00114564	LC	3m
Fn1	14268	0.73750871	6.86605163	4.86447975	2.9091E-05	0.00124816	LC	3m
Scrg1	20284	0.72611378	6.91959583	4.84649864	3.0652E-05	0.00127854	LC	3m
Ppp2r3c	59032	-0.65259949	7.62457264	-4.84565924	3.0727E-05	0.00127933	LC	3m
Cetn3	12626	-0.66431535	9.86810953	-4.80573244	3.4507E-05	0.00138124	LC	3m
Igsf5	72058	-0.70178874	7.63776325	-4.80285482	3.4796E-05	0.00139039	LC	3m
Nxpe4	244853	0.64089811	6.0905466	4.78482806	3.6666E-05	0.00143005	LC	3m
A2m	232345	0.68395112	5.84148895	4.73828275	4.1968E-05	0.00155219	LC	3m
Gast	14459	-0.69441748	6.7046087	-4.72434562	4.3699E-05	0.00158765	LC	3m
Olfr111	545205	0.72862031	4.21234383	4.71983246	4.4275E-05	0.00159745	LC	3m
Lhfp13	269629	0.79410004	7.84418343	4.67496761	5.0421E-05	0.00171825	LC	3m
Drd2	13489	0.68350922	7.12061324	4.67025478	5.1114E-05	0.00172773	LC	3m
Radx	102871	-0.66887662	5.81896358	-4.66949303	5.1227E-05	0.00172898	LC	3m
Dgkk	331374	0.74005146	6.47914887	4.65911358	5.279E-05	0.00176864	LC	3m
Gtf2b	229906	-0.60137406	8.54323839	-4.61425095	6.0105E-05	0.00192215	LC	3m
Efcab10	75040	-0.79717735	7.82019093	-4.59057554	6.4362E-05	0.00200337	LC	3m
Irgm2	54396	0.72656175	4.91891891	4.57930105	6.6493E-05	0.00203364	LC	3m
Kctd16	383348	0.6223708	6.07829455	4.52525499	7.7716E-05	0.00226748	LC	3m
Plpp4	381925	0.67370035	7.28867697	4.52176767	7.8501E-05	0.00228164	LC	3m
Tlr7	170743	0.61848325	4.1452496	4.49992213	8.3603E-05	0.00239633	LC	3m
Plxnc1	54712	0.61917941	6.80532594	4.48185117	8.8069E-05	0.002482	LC	3m
Slc43a3	58207	0.80527876	5.93849779	4.4587608	9.4121E-05	0.00260931	LC	3m
Alox5ap	11690	0.71950111	6.5613048	4.41685117	0.00010617	0.00284991	LC	3m
Rorb	225998	0.62976221	6.72898254	4.41000115	0.00010828	0.00287943	LC	3m
Shisal2b	77803	-0.93186096	8.58678633	-4.40030569	0.00011134	0.00293337	LC	3m
Osmr	18414	0.75254876	5.20291286	4.38502636	0.00011633	0.00300926	LC	3m
Gpx2-ps1	14777	-0.61664282	5.56495364	-4.36000618	0.00012498	0.00317197	LC	3m
Gira2	237213	-0.79626058	9.19608845	-4.34548826	0.00013029	0.00327393	LC	3m
Txnip	56338	0.62851771	7.62568567	4.33836297	0.00013298	0.00331566	LC	3m
Slc9b2	97086	-0.6365476	6.7183966	-4.32166782	0.00013949	0.00340379	LC	3m
Calca	12310	-0.63996224	8.78406531	-4.30703245	0.00014545	0.00350481	LC	3m
Pla2g4e	329502	-0.66866364	7.46369822	-4.30698753	0.00014547	0.00350481	LC	3m

Igfbp7	29817	0.73389856	7.80078338	4.27450522	0.00015962	0.00375796	LC	3m
Chst1	76969	0.59083571	8.75983164	4.19985722	0.00019748	0.00429282	LC	3m
Kcnj10	16513	0.66779741	7.86399005	4.1554825	0.00022403	0.00469112	LC	3m
Agt	11606	0.59284459	9.57287472	4.14207382	0.00023272	0.00481779	LC	3m
Parp12	243771	0.70539462	6.51157297	4.13733554	0.00023587	0.00486578	LC	3m
Gabrg3	14407	0.58630399	6.79134928	4.08215208	0.00027578	0.00541295	LC	3m
Mir692-1	751529	0.63581027	8.79229536	4.05004151	0.00030197	0.0057464	LC	3m
Fam183b	75429	-0.65964125	9.22764054	-4.04613267	0.00030532	0.00578109	LC	3m
Znhit6	229937	-0.63351209	8.31100699	-4.0434396	0.00030765	0.00580355	LC	3m
Ctla2b	13025	0.61562003	5.59698834	3.9736618	0.00037446	0.00653689	LC	3m
Tmc3	233424	-0.68478285	7.94237804	-3.96530632	0.00038336	0.00663632	LC	3m
Kcnh5	238271	0.61484068	7.36802424	3.92690077	0.00042697	0.00713306	LC	3m
Rbp4	19662	-0.62866409	9.55907636	-3.92501072	0.00042924	0.00714986	LC	3m
Mir431	723866	-0.68959662	5.3286082	-3.90112468	0.00045892	0.00750243	LC	3m
Tlr3	142980	0.67961185	6.28650768	3.85933997	0.00051574	0.0081209	LC	3m
Bcap31	27061	-0.59163198	10.9875735	-3.80737878	0.00059603	0.0088824	LC	3m
Lgals1	16852	0.7511119	8.43584434	3.79454276	0.00061766	0.00912733	LC	3m
Ly6a	110454	0.72363783	6.71545783	3.78270549	0.00063829	0.00932423	LC	3m
C1ql3	227580	0.58826477	7.17707763	3.70345608	0.00079471	0.01073545	LC	3m
Gm14405	626877	-0.59011646	7.39889174	-3.66981317	0.00087185	0.01143225	LC	3m
Aasdhpt	67618	-0.6567677	7.88464185	-3.62412523	0.00098832	0.01237623	LC	3m
Rtl9	209540	-0.64229691	6.40076894	-3.60027577	0.00105497	0.01292011	LC	3m
Slitrk6	239250	0.59301728	5.62441202	3.55535357	0.00119251	0.01401057	LC	3m
Slc17a6	140919	0.6001616	7.94101096	3.54804404	0.00121648	0.01419699	LC	3m
Aldh1a1	11668	1.05932152	6.58744383	3.50414621	0.00137047	0.01544031	LC	3m
Ly6c2	100041546	0.63808669	8.39702501	3.46427618	0.00152651	0.01661684	LC	3m
Mir376c	723856	-0.60061593	3.72957333	-3.45408943	0.00156905	0.01684678	LC	3m
Zfp971	626848	-0.5886623	8.74409999	-3.32361959	0.00222547	0.02146086	LC	3m
Nps	100043254	0.79079509	9.34647729	3.12647263	0.00373801	0.03054671	LC	3m
Ptgds	19215	0.6329098	8.8339134	3.06407125	0.00439339	0.0340719	LC	3m
Npy	109648	0.72580844	7.69143097	2.76777744	0.00928265	0.05793021	LC	3m
Stat1	20846	0.60064559	6.68913816	2.75774436	0.00951518	0.0588981	LC	3m
Lyz2	17105	4.51516771	7.03153528	14.6024661	9.5088E-16	9.7421E-12	LC	12m
Gfap	14580	2.82749333	9.58255376	14.5410298	1.0703E-15	9.7421E-12	LC	12m

Cd68	12514	2.78558605	6.94442005	14.4415208	1.2974E-15	9.7421E-12	LC	12m
Cyba	13057	1.30988127	7.23141694	14.3002532	1.7079E-15	9.7421E-12	LC	12m
Gpnmb	93695	2.14163137	5.9171108	13.6063622	6.7879E-15	3.0974E-11	LC	12m
Apobec1	11810	0.93964538	5.25235833	12.583782	5.6975E-14	2.1666E-10	LC	12m
Lyz1	17110	2.11961567	6.34911727	12.3015535	1.0464E-13	3.4106E-10	LC	12m
Tyrobp	22177	2.47906332	8.3209597	11.9914956	2.0624E-13	5.882E-10	LC	12m
Ms4a7	109225	1.54937023	4.26833616	11.3979428	7.8064E-13	1.8233E-09	LC	12m
Cd84	12523	1.52890646	4.57210783	11.387661	7.9915E-13	1.8233E-09	LC	12m
Anpep	16790	0.99096403	5.38836294	11.2182596	1.178E-12	2.3844E-09	LC	12m
Mpeg1	17476	1.92701013	5.14017314	11.1670746	1.3255E-12	2.3844E-09	LC	12m
Lilrb4a	14728	2.59060074	5.46165604	11.1563814	1.3586E-12	2.3844E-09	LC	12m
Ctss	13040	1.73363418	8.49509081	10.9080323	2.4198E-12	3.9436E-09	LC	12m
C4b	12268	2.12125971	7.73936843	10.4982405	6.3806E-12	9.7054E-09	LC	12m
Ctsh	13036	1.53173681	6.68763361	10.2761068	1.089E-11	1.4795E-08	LC	12m
Vim	22352	1.08066598	7.1676994	10.2710729	1.1024E-11	1.4795E-08	LC	12m
Bcl2a1a	12044	2.30669015	6.14800716	10.2338246	1.2065E-11	1.5293E-08	LC	12m
Lilr4b	14727	1.8391088	4.74746731	10.054958	1.8661E-11	2.2408E-08	LC	12m
Itgb2	16414	1.08750108	5.92366192	9.94636387	2.4366E-11	2.6659E-08	LC	12m
Slc11a1	18173	0.717803	5.95021655	9.94352306	2.4538E-11	2.6659E-08	LC	12m
Csf3r	12986	0.88501913	5.74239542	9.52999668	6.8746E-11	7.1296E-08	LC	12m
Man2b1	17159	0.85938148	8.0815004	9.24440003	1.4189E-10	1.4075E-07	LC	12m
Apod	11815	1.13895967	8.9668162	9.214734	1.5307E-10	1.4552E-07	LC	12m
Hexb	15212	0.86862319	9.12576155	9.02838493	2.472E-10	2.1304E-07	LC	12m
Gpam	14732	0.73028133	7.3759425	9.01395133	2.5659E-10	2.1304E-07	LC	12m
Itgax	16411	1.24398255	5.06455331	9.00997476	2.5925E-10	2.1304E-07	LC	12m
Myo1f	17916	0.83823935	5.83651588	9.0067099	2.6145E-10	2.1304E-07	LC	12m
Ms4a6d	68774	0.62961691	4.77942448	8.96596568	2.9054E-10	2.2858E-07	LC	12m
Clec7a	56644	2.86756459	5.84474282	8.86771987	3.7504E-10	2.8523E-07	LC	12m
Cd33	12489	0.74866444	6.4564277	8.78045272	4.7101E-10	3.4666E-07	LC	12m
C4a	625018	1.24052595	6.94315648	8.67759118	6.1688E-10	4.3984E-07	LC	12m
Ucp2	22228	0.59395646	6.97673221	8.57487235	8.0873E-10	5.5915E-07	LC	12m
Cxcl16	66102	0.86691098	5.52859917	8.46666929	1.0773E-09	6.7988E-07	LC	12m
Bcl2a1d	12047	0.77598448	3.56521457	8.45794199	1.1025E-09	6.7988E-07	LC	12m
Grn	14824	0.73220145	8.02747572	8.40794339	1.2594E-09	7.4591E-07	LC	12m

Laptm5	16792	0.90904666	6.25101019	8.40332655	1.275E-09	7.4591E-07	LC	12m
Pld4	104759	1.16743133	6.66832666	8.22597326	2.0493E-09	1.1689E-06	LC	12m
Fcer1g	14127	1.17400539	6.44410744	8.07986564	3.0387E-09	1.691E-06	LC	12m
Ctsc	13032	0.7301082	5.59047562	8.03293438	3.4505E-09	1.8268E-06	LC	12m
Cd9	12527	0.82224717	7.80037964	8.02526394	3.523E-09	1.8268E-06	LC	12m
Itgb5	16419	0.79163632	7.38959877	7.93014927	4.5621E-09	2.2493E-06	LC	12m
Mmp12	17381	1.12094027	4.00400427	7.92444695	4.6335E-09	2.2493E-06	LC	12m
Cst7	13011	1.29367849	5.04571578	7.83980207	5.8376E-09	2.7748E-06	LC	12m
Ptprj	19271	0.73481005	7.42489139	7.79870332	6.5324E-09	3.0417E-06	LC	12m
Serping1	12258	0.79571375	6.30172765	7.78334847	6.8131E-09	3.109E-06	LC	12m
C3ar1	12267	1.47774634	4.90094889	7.75123969	7.4403E-09	3.2289E-06	LC	12m
Blnk	17060	0.77494916	4.72924135	7.72317557	8.0364E-09	3.3602E-06	LC	12m
C1qb	12260	1.4517427	6.80260502	7.70785705	8.382E-09	3.3795E-06	LC	12m
Unc93b1	54445	0.66572041	6.1878901	7.70523355	8.4427E-09	3.3795E-06	LC	12m
Nrp2	18187	0.66090091	6.92127387	7.64248098	1.0035E-08	3.9476E-06	LC	12m
Cybb	13058	1.38699381	4.79731205	7.61383196	1.0861E-08	4.0622E-06	LC	12m
Igfbp5	16011	0.83960961	8.80517231	7.58707597	1.1694E-08	4.256E-06	LC	12m
Ptprb	19263	0.67108745	6.47041274	7.58528196	1.1752E-08	4.256E-06	LC	12m
Nckap11	105855	0.89956343	5.57220629	7.49793334	1.4967E-08	5.3357E-06	LC	12m
Cd48	12506	1.33252651	4.8978693	7.48352215	1.5577E-08	5.4679E-06	LC	12m
Tcn2	21452	0.63057861	7.14146042	7.46113281	1.6576E-08	5.6549E-06	LC	12m
Trem2	83433	0.58734694	5.55509047	7.43966188	1.7596E-08	5.9039E-06	LC	12m
H2-K1	14972	1.18636894	7.74916453	7.40947205	1.9137E-08	6.328E-06	LC	12m
Cd86	12524	0.79408153	4.58912449	7.37960569	2.0797E-08	6.7787E-06	LC	12m
Npl	74091	0.71533379	5.87400517	7.34511551	2.2897E-08	7.084E-06	LC	12m
H2-DMb1	14999	0.61721415	4.77659004	7.34388186	2.2976E-08	7.084E-06	LC	12m
Fn1	14268	1.10793073	6.86605163	7.30771925	2.5417E-08	7.7323E-06	LC	12m
Igsf6	80719	0.91547506	4.60880714	7.27113832	2.8155E-08	8.4371E-06	LC	12m
C1qa	12259	1.12293781	7.84430879	7.267117	2.8474E-08	8.4371E-06	LC	12m
Flt1	14254	0.79849604	7.12637617	7.24658261	3.0159E-08	8.8218E-06	LC	12m
Vgf	381677	0.68227766	6.70022787	7.24022225	3.0701E-08	8.8667E-06	LC	12m
P2rx7	18439	0.85273537	6.08616377	7.19472276	3.4879E-08	9.9474E-06	LC	12m
Casp12	12364	0.59886312	4.40481583	7.17964743	3.6386E-08	1.0249E-05	LC	12m
Anxa3	11745	0.83734116	5.60946892	7.14995666	3.9552E-08	1.0879E-05	LC	12m

Ctse	13034	0.9730505	4.8497826	7.14237819	4.0404E-08	1.088E-05	LC	12m
Plxdc2	67448	0.83133498	7.4886004	7.14125134	4.0532E-08	1.088E-05	LC	12m
Ctla2b	13025	1.10258914	5.59698834	7.11691644	4.3404E-08	1.1383E-05	LC	12m
Xdh	22436	0.72609243	6.01466378	7.09615604	4.6017E-08	1.1931E-05	LC	12m
Ctla2a	13024	1.20345219	6.51250764	7.03835349	5.4162E-08	1.358E-05	LC	12m
Ilgam	16409	0.80437206	6.01116586	7.0234301	5.6493E-08	1.401E-05	LC	12m
Fcgr3	14131	0.84284815	6.82266634	6.94666521	7.0188E-08	1.6857E-05	LC	12m
Csf1r	12978	0.87415143	6.92784838	6.93043103	7.349E-08	1.7377E-05	LC	12m
Ptpn5	19259	0.66163109	7.18991332	6.92858845	7.3875E-08	1.7377E-05	LC	12m
Fcgr2b	14130	0.73805343	4.89665472	6.91405657	7.698E-08	1.7741E-05	LC	12m
Osmr	18414	1.16640005	5.20291286	6.79649649	1.0749E-07	2.3493E-05	LC	12m
Tnr	21960	0.77810437	7.3969493	6.78207255	1.12E-07	2.4107E-05	LC	12m
Cdkn1a	12575	1.38365201	6.78807803	6.73039084	1.2976E-07	2.7162E-05	LC	12m
Txnip	56338	0.97121653	7.62568567	6.70385218	1.3997E-07	2.881E-05	LC	12m
Dock2	94176	0.66209631	4.95596291	6.67256459	1.5304E-07	3.0901E-05	LC	12m
Ephb1	270190	0.6412532	6.75241345	6.65269718	1.6198E-07	3.2137E-05	LC	12m
Nr4a2	18227	0.79066294	7.56315589	6.64870124	1.6384E-07	3.2226E-05	LC	12m
Olfr111	545205	1.02177983	4.21234383	6.61885143	1.7844E-07	3.4503E-05	LC	12m
9530091C08Rik	320440	0.76699895	5.78402534	6.5455368	2.2013E-07	4.0834E-05	LC	12m
Cebpa	12606	0.73271706	5.88384144	6.50517978	2.4715E-07	4.4754E-05	LC	12m
Emp3	13732	0.64064337	6.2185497	6.49222781	2.5651E-07	4.6083E-05	LC	12m
Hpgd	15446	0.98394057	6.46314754	6.48487339	2.6198E-07	4.6623E-05	LC	12m
Slc43a3	58207	1.17065875	5.93849779	6.48183906	2.6428E-07	4.6623E-05	LC	12m
Cd63	12512	0.67986254	10.109128	6.4800372	2.6565E-07	4.6623E-05	LC	12m
Angpt1	11600	0.64029843	4.99254732	6.44590985	2.9302E-07	5.0267E-05	LC	12m
Ptprc	19264	0.76003854	4.14067362	6.41785591	3.1763E-07	5.2899E-05	LC	12m
Rac2	19354	0.80512711	6.44805841	6.39265174	3.4153E-07	5.5264E-05	LC	12m
Cp	12870	0.81222834	4.70765576	6.38140555	3.5276E-07	5.6681E-05	LC	12m
Ms4a6c	73656	0.85800754	4.77555521	6.36386798	3.7104E-07	5.92E-05	LC	12m
Dusp6	67603	0.73673013	6.8094519	6.35725839	3.7817E-07	5.9919E-05	LC	12m
B2m	12010	1.67299277	9.37812206	6.33202295	4.067E-07	6.3556E-05	LC	12m
Slc14a1	108052	0.88122086	8.05862975	6.27424316	4.8046E-07	7.2597E-05	LC	12m
Ptafr	19204	0.7347263	5.31714829	6.26996297	4.8643E-07	7.3016E-05	LC	12m
Lipk	240633	-0.6706185	4.99846018	-6.2478914	5.1845E-07	7.5651E-05	LC	12m

Gm3002	100040852	0.65478209	8.16050461	6.24428209	5.2388E-07	7.5651E-05	LC	12m
Atp1b2	11932	0.62617068	8.917414	6.22987932	5.4614E-07	7.7383E-05	LC	12m
Plec1	74055	0.80040773	6.91854837	6.22779311	5.4944E-07	7.7383E-05	LC	12m
Adgrf5	224792	0.66719238	6.91381667	6.1521779	6.8374E-07	9.2578E-05	LC	12m
Trf	22041	0.72430603	9.20185094	6.15117231	6.8573E-07	9.2578E-05	LC	12m
Grm1	14816	0.68241994	6.67922974	6.12536723	7.3892E-07	9.8019E-05	LC	12m
Mertk	17289	0.67243856	6.38070109	6.11911182	7.5243E-07	9.8246E-05	LC	12m
Sst	20604	0.94063243	9.70261388	6.1091783	7.744E-07	9.9262E-05	LC	12m
H2-Q5	15016	0.71735596	6.82995738	6.05423915	9.0806E-07	0.0001126	LC	12m
Gm3500	100041678	0.61158751	8.02358904	6.02714265	9.8231E-07	0.0001205	LC	12m
Noval	664883	0.6401514	7.7830854	6.0198032	1.0035E-06	0.00012232	LC	12m
Casp1	12362	0.96320489	4.34379773	6.01090826	1.0297E-06	0.0001243	LC	12m
Ftl1	14325	0.65950442	8.50027312	5.98299807	1.1166E-06	0.00012998	LC	12m
Pdgfd	71785	-0.69736317	7.72404054	-5.97779005	1.1336E-06	0.00013129	LC	12m
Gm3411	100861615	0.6363768	7.5739692	5.96936477	1.1617E-06	0.00013386	LC	12m
Maoa	17161	-0.91100633	11.2556516	-5.95278341	1.219E-06	0.00013837	LC	12m
Arhgap25	232201	0.65179189	5.37946825	5.9241142	1.3249E-06	0.00014603	LC	12m
Ifitm2	80876	0.75557605	6.33164939	5.90056795	1.4187E-06	0.00015375	LC	12m
Uba6	231380	-0.61042997	7.76044878	-5.89981091	1.4219E-06	0.00015375	LC	12m
Mobp	17433	0.79474608	8.66807524	5.85680214	1.6113E-06	0.00016864	LC	12m
Igfbp7	29817	1.00031257	7.80078338	5.82620202	1.7613E-06	0.00017871	LC	12m
Gla1	14654	0.6114605	7.41313523	5.8233034	1.7763E-06	0.00017893	LC	12m
Tnfaip8l3	244882	-0.87798814	6.54004201	-5.78753426	1.9712E-06	0.00018662	LC	12m
Serpina3n	20716	0.97539275	9.26374305	5.78566538	1.9819E-06	0.00018686	LC	12m
Esyt3	272636	-0.7548604	7.72613537	-5.74847945	2.2086E-06	0.00020149	LC	12m
Cx3cr1	13051	0.66795427	7.82584539	5.74724606	2.2166E-06	0.00020149	LC	12m
Slc8a1	20541	0.58852865	7.38025313	5.74019543	2.2626E-06	0.00020324	LC	12m
Rbp1	19659	0.76669792	7.0531915	5.72739245	2.3486E-06	0.0002085	LC	12m
S100a6	20200	0.72260702	5.16840592	5.70367803	2.5166E-06	0.00021902	LC	12m
Tlr7	170743	0.77973139	4.1452496	5.67312132	2.751E-06	0.0002295	LC	12m
Sema5a	20356	0.66443763	7.2607231	5.67307454	2.7514E-06	0.0002295	LC	12m
Gjc3	118446	0.59878841	7.94000536	5.62589075	3.1572E-06	0.00025454	LC	12m
Magea13	75352	-1.01789454	6.78288302	-5.6131236	3.277E-06	0.00025961	LC	12m
Tnfrsf12a	27279	1.10889766	7.53378377	5.59137737	3.4916E-06	0.00027445	LC	12m

Penk	18619	0.60275958	7.63671945	5.58155001	3.5931E-06	0.00028076	LC	12m
Gm3696	100042149	0.59891093	7.25268138	5.55898247	3.8377E-06	0.00029782	LC	12m
Slc18a2	214084	-0.81419201	11.4192142	-5.51565262	4.3549E-06	0.00032685	LC	12m
Hspb3	56534	-0.75228275	6.51087337	-5.50244868	4.526E-06	0.00033528	LC	12m
Chrn3	108043	-1.24511937	9.58160403	-5.47450141	4.9107E-06	0.00036142	LC	12m
Drd2	13489	0.79941637	7.12061324	5.4622206	5.0899E-06	0.000372	LC	12m
Gla2	237213	-0.99881561	9.19608845	-5.45090593	5.2608E-06	0.00037745	LC	12m
Gm3264	100041306	0.60163727	8.827613	5.44599952	5.3367E-06	0.0003817	LC	12m
Ly6a	110454	1.04010918	6.71545783	5.43701085	5.4786E-06	0.00038699	LC	12m
Hsd17b2	15486	-0.76415686	7.80167702	-5.42795582	5.6253E-06	0.0003937	LC	12m
Cnn3	71994	0.63493315	8.41055754	5.41893428	5.7754E-06	0.00040155	LC	12m
Gabbr2	14401	0.73139061	8.04136408	5.41702257	5.8078E-06	0.00040155	LC	12m
Cabp7	192650	0.68072354	7.11605673	5.40771884	5.9677E-06	0.00040888	LC	12m
Zmat4	320158	-0.59752863	7.4051783	-5.37961697	6.4779E-06	0.00043095	LC	12m
Scrg1	20284	0.80591143	6.91959583	5.37911378	6.4874E-06	0.00043095	LC	12m
C1qc	12262	0.5864295	6.42329166	5.37278864	6.6084E-06	0.00043356	LC	12m
Rgs9	19739	-0.6134605	9.87406503	-5.34315555	7.2055E-06	0.0004631	LC	12m
Chrna4	11438	0.59298487	7.21582653	5.29943829	8.1865E-06	0.00050482	LC	12m
6330407A03Rik	70720	0.58742067	4.15663385	5.27843723	8.7041E-06	0.00052755	LC	12m
Mgarp	67749	-0.63743568	6.27624093	-5.22311608	1.0229E-05	0.00058203	LC	12m
Dcn	13179	0.7596913	6.50639904	5.21053387	1.0612E-05	0.00059438	LC	12m
Nr4a3	18124	-0.62188962	7.37908807	-5.19560194	1.1085E-05	0.00060958	LC	12m
Plcl2	224860	0.63061321	7.35081217	5.15956505	1.2314E-05	0.00064736	LC	12m
Cyb561	13056	-0.64951172	8.43962387	-5.15636452	1.2429E-05	0.00064747	LC	12m
Ifitm3	66141	0.86404901	6.57619073	5.14246472	1.2944E-05	0.00066515	LC	12m
Fbxo30	71865	-0.60629885	6.91203993	-5.14150477	1.298E-05	0.00066552	LC	12m
Ly6c1	17067	0.8116204	7.73241475	5.11756898	1.3919E-05	0.00070104	LC	12m
Fam107a	268709	0.5889155	8.31705075	5.11236337	1.4132E-05	0.00070864	LC	12m
Il1a	16175	0.60497801	4.0252254	5.0791423	1.5569E-05	0.00074943	LC	12m
Akr1e1	56043	-1.52990117	7.7845498	-5.07358445	1.5824E-05	0.0007553	LC	12m
Mir692-1	751529	0.7907852	8.79229536	5.03721481	1.7594E-05	0.00080422	LC	12m
Dgkk	331374	0.79637078	6.47914887	5.01368094	1.8843E-05	0.00084883	LC	12m
Maob	109731	-0.5979213	9.07549704	-5.01265153	1.8899E-05	0.00084883	LC	12m
Uts2b	224065	-1.11318959	8.15124808	-4.97683809	2.0978E-05	0.00091515	LC	12m

Ddc	13195	-0.62369346	9.75389224	-4.9605102	2.1999E-05	0.00094704	LC	12m
Kcnd2	16508	0.68703777	9.3484545	4.93553229	2.3659E-05	0.00100147	LC	12m
Gm3383	100041515	0.60389809	8.44578111	4.93418652	2.3751E-05	0.00100354	LC	12m
Calb2	12308	0.58948341	9.86069835	4.93178358	2.3918E-05	0.00100537	LC	12m
Rtl9	209540	-0.87232938	6.40076894	-4.88967997	2.7035E-05	0.0010879	LC	12m
A2m	232345	0.70483057	5.84148895	4.88293164	2.7571E-05	0.00110363	LC	12m
Fndc9	320116	0.87159933	5.9462501	4.88085765	2.7738E-05	0.00110836	LC	12m
Gent2	14538	-0.62797539	7.86723613	-4.86030617	2.9446E-05	0.00116438	LC	12m
Sting1	72512	0.59303794	4.95356131	4.85310603	3.0069E-05	0.0011807	LC	12m
Shc3	20418	0.72689421	8.00540328	4.81460042	3.3629E-05	0.0012699	LC	12m
Calcr	12311	-0.62075932	10.0152293	-4.8100442	3.4077E-05	0.00128302	LC	12m
Lratd1	105005	0.61598143	7.91623825	4.79533942	3.5564E-05	0.00132371	LC	12m
Plxnc1	54712	0.66228832	6.80532594	4.79388956	3.5714E-05	0.00132713	LC	12m
Ly6c2	100041546	0.88041557	8.39702501	4.77991896	3.7193E-05	0.00135774	LC	12m
Vtn	22370	0.59122719	7.90943003	4.773211	3.7924E-05	0.00137782	LC	12m
Mc4r	17202	0.73565874	5.44464308	4.75716771	3.9731E-05	0.00142673	LC	12m
Mfsd2a	76574	0.67315392	8.2947974	4.72745789	4.3307E-05	0.00151315	LC	12m
Adgrl4	170757	0.6535739	6.25996556	4.7103759	4.5505E-05	0.00155562	LC	12m
Tac1	21333	0.69367419	6.31259971	4.69587188	4.7459E-05	0.00160894	LC	12m
Spink10	328971	-0.62462786	7.01370963	-4.63714488	5.6255E-05	0.00184147	LC	12m
Nps	100043254	1.16937961	9.34647729	4.62323729	5.8564E-05	0.00188727	LC	12m
Cntnap5b	241175	0.58861954	6.90455146	4.62107147	5.8932E-05	0.00189645	LC	12m
Slc38a5	209837	0.5916827	5.86136681	4.58026181	6.6308E-05	0.00208675	LC	12m
Shisal2b	77803	-0.96737985	8.58678633	-4.56802809	6.8693E-05	0.0021382	LC	12m
Tmc3	233424	-0.78792142	7.94237804	-4.56254095	6.979E-05	0.00216055	LC	12m
Wfikkn2	278507	-0.59431292	7.30995642	-4.55034383	7.229E-05	0.00222288	LC	12m
Alox5ap	11690	0.73701726	6.5613048	4.52437876	7.7913E-05	0.00234519	LC	12m
Calb1	12307	0.61299696	6.78122682	4.51620938	7.9769E-05	0.0023798	LC	12m
Gpr101	245424	0.64739646	8.16301419	4.50330822	8.2791E-05	0.0024311	LC	12m
Gm20172	100504323	0.64097655	5.05766809	4.48221856	8.7976E-05	0.00254627	LC	12m
Lgals9	16859	0.66110677	7.18354785	4.47054552	9.0983E-05	0.00261115	LC	12m
Cpne5	240058	-0.60158597	8.22633038	-4.46642395	9.2068E-05	0.00263037	LC	12m
Npy	109648	1.1712082	7.69143097	4.46625234	9.2114E-05	0.00263037	LC	12m
C1ql3	227580	0.70778264	7.17707763	4.45588797	9.4902E-05	0.00268313	LC	12m

AW112010	107350	0.6782276	4.31335416	4.41983332	0.00010527	0.00287636	LC	12m
C3	12266	1.52733618	5.78218856	4.39577461	0.0001128	0.00301706	LC	12m
Cryab	12955	0.60424508	8.63838308	4.37699034	0.00011904	0.00313196	LC	12m
Ovgp1	12659	-0.70764172	8.55783029	-4.37352541	0.00012023	0.00315193	LC	12m
Stk32a	269019	-0.60964203	7.48525131	-4.37295199	0.00012043	0.00315193	LC	12m
Chst1	76969	0.61098865	8.75983164	4.343111	0.00013118	0.00333301	LC	12m
Nanos1	332397	-0.62155834	8.66324954	-4.32072752	0.00013986	0.00349999	LC	12m
Cfh	12628	0.62354125	5.36253047	4.30725122	0.00014536	0.00359323	LC	12m
Ch25h	12642	0.72634083	4.82448192	4.30618302	0.00014581	0.00360032	LC	12m
Radx	102871	-0.61639773	5.81896358	-4.30313277	0.00014708	0.00361594	LC	12m
Calca	12310	-0.63789721	8.78406531	-4.29313448	0.00015135	0.00368926	LC	12m
Fat1	14107	0.60426408	7.13822443	4.26393881	0.00016451	0.00393445	LC	12m
Cybrd1	73649	0.6123876	6.97940281	4.26271346	0.00016509	0.0039441	LC	12m
Kctd16	383348	0.58596085	6.07829455	4.26051843	0.00016612	0.00395247	LC	12m
Npb	208990	-0.96717731	5.97301332	-4.26050616	0.00016613	0.00395247	LC	12m
Htr2a	15558	0.59225508	6.75101213	4.25158816	0.00017041	0.00401664	LC	12m
Mir6994	102465601	0.82638763	7.08474095	4.25072688	0.00017083	0.00401898	LC	12m
Gast	14459	-0.62411182	6.7046087	-4.24603358	0.00017313	0.00405565	LC	12m
Cdkn3	72391	-0.61368657	7.23149547	-4.21055996	0.00019155	0.00434867	LC	12m
Lcn2	16819	0.7015406	4.96583739	4.19432812	0.00020061	0.00448778	LC	12m
Chrna6	11440	-1.1421099	9.76636456	-4.17856804	0.0002098	0.00460023	LC	12m
Slc6a2	20538	-0.85181958	11.3790813	-4.13931449	0.00023455	0.00490057	LC	12m
Cited2	17684	0.63627958	8.94972283	4.12697684	0.0002429	0.00497486	LC	12m
Dbh	13166	-0.66135199	12.0949121	-4.12427304	0.00024477	0.00499827	LC	12m
Ecell1	13599	0.6624899	7.92178325	4.11215829	0.00025332	0.00512386	LC	12m
Ifi207	226691	0.77075197	4.26273829	4.06274041	0.00029133	0.00570071	LC	12m
Ednra	13617	0.59016468	6.52783622	4.05774876	0.00029547	0.00575267	LC	12m
Erdr1	170942	0.9083137	9.6547083	4.05768512	0.00029552	0.00575267	LC	12m
Ccl8	20307	0.59859678	3.74949298	4.04361232	0.0003075	0.00591882	LC	12m
Slc17a6	140919	0.67177873	7.94101096	3.97143121	0.00037682	0.00683422	LC	12m
Hsd17b7	15490	-0.65970643	7.56767381	-3.934722	0.00041771	0.00738802	LC	12m
Znhit6	229937	-0.61561295	8.31100699	-3.92919698	0.00042423	0.00745708	LC	12m
Lgals1	16852	0.77398763	8.43584434	3.91010866	0.00044753	0.0077355	LC	12m
Chodl	246048	-0.60429066	8.9921807	-3.85436056	0.00052295	0.00859635	LC	12m

Cartpt	27220	0.68145281	8.53638971	3.85022741	0.00052902	0.00868348	LC	12m
Mir342	723909	0.78578085	7.69297994	3.72165785	0.00075579	0.01110684	LC	12m
Cd8b1	12526	0.71205643	5.6003898	3.66747655	0.00087747	0.01238115	LC	12m
Ajap1	230959	0.59761175	7.235602	3.64799477	0.00092571	0.01283793	LC	12m
Mir101c	100628572	0.61174058	4.14830539	3.50780636	0.00135694	0.01656502	LC	12m
Lcat	16816	0.60581026	8.02218641	3.48924355	0.00142691	0.0171439	LC	12m
Aasdhppt	67618	-0.59988588	7.88464185	-3.31024432	0.00230603	0.02388703	LC	12m
Ly86	17084	0.59700112	6.03241989	3.19199501	0.00315045	0.02982193	LC	12m
Tmem252	226040	0.60684982	5.02223715	3.18264684	0.00322853	0.03023902	LC	12m
Olfir690	56860	0.69884969	5.37289893	3.18103444	0.00324219	0.03034198	LC	12m
Mir153	387171	0.90787523	5.31445423	3.03507967	0.00473369	0.03950149	LC	12m
Ccl21a	18829	-1.04653382	6.31271739	-2.99068937	0.0053035	0.04275179	LC	12m
Crh	12918	0.74549313	6.88469701	2.92995003	0.00618885	0.04744783	LC	12m
Padi2	18600	0.8381169	7.78329177	2.90125767	0.00665392	0.04997032	LC	12m
Mir300	723833	0.59230649	6.67781964	2.79805915	0.0086126	0.0600382	LC	12m

Annex Data Table 3. TOP 30 miR-692 targets from mirDB database.

Target Rank	Target Score	miRNA Name	Gene Symbol	Gene Description
1	100	mmu-miR-692	Pcdh20	protocadherin 20
2	100	mmu-miR-692	Synj2bp	synaptojanin 2 binding protein
3	99	mmu-miR-692	Chrdl1	chordin-like 1
4	99	mmu-miR-692	Hoxd8	homeobox D8
5	99	mmu-miR-692	Grm4	glutamate receptor, metabotropic 4
6	99	mmu-miR-692	Bnc2	basonuclin 2
7	98	mmu-miR-692	Cnot9	CCR4-NOT transcription complex, subunit 9
8	98	mmu-miR-692	Adam10	a disintegrin and metallopeptidase domain 10
9	98	mmu-miR-692	Slc38a9	solute carrier family 38, member 9
10	98	mmu-miR-692	Galnt2	polypeptide N-acetylgalactosaminyltransferase 2
11	98	mmu-miR-692	Rsb1	rosbin, round spermatid basic protein 1
12	98	mmu-miR-692	Atxn3	ataxin 3
13	98	mmu-miR-692	Rpn2	ribophorin II
14	98	mmu-miR-692	Plp1	proteolipid protein (myelin) 1
15	98	mmu-miR-692	Phactr2	phosphatase and actin regulator 2

16	98	mmu-miR-692	Cask	calcium/calmodulin-dependent serine protein kinase (MAGUK family)
17	98	mmu-miR-692	Lbh	limb-bud and heart
18	98	mmu-miR-692	Slk	STE20-like kinase
19	98	mmu-miR-692	Cnr1	cannabinoid receptor 1 (brain)
20	98	mmu-miR-692	Pter	phosphotriesterase related
21	98	mmu-miR-692	Fut9	fucosyltransferase 9
22	97	mmu-miR-692	Nufip1	nuclear fragile X mental retardation protein interacting protein 1
23	97	mmu-miR-692	Rbm20	RNA binding motif protein 20
24	97	mmu-miR-692	Tbc1d8b	TBC1 domain family, member 8B
25	97	mmu-miR-692	Iqsec3	IQ motif and Sec7 domain 3
26	97	mmu-miR-692	Ankfy1	ankyrin repeat and FYVE domain containing 1
27	97	mmu-miR-692	Raly	hnRNP-associated with lethal yellow
28	97	mmu-miR-692	Adam22	a disintegrin and metallopeptidase domain 22
29	97	mmu-miR-692	Sec11c	SEC11 homolog C, signal peptidase complex subunit
30	97	mmu-miR-692	Hivep2	human immunodeficiency virus type I enhancer binding protein 2

Annex Data Table 4. DEGs ($p < 0.01$, $FC > |1.5|$) in tgNM mice NM-containing neurons compared to wt non pigmented neurons.

Gene Symbol	Entrez	logFC	AveExpr	t	P.Value	adj.P.Val	Region	Age
Mir1912	100526529	-2.03662244	5.45650934	-5.63950115	7.29E-05	0.60515287	SNneurons	3m
Pisd-ps3	66776	0.89241715	6.51763043	5.02031455	0.00021588	0.89655384	SNneurons	3m
Mir7652	102465760	1.20664769	4.19071233	4.54836752	0.00051109	0.99972667	SNneurons	3m
Gad2	14417	-0.84370788	5.49030414	-4.27728754	0.00084859	0.99972667	SNneurons	3m
Kcnab3	16499	-0.66205196	4.32619257	-4.14323502	0.00109355	0.99972667	SNneurons	3m
Eif2s3y	26908	-1.27890659	4.41846967	-3.7476308	0.00233314	0.99972667	SNneurons	3m

Nmnat2	226518	0.65228641	7.80223345	3.7199134	0.00246144	0.99972667	SNneurons	3m
Kdm5d	20592	-0.66154318	3.40422811	-3.66345509	0.00274541	0.99972667	SNneurons	3m
Ddx3y	26900	-1.04567782	3.42841695	-3.42196489	0.00438722	0.99972667	SNneurons	3m
Laptm4b	114128	0.76997269	9.44726863	3.36447629	0.00490666	0.99972667	SNneurons	3m
Snora16a	100310813	0.88364416	2.76610052	3.33410748	0.00520558	0.99972667	SNneurons	3m
Rnu3b4	19861	-0.69836823	5.26885404	-3.30024077	0.00556057	0.99972667	SNneurons	3m
Mir1927	100316784	-0.90573255	3.06573196	-3.26901021	0.0059094	0.99972667	SNneurons	3m
Gad1	14415	-0.65266428	5.74539165	-3.12436189	0.00783324	0.99972667	SNneurons	3m
Trav3-3	320898	1.08432173	5.48134263	3.12278156	0.00785739	0.99972667	SNneurons	3m
Syn2	20965	-0.63175947	5.69602423	-3.09493776	0.00829526	0.99972667	SNneurons	3m
Rnu3b2	19859	-0.71605173	5.38353767	-3.08020171	0.00853673	0.99972667	SNneurons	3m
Rnu3b3	19860	-0.71605173	5.38353767	-3.08020171	0.00853673	0.99972667	SNneurons	3m
Rnu3b1	19858	-0.71605173	5.38353767	-3.08020171	0.00853673	0.99972667	SNneurons	3m
Sptssb	66183	-0.62648809	4.1178988	-3.06975455	0.00871214	0.99972667	SNneurons	3m
Pcdhb4	93875	0.69820766	4.21717146	3.0634923	0.008819	0.99972667	SNneurons	3m
Xist	213742	2.44131644	4.19104323	3.04278711	0.00918168	0.99972667	SNneurons	3m
Hddc3	68695	-0.70028911	6.42426528	-3.03682787	0.00928878	0.99972667	SNneurons	3m
Nmnat2	226518	1.09659686	7.96638952	5.6692763	2.97E-05	0.08409193	SNneurons	12m
Rec114	73673	-0.81067464	4.46955614	-5.5577443	3.71E-05	0.08409193	SNneurons	12m
Lyz2	17105	1.3818979	3.60434067	5.44189762	4.69E-05	0.08409193	SNneurons	12m
Gm19825	100503674	0.82024672	5.93720384	5.42145058	4.89E-05	0.08409193	SNneurons	12m
Impact	16210	0.81359097	9.25548936	5.40395876	5.06E-05	0.08409193	SNneurons	12m

Slc9a7	236727	0.82317785	6.49372371	5.16834861	8.18E-05	0.09107585	SNneurons	12m
Dennd1a	227801	0.94813143	5.28542641	5.0102862	0.00011326	0.09107585	SNneurons	12m
Fgf5	14176	-0.76172392	4.29853925	-4.95926679	0.00012588	0.09107585	SNneurons	12m
Lnpep	240028	0.9161698	5.18804339	4.94251366	0.00013033	0.09107585	SNneurons	12m
Gm19445	100502904	0.92618643	3.60967805	4.92328301	0.00013564	0.09107585	SNneurons	12m
Grp	225642	-0.83293423	5.82219083	-4.91856973	0.00013697	0.09107585	SNneurons	12m
Scn2a	110876	0.79982513	6.33484337	4.91632088	0.00013761	0.09107585	SNneurons	12m
Fam135b	70363	0.91606692	6.56226006	4.87765674	0.00014914	0.09107585	SNneurons	12m
Rtn4rl1	237847	-0.79343798	4.18351005	-4.86378015	0.00015351	0.09107585	SNneurons	12m
Pex5l	58869	0.80940717	6.67166243	4.82577853	0.00016617	0.09201445	SNneurons	12m
Cacna1e	12290	0.86703212	6.43013313	4.67007869	0.00023025	0.10447637	SNneurons	12m
A830029E22Rik	320566	-1.05077157	3.02172266	-4.65039583	0.00023998	0.10447637	SNneurons	12m
Nbea	26422	0.75073195	6.22362263	4.58065981	0.00027797	0.10447637	SNneurons	12m
Ubqln1	56085	0.61622782	6.50646401	4.58009294	0.0002783	0.10447637	SNneurons	12m
Crebbp	12914	0.70553916	7.08988593	4.50266211	0.00032778	0.10447637	SNneurons	12m
Gtf2i	14886	0.68908231	6.2298567	4.48228762	0.00034223	0.10447637	SNneurons	12m
Necab1	69352	0.80255017	7.08405424	4.47394224	0.00034834	0.10447637	SNneurons	12m
Mir6352	102465180	1.52241892	4.42966753	4.46157882	0.00035758	0.10447637	SNneurons	12m
Lyst	17101	0.83026696	4.89236003	4.45344911	0.0003638	0.10447637	SNneurons	12m
Usp9x	22284	0.76060358	6.42020707	4.4514236	0.00036537	0.10447637	SNneurons	12m
Fry	320365	0.71042117	6.29202345	4.44967938	0.00036672	0.10447637	SNneurons	12m
Gfap	14580	0.89159657	4.95506715	4.43239853	0.00038041	0.10447637	SNneurons	12m

Cntnap2	66797	0.82801082	6.86359305	4.42607279	0.00038556	0.10447637	SNneurons	12m
Mir154	387172	1.56404399	3.35213617	4.36837739	0.00043584	0.10447637	SNneurons	12m
Timm21	67105	-1.13420329	6.24670031	-4.33936128	0.00046359	0.10447637	SNneurons	12m
Golph3l	229593	0.72158898	5.19909496	4.33352058	0.00046939	0.10447637	SNneurons	12m
Mir493	100124466	2.17446236	5.59222657	4.31993027	0.00048318	0.10447637	SNneurons	12m
Ppme1	72590	0.85355883	6.66684235	4.31295628	0.00049041	0.10447637	SNneurons	12m
Fat4	329628	0.93182061	5.61118566	4.30738219	0.00049627	0.10447637	SNneurons	12m
Hmgcs1	208715	0.68021761	6.6142877	4.29470135	0.00050986	0.10447637	SNneurons	12m
Brinp1	56710	0.82683711	7.67816839	4.29074726	0.00051418	0.10447637	SNneurons	12m
Stbd1	52331	-0.75721783	5.08255936	-4.27606292	0.00053054	0.10447637	SNneurons	12m
Cpne4	74020	0.65125484	7.13088478	4.27037441	0.00053701	0.10447637	SNneurons	12m
Lrrtm2	107065	0.70329389	6.01752675	4.26827673	0.00053942	0.10447637	SNneurons	12m
Huwe1	59026	0.65173152	6.38714643	4.26485483	0.00054337	0.10447637	SNneurons	12m
Ap3s2	11778	0.90941005	6.93493167	4.25182482	0.0005587	0.10447637	SNneurons	12m
Pld5	319455	0.73211585	5.83226504	4.23095453	0.00058415	0.10447637	SNneurons	12m
Rnfl13a2	66381	-0.63264175	4.67430237	-4.22568371	0.00059077	0.10447637	SNneurons	12m
Gpatch8	237943	0.64318306	5.84999771	4.21996859	0.00059802	0.10447637	SNneurons	12m
Lrrc7	242274	0.81393637	5.89948905	4.19107725	0.00063611	0.10447637	SNneurons	12m
Usp32	237898	0.68736101	5.82108468	4.1908169	0.00063647	0.10447637	SNneurons	12m
Arfgef3	215821	0.69585772	6.86183829	4.18331533	0.00064676	0.10447637	SNneurons	12m
Lncpint	232685	0.64061219	5.45978462	4.17161679	0.00066314	0.10447637	SNneurons	12m
Cryga	12964	-0.82582435	4.31850252	-4.16797592	0.00066833	0.10447637	SNneurons	12m

Mir341	723846	1.07308627	8.62229739	4.16565547	0.00067166	0.10447637	SNneurons	12m
Clock	12753	0.77491245	6.09367813	4.1576001	0.00068333	0.10447637	SNneurons	12m
Vps13b	666173	0.59410036	5.15352435	4.15751049	0.00068346	0.10447637	SNneurons	12m
Arhgef11	213498	0.7170143	6.42936429	4.14904212	0.00069596	0.10447637	SNneurons	12m
Galnt16	270049	0.72580557	5.36386072	4.14751597	0.00069824	0.10447637	SNneurons	12m
Acs14	50790	0.75079215	6.30327785	4.13601176	0.00071565	0.10447637	SNneurons	12m
Mycbp2	105689	0.75739239	6.82691989	4.13433991	0.00071821	0.10447637	SNneurons	12m
Pgm211	70974	0.6475973	7.08537136	4.11217481	0.00075313	0.10447637	SNneurons	12m
Fam71e1	75538	-0.61342698	4.79026644	-4.10067226	0.00077192	0.10447637	SNneurons	12m
Mir300	723833	2.14893197	4.54882414	4.07766059	0.00081094	0.10447637	SNneurons	12m
Ash11	192195	0.71121832	5.93575774	4.05433881	0.00085253	0.10447637	SNneurons	12m
Gm16488	791267	0.69424214	4.42662895	4.05138876	0.00085794	0.10447637	SNneurons	12m
Rrn3	106298	0.77212643	6.6846337	4.04818779	0.00086385	0.10447637	SNneurons	12m
Efr3b	668212	0.75281111	5.93858593	4.0438999	0.00087183	0.10447637	SNneurons	12m
Mir882	100124461	1.07260672	3.14568156	4.03091704	0.00089646	0.10447637	SNneurons	12m
Zdhhc15	108672	0.68790293	4.27562201	4.0240333	0.0009098	0.10447637	SNneurons	12m
Fgf14	14169	0.65819484	5.59094097	4.01299925	0.0009316	0.10447637	SNneurons	12m
Gabbr2	242425	0.71990915	7.94137639	4.01255911	0.00093248	0.10447637	SNneurons	12m
Atg2b	76559	0.7125307	5.8560946	4.0108399	0.00093593	0.10447637	SNneurons	12m
Rbms3	207181	0.66143625	7.0257076	4.00823336	0.00094118	0.10447637	SNneurons	12m
Kcnj6	16522	0.68124378	5.99074184	4.00479094	0.00094816	0.10447637	SNneurons	12m
Hectd4	269700	0.83548787	6.8647606	3.99984746	0.00095828	0.10447637	SNneurons	12m

Aff4	93736	0.69950579	7.10264813	3.9949994	0.00096831	0.10447637	SNneurons	12m
Gm10723	100038361	0.93821581	6.75396675	3.97692725	0.00100662	0.10447637	SNneurons	12m
Csmd1	94109	0.62170471	5.3879248	3.97012385	0.00102144	0.10447637	SNneurons	12m
Wdr7	104082	0.87274356	6.47985829	3.96776172	0.00102664	0.10447637	SNneurons	12m
Dync1h1	13424	0.81437412	7.24378405	3.96474979	0.0010333	0.10447637	SNneurons	12m
St6gal2	240119	0.61427823	5.7423041	3.96345592	0.00103618	0.10447637	SNneurons	12m
Mapk9	26420	0.73354219	8.48870618	3.9616145	0.00104029	0.10447637	SNneurons	12m
Ascc3	77987	0.60346908	4.46526843	3.94098106	0.00108744	0.1046073	SNneurons	12m
Gm16294	432945	-1.12967921	2.68896753	-3.93577869	0.00109967	0.1046073	SNneurons	12m
Miga1	215708	0.61652897	6.37746664	3.9348027	0.00110198	0.1046073	SNneurons	12m
Clstn2	64085	0.74500066	7.29023913	3.92856684	0.00111685	0.1046073	SNneurons	12m
Mir6941	102465567	-0.61230517	6.90947527	-3.92688878	0.00112088	0.1046073	SNneurons	12m
Cbl	12402	0.62690713	6.83832759	3.91576255	0.00114801	0.10478461	SNneurons	12m
Ncam2	17968	0.66445715	6.83876717	3.9074191	0.00116879	0.10552153	SNneurons	12m
Glg1	20340	0.68052089	6.67445703	3.88423882	0.00122853	0.10613669	SNneurons	12m
ErbB4	13869	0.87342696	6.79499546	3.8743978	0.0012548	0.10613669	SNneurons	12m
Mir7002	102465982	-0.62524959	4.87499807	-3.86831937	0.00127132	0.10613669	SNneurons	12m
Wasf3	245880	0.70715991	7.29118264	3.85869275	0.00129792	0.10613669	SNneurons	12m
Marf1	223989	0.61404373	7.26683782	3.85355889	0.00131233	0.10613669	SNneurons	12m
Dgkh	380921	0.59231573	5.33914458	3.84474713	0.00133745	0.10613669	SNneurons	12m
Mir872	100124456	0.88940823	2.10623565	3.84014882	0.00135074	0.10613669	SNneurons	12m
Nploc4	217365	0.81400287	6.52931024	3.83790194	0.00135729	0.10613669	SNneurons	12m

Kmt2a	214162	0.64442749	7.12174612	3.83748179	0.00135852	0.10613669	SNneurons	12m
Cadps	27062	0.7292363	8.62084281	3.82853856	0.00138491	0.10613669	SNneurons	12m
Mir453	100124484	0.66281926	10.1176842	3.82231063	0.0014036	0.10613669	SNneurons	12m
Snord88c	100217434	-0.70396972	4.41929189	-3.81235064	0.00143401	0.10613669	SNneurons	12m
Tnpo2	212999	0.73100578	6.58117434	3.80677494	0.00145132	0.10613669	SNneurons	12m
Mir665	751555	0.94042694	7.18741587	3.8061016	0.00145342	0.10613669	SNneurons	12m
Acaca	107476	0.59866171	5.21765107	3.80369254	0.00146098	0.10613669	SNneurons	12m
Ppp6r3	52036	0.58834112	5.25548471	3.79410171	0.00149145	0.10613669	SNneurons	12m
Ube4b	63958	0.64780547	6.70570977	3.76892807	0.0015745	0.10613669	SNneurons	12m
Srgap3	259302	0.77794776	5.8021927	3.76759457	0.00157902	0.10613669	SNneurons	12m
Gm7697	665578	0.69578603	3.77891967	3.76750476	0.00157933	0.10613669	SNneurons	12m
Slc32a1	22348	-0.85992057	5.74119427	-3.76689849	0.00158139	0.10613669	SNneurons	12m
Cdkn3	72391	-0.83150251	4.39832991	-3.74820406	0.00164633	0.10613669	SNneurons	12m
Kdm7a	338523	0.60509236	4.74938783	3.74209064	0.00166814	0.10613669	SNneurons	12m
Nf1	18015	0.6858518	6.40033627	3.74198541	0.00166852	0.10613669	SNneurons	12m
Gpr26	233919	0.6478931	6.6705431	3.73961655	0.00167705	0.10613669	SNneurons	12m
Dcaf5	320808	0.6487153	6.15631442	3.73852216	0.00168101	0.10613669	SNneurons	12m
Arfgef2	99371	0.6225695	6.00759108	3.71837271	0.00175554	0.10613669	SNneurons	12m
Unc80	329178	0.75715413	7.23822121	3.71539862	0.00176681	0.10613669	SNneurons	12m
Pi4ka	224020	0.67882003	6.92999898	3.71401254	0.0017721	0.10613669	SNneurons	12m
Psd3	234353	0.80766802	7.78194376	3.70937305	0.00178989	0.10613669	SNneurons	12m
Stxbp1	20910	0.70936079	9.46414113	3.70651061	0.00180095	0.10613669	SNneurons	12m

Etnk1	75320	0.99820929	7.1092614	3.70556611	0.00180462	0.10613669	SNneurons	12m
Ralgps1	241308	0.59762586	5.36542358	3.69374604	0.00185114	0.10613669	SNneurons	12m
Dmx12	235380	0.5868119	7.48998036	3.69027701	0.00186501	0.10613669	SNneurons	12m
Dst	13518	0.67275897	5.9114606	3.6851858	0.00188557	0.10613669	SNneurons	12m
Mir543	723881	1.15309292	3.18397894	3.68406825	0.00189011	0.10613669	SNneurons	12m
Dzank1	241688	0.59944429	7.31754047	3.68294456	0.00189469	0.10613669	SNneurons	12m
Zw10	26951	0.6615505	5.56679955	3.67866715	0.00191222	0.10613669	SNneurons	12m
Dock4	238130	0.75858527	5.61270415	3.67756944	0.00191675	0.10613669	SNneurons	12m
Mir3091	100526556	-0.80049699	6.26636348	-3.67099389	0.00194408	0.10624075	SNneurons	12m
Washc4	319277	0.68324315	4.48717723	3.6664055	0.00196338	0.10624075	SNneurons	12m
Tnks	21951	0.74221145	5.85273359	3.66548284	0.00196728	0.10624075	SNneurons	12m
Sv2c	75209	0.89374958	8.36526375	3.64727722	0.00204593	0.10647668	SNneurons	12m
Mir379	723858	0.8660345	3.108648	3.64304406	0.00206466	0.10647668	SNneurons	12m
Mir344c	100526506	1.10978947	4.35125872	3.636611	0.00209346	0.10647668	SNneurons	12m
Cacna1b	12287	0.62374575	6.44545706	3.63461656	0.00210247	0.10647668	SNneurons	12m
Herc1	235439	0.6592372	5.77990778	3.62142672	0.00216303	0.10647668	SNneurons	12m
Zfp867	237775	-0.73203255	3.49232004	-3.61840608	0.00217714	0.10647668	SNneurons	12m
Nedd4	17999	0.61586024	7.19491779	3.61766382	0.00218062	0.10647668	SNneurons	12m
Abhd1	57742	-0.61424437	4.88382679	-3.61114606	0.00221144	0.10647668	SNneurons	12m
Thrsp	21835	-0.83885185	4.44164412	-3.60785761	0.00222715	0.10647668	SNneurons	12m
Gm10862	100038349	0.64433186	4.29469156	3.60726646	0.00222999	0.10647668	SNneurons	12m
Vps33a	77573	0.81314833	6.92917463	3.60551706	0.0022384	0.10647668	SNneurons	12m

Grik3	14807	0.76202348	6.84544616	3.60445382	0.00224353	0.10647668	SNneurons	12m
Mir1954	100316776	0.59917578	10.7392275	3.59859656	0.002272	0.10647668	SNneurons	12m
Myo5a	17918	0.61009827	6.26862836	3.59575564	0.00228593	0.10647668	SNneurons	12m
Wdr35	74682	0.58961613	5.62793125	3.5939887	0.00229465	0.10647668	SNneurons	12m
Nrtn	18188	-0.59063636	4.92149864	-3.58765259	0.00232616	0.10648219	SNneurons	12m
Snora68	104370	-0.69036996	5.04507922	-3.58750032	0.00232692	0.10648219	SNneurons	12m
Cartpt	27220	-0.83489544	6.63115198	-3.58167523	0.00235628	0.10652709	SNneurons	12m
Cnm1	83674	0.70271954	6.08839398	3.58085289	0.00236046	0.10652709	SNneurons	12m
Cyfp2	76884	0.61701718	7.22103868	3.57046077	0.00241385	0.10652709	SNneurons	12m
Mir138-2	723956	1.16208607	5.43964852	3.56909853	0.00242094	0.10652709	SNneurons	12m
Usp34	17847	0.65128908	5.99907989	3.56674448	0.00243323	0.10652709	SNneurons	12m
Kcnma1	16531	0.59888038	6.4700254	3.56606204	0.00243681	0.10652709	SNneurons	12m
Plxna2	18845	0.62507883	6.41204471	3.55718065	0.00248384	0.10745183	SNneurons	12m
Snx19	102607	0.61253419	5.74268461	3.54829022	0.00253182	0.10895998	SNneurons	12m
Mir1188	100316669	0.79772984	7.11043948	3.53369115	0.00261262	0.10953069	SNneurons	12m
Fam167a	219148	0.66864278	6.05683827	3.53067809	0.00262961	0.10953069	SNneurons	12m
Vcp	269523	0.59430462	6.99814277	3.52951579	0.00263619	0.10953069	SNneurons	12m
Mir6388	102465205	-0.58655896	4.29455134	-3.52793219	0.00264519	0.10953069	SNneurons	12m
Pappa	18491	0.63481182	5.95823859	3.52322476	0.00267212	0.10953069	SNneurons	12m
Gm15319	100040599	0.74334213	4.39702881	3.5152269	0.0027185	0.10953069	SNneurons	12m
Ap2b1	71770	0.70436698	8.0561477	3.51408944	0.00272516	0.10953069	SNneurons	12m
Dpysl2	12934	0.75530066	8.70148769	3.50889063	0.0027558	0.10953069	SNneurons	12m

Gm9938	791290	0.99690317	5.06197725	3.50884582	0.00275607	0.10953069	SNneurons	12m
Kif1b	16561	0.75279072	7.21868404	3.49855409	0.00281776	0.11144925	SNneurons	12m
Kif21a	16564	0.76512565	7.52131595	3.49421516	0.00284418	0.11145326	SNneurons	12m
Mir6928	102466767	1.29492707	3.71768847	3.47925491	0.00293718	0.11145326	SNneurons	12m
Map3k13	71751	0.64512612	5.24077919	3.47523804	0.00296266	0.11145326	SNneurons	12m
8430431K14Rik	78103	0.61369816	2.35416159	3.47354031	0.00297349	0.11145326	SNneurons	12m
Rragb	245670	0.76613281	5.30142902	3.46772765	0.00301089	0.11145326	SNneurons	12m
A330041J22Rik	319556	-0.60838663	5.83545546	-3.46494031	0.00302899	0.11145326	SNneurons	12m
Hist1h1c	50708	-0.83888978	5.99477106	-3.46479936	0.00302991	0.11145326	SNneurons	12m
2610005L07Rik	381598	0.60790332	8.36652102	3.46292206	0.00304216	0.11145326	SNneurons	12m
Neo1	18007	0.72384044	5.99691221	3.46079348	0.00305611	0.11145326	SNneurons	12m
Chrb3	108043	0.77256176	8.05102037	3.45606073	0.00308737	0.11145326	SNneurons	12m
Mblac1	330216	-0.69257804	6.8118919	-3.4523919	0.00311181	0.11145326	SNneurons	12m
Fgf11	14166	-0.62597692	5.53569907	-3.45198676	0.00311452	0.11145326	SNneurons	12m
Robo2	268902	0.67513936	7.03172308	3.44982024	0.00312906	0.11145326	SNneurons	12m
Gpi1	14751	0.58989872	9.1109576	3.44935961	0.00313216	0.11145326	SNneurons	12m
Cntnap4	170571	0.6381484	6.77300759	3.4425993	0.003178	0.11145326	SNneurons	12m
Kif1a	16560	0.76644131	8.27929352	3.44064243	0.0031914	0.11145326	SNneurons	12m
Fam84a	105005	-0.97719437	5.76983816	-3.43996562	0.00319604	0.11145326	SNneurons	12m
Gns	75612	0.61522939	6.49621255	3.42921495	0.00327074	0.11145326	SNneurons	12m
Dctn4	67665	0.63495412	7.55961609	3.42576739	0.00329506	0.11145326	SNneurons	12m
Gm9495	670593	0.59755941	3.64598706	3.42398839	0.00330768	0.11145326	SNneurons	12m

Plcb4	18798	0.63047934	7.03850807	3.42352212	0.00331099	0.11145326	SNneurons	12m
D630041G03Rik	320749	0.94605365	4.3890046	3.42226773	0.00331993	0.11145326	SNneurons	12m
Fnip1	216742	0.59980907	4.23017135	3.41975711	0.00333789	0.11145326	SNneurons	12m
Amph	218038	0.62501665	6.45860856	3.41601159	0.00336485	0.11179388	SNneurons	12m
Ogfod1	270086	0.70008446	7.95278877	3.40939679	0.00341301	0.11208257	SNneurons	12m
Cd68	12514	1.0005025	4.88321011	3.4051902	0.00344399	0.11208257	SNneurons	12m
Pno1	66249	-0.58703935	4.45645015	-3.40060073	0.0034781	0.11208257	SNneurons	12m
Kif5c	16574	0.67046257	6.8385323	3.3982296	0.00349586	0.11208257	SNneurons	12m
Igsf10	242050	0.74638282	4.43880702	3.37603057	0.00366652	0.11541839	SNneurons	12m
Lrp1b	94217	0.59392781	4.54013537	3.3732437	0.00368852	0.11541839	SNneurons	12m
Soat1	20652	0.58586543	5.49387632	3.36957036	0.00371772	0.11541839	SNneurons	12m
Snord11612	64245	1.33269937	8.72355388	3.36833834	0.00372757	0.11541839	SNneurons	12m
Snord11611	64244	1.33269937	8.72355388	3.36833834	0.00372757	0.11541839	SNneurons	12m
Gm5512	433224	-0.61228606	6.07172444	-3.36666195	0.003741	0.11541839	SNneurons	12m
Fabp7	12140	-0.87177113	6.67544356	-3.36392644	0.00376303	0.11541839	SNneurons	12m
Sox6	20679	0.64794392	5.84906826	3.35336665	0.00384927	0.11583022	SNneurons	12m
Gbf1	107338	0.67104661	6.39701289	3.3393775	0.00396654	0.11669251	SNneurons	12m
Sptbn1	20742	0.73121048	6.71168802	3.33331233	0.00401848	0.11747314	SNneurons	12m
Exoc2	66482	0.64638578	5.35524406	3.31593906	0.004171	0.11808315	SNneurons	12m
1700124L16Rik	67934	-0.72044394	6.00457717	-3.31544467	0.00417542	0.11808315	SNneurons	12m
Pigf	18701	-0.78224203	6.63509829	-3.31033402	0.00422141	0.11845625	SNneurons	12m
Rbm4	19653	1.0046664	5.42331977	3.30053693	0.00431099	0.12015785	SNneurons	12m

Peg3	18616	0.60216364	8.28985638	3.28551659	0.00445197	0.1208351	SNneurons	12m
Drp2	13497	0.59266948	5.85609355	3.27532089	0.00455025	0.1208351	SNneurons	12m
Igfbp5	16011	0.60419002	6.91439829	3.27498762	0.0045535	0.1208351	SNneurons	12m
Eef2	13629	0.62065146	8.27405416	3.26832019	0.00461898	0.1217943	SNneurons	12m
Rbp1	19659	-0.59212522	4.87093349	-3.26026501	0.00469932	0.12313094	SNneurons	12m
Snrpf	69878	-0.59770366	5.77844325	-3.24782866	0.00482607	0.12333782	SNneurons	12m
Mir544	100124450	1.05665994	9.38361641	3.2438792	0.00486702	0.12333782	SNneurons	12m
Gabra3	14396	0.60283607	8.1753977	3.24325107	0.00487356	0.12333782	SNneurons	12m
2900009J06Rik	100502745	-0.64610727	3.82291235	-3.24253655	0.00488102	0.12333782	SNneurons	12m
Atp6v0a1	11975	0.63933698	7.71888738	3.24228323	0.00488366	0.12333782	SNneurons	12m
Ints3	229543	0.60051787	5.89127526	3.24228317	0.00488367	0.12333782	SNneurons	12m
D130012P04Rik	319377	0.70420819	3.22248614	3.23710364	0.00493808	0.12333782	SNneurons	12m
Dnm1	13429	0.63721852	8.12804518	3.23550138	0.00495503	0.12333782	SNneurons	12m
Gm10654	665828	-0.61591053	3.41188044	-3.23223083	0.00498981	0.12333782	SNneurons	12m
Pdxk	216134	0.71206249	6.85704398	3.22976676	0.00501617	0.12333782	SNneurons	12m
Rictor	78757	0.64900827	4.56950687	3.22679323	0.00504817	0.12333782	SNneurons	12m
Adamts6	108154	0.61972037	4.49976612	3.21874259	0.00513581	0.12366231	SNneurons	12m
Snord35b	27212	-0.71165413	4.68185276	-3.21846068	0.00513891	0.12366231	SNneurons	12m
Dscam	13508	0.62717083	6.56381744	3.21695665	0.00515546	0.12366231	SNneurons	12m
Sstr2	20606	-0.58541659	4.05992361	-3.20275043	0.00531437	0.12423603	SNneurons	12m
Lamtor4	66096	-0.68127051	5.95937665	-3.20152628	0.00532829	0.12423603	SNneurons	12m
Apa1	319924	0.66244562	7.18209208	3.2007278	0.00533739	0.12423603	SNneurons	12m

Arnt	11863	0.59308248	5.29957124	3.19681254	0.00538222	0.12423603	SNneurons	12m
Slc36a4	234967	0.60180479	7.40781397	3.19155806	0.00544296	0.12461622	SNneurons	12m
Ret	19713	0.76160215	9.54927988	3.18867185	0.00547662	0.12461622	SNneurons	12m
App	11820	0.72555553	8.57676092	3.18720641	0.00549378	0.12461622	SNneurons	12m
C1ql3	227580	-0.7683925	5.33607281	-3.17210233	0.00567381	0.12562119	SNneurons	12m
Plekhh2	213556	0.6510298	4.9689533	3.17202581	0.00567474	0.12562119	SNneurons	12m
Agk	69923	0.62777291	7.51433286	3.17137965	0.00568257	0.12562119	SNneurons	12m
Cntnap1	53321	0.606767	6.2647797	3.17104093	0.00568668	0.12562119	SNneurons	12m
Ahl1	52906	0.58601539	7.43482602	3.16550028	0.00575432	0.12603941	SNneurons	12m
Nell2	54003	0.81786301	6.19989263	3.15997739	0.00582252	0.12693398	SNneurons	12m
Edem3	66967	0.59501508	6.33950877	3.14426359	0.00602095	0.12862704	SNneurons	12m
Phlpp2	244650	0.6484526	5.33842033	3.12586773	0.00626169	0.12929882	SNneurons	12m
Ubqln2	54609	0.62592877	7.3303563	3.11532379	0.00640391	0.13005094	SNneurons	12m
Zfp106	20402	0.6344767	5.86194387	3.11417019	0.00641966	0.13005282	SNneurons	12m
Atad3aos	70448	-0.70359268	4.24556781	-3.09737368	0.00665333	0.13193294	SNneurons	12m
Gucy2c	14917	0.71506747	6.19316309	3.07451281	0.00698481	0.13367706	SNneurons	12m
Mrln	69563	-0.92087173	6.18563745	-3.06789553	0.00708374	0.13436297	SNneurons	12m
Cntnap5a	636808	0.67439925	5.73662785	3.05957255	0.00721012	0.13498644	SNneurons	12m
Mir598	100124452	0.65705618	5.89507366	3.04692657	0.00740637	0.1352672	SNneurons	12m
Mir31	723895	-0.6336936	2.91011865	-3.04332613	0.0074632	0.1352672	SNneurons	12m
Cs	12974	0.58881696	7.42812745	3.02173393	0.00781302	0.13604803	SNneurons	12m
Acp2	11432	0.72755814	5.02912659	3.01046251	0.00800194	0.13675232	SNneurons	12m

Ifitm2	80876	-0.60588418	4.41091084	-3.00971504	0.00801462	0.13675232	SNneurons	12m
Ankrd28	105522	0.71729064	4.62948243	3.00903773	0.00802613	0.13675232	SNneurons	12m
Eef1akmt2	72096	-0.60446617	5.7552782	-2.9974114	0.00822626	0.13675232	SNneurons	12m
Tmem150c	231503	0.60902191	6.23086609	2.9944438	0.00827811	0.13675232	SNneurons	12m
Gm19816	100503654	0.66671784	4.65763152	2.99288232	0.00830553	0.13687641	SNneurons	12m
Snora7a	100217451	-0.69603751	4.07389772	-2.98903065	0.00837353	0.13691045	SNneurons	12m
Tubb3	22152	0.69204063	7.51802624	2.98286868	0.00848344	0.13762397	SNneurons	12m
Tctex1d2	66061	-0.61742422	7.14822896	-2.97661153	0.0085965	0.13810925	SNneurons	12m
2900055J20Rik	73001	-1.00081834	4.49170384	-2.9743829	0.00863711	0.1381553	SNneurons	12m
Gm20290	100504566	0.77005049	4.6764437	2.96578344	0.00879561	0.1381553	SNneurons	12m
Csrnp3	77771	0.60090171	5.70168314	2.96513661	0.00880765	0.1381553	SNneurons	12m
Mir329	723842	0.91057402	7.66591537	2.96249644	0.00885694	0.1381553	SNneurons	12m
Hsbp111	66255	-0.76026023	4.00638853	-2.96005168	0.00890282	0.1381553	SNneurons	12m
Mir342	723909	0.81639773	5.73837953	2.95850202	0.00893202	0.1381553	SNneurons	12m
Cpeb4	67579	0.61761834	5.83236839	2.94790771	0.00913419	0.13999861	SNneurons	12m
Snord98	100217463	1.07762797	2.37497392	2.93781704	0.00933088	0.14139745	SNneurons	12m
Mir7668	102465770	-0.61115811	3.46555612	-2.93452461	0.00939594	0.14139745	SNneurons	12m
Mir6361	102465186	-0.59139188	4.6335838	-2.93283344	0.00942953	0.14139745	SNneurons	12m
March4	381270	0.7287671	7.21124192	2.92727934	0.00954068	0.1420875	SNneurons	12m
Hspa1a	193740	-0.58769884	3.70168822	-2.90932989	0.00990863	0.14494585	SNneurons	12m
Nmnat2	226518	0.9268523	8.0166549	6.43363993	1.33E-05	0.11076125	SNneurons	20m
Ift57	73916	-0.61682834	7.05724215	-5.02746482	0.00016706	0.40905655	SNneurons	20m

Chrna3	110834	-0.6087248	7.00172774	-4.95445637	0.00019186	0.40905655	SNneurons	20m
Gm9958	791294	-0.74912105	3.56333883	-4.18815012	0.00085074	0.50710328	SNneurons	20m
Mir679	751539	0.63460149	4.05713125	3.98399381	0.00127714	0.50710328	SNneurons	20m
Bcl1	100568459	0.58846233	8.32364127	3.91718062	0.0014597	0.50710328	SNneurons	20m
Snord35a	27211	-0.84461342	4.43137071	-3.91515187	0.00146564	0.50710328	SNneurons	20m
Acadl	11363	-0.86492066	5.7256087	-3.89919124	0.00151324	0.50710328	SNneurons	20m
Mir431	723866	0.60751168	3.36644431	3.85341669	0.00165865	0.50710328	SNneurons	20m
Anxa1	16952	-0.89053499	5.98878548	-3.75542921	0.00201937	0.50710328	SNneurons	20m
Mir7236	102465713	-0.59703291	2.53057996	-3.65382127	0.00247765	0.52555618	SNneurons	20m
Aurkaip1	66077	-0.63498598	7.50684473	-3.65147652	0.00248939	0.52555618	SNneurons	20m
Mir669h	100316831	0.77729115	8.92349447	3.59450448	0.00279235	0.52555618	SNneurons	20m
Mir341	723846	0.70894074	8.58852186	3.57190741	0.00292257	0.52555618	SNneurons	20m
Pigf	18701	-0.67770965	6.60167176	-3.50918792	0.00331691	0.55568989	SNneurons	20m
Akr1e1	56043	-0.9683167	6.36759259	-3.46622156	0.00361749	0.56896665	SNneurons	20m
Mir6371	102465193	-0.75306329	2.56202618	-3.45118376	0.00372903	0.56896665	SNneurons	20m
Rbp4	19662	-0.81093033	7.32031981	-3.28382848	0.00522858	0.56896665	SNneurons	20m
Necab1	69352	0.81951902	7.0687159	3.25782836	0.00551036	0.56896665	SNneurons	20m
Mir665	751555	0.65235478	7.13373206	3.24322354	0.00567523	0.56896665	SNneurons	20m
Mir8115	102465902	-0.64130423	5.71084993	-3.2057982	0.00612044	0.56896665	SNneurons	20m
Mir466f-1	100124486	0.87255478	8.2060099	3.10472273	0.00750367	0.56986718	SNneurons	20m
Gm16503	100038537	-0.62101771	3.61204983	-3.05610304	0.00827515	0.56986718	SNneurons	20m
Tyrobp	22177	1.81945591	6.10553029	11.0866145	1.74E-07	0.00144171	VTAneurons	3m

Fcer1g	14127	0.98507263	4.23651521	6.76346045	2.49E-05	0.08985784	VTAneurons	3m
Bcl2a1a	12044	1.31838524	4.18726627	6.47089891	3.75E-05	0.08985784	VTAneurons	3m
Mir677	751518	1.66152423	4.51746432	6.22544091	5.33E-05	0.08985784	VTAneurons	3m
Lilrb4a	14728	1.38234364	2.95460589	6.17775809	5.71E-05	0.08985784	VTAneurons	3m
Ctss	13040	1.07902003	6.37345193	6.09095695	6.49E-05	0.08985784	VTAneurons	3m
Gm20172	100504323	-1.06994228	4.46051936	-5.61095009	0.00013377	0.15023328	VTAneurons	3m
Lyz2	17105	1.14248094	3.37762821	5.56008208	0.0001447	0.15023328	VTAneurons	3m
Mir6896	102466987	1.63968015	4.30489315	5.29991062	0.00021746	0.20068691	VTAneurons	3m
Ly86	17084	1.3673979	4.22410085	5.13122929	0.00028463	0.23641659	VTAneurons	3m
Itih3	16426	0.69375465	5.48277141	4.99046721	0.00035742	0.26988683	VTAneurons	3m
Bmp7	12162	-0.95106241	4.9492013	-4.92540129	0.00039747	0.27511477	VTAneurons	3m
C1qb	12260	0.86477119	4.54502099	4.83006021	0.00046489	0.28427291	VTAneurons	3m
Mir6417	102466648	-0.89799038	4.32311938	-4.81175475	0.00047915	0.28427291	VTAneurons	3m
Plip	67801	0.75555841	5.99420826	4.71566704	0.00056195	0.29991288	VTAneurons	3m
Mir325	723929	-1.24981234	7.64637724	-4.69905765	0.00057773	0.29991288	VTAneurons	3m
Nmnat2	226518	0.79654746	7.66476936	4.59626836	0.00068625	0.30683847	VTAneurons	3m
Rab1b	76308	0.67602517	6.52894417	4.56052463	0.00072883	0.30683847	VTAneurons	3m
Gfap	14580	0.9705544	4.97775045	4.53500819	0.00076091	0.30683847	VTAneurons	3m
Man2b1	17159	0.68831032	5.81645959	4.52976391	0.00076768	0.30683847	VTAneurons	3m
Gm14399	100043761	0.64968731	7.50896323	4.52355776	0.00077578	0.30683847	VTAneurons	3m
4930426L09Rik	74629	0.69477405	3.48584385	4.41377381	0.00093479	0.35292573	VTAneurons	3m
Ltv1	353258	0.67234809	6.45722608	4.37809061	0.00099353	0.35369913	VTAneurons	3m

Pmch	110312	0.94381265	4.36353985	4.36157412	0.00102201	0.35369913	VTAnurons	3m
Gm10115	791270	-1.04868859	3.75995084	-4.2894472	0.00115672	0.36611268	VTAnurons	3m
Pisd-ps3	66776	1.00865381	6.59919627	4.21837128	0.00130765	0.36611268	VTAnurons	3m
Smco3	654818	0.74205234	3.89456798	4.18765164	0.0013791	0.36611268	VTAnurons	3m
Anxa1	16952	-0.70023329	5.03426453	-4.15887074	0.00144973	0.36611268	VTAnurons	3m
C1qa	12259	0.68321134	5.30557727	4.15629815	0.00145622	0.36611268	VTAnurons	3m
Gm14305	100043387	1.04053483	8.84156602	4.14198144	0.00149291	0.36611268	VTAnurons	3m
Csta2	76770	1.19729293	4.12971982	4.14057883	0.00149656	0.36611268	VTAnurons	3m
Timp4	110595	0.60083027	6.17086847	4.09614975	0.00161697	0.36611268	VTAnurons	3m
Gm2026	100039060	0.81322261	8.00743334	4.08960598	0.00163553	0.36611268	VTAnurons	3m
Clec7a	56644	0.80644503	2.68433157	4.08304661	0.00165437	0.36611268	VTAnurons	3m
Laptm4b	114128	0.65168767	9.1165926	4.06318336	0.00171278	0.36611268	VTAnurons	3m
Ppp1r3e	105651	0.84454483	5.37139146	4.04872677	0.00175664	0.36611268	VTAnurons	3m
Aktip	14339	0.70077463	7.83758576	4.02721383	0.00182408	0.36611268	VTAnurons	3m
Gm14295	100039123	0.93851849	8.05905981	4.01876698	0.00185128	0.36611268	VTAnurons	3m
Mir153	387171	-1.83305078	6.13504597	-3.9763399	0.00199443	0.37649364	VTAnurons	3m
Gabra4	14397	0.63992912	6.22716859	3.96149281	0.00204719	0.37786564	VTAnurons	3m
Nr2c2ap	75692	0.61543315	5.15058504	3.93994032	0.00212636	0.3839471	VTAnurons	3m
Ms4a7	109225	0.85419494	2.57740333	3.89155399	0.00231586	0.40214395	VTAnurons	3m
Mir669b	735255	-1.29351049	2.12870207	-3.88957498	0.00232397	0.40214395	VTAnurons	3m
Mir692-1	751529	0.76655	7.74507727	3.74710683	0.00299231	0.47173792	VTAnurons	3m
Irak1bp1	65099	0.61322839	5.84612317	3.73239749	0.00307177	0.47173792	VTAnurons	3m

Ide	15925	0.7491577	6.15903733	3.73222831	0.0030727	0.47173792	VTAneurons	3m
Dcxr	67880	0.64185392	6.26428195	3.71249754	0.00318275	0.47173792	VTAneurons	3m
Apln	30878	0.60005726	5.78551026	3.70152707	0.00324568	0.47173792	VTAneurons	3m
Pisd-ps1	236604	0.75976296	6.00015367	3.69323487	0.0032941	0.47173792	VTAneurons	3m
Mpeg1	17476	0.68585553	2.87510584	3.67606113	0.00339675	0.47404137	VTAneurons	3m
Llcfcl	76606	-0.66202986	3.60798197	-3.67153837	0.00342433	0.47404137	VTAneurons	3m
Gm14403	433520	0.67850827	7.01522595	3.6548135	0.00352832	0.48043004	VTAneurons	3m
Ankrd34c	330998	0.68474533	4.69742059	3.63661718	0.00364515	0.48058138	VTAneurons	3m
Hexb	15212	0.60090837	7.05989159	3.60546383	0.00385448	0.49254267	VTAneurons	3m
Serpina3n	20716	0.84168929	5.08479482	3.57991694	0.00403531	0.49681678	VTAneurons	3m
Timm13	30055	0.60457285	8.01712237	3.56358514	0.00415545	0.49681678	VTAneurons	3m
Snord82	80828	-1.136333	3.21658562	-3.55737042	0.00420212	0.49681678	VTAneurons	3m
Siah3	380918	0.77521735	6.5918808	3.5438945	0.00430518	0.49681678	VTAneurons	3m
Dcn	13179	-1.03491001	4.07340499	-3.5437086	0.00430662	0.49681678	VTAneurons	3m
3110039I08Rik	73144	0.61327523	4.3092908	3.52248512	0.00447427	0.50908564	VTAneurons	3m
Olfir690	56860	-0.87918167	3.25093641	-3.47336939	0.00488831	0.51540246	VTAneurons	3m
Gm10855	100038708	-0.70745543	3.35164175	-3.45323604	0.00506915	0.51540246	VTAneurons	3m
Tmem98	103743	0.79196711	5.74969859	3.42819254	0.00530368	0.51540246	VTAneurons	3m
Pisd-ps2	328734	0.69045379	6.60448749	3.42046851	0.00537822	0.51540246	VTAneurons	3m
Cdkn3	72391	0.64521385	4.36995984	3.41833733	0.00539898	0.51540246	VTAneurons	3m
Gatd3a	28295	1.05268565	7.05924429	3.40170502	0.00556379	0.51540246	VTAneurons	3m
Nat8f5	69049	0.71201411	3.10471251	3.39835944	0.00559755	0.51540246	VTAneurons	3m

Ddx3y	26900	-1.00189213	3.41423106	-3.39451436	0.00563662	0.51540246	VTAneurons	3m
Lypd1	72585	0.66022466	5.50678589	3.35953167	0.00600505	0.51540246	VTAneurons	3m
2810013P06Rik	100503178	0.62517004	5.67086174	3.34168311	0.00620238	0.51540246	VTAneurons	3m
Cd48	12506	0.97823964	2.83707675	3.26669474	0.00710614	0.51540246	VTAneurons	3m
Acadl	11363	0.68481644	5.33794755	3.25476242	0.00726181	0.51540246	VTAneurons	3m
Snord71	100217432	-0.92778661	6.19665865	-3.25140888	0.00730618	0.51540246	VTAneurons	3m
Ctsz	64138	0.6100797	5.21387966	3.2465904	0.00737042	0.51540246	VTAneurons	3m
Trav3-3	320898	1.45498458	5.7843045	3.22120851	0.00771835	0.51540246	VTAneurons	3m
Atg14	100504663	0.66746982	3.38904252	3.21175127	0.00785221	0.51540246	VTAneurons	3m
Reep4	72549	0.80330151	6.06091156	3.18091572	0.00830518	0.51540246	VTAneurons	3m
Tfblm	224481	0.6079172	5.63013863	3.17265067	0.00843102	0.51540246	VTAneurons	3m
Gm14326	665211	0.72601466	8.3285126	3.13039076	0.00910521	0.51540246	VTAneurons	3m
Gsg11	269994	0.80253209	5.85732964	3.11429538	0.00937607	0.51540246	VTAneurons	3m
Tacr1	21336	0.77647831	5.30912371	3.10193111	0.00958965	0.51540246	VTAneurons	3m
Mllt11	56772	0.62898834	6.45757717	3.09507744	0.00971015	0.51540246	VTAneurons	3m
Mir6352	102465180	-0.85899174	4.42265875	-3.08862165	0.00982504	0.51540246	VTAneurons	3m
Lyz2	17105	4.21249198	4.83026395	15.9079232	1.51E-10	1.25E-06	VTAneurons	12m
Cd68	12514	3.30127003	5.79711403	13.5463899	1.33E-09	5.54E-06	VTAneurons	12m
Tyrobp	22177	2.81242659	7.41140194	12.37337	4.47E-09	1.24E-05	VTAneurons	12m
Ms4a7	109225	2.81047364	3.30166053	11.1548407	1.75E-08	2.93E-05	VTAneurons	12m
Gpnmb	93695	2.78858001	4.02079291	11.1469352	1.76E-08	2.93E-05	VTAneurons	12m
Lilrb4a	14728	2.27196741	3.70022686	9.89804739	8.12E-08	0.00011243	VTAneurons	12m

Ctss	13040	1.94099261	7.15626209	9.60571561	1.19E-07	0.00014077	VTAneurons	12m
Cyba	13057	1.70221389	5.9542177	8.1445743	9.04E-07	0.00093879	VTAneurons	12m
Bcl2a1a	12044	3.40369547	5.27741538	7.89518146	1.31E-06	0.00120971	VTAneurons	12m
Lilr4b	14727	1.54399443	2.95152106	7.016348	5.16E-06	0.00420414	VTAneurons	12m
Cd84	12523	1.59940072	2.83773911	6.93399108	5.90E-06	0.00420414	VTAneurons	12m
Serpina3n	20716	2.03817952	5.62673571	6.91650821	6.07E-06	0.00420414	VTAneurons	12m
H2-K1	14972	1.07943462	6.14183073	6.42851792	1.37E-05	0.00834896	VTAneurons	12m
Hexb	15212	1.28810705	7.39386663	6.41197663	1.41E-05	0.00834896	VTAneurons	12m
Lyz1	17110	1.4823108	3.11933875	6.24267383	1.88E-05	0.01041154	VTAneurons	12m
C3ar1	12267	1.21852654	3.04177703	6.18333111	2.08E-05	0.01081444	VTAneurons	12m
Cst7	13011	1.78011048	3.6937614	6.09797546	2.42E-05	0.01180533	VTAneurons	12m
Lcn2	16819	1.09065478	3.5147169	5.87083717	3.60E-05	0.01581049	VTAneurons	12m
Gfap	14580	2.12271965	5.70541094	5.86868437	3.62E-05	0.01581049	VTAneurons	12m
Cd48	12506	1.75613054	3.51076285	5.79122367	4.15E-05	0.01724085	VTAneurons	12m
Trem2	83433	0.88984895	4.28491514	5.71244583	4.78E-05	0.01890796	VTAneurons	12m
Spp1	20750	1.17712654	4.17704136	5.68127969	5.06E-05	0.01908908	VTAneurons	12m
Snord90	100217435	1.9699945	3.2429811	5.53798752	6.55E-05	0.02366705	VTAneurons	12m
Ms4a6c	73656	0.9859372	3.34638614	5.33179785	9.57E-05	0.03310466	VTAneurons	12m
C1qb	12260	1.49769601	5.18013474	5.20667434	0.00012066	0.04008794	VTAneurons	12m
Itgb5	16419	0.64600899	5.17915609	5.18110307	0.00012656	0.04042973	VTAneurons	12m
Ctsh	13036	0.85981173	4.65913314	5.06401867	0.00015762	0.0451645	VTAneurons	12m
C4b	12268	1.14611314	5.29472859	5.04621287	0.000163	0.0451645	VTAneurons	12m

Grn	14824	0.65299445	6.0226023	5.04620761	0.000163	0.0451645	VTAneurons	12m
Clec7a	56644	2.04279554	3.12450147	5.04579783	0.00016313	0.0451645	VTAneurons	12m
Snord93	100217436	-0.95405296	5.47719244	-5.01497111	0.0001729	0.04632493	VTAneurons	12m
B2m	12010	1.2735586	8.84726671	4.96336342	0.00019063	0.04874357	VTAneurons	12m
Pycard	66824	0.67500183	3.7858623	4.95503685	0.00019366	0.04874357	VTAneurons	12m
Tlr7	170743	1.31729996	3.13611494	4.93042782	0.00020292	0.04957152	VTAneurons	12m
Vim	22352	1.00006462	4.82479903	4.86514345	0.00022976	0.05452533	VTAneurons	12m
Laptm5	16792	0.77503026	4.72874896	4.84220901	0.00024004	0.05538235	VTAneurons	12m
Cd9	12527	0.80663521	6.79428598	4.82209325	0.00024945	0.05579577	VTAneurons	12m
Mpeg1	17476	1.45802098	3.40212068	4.81003508	0.00025527	0.05579577	VTAneurons	12m
Fcer1g	14127	1.02895654	4.66961449	4.75802109	0.00028203	0.06006409	VTAneurons	12m
Nmnat2	226518	0.68114468	7.77430724	4.70907815	0.00030985	0.06418031	VTAneurons	12m
Alox5ap	11690	1.36463155	4.7207906	4.69754949	0.00031681	0.06418031	VTAneurons	12m
Kcna1	16485	0.75147363	5.62964226	4.50697493	0.00045827	0.09062921	VTAneurons	12m
Anxa1	16952	-1.00740411	5.08087657	-4.47707619	0.00048577	0.09383332	VTAneurons	12m
Ctsz	64138	1.33978486	5.83950595	4.46255146	0.00049974	0.09433697	VTAneurons	12m
Cd63	12512	0.71541997	8.65171397	4.38621391	0.00058021	0.10709462	VTAneurons	12m
Omg	18377	-0.70158604	6.33299907	-4.35655236	0.00061497	0.11104174	VTAneurons	12m
Man2b1	17159	0.84288617	6.09275014	4.34320766	0.00063129	0.11156411	VTAneurons	12m
Casr	12374	-0.72521664	5.34037301	-4.25153865	0.00075612	0.13083938	VTAneurons	12m
C4a	625018	0.61783639	4.66422116	4.19954967	0.00083787	0.14202668	VTAneurons	12m
Fnip2	329679	0.60790414	3.78044019	4.13929727	0.000944	0.15681773	VTAneurons	12m

H2-K2	630499	0.61125032	4.82676304	4.10717845	0.0010061	0.16186111	VTAnurons	12m
Anxa3	11745	0.91645571	3.68046076	4.10356463	0.00101334	0.16186111	VTAnurons	12m
Mir669h	100316831	0.81404874	8.98809687	4.04899214	0.0011294	0.17699606	VTAnurons	12m
Mir692-1	751529	1.23735265	8.07312456	4.02577233	0.00118281	0.18193361	VTAnurons	12m
Snord4a	100216539	-1.53571676	5.52013219	-3.99272962	0.00126328	0.1907786	VTAnurons	12m
Fcgr2b	14130	0.6400427	3.12096255	3.91255509	0.0014825	0.21602917	VTAnurons	12m
P2ry13	74191	0.69077953	4.2123733	3.84187538	0.00170768	0.23941434	VTAnurons	12m
Casp1	12362	1.17245713	2.73339507	3.83554808	0.00172946	0.23941434	VTAnurons	12m
Pip4k2a	18718	0.64697723	5.90342322	3.78367976	0.00191894	0.26129027	VTAnurons	12m
Mir708	735284	-0.62723048	3.65022524	-3.76574634	0.00198924	0.26649339	VTAnurons	12m
Cd53	12508	0.7247697	3.12902507	3.74789709	0.00206179	0.27182914	VTAnurons	12m
Mir6352	102465180	0.75300108	4.21681209	3.70457251	0.00224924	0.28055824	VTAnurons	12m
Plpp4	381925	-1.07337855	6.28749032	-3.70384964	0.00225251	0.28055824	VTAnurons	12m
Soat1	20652	0.61478108	5.40439268	3.653506	0.00249242	0.30002968	VTAnurons	12m
Ctsb	13030	0.65663838	9.2889867	3.64203739	0.00255059	0.30264563	VTAnurons	12m
Mir6957	102466773	-0.80960666	4.35607712	-3.59298869	0.00281521	0.31598877	VTAnurons	12m
Zfp566	72556	-0.63432279	5.32909618	-3.57141264	0.00294022	0.32561957	VTAnurons	12m
Cxcl16	66102	0.76989982	4.26537954	3.51214092	0.00331313	0.35193624	VTAnurons	12m
Igfbp5	16011	0.64657075	6.62714608	3.50438998	0.00336529	0.35193624	VTAnurons	12m
Pld4	104759	0.64453231	4.92930053	3.50388804	0.0033687	0.35193624	VTAnurons	12m
Gm20172	100504323	0.85733262	4.55421241	3.47649561	0.00355992	0.36504602	VTAnurons	12m
Snora78	100306952	-0.78258816	5.24851833	-3.44171393	0.00381851	0.37849227	VTAnurons	12m

Pglyrp1	21946	0.90097749	5.4127603	3.4392848	0.00383726	0.37849227	VTAneurons	12m
Mir5123	100628614	1.6949776	3.15523583	3.43428387	0.00387615	0.37849227	VTAneurons	12m
Bcl2a1d	12047	0.65292968	2.48939329	3.43032129	0.00390724	0.37849227	VTAneurons	12m
Cxcr4	12767	0.8872439	3.25178459	3.39127096	0.00422735	0.40359022	VTAneurons	12m
Rnu3a	19850	-0.63469986	4.8223959	-3.34414296	0.00464881	0.43282743	VTAneurons	12m
Rac2	19354	0.69457071	4.32844616	3.32515687	0.00483023	0.43282743	VTAneurons	12m
C1qa	12259	0.66411458	5.57196929	3.27025978	0.00539555	0.45802575	VTAneurons	12m
Ifi30	65972	0.92456283	5.54135222	3.23042327	0.00584661	0.47953632	VTAneurons	12m
Ftl1	14325	0.82741612	7.31717472	3.21939726	0.00597796	0.48206695	VTAneurons	12m
Gm19817	100503655	0.81756701	5.69963803	3.19370989	0.00629544	0.49038691	VTAneurons	12m
AW112010	107350	1.34832155	3.05370001	3.17719909	0.00650829	0.50053577	VTAneurons	12m
Tmem176a	66058	0.60420585	5.74990595	3.16124105	0.0067208	0.50573552	VTAneurons	12m
D10Jhu81e	28295	-0.64418621	7.1144141	-3.14226507	0.00698247	0.50573552	VTAneurons	12m
Nsmce2	68501	0.65584575	6.84338593	3.14130878	0.00699593	0.50573552	VTAneurons	12m
Gm9982	791357	0.59579467	3.84896363	3.1408692	0.00700212	0.50573552	VTAneurons	12m
Ifit1	15957	0.65032756	3.34631707	3.09904402	0.00761676	0.53157958	VTAneurons	12m
Hexa	15211	0.61691309	6.7436239	3.09493622	0.00767994	0.53157958	VTAneurons	12m
Gkn1	66283	-0.88562738	6.09795535	-3.09033121	0.00775137	0.53209004	VTAneurons	12m
Zfp72	238722	-0.66182021	5.34454176	-3.07595609	0.00797862	0.54281878	VTAneurons	12m
Neurod6	11922	-0.90489599	3.58953369	-3.05909084	0.00825364	0.54843793	VTAneurons	12m
Adgrl4	170757	0.61064829	3.93509593	3.04839126	0.00843295	0.55189221	VTAneurons	12m
Ctla2b	13025	0.96574628	4.19305328	3.04365702	0.00851351	0.55189221	VTAneurons	12m

Mir6386	102465203	-0.62156193	4.08096905	-3.03297472	0.00869809	0.55189221	VTAnurons	12m
Mir3088	100526498	0.65319708	3.07397593	3.02408982	0.00885461	0.5529806	VTAnurons	12m
Xlr	22441	0.62234234	2.42055445	2.98445928	0.00958727	0.57289081	VTAnurons	12m
Usp18	24110	0.82314774	3.75608422	2.96568699	0.00995483	0.58641718	VTAnurons	12m
Tyrobp	22177	2.89501388	7.83327428	11.1177153	2.14E-08	0.00017798	VTAnurons	20m
Bcl2a1a	12044	2.90473289	5.47859951	9.55375758	1.45E-07	0.00044114	VTAnurons	20m
AW112010	107350	2.32672001	3.42594483	9.48274701	1.59E-07	0.00044114	VTAnurons	20m
Mir692-1	751529	1.49789928	8.13197797	9.23107046	2.22E-07	0.00046109	VTAnurons	20m
Cst7	13011	1.73830296	3.89978041	8.94431045	3.27E-07	0.00054284	VTAnurons	20m
H2-K1	14972	1.09247542	6.14400859	8.74950244	4.27E-07	0.0005604	VTAnurons	20m
B2m	12010	1.6191076	9.00478311	8.67696624	4.72E-07	0.0005604	VTAnurons	20m
Cyba	13057	2.00890675	6.06853458	8.52995094	5.80E-07	0.0006025	VTAnurons	20m
Lgals9	16859	1.65861093	5.35479448	8.21373004	9.11E-07	0.00084118	VTAnurons	20m
Mpeg1	17476	2.20165121	3.800926	8.13809239	1.02E-06	0.00084488	VTAnurons	20m
Lyz1	17110	2.53947287	3.34027393	7.48875233	2.69E-06	0.00202823	VTAnurons	20m
Car8	12319	-1.17127506	5.16873739	-7.41455888	3.01E-06	0.0020844	VTAnurons	20m
Ctss	13040	1.677903	7.50928638	7.35679631	3.29E-06	0.00210421	VTAnurons	20m
Ftl1	14325	1.04854458	7.36409612	7.30876629	3.55E-06	0.00210557	VTAnurons	20m
Cd68	12514	3.34451285	6.23946486	7.25767032	3.84E-06	0.00212856	VTAnurons	20m
Casp1	12362	1.46748908	2.9646876	7.04552712	5.37E-06	0.0027902	VTAnurons	20m
Vim	22352	1.0240399	4.70849664	6.67526286	9.79E-06	0.00460091	VTAnurons	20m
Lyz2	17105	4.98146286	5.44737595	6.65796697	1.01E-05	0.00460091	VTAnurons	20m

Ctsz	64138	1.53079591	5.87738974	6.60097196	1.11E-05	0.00460091	VTAneurons	20m
Lilr4b	14727	2.13329678	3.01144779	6.60017297	1.11E-05	0.00460091	VTAneurons	20m
Gm14305	100043387	-1.07877287	8.56963574	-6.49789063	1.31E-05	0.00519336	VTAneurons	20m
Cd48	12506	2.35665434	3.81295279	6.34027727	1.71E-05	0.00645924	VTAneurons	20m
Hexb	15212	0.8594792	7.5800927	6.29802947	1.84E-05	0.00663647	VTAneurons	20m
Clec7a	56644	2.41189325	3.52010444	6.092227	2.61E-05	0.00904265	VTAneurons	20m
0610010B08Rik	100039060	-0.89329	7.7937325	-5.85849096	3.92E-05	0.01303897	VTAneurons	20m
Degs2	70059	-0.79958862	3.94284855	-5.81886923	4.21E-05	0.01344264	VTAneurons	20m
Cxcl16	66102	0.86454822	4.38893912	5.70236562	5.17E-05	0.01590956	VTAneurons	20m
Bcl2a1d	12047	0.83593625	2.56376429	5.61320865	6.06E-05	0.0174262	VTAneurons	20m
Gm14295	100039123	-0.98057784	7.7836846	-5.6112914	6.08E-05	0.0174262	VTAneurons	20m
Ctsh	13036	1.09071759	4.83928507	5.57942055	6.44E-05	0.01770259	VTAneurons	20m
Cd63	12512	0.74919726	8.76895504	5.56533949	6.61E-05	0.01770259	VTAneurons	20m
Man2b1	17159	0.71044862	6.30334604	5.53294461	7.00E-05	0.01782798	VTAneurons	20m
Lgals3bp	19039	0.8695457	5.27517847	5.52667487	7.08E-05	0.01782798	VTAneurons	20m
Cd84	12523	1.3048511	2.91274816	5.48558137	7.63E-05	0.01863587	VTAneurons	20m
Gpnmb	93695	2.66078363	4.20897514	5.30089378	0.00010677	0.02533693	VTAneurons	20m
Ifi30	65972	1.09890155	5.52096992	5.16506659	0.00013711	0.03163337	VTAneurons	20m
Tlr7	170743	1.93816473	3.37348118	5.1103719	0.00015174	0.03385752	VTAneurons	20m
Creg1	433375	0.68386389	6.40945707	5.08207286	0.00015994	0.03385752	VTAneurons	20m
Ms4a7	109225	3.13852626	3.60315875	5.06846929	0.00016404	0.03385752	VTAneurons	20m
Calhm6	215900	0.84984669	3.56285867	5.06168636	0.00016612	0.03385752	VTAneurons	20m

Gpr137b-ps	664862	0.91034959	5.34686041	5.0584562	0.00016713	0.03385752	VTAneurons	20m
C1qb	12260	0.89721389	5.38671745	5.01762572	0.00018036	0.03484236	VTAneurons	20m
Mir107	723826	-0.79460589	3.11009057	-5.01758136	0.00018038	0.03484236	VTAneurons	20m
Lgals1	16852	0.88700332	6.7644519	4.98362364	0.00019221	0.03628461	VTAneurons	20m
Ms4a6c	73656	1.08331297	3.47026021	4.91416874	0.00021899	0.04042104	VTAneurons	20m
Anxa3	11745	0.91854166	3.60201004	4.89903972	0.00022532	0.04068509	VTAneurons	20m
AU020206	100504230	0.9472799	4.56231322	4.84917594	0.00024755	0.0431711	VTAneurons	20m
Usp18	24110	2.074933	4.08795527	4.84506601	0.00024948	0.0431711	VTAneurons	20m
Nppc	18159	-0.66762075	4.31607445	-4.78192194	0.00028119	0.04766405	VTAneurons	20m
Gpr137b	83924	0.80013912	5.64318531	4.76143219	0.00029235	0.04823904	VTAneurons	20m
Rgl1	19731	0.61645019	5.18727405	4.74789578	0.00029997	0.04823904	VTAneurons	20m
Nmnat2	226518	0.92833549	7.84161757	4.74434507	0.000302	0.04823904	VTAneurons	20m
Serpina3n	20716	1.62143331	5.93188421	4.66815801	0.00034923	0.0547305	VTAneurons	20m
9530091C08Rik	320440	0.63340418	4.33355707	4.65150735	0.00036053	0.0554551	VTAneurons	20m
Ccl2	20296	0.67173488	3.46108743	4.58258482	0.00041147	0.06213899	VTAneurons	20m
Cebpa	12606	0.74376702	4.22634492	4.55646441	0.00043266	0.06417255	VTAneurons	20m
Lilrb4a	14728	2.39031548	3.85978356	4.47457164	0.00050668	0.07383318	VTAneurons	20m
Lipa	16889	0.83228303	5.38317464	4.45891691	0.00052225	0.07479032	VTAneurons	20m
Gm9958	791294	-0.6354143	3.5835882	-4.28588641	0.000731	0.10119425	VTAneurons	20m
Hapln1	12950	-0.63971947	4.28179053	-4.22920283	0.00081664	0.10805609	VTAneurons	20m
Gfap	14580	1.77047782	6.21698565	4.22735704	0.00081959	0.10805609	VTAneurons	20m
Xlr	22441	0.74620108	2.6102721	4.2076387	0.00085186	0.10923091	VTAneurons	20m

Gm14326	665211	-0.66341954	8.17790855	-4.20587513	0.00085481	0.10923091	VTAneurons	20m
Hcar2	80885	1.02285821	3.48335507	4.16690941	0.00092268	0.11270251	VTAneurons	20m
Agt	11606	-0.92899829	6.55665656	-4.03273135	0.00120155	0.13083499	VTAneurons	20m
Mars2	212679	-0.75601416	3.1816445	-4.03238469	0.00120238	0.13083499	VTAneurons	20m
Camk2n1	66259	-0.59919497	6.01592116	-4.02797187	0.00121289	0.13083499	VTAneurons	20m
Fcgr2b	14130	0.89691916	3.24965231	3.93153564	0.00146772	0.15261174	VTAneurons	20m
Ifit2	15958	0.74936929	3.70859447	3.91713568	0.0015102	0.15486019	VTAneurons	20m
Gira3	110304	-0.80616743	4.98906768	-3.84243509	0.00175148	0.1774121	VTAneurons	20m
Ly86	17084	1.09869238	5.14857071	3.81791153	0.00183895	0.18293346	VTAneurons	20m
Ctla2a	13024	1.1904686	5.29695286	3.81488837	0.00185004	0.18293346	VTAneurons	20m
Bend7	209645	-0.62167638	5.14598683	-3.78481233	0.00196409	0.18711786	VTAneurons	20m
Mir7060	102465642	0.60806181	5.28077255	3.76128714	0.00205824	0.18711786	VTAneurons	20m
Gm10941	100169878	-0.59479897	5.3101897	-3.75818718	0.00207098	0.18711786	VTAneurons	20m
Gm14405	626877	-0.62617549	5.68301883	-3.74320715	0.0021337	0.18711786	VTAneurons	20m
Serpini1	20713	-0.60836025	6.53498951	-3.74014724	0.00214675	0.18711786	VTAneurons	20m
Igfbp5	16011	0.60185842	6.69264395	3.73589664	0.002165	0.18711786	VTAneurons	20m
Mafb	16658	0.78085971	4.06804126	3.64963515	0.0025714	0.20939283	VTAneurons	20m
Alox5ap	11690	0.82673475	4.80108826	3.62878387	0.00268071	0.2140959	VTAneurons	20m
Ifit1	15957	1.34603972	3.51819126	3.6168449	0.0027454	0.21512507	VTAneurons	20m
Rtp4	67775	0.81009687	3.66604543	3.61103791	0.00277743	0.21560091	VTAneurons	20m
C4b	12268	0.95253407	5.80807981	3.58726135	0.00291255	0.22223434	VTAneurons	20m
Wfdc17	100034251	0.6166812	3.34202285	3.57713601	0.00297209	0.22223434	VTAneurons	20m

Ctla2b	13025	1.06026055	4.42318015	3.57142051	0.00300624	0.22223434	VTAnurons	20m
Lcn2	16819	0.64801767	3.45971974	3.56856986	0.00302341	0.22223434	VTAnurons	20m
AA667203	100503467	0.70827629	3.7236164	3.5346419	0.00323563	0.23554703	VTAnurons	20m
Grn	14824	0.59206419	6.02463956	3.5306986	0.00326125	0.23554703	VTAnurons	20m
1700001L19Rik	69315	-0.61911592	4.85466863	-3.52060583	0.00332775	0.23827825	VTAnurons	20m
Perp	64058	-0.65857535	4.97311101	-3.49680524	0.00349003	0.24051427	VTAnurons	20m
Fcer1g	14127	1.0366968	4.95340282	3.4748296	0.00364692	0.24627061	VTAnurons	20m
Bcl2a1c	12046	0.59890209	2.6733551	3.4389071	0.00391878	0.25906769	VTAnurons	20m
Trem2	83433	0.68008395	4.25696186	3.42715336	0.00401208	0.25906769	VTAnurons	20m
Akr1e1	56043	-1.23442735	6.41068241	-3.39460692	0.00428221	0.26742907	VTAnurons	20m
Nkain4	58237	-0.66244979	6.13850585	-3.34320159	0.00474647	0.29203111	VTAnurons	20m
Stbd1	52331	-0.70624427	5.72061412	-3.32767316	0.00489638	0.29344739	VTAnurons	20m
Snapc5	330959	-0.62172344	5.10619658	-3.32620353	0.00491081	0.29344739	VTAnurons	20m
Stat2	20847	0.58649384	5.01584412	3.30777881	0.00509537	0.30015698	VTAnurons	20m
Gm14327	665205	-0.63991929	8.18693854	-3.30226024	0.00515199	0.30135482	VTAnurons	20m
Snord35b	27212	-0.70372743	4.61386965	-3.28251486	0.00535975	0.30491828	VTAnurons	20m
Zfp971	626848	-0.64354734	7.49941801	-3.26928186	0.00550365	0.31097473	VTAnurons	20m
Zfp965	100503949	-0.59149788	7.75652221	-3.24755403	0.00574832	0.32044	VTAnurons	20m
Anxa1	16952	-0.80485718	5.03705029	-3.2138729	0.00614919	0.33155572	VTAnurons	20m
Pcdhb9	93880	-0.81854713	5.31290207	-3.17649937	0.00662664	0.34186889	VTAnurons	20m
Mc4r	17202	0.61705697	3.07244951	3.15507764	0.00691673	0.34196665	VTAnurons	20m
Npy	109648	0.65991832	5.41813462	3.14610201	0.007042	0.34406378	VTAnurons	20m

Hddc3	68695	-0.73323022	6.28960529	-3.12787286	0.00730338	0.34877335	VTAneurons	20m
Neurod6	11922	-0.69309804	3.65327654	-3.12273843	0.00737872	0.34877335	VTAneurons	20m
Cyp2j9	74519	-0.6779726	4.70770416	-3.12070008	0.00740884	0.34877335	VTAneurons	20m
Mir1193	100316673	0.919553	3.98489871	3.03822218	0.00873547	0.39433046	VTAneurons	20m
Cd53	12508	0.66395181	3.34035876	3.00192086	0.00939136	0.41937996	VTAneurons	20m
Ly6a	110454	0.71030374	5.24440764	2.99864153	0.00945296	0.41952616	VTAneurons	20m

Annex Data Table 5. GEO datasets Info used for correlation of tgNM transcriptomic profiles with human postmortem PD studies.

GEO	Publication	Brain region(s)	Patients	Platform
GSE34516	22634372	LC	4C (2M, 2F), 4iPD (1M, 3F), 2LRRK2PD (2F)	[HuEx-1_0-st] Affymetrix Human Exon 1.0 ST Array
GSE7621	17571925	SN	9C (4M, 5F), 16PD (13M, 3F)	[HG-U133_Plus_2] Affymetrix Human Genome U133 Plus 2.0 Array
GSE43490	25525598	SN	5C (4M, 1F), 8PD (5M, 3F)	Agilent-014850 Whole Human Genome Microarray 4x44K G4112F
GSE20164	20926834	SN	5C (1M, 4F), 6PD (4M, 2F)	[HG-U133A] Affymetrix Human Genome U133A Array
GSE20163	20926834	SN	9C (M/F not specified), 8PD (M/F not specified)	[HG-U133A] Affymetrix Human Genome U133A Array
GSE20292	15965975, 20926834	SN	18C (13M, 5F), 11PD (6M, 5F)	[HG-U133A] Affymetrix Human Genome U133A Array
GSE20333	-	SN	6C (5M, 1F), 6PD (2M, 4F)	[HG-Focus] Affymetrix Human HG-Focus Target Array
GSE24378	20926834	SN (LCM DA neurons)	9C (M/F not specified), 8PD (M/F not specified)	[U133_X3P] Affymetrix Human X3P Array
GSE20141	20926834	SN (LCM DA neurons)	8C (M/F not specified), 10PD (M/F not specified)	[HG-U133_Plus_2] Affymetrix Human Genome U133 Plus 2.0 Array

Annex Data Table 6. Expression values of GPNMB in bulk (upper table) and LCM-isolated neurons (lower table). RNA quality is reported with RIN number (0-totally degraded, 10-intact). GPNMB expression values are represented as relative quantity (RQ, $2^{-\Delta\Delta CT}$) normalized to FOXO1, GOLGA3, HPRT1 and UGGT1 (bulk analysis) or HPRT1 and UGGT (LCM-isolated neurons). Red values indicate excluded samples because of bad RNA quality. Orange values indicate statistical outliers removed. Disease duration in years, Dis. Dur. (y), Postmortem

interval, PMI. Substantia nigra, SN, Locus coeruleus, LC, Frontal cortex, FC. * Present in both experiments.

Case	Diagnostic	Dis. Dur. (y)	Sex	Age (y)	PMD (h)	RIN SN	SN GPNMB	RIN LC	LC GPNMB	RIN FC	FC GPNMB
BK-1491*	Control	-	M	83	13	5.4	6.8	5.9	5.0	6.0	27.3
BK-1570*	Control	-	F	86	4	6.9	4.2	7.4	5.4	7.4	3.2
BK-1679*	Control	-	F	90	12.25	5.3	7.2	7.5	6.7	7.8	12.5
BK-1694	Control	-	M	58	5	6.3	4.5	5.6	12.3	5.7	17.2
BK-1733	Control	-	M	76	11.5	6.2	7.2	6.8	3.6	8.1	0.8
BK-1749*	Control	-	F	70	14	6.9	10.6	6.6	9.0	7.6	11.0
BK-1889*	Control	-	M	70	4.5	5.9	355.2	7.1	7.4	7.5	10.2
BK-1937*	Control	-	F	83	7.2	4.4	79.8	4.7	17.6	7.2	11.8
BK-0902	PD	32	M	83	14	7.0	52.1	6.8	8.8	7.9	5.1
BK-0962	PD	16	F	85	7	5.5	7.6	5.7	32.3	6.8	3.8
BK-1027	PD	30	F	77	7.5	6.6	11.7	7.5	182.6	5.9	19.5
BK-1094	PD	21	M	77	6.25	7.2	13.8	5.4	9.1	6.5	10.4
BK-1100*	PD	22	M	76	12	5.8	36.0	5.7	14.7	5.0	13.0
BK-1006	PD	1	M	77	7.5	5.9	5.7	5.0	7.0	7.1	34.0
BK-1049*	PD	8	F	73	3.75	6.8	10.3	6.2	6.7	5.5	14.3
BK-0930	PD	12	F	88	16.5	2.2	7.9	-	-	5.7	9.4
BK-0988	PD	29	M	81	7	7.1	47.9	7.3	4.8	6.7	16.8
BK-1082	PD	14	M	80	7.5	6.7	41.5	6.3	14.3	7.9	4.1

Case	DX	Braak	Dis. Dur.(y)	Sex	Age(y)	PMI(h)	SN neurons GPNMB	RIN
BK-1679*	Control			F	90	12.25	0.00	5.2
BK-1937*	Control			F	83	7.2	26.31	2.8
BCPA-587	Control			F	83	4	0.34	5.1
BK-1570*	Control			F	86	4	0.87	5.4
BK-1889*	Control			M	70	4.5	0.52	3
BK-1491*	Control			M	83	13	0.04	5.3
BK-1749*	Control			F	70	14	0.17	5.9
BK-1049*	PD	Braak 5	8	F	81	3.75	0.65	5.3
BK-1100*	PD		22	M	76	12	331.36	3.4
1224	PD	Braak4-5		M	82	7	1.02	6
1210	PD	Braak 5		M	85	12	2.18	4.7
1244	PD	Braak 6		F	86	16	66.68	5.1
1246	PD	Braak 4		F	69	5	0.07	3.8
1238	PD	Braak 5		M	76	17	2.35	4